Modification and Application of Hyperbranched Polyglycerol and Polyethylenimine

Dissertation

for attaining the degree of

Doctor of Natural Sciences

am Fachbereich 09

Chemie, Pharmazie und Geowissenschaften

of Johannes Gutenberg University Mainz

Zhong SHEN

born in Shandong Province, P. R. China

Mainz, 06. 2006

Abstract

Branched macromolecules are powerful motifs for the design of supramolecular assemblies and nanomaterials due to their specific shape and multifunctionality. The present thesis deals with modification of hyperbranched polymers, namely hyperbranched polyglycerol (PG) and hyperbranched polyethylenimine (HPEI).

Well-defined multi-arm star copolymers PG-*b*-poly(*tert*-butyl acrylate) with 17, 27, 36, 66, 90 arms have been prepared using a core-first strategy with PG as core macroinitiator. The arms were grafted by ATRP of *t*BA in acetone. Polydispersities of the multi-arm stars were in the range of 1.2-1.4. Kinetic studies show a linear dependence of $\ln([M]_0/[M]_t)$ on time, indicating the radical concentration remained stable during the reaction. Full hydrolysis of the *tert*-butyl ester groups was achieved upon reacting with HCl in dioxane, resulting in star polyacrylic acid (PAA). Viscosity measurements show these star PAAs display typical polyelectrolyte behaviors.

Star PAA was successfully utilized as template to synthesize silver nanoparticles (NPs) and nanoclusters. The nanoclusters obtained from star PAA template via UV-reduction show fluorescent properties. The fluorescent properties show both arm-density and arm length dependence. The “cage effect” associated with densely grafted PAA arms and strong binding of protonated AA groups with Ag^+ are two essential factors for the formation of the fluorescent nanoclusters.

A well-defined multi-arm star copolymer PG-*b*-P(2-dimethylamino ethyl methacrylate) (DMAEMA) with 36 arms was also prepared via ATRP of DMAEMA in ethyl acetate or anisole. The polydispersities of the stars are in the range of 1.4-1.9. Kinetic studies do not show a linear dependence of $\ln([M]_0/[M]_t)$ on time, indicating the polymerizations are only in a relative controlled mode. The star polymers can be turned into inverted micelle by modification with aliphatic bromide. These inverted micelles can be used to transfer water soluble dyes from water phase into organic phase.

The works carried out with HPEI include the synthesis of hyperbranched macroligands for ATRP and non-covalently or covalently bonded nanocapsules for liquid-liquid phase transfer protocols.

Hyperbranched macroligands were prepared by facile Michael addition reaction of HPEI with Ethyl Acrylate or Butyl Acrylate. The resulting hyperbranched macroligand/Cu(I) complexes are efficient catalyst systems for the ATRP of MMA. The ATRP of MMA with hyperbranched macroligands is a controlled process. Molecular weight distributions are fairly narrow (<1.4) even at very high conversion. The compact structure not only leads to very low viscosity compared to the synthesized linear PMMA, but also imparts facile separation from the PMMA product by precipitation of the polymerization mixture in methanol. Copper is separated together with the hyperbranched macroligands, when precipitating the reactants in methanol, and no additional steps are required to purify the polymer from copper contamination. The hyperbranched macroligand/Cu(I) system can be recycled for the ATRP of MMA, keeping relatively high activity.

Self-assembly of HPEI and fatty acids leads to inverted micellar nanocapsules that are able to irreversibly transfer water-soluble guest molecules into organic solvents. The synergy between both components affords phase transfer properties due to the polyelectrolyte-surfactant complexes.

Partially amidated HPEIs with cationic interiors are attractive molecular nanocapsules. Our data confirm the crucial role of both the hyperbranched structure and the polarity difference between core-shell components for molecular nanocapsules. It can be used to transfer water-soluble dyes and Au NPs into organic solvents.

TABLE OF CONTENTS

Chapter 1. General Introduction

1.1. Hyperbranched polymers

It is well known that polymers can possess different topological structures: they may either be linear, branched or networks.[1]

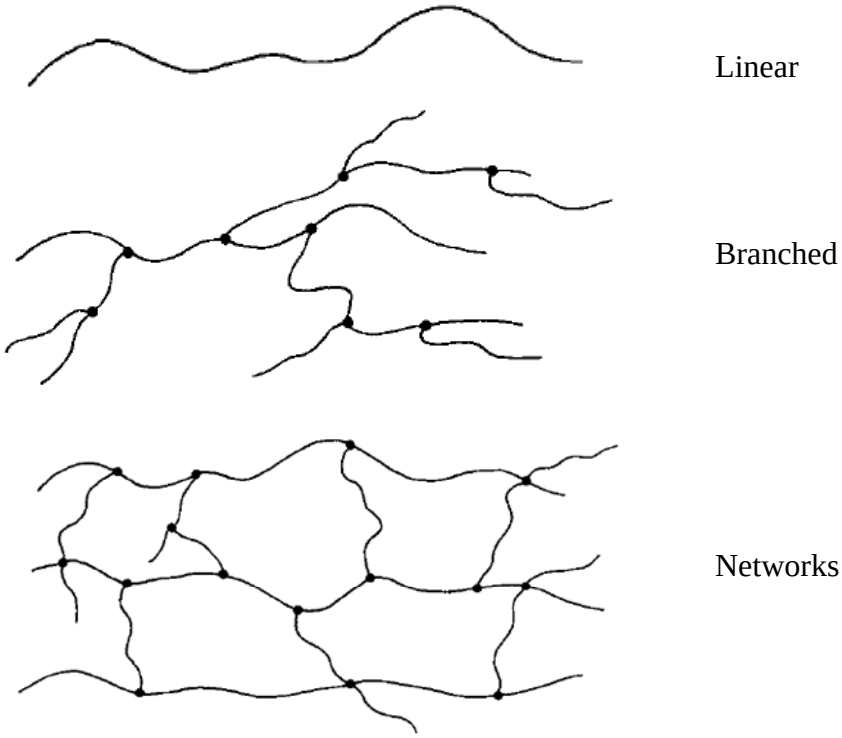

Scheme 1-1. Structure of polymers

Branched polymers can be further subdivided into three different categories according to their topology: comb (the branching points distributed along one single chain), star (one single branching point), and hyperbranched polymers (the branching points are distributed randomly),[1] as illustrated in Scheme 1-2. In this thesis we will focus on the study of hyperbranched polymers and multi-arm stars derived from such topologies.

Branched/hyperbranched polymers are a family of polymers with three-dimensional dendritic architecture.[2, 3] They are characterized by the peculiarity that

there is no connecting line between any two end groups that passes all branching points. Generally dendritic polymers can be divided into two main categories: Dendrimers with perfectly branched structure and hyperbranched polymers with randomly branched structure.[2] (as shown in Scheme1-3)

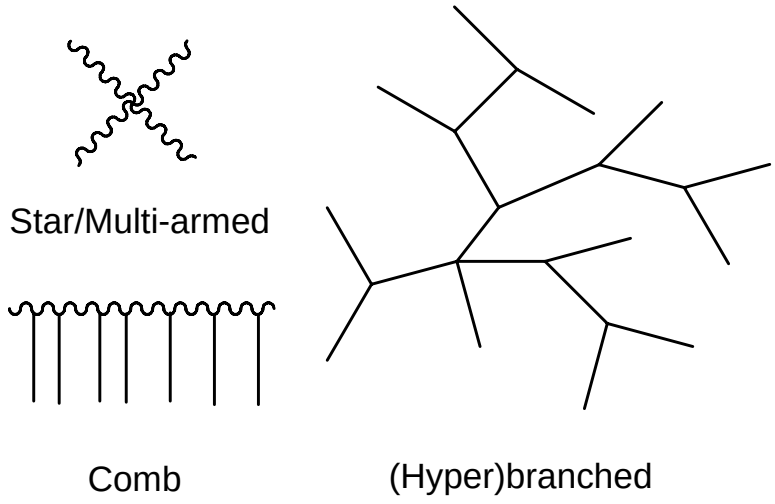

Scheme 1-2. Topology of branched polymers

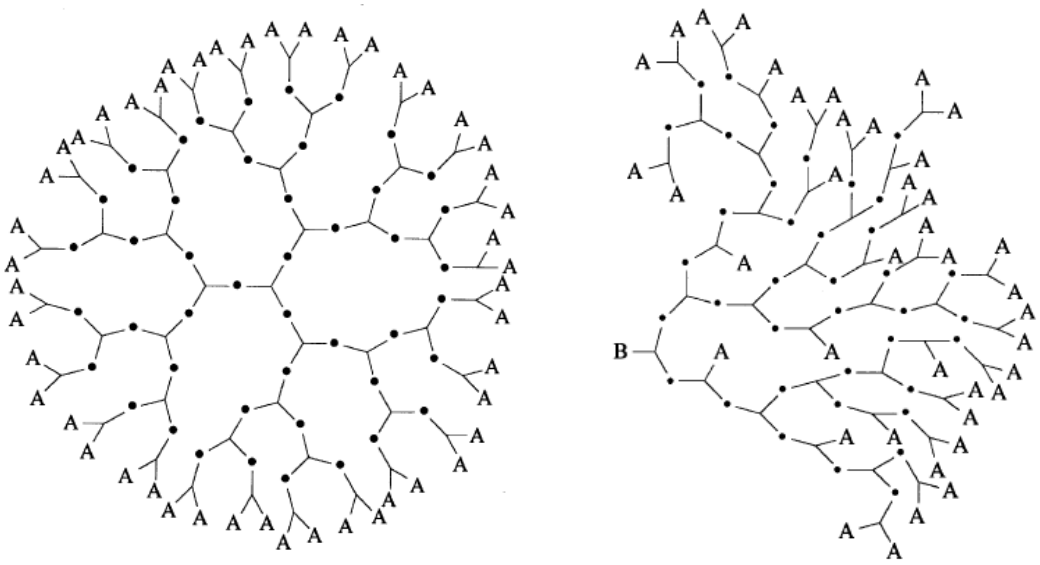

Scheme 1-3. Schematic comparison between a perfect dendrimer and a hyperbranched polymer with a core B, A in the periphery

There are commonly three major parameters used to describe those branched polymers.[2, 4] Apart from molecular weight, polydispersity and functionality, there is a very special and important parameter, the so called “degree of branching (DB)”,

which can be used to tell the difference between dendrimer and hyperbranched polymers. The DB can be calculated using the following Equation 1-1.[5]

$$DB_{Frey} = \frac{2D}{2D + L} \qquad (1\text{-}1)$$

Here D is dendritic unit, while L is linear unit. (as shown in scheme 1-4.)

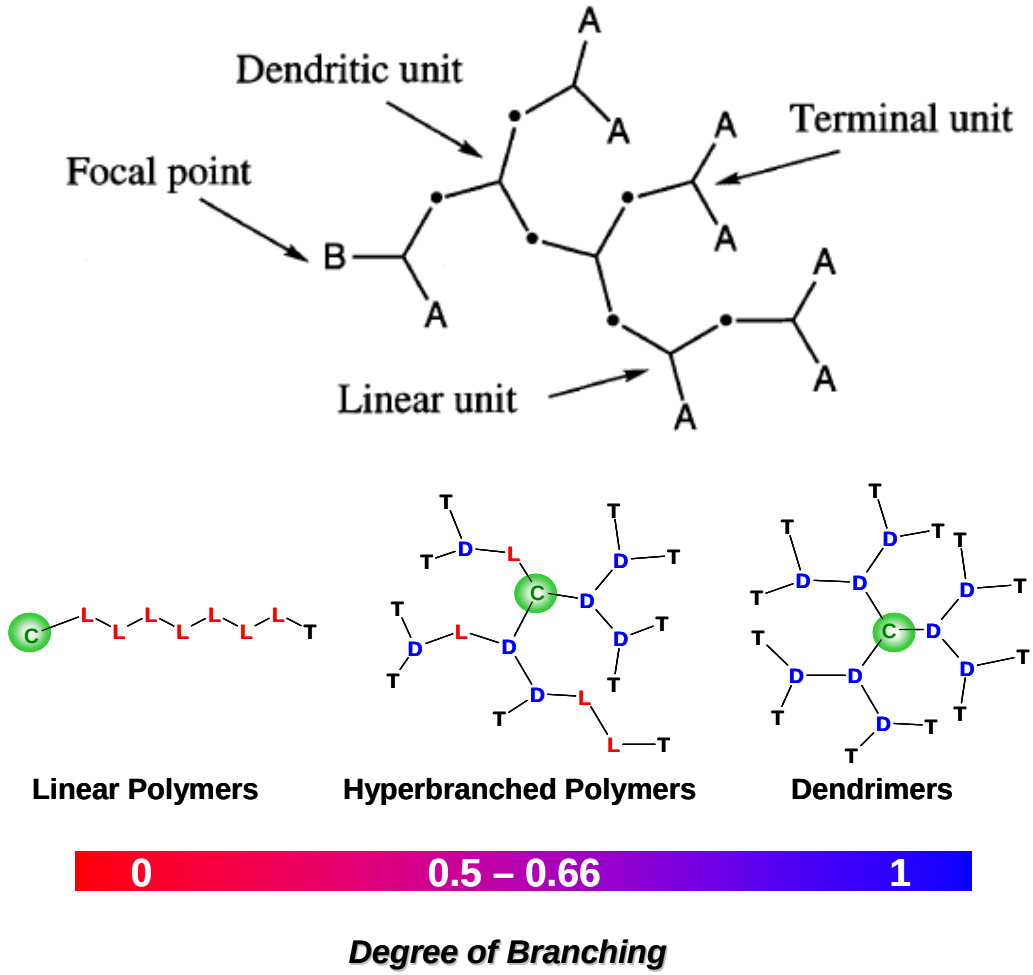

Scheme 1-4. Comparison of polymeric architectures as a function of the degree of branching DB (D, L, T: dendritic, linear and terminal units, respectively. The scheme is reproduced from Prof. Dr. H. Frey's homepage)

Dendrimers do not possess linear units, in this perfect case the degree of branching is calculated as 1, while on the other hand linear polymers do not possess dendritic units, the degree of branching can be calculated according to Equation 1-1 as 0. Accordingly, hyperbranched polymers should then exhibit an intermediate DB

between 0 and 1. For hyperbranched polymers studied in this thesis, a DB at around 0.5-0.66 was determined by NMR-spectroscopy.

Over the past twenty years, dendrimers with perfect structure have received immense interest from academic as well as industrial researchers.[6-8] However, commercial applications of these perfectly branched materials are scarce, since the tedious multi-step syntheses result in inacceptable costs for most applications.

The synthesis of hyperbranched polymers can often be simplified compared to that of dendrimers, as it does not require the use of protection/deprotection steps. This is due to the fact that hyperbranched polymers always contain a fraction of linearly incorporated A_nB monomers. [2] The most common synthesis route follows a one-pot procedure, where A_nB monomers are condensed in the presence of a catalyst (as shown in Scheme 1-5) Hyperbranched materials can be produced with an A_f core and A_nB monomers as well.

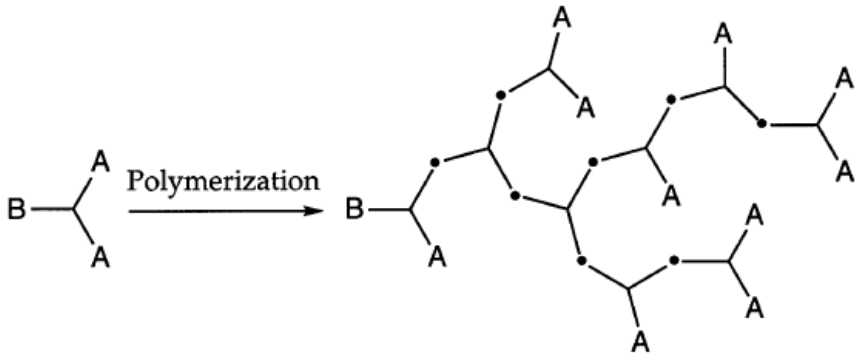

Scheme 1-5. General strategy for the synthesis of hyperbranched polymers with A_2B monomer

Although the properties of hyperbranched polymers are intermediate between those of dendrimers and linear polymers, the low cost for the synthesis of hyperbranched polymers permits to produce them on a large scale, giving them an advantage over dendrimers in applications. Hyperbranched polymers are thus considered as an alternative to dendrimers for different applications both in academia and in industry.[2, 4]

1.2. Properties and applications of hyperbranched polymers

The dendritic architecture with random branch-on-branch topology and compact molecular structures leads to unique physical and chemical properties. [4]

Due to the large number of end groups, one at every end of a branch, they are highly functional and have improved accessibility of functional groups. It can be used for catalysis support applications. We will have one chapter in the thesis discussing the application for catalysis purpose.

The high degree of branching enables them to be amorphous since branching prevents or impedes crystallization. Normally, these materials are soluble in numerous organic solvents. They normally have improved solubility compared to linear analogs. Furthermore, hyperbranched polymers are characterized by the absence of entanglements, at high molecular weight they were found to be globular, contrarily to the linear polymers they behaved more like molecular micelles, which results in low melt and solution viscosities,[2] this will bring great benefit to the processing.

Increasing academic and industrial interest has been sparked by the potential for developing advanced nanomaterials, biomaterials and biological, rheology modifiers, structural hydrogels, functional crosslinkers, dental components and catalytic support based on the low viscosity and high functionality of hyperbranched polymers. Also novel structure property correlations might arise from the studies.[2, 3]

1.3. Hyperbranched Polyglycerol (PG)

Current efforts are devoted to hyperbranched polymers. However, to approach dendrimer features, one has to overcome the usually obtained broad, statistical molecular-weight distributions. This necessitates the development of new polymerization methodologies.

In this regard, our group recently developed an efficient method in Freiburg to generate well-defined hyperbranched polyglycerol (PG), based on the ring-opening polymerization of glycidol under slow monomer addition technique.[9] This process is currently carried out on a kilogramm scale. The obtained polymers possess relatively narrow molecular weight distribution (M_w/M_n is around 1.5, determined by size

exclusion chromatography vs. poly(propylene oxide) standards, compared this PDI with the normal range 3-5), and molecular weight can range from 1000 to 25000 g/mol.

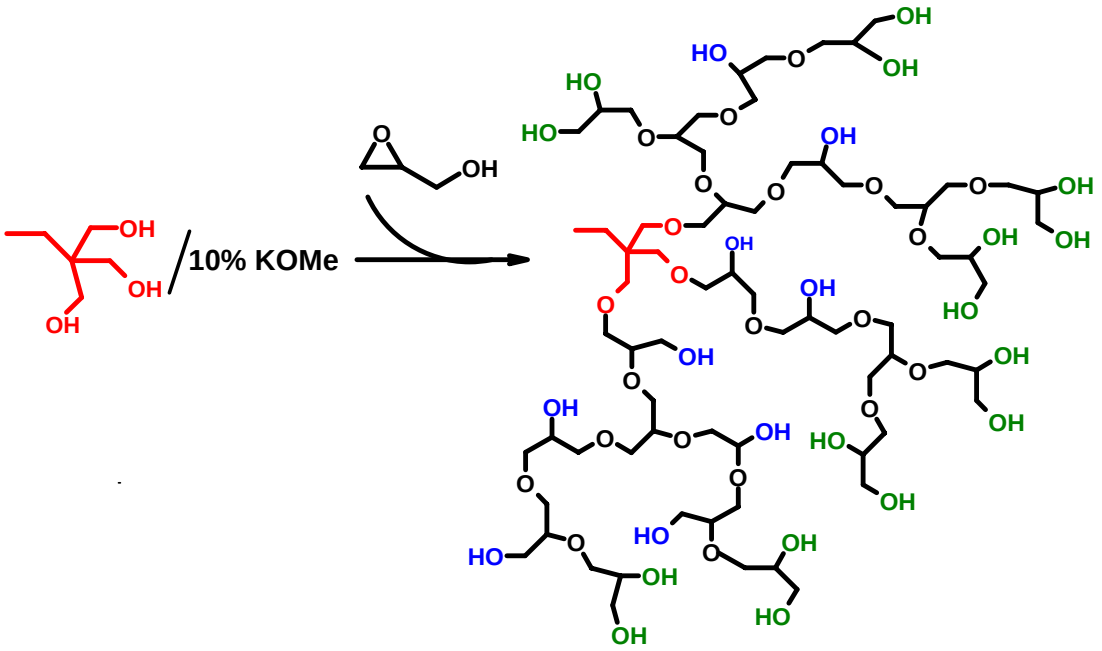

Scheme 1-6. Synthetic route and structure of hyperbranched polyglycerol

The obtained hyperbranched PG is a clear, viscous liquid. The glass transition temperature is considerably below room temperature, typically around -25 ^{o}C. At room temperature it is highly viscous, the viscosity increasing with molecular weight. By simple heating to elevated temperatures (80 ^{o}C) PG becomes a free-flowing liquid. Hyperbranched polyglycerol is highly soluble in water and also polar organic solvents, such as methanol. By comparison to linear, the solution-viscosity of non-branched polymers is considerably lower. Polyglycerols are essentially non-volatile at room temperature.[4]

Biocompatibility is one particularly advantageous feature of PG.[10] It can be used as a delivery agent for biologically active compounds, cosmetics etc. In containing hydroxy-end groups and a polyether-backbone, the hyperbranched polyglycerols resemble the well-known linear polyethylene glycols (PEG, PEO) which are approved for a large variety of medical and biomedical applications.[11]

The main difference probably lies in the inability of PG to crystallize.

Hyperbranched PG possesses an inert polyether scaffold. Each branch terminates in a hydroxyl-function, which renders hyperbranched PG a highly functional material, e.g., a molecule with a molecular weight of 2000 g/mol possesses 28 hydroxyl end groups. This high functionality in combination with the versatile and well-investigated reactivity of hydroxyl-functions is the basis for a broad variety of derivatives.

Partial esterification with fatty acids yields amphiphilic materials, which behave as nanocapsules. Such nanocapsules can, for example, incorporate polar molecules as guests and solubilize them in an apolar environment. [12] Selective modification can be achieved utilizing the reactivity of 1,2-diol units, located preferentially at the periphery of the molecule. [4, 11] Complementary to functionalization by reactions of the large number of hydroxy-groups, a single functionality can also be introduced selectively as the 'core' of the molecule. A number of single core functionalities, such as a vinylic group, amines and thiols, have been incorporated.[4, 11, 13, 14]

Apart from these modifications, PG is also employed as core molecules to build different star-branched block copolymers. This part of the work will be summarized in Chapter 2.

1.4. Hyperbranched Polyethylenimine (HPEI)

In continuation of our aim to design and construct new supramolecular systems based on hyperbranched polymers, hyperbranched polyethylenimine (HPEI) was also used for the research discussed in this thesis.

HPEI is another important and commercial available widely used hyperbranched polymer. Dendritic HPEI is a highly functional aliphatic polyamine with a globular structure. It can be obtained via catonic ring-opening polymerization of Aziridine (ethylene imine). The procedure and structure is illustrated in Scheme 1-7. HPEIs with molecular weights of up to 25000 g/mol are produced on a ton scale with relatively narrow molecular weight distributions and high degrees of branching between 65-75%. [15]

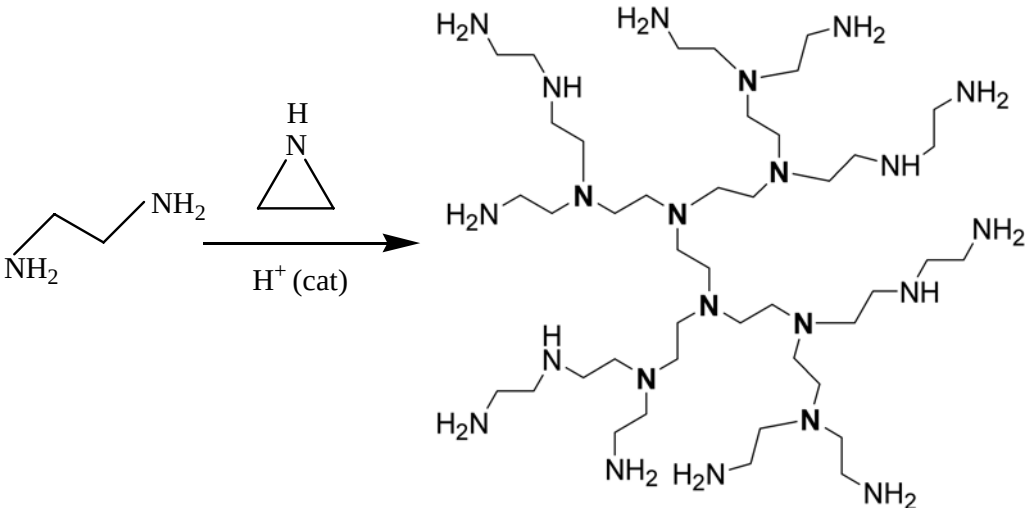

Scheme 1-7. Synthetic route and idealized structure of hyperbranched polyethylenimine

HPEI is a transparent viscous liquid with low intrinsic viscosity in solution. Polyethylenimines possess good thermal stability compared to other polyelectrolytes, as evidenced by endothermic degradation in a nitrogen environment. Substantial decomposition in air does not occur below 300 ^{o}C, as can be seen by thermo-gravimetric analysis.[16]

Previous studies indicated that branching sites are separated largely by secondary amine groups, with one branch occurring for every 3-3.5 nitrogen atoms along a linear segment.[15]

This branching distribution yields presumably spheroid-shaped molecules which may possess many charged nitrogens. The charge density will vary according to the position of equilibrium with various proton sources. Alternatively, permanent charges can be affixed to the spheroidal molecule by quaternization with appropriate alkylating agents.[16]

Thus, PEI can function as a cationic polyelectrolyte and is strongly attracted to anionically charged organic and inorganic materials, colloids and surfaces. Furthermore, the multiplicity of amine functions provides ideal ligand sites for complexation with various heavy-metal ions. We will utilize this property in this thesis, using modified HPEI as ligand for the ATRP.

Essentially, all modifications at HPEI involve replacement of the hydrogen atoms on the nitrogens. Among them the most common route is alkylation. This allows modification of solubility, introduction of functional groups or control of charge density, etc.

There is one report[17] on a general method for converting hyperbranched PEI into a fully branched dendritic polymer by applying one dendrimer sequence to prepare close analogues of the PPI and the PAMAM dendrimers. This simple process allows the generation of high-molecular-weight dendritic polymers in only two synthetic steps, (as shown in Scheme 1-8) while the corresponding effect structures have to be prepared by a multi-step process.

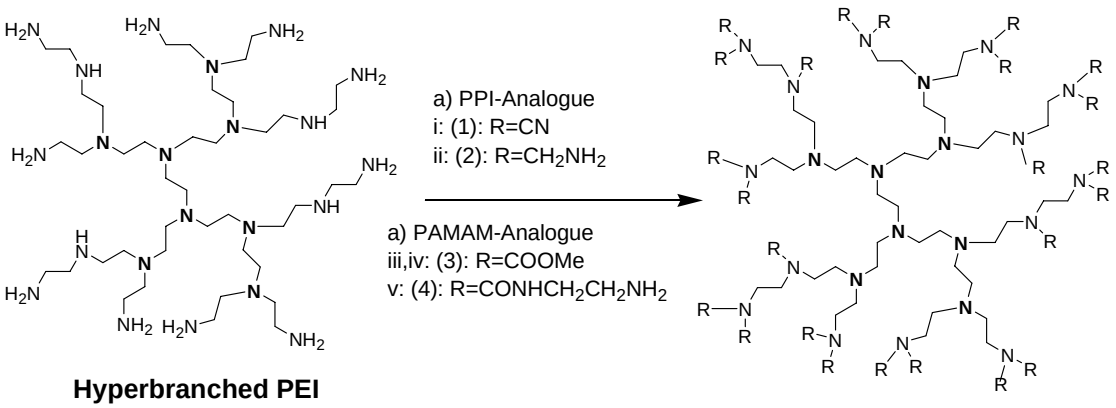

Scheme 1-8. Schematic image of modification of HPEI

After modification, core-shell type architectures from hyperbranched PEI are expected. After attaching pH-sensitive shells via acetal or imine bonds the obtained pH-responsive nanocarriers showed extremely high transport capacities and necessary release profile for tumor tissue: fast release at pH 6 and no release at pH 7.4.[18, 19]

Modified and unmodified polyethylenimine is also used as DNA transfection agent, since complexes of DNA and HPEI are known to pass through cell walls, and studies have reported that HPEI's efficiency as a gene delivery vehicle depends on its molecular mass.

In industry, PEI can be used for detergents, adhesives, water treatment, printing inks, dyes, cosmetics, and paper modification, as adhesion promoter, lamination

primer, fixative agent, flocculant, cationic dispersant, stability enhancer, surface activator, chelating agent, scavenger for aldehydes and oxides.[16]

In this thesis we will focus on using HPEI for modern catalyst separation techniques.

1.5. Structure of the thesis

The desire to discover new properties of hyperbranched architectures motivates many research groups at present. In this thesis, we will use hyperbranched polyglycerol (PG) and hyperbranched polyethylenimine (HPEI), as core molecules for building multi-arm star polymers using the atom transfer radical polymerization (ATRP) method (Chapter 2, 4). It will be demonstrated that the obtained star polymers of poly acrylic acid (PAA) possess unusual solution properties and can be used for stabilizing silver nanoparticles and nanoclusters (Chapter 3). Furthermore, the materials will be employed for biomineralization of $CaCO_3$ (Appendix); for liquid-liquid (water and oil) guest molecule transfer both for dye molecules and nanoparticles (Chapter 6, 7) as well as for catalysis in ATRP (Chapter 5).

1.6. References

[1] Odian, G., *Principle of Polymerization*. 4th Ed.; Wiley: 2004.
[2] Hult, A.; Johansson, M.; Malmström, E. *Adv. Polym. Sci.* **1999,** 143, 1.
[3] Gao, C.; Yan, D. *Prog. Polym. Sci.* **2004,** 29, 183.
[4] Frey, H.; Barriau, E.; Chen, Y.; Stiriba, S. *Acc. Chem. Res.* **2006**, In press.
[5] Holter, H.; Burgath, A.; Frey, H. *Acta Polym.* **1997,** 48, 30.
[6] Newkome, G. R.; Moorefield, C. N.; Vötle, F., *Dendrimers and Dendrons: Concepts, Syntheses, Applications,*. Wiley-VCH: 2001.
[7] Fréchet, J. M. J.; Tomalia, D. A., *Dendrimers and other Dendritic Polymers,*. John Wiley & Sons: 2001.
[8] Malik, N.; Wiwattanapatapee, R.; Klopsch, R.; Lorenz, K.; Frey, H.; Weener, J. W.; Meijer, E. W.; Paulus, W.; Duncan, R. *J. Controlled Release* **2000,** 65, 133.
[9] Sunder, A.; Hanselmann, R.; Frey, H.; Mülhaupt, R. *Macromolecules* **1999,** 32, 4240.
[10] Kainthan, R. K.; Janzen, J.; Levin, E.; Devine, D. V.; Brooks, D. E. *Biomacromolecules* **2006,** 7, 703.
[11] Frey, H.; Haag, R.; Mecking, S., http://www.hyperpolymers.com/.

[12] Sunder, A.; Krämer, M.; Hanselmann, R.; Mülhaupt, R.; Frey, H. *Angew. Chem. Int. Ed.* **1999,** 38, 3552.
[13] Sunder, A.; Turk, H.; Haag, R.; Frey, H. *Macromolecules* **2000,** 33, 7682.
[14] Sunder, A.; Mülhaupt, R.; Haag, R.; Frey, H. *Adv. Mater.* **2000,** 12, 235.
[15] Ivin, K. J.; Saegusa, T., *Ring-Opening Polymerization*. Elsevier: 1984; Vol. 2.
[16] Herman, M. F., *Encyclopedia of Polymer Science and Technology*, 3rd Ed.; 2004.
[17] Kreamer, M.; Stumb, J.; Grimm, G.; Kaufmann, B.; Kreager, U.; Weber, M.; Haag, R. *ChemBioChem* **2004,** 5, 1081.
[18] Haag, R. *Angew. Chem. Int. Ed.* **2004,** 43, 278.
[19] Garcia-Bernabe, A.; Krämer, M.; Olah, B.; Haag, R. *Chem. Eur. J.* **2004,** 10, 2822.

Chapter 2. Synthesis of Multi-Arm Star Polyglycerol-*b*-Poly-(*tert*-butyl acrylate) and Polyglycerol-*b*-Poly(acrylic acid) using Atom-Transfer Radical Polymerization (ATRP)

2.1. Introduction

2.1.1. ATRP

In recent years, several procedures for the controlled or "living" radical polymerization have been developed and used to prepare various well-defined polymers as well as materials with complex polymer architectures.[1-4]

Living radical polymerization methods include atom-transfer radical polymerization (ATRP)[1, 5, 6] and stable free-radical polymerization (SFRP),[7, 8] which proceed with reversible termination, and reversible addition-fragmentation transfer (RAFT)[9, 10], which proceeds with reversible chain transfer. The extensive exploration of these living polymerizations started in the mid-1990s, driven by the belief that well-defined materials from living radical polymerization would offer substantial advantages to generate nanostructures for microelectronics, biotechnology, and other areas.[4, 10] Among these methods, ATRP is very useful and has attracted broad attention.

ATRP proceeds via reversible activation of carbon-halogen terminal groups by the transition metal complex, where the metal center (such as copper) undergoes redox reactions[5, 6] (an electron transfer with simultaneous halogen atom abstraction) via interaction with the halogens at the polymer terminal, as shown in Eqs. 2-1 through 2-3:

$$R\text{-}Br + CuBr(L) \underset{k_d}{\overset{k_a}{\rightleftharpoons}} R\bullet + CuBr_2\,(L) \qquad (2\text{-}1)$$

$$R\bullet \xrightarrow{M} RM_n\bullet \qquad (2\text{-}2)$$

$$RM_n\bullet \xrightleftharpoons{CuBr_2(L)} RM_n\text{—}Br + CuBr\,(L) \qquad (2\text{-}3)$$

where R-Br is initiator, L is a ligand, k_a and k_d are rate constants for activation and deactivation of the initiator, R• is the reactive radical that initiates polymerization. Ligand is used to complex with the metal (here is Cu) salt and help to solubilize them in the organic reaction system. The generated $CuBr_2$ (L) is called the persistent radical or "deactivator", it can reduce the steady-state concentration of propagating radicals and minimizes normal termination of living polymers.

The free-radical nature of ATRP has been thoroughly studied through a large number of studies.[5, 6] The living nature arises from the reversible process of redox process, while for traditional metal assisted polymerization, the redox process is irreversible. However, the effects of inhibitors and retarders, solvents, chain transfer agents, regioselectivity, stereoselectivity, and copolymerization behaviors are the same in ATRP as in conventional radical polymerization.

From the equilibrium of Eq. 2-1, the concentration of propagating radicals in ATRP is obtained as

$$[R\bullet] = \frac{K[I][Cu^+]}{[Cu^{2+}]} \tag{2-4}$$

where K = k_a / k_d, I is the initiator, in this case RBr. The polymerization rate can be expressed as

$$R_p = \frac{k_p K[M][I][Cu^+]}{[Cu^{2+}]} \tag{2-5}$$

Thus the change in monomer concentration with time can be expressed as:

$$\ln\frac{[M]_0}{[M]} = \frac{k_p K[I][Cu^+]}{[Cu^{2+}]}t \tag{2-6}$$

The living nature of ATRP will result in a narrow molecular weight distribution. A fast and quantitative initiation can ensures all propagating species grow at the same time, the following rapid reversible deactivation of propagating radicals will help to maintain low radical concentrations and minimize normal termination of living polymers, which ensures all propagating chains grow at the same rate and for the same period of time and results in a narrow molecular weight distribution.

Based on these conditions, the number-average degree of polymerization can be calculated by

$$\overline{X}_n = \frac{[M]_0 - [M]}{[I]_0} = \frac{p[M]_0}{[I]_0} \tag{2-7}$$

where $[M]_0$ and [M] are initial concentrations of monomer and monomer concentration in the reaction, respectively. $[I]_0$ and p are the starting initiator concentration and fractional conversion of monomer in the reaction. The number-average degree of polymerization can be calculated as $[M]_0/[I]_0$ at 100% monomer conversion.

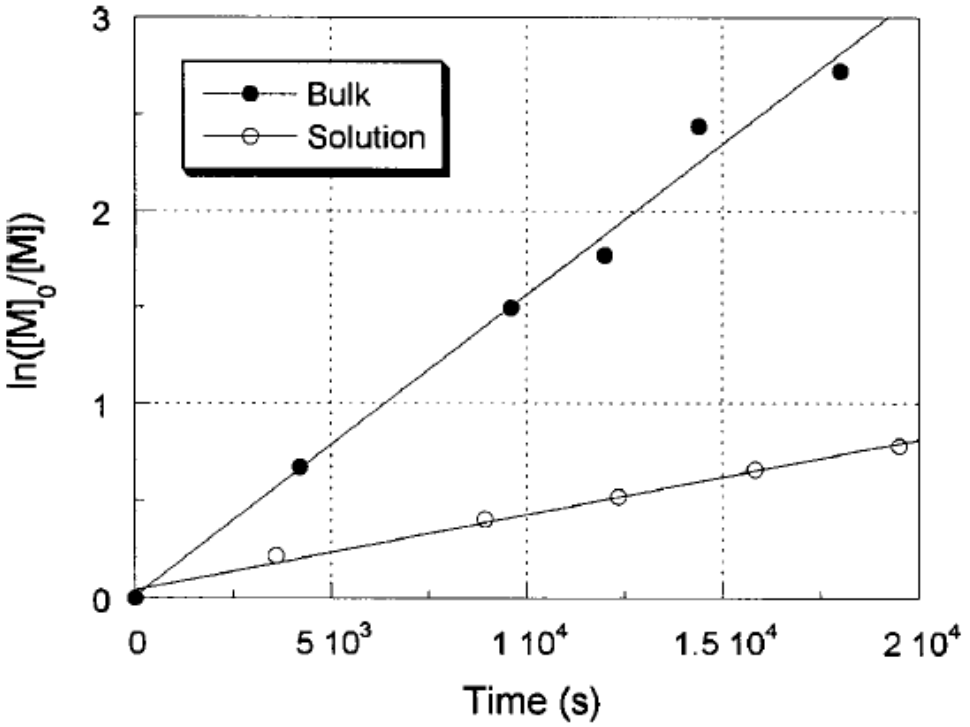

Figure 2-1. Plots of $\ln([M]_0/[M])$ versus time for ATRP polymerizations of styrene at 110°C with CuBr, 1-phenylethyl bromide (I), and 4,4-di-5-nonyl-2,2'-bipyridine (L). Bulk polymerization (●): [M] = 8.7 M, $[CuBr]_0 = [L]_0/2 = [I] = 0.087$ M; Solution polymerization in diphenyl ether (○): [M] = 4.3 M, $[CuBr]_0 = [L]_0/2 = [I] = 0.045$ M. According to Matyjaszewski et al. [11]

An example from Matyjaszewski et al[11] was given in Figure 2-1 and 2-2. This is the ATRP of styrene using 1-phenylethyl bromide as the initiator, with CuBr/4,4-di-5- nonyl-2,2'-bipyridine as catalyst/ligand. Figure 2-1 shows linear dependence of the decrease in monomer concentration with time, as can be expected from Eq. 2-6. This indicates the concentration of propagating radicals is constant throughout the polymerization. Figure 2-2 shows the molecular weight to be first-order in conversion, as required by Eq. 2-7. This behavior defines the living nature of ATRP in which fast initiation and growth with negligible occurrence of chain-breaking reactions until high conversion of monomer is reached.

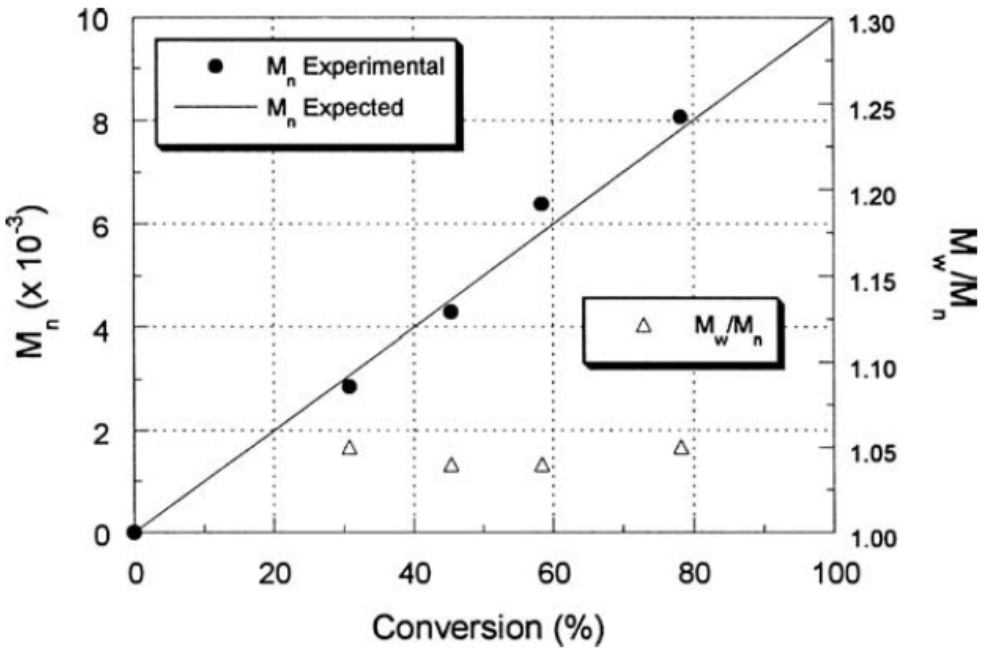

Figure 2-2. Dependence of number-average molecular weight (●) and polydispersity index (Δ) on monomer conversion for ATRP polymerization of bulk styrene at 110 °C with CuBr, 1-phenylethyl bromide (I), and 4,4'-di-5-nonyl-2,2'-bipyridine (L). [M] = 8.7 M, $[CuBr]_0 = [L]_0/2 = [I] = 0.087$ M. According to Matyjaszewski et al.[11]

The polymer should be monodisperse under living conditions. For the current case, the polydispersity index (PDI) is given by

$$PDI = 1 + \left\{\frac{[I]_0 k_p}{k_d [D]}\right\}\left\{\frac{2}{p} - 1\right\} \tag{2-8}$$

where D is the concentration of deactivator. It can be expected that the molecular weight distributions will become narrow with lowering of the initiator concentration, higher conversion, rapid deactivation (higher values of k_d and [D]), and lower k_p values. Given these conditions fulfilled, the molecular weight distribution will follow the Poisson distribution[12]

$$PDI = 1 + \frac{\overline{X_n}}{\left(\overline{X_n} + 1\right)^2} = 1 + \frac{1}{\overline{X_n}} \tag{2-9}$$

According to Equation 2-9, for a polymer of number average degree of polymerization of 50 having a Poisson distribution, the PDI would be 1.02. The PDI of the ATRP in Figure 2-2 is about 1.05, very close to the theoretical value. However, many ATRP polymerizations have broader distributions (PDI ≤ 1.2–1.3). This might be from the following two reasons. First, there is the very initial period (up to 5%

conversion) before the deactivator concentration has grown sufficiently large to suppress normal termination. This problem can be avoided by initially adding $CuBr_2$ (~5-10 mol% of CuBr). Second, the polymerization rate decreases significantly at very high conversion (~90%) and leads to the normal termination can not be sufficiently suppressed.

A variety of vinyl monomers, mostly conjugated ones, including styrene, acrylonitrile, (meth)acrylates, (meth)acrylamides, 1,3-dienes, and 4-vinylpyridine, undergo ATRP. Less conjugated monomers such as vinyl acetate, vinyl chloride are still difficult to polymerize via ATRP. As described above, ATRP involves a multi-component system of initiator, catalyst, deactivator either formed spontaneously or deliberately added, ligands, and solvent. Successful ATRP of a specific monomer requires matching the various components so that the dormant species concentration exceeds the propagating radical concentration by a factor of $\sim 10^6$.[5, 6]

Various organic halides are used as initiators, including alkyl halides, allyl and benzyl halides, α-haloesters, α-haloketones, α-halonitriles, and sulfonyl halides. Fast and quantitative initiation is necessary to achieve narrow PDI, however, an initiator that decomposes too rapidly will result in increased bimolecular termination of propagating radicals and broaden the PDI. Bromides are more reactive than chlorides, iodides are highly reactive, but undergo light-induced side reactions, and fluorides are unreactive. The initiator reactivity should be matched to the monomer reactivity, which is achieved by using a halide with an organic group similar in structure to the propagating radical, for example, benzyl halide and α-haloester for styrene and acrylate polymerizations, respectively. [5, 6]

The metal catalyst induces a reversible redox process during ATRP, it thus must have two oxidation states easily accessed by a one electron transfer, an affinity for halogen, and a strong complexation with the ligand. The catalyst is the key to ATRP, since it determines the position of equilibrium and rate of exchange between dormant and propagating species. Various middle and late transition metals (groups 6–11) have been investigated. Catalysts based on copper are the most studied and have found the greatest utility, as they are useful irrespective of the monomer.[6]

Proper functioning of a metal catalyst requires appropriate ligands. Ligands solubilize the transition metal salt in organic media and adjust the redox potential of the metal center for appropriate activity. For copper catalysts, bidentate and

multidentate nitrogen ligands work best. Bridged and cyclic ligands as well as branched aliphatic polyamines yield more active catalysts than do simple linear ligands. 4,4-Dialkyl-2,2'- bipyridines and tris-(2-dimethylaminoethyl)amine are examples of active ligands. Longer alkyl chains in 4,4-dialkyl-2,2'-bipyridine are useful for achieving solubility of the catalyst in the less polar monomers such as styrene. Phosphorus ligands such as triphenyl phosphine are useful for most other transition metals, but not for copper. The optimum ligand to Cu^+ ratio depends in a complex manner on the ligand and counterion. For complex anions such as triflate and hexafluorophosphate, two bidentate or one tetradentate ligands are needed per Cu^+. For bromide counterions, one bidentate ligand or one-half tetradentate ligand is needed per Cu^+. The optimal ratio may change with temperature and solvent. Polymerization rates are lower below the optimum ratio and constant above. The initial addition of metallic copper is advantageous for achieving a better control of polymerization since it will enable a fast polymerization and decrease the amount of normal termination. [5, 6]

ATRP can be carried out either in bulk, solution, suspension, or in aqueous emulsion. A variety of solvents have been used for solution polymerization, including toluene, ethyl acetate, alcohols, water, ethylene carbonate, DMF, and supercritical carbon dioxide. To select the proper solvent, one needs to consider if a solvent interacts with and affects the catalyst system, such as by displacement of ligands.

Temperatures for ATRP are generally in the range 30-120 ^oC. The polymerization rate increases with increased temperature since the equilibrium process is endothermic in the forward direction. The tendency toward a living polymerization is enhanced at higher temperature but chain transfer will also increase with increasing temperature. Normally, there is an optimum temperature for any specific ATRP reaction system.

The components of the system and reaction conditions need to be adjusted according to the monomer, so that radical concentrations are sufficiently low to effectively suppress normal termination. Acidic monomers such as acrylic acid can not be polymerized by ATRP since they interfere with the initiator by protonation of the ligands. The carboxylate salts of acidic monomers are polymerized without difficulty. New ATRP initiators and catalysts together with modification of reaction conditions may broaden the range of polymerizable monomers in the future. [5, 6]

ATRP can be used to prepare polymers with different topology, composition, functionality. [13](As illustrated in Scheme 2-1)

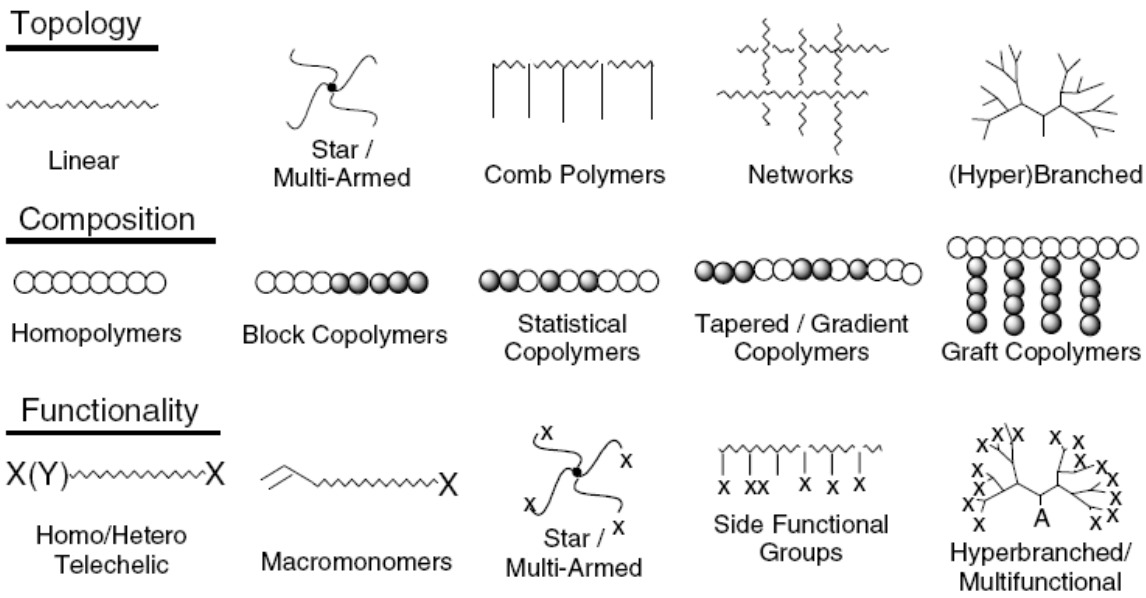

Scheme 2-1. Examples of structures prepared by controlled macromolecular synthesis

As we see from the above scheme, it is possible to synthesize many different types of copolymers with ATRP: statistical (random), gradient, block, and graft copolymers.

Block copolymers can be synthesized via ATRP either by the one-pot sequential or isolated macroinitiator methods. Both methods require that the polymerization of the first monomer should not be carried to 90% completion, since the extent of bimolecular termination increases as the monomer concentration decreases at 90% monomer conversion. This will result in the loss of polymer chains with halogen end groups and a corresponding loss of the ability to propagate. The final product would be a block copolymer contaminated with homopolymer A. Similarly, the isolated macroinitiator method requires isolation of A_nX prior to complete conversion (also less than 90%) so that there is a minimum loss of functional groups for initiation. Loss of functionality is also minimized by adjusting the choice and amount of the components of the reaction system (activator, deactivator, ligand, solvent) and other reaction conditions (concentration, temperature) to minimize normal termination.[4-6]

The one-pot sequential method has the disadvantage that the reactant is a mixture of the second monomer plus unreacted first monomer. The second block is actually a random copolymer. To avoid this ‘contamination’ of the second block, the isolated macroinitiator method is the method of choice

Tri- and higher block copolymers, such as ABA, ABC, ABCB, can be synthesized by a continuation of the processes with the successive additions of the appropriate monomers. A symmetric block copolymer such as ABA or CABAC can be made efficiently by using a difunctional initiator, such as α-dichloro-p-xylene or dimethyl 2,6-dibromoheptanedioate instead of the monofunctional initiator.[4-6]

The exact sequence of monomer addition is also critical for success in producing the desired block copolymer. For example, how can AB block copolymer be produced, by adding A first or B first? The answer depends on the reactivity of an A-X chain end toward monomer B compared to the reactivity of a B-X chain end toward monomer A. if The two monomers are in the same family, both addition sequence work, (e.g., methyl acrylate and butyl acrylate or methyl methacrylate and butyl methacrylate), because the equilibrium constants (for activation) for both types of chain ends have about the similar value. It will be quite different for pairs of monomers from different families. Chain ends from monomers with large equilibrium constants can initiate the polymerization of monomers with lower equilibrium constants; thus, cross-propagation is efficient. Methacrylate works well as the first monomer to form methacrylate-acrylate and methacrylate-styrene blocks. However, styrene or acrylate monomers are inefficient as the first monomer to form those block copolymers. The problem is that there is a slow activation of styrene or acrylate chain ends, cross-propagation is fast (because methacrylate is very reactive), and subsequent activation of methacrylate chain ends is fast, resulting in considerable conversion of the second monomer before all the styrene or acrylate chain ends are activated-all of which leads to increased polydispersity in methacrylate block lengths and molecular weight. If styrene or acrylate first is the desired sequence for some reason, for instance, as the prelude to some other block sequence, it may be possible to achieve it by employing a halogen exchange. One starts polymerization of the acrylate or styrene monomer with a bromo initiator and CuBr. Prior to the addition of methacrylate, CuCl is added to convert bromo-terminated chain ends to chloro-terminated chain ends. The equilibrium constant for the latter is lower, activation and cross-propagation are slowed sufficiently that complete activation and cross propagation are achieved before significant conversion of methacrylate occurs. Styrene-acrylate block copolymers can be synthesized with either monomer as the first monomer because the equilibrium constants for both chain ends are similar. [4-6]

Other polymer architectures are also possible: hyperbranched, comb, brush and star polymers, and functionalized polymers.

Hyperbranched polymers are produced via self-condensing vinyl polymerization (SCVP). This is to utilize inimers that contain both a polymerizable double bond and an initiating function, such as *p*-(chloromethyl) styrene. The product is highly branched with one double bond end group and many chloromethyl end groups. [4-6]

Comb or brush polymer can be produced using the polymeric initiator contains many halogens. A variety of polymers can be used as the polymeric initiator, including polymers containing vinyl chloride and 4-chloromethylstyrene units. A star polymer contains polymer chains as arms emanating from a branch point. Star polymers can be synthesized via ATRP by using an initiator containing three or more halogens.

The synthesis of complex polymer architectures by ATRP is useful, but relatively restricted, because the occurrence of bimolecular termination increases with the number of initiator sites on a polymeric species. However, on the other hand, this is an intriguing synthetic challenge.

2.1.2. Star polymer

Multi-arm star polymers have recently attracted considerable attention due to their unusual bulk and solution properties.[14] For example, stars with many arms represent good model polymers for polymeric micelles.[15, 16] Therefore to build star polymers for model study is of great importance.

There are two major strategies that have been employed for their preparation: (1) the *arm-first* approach:[17-20] quenching of mono-functional living polymers with a multifunctional coupling agent or linking reactions of living polymers with a small amount of bi-functional vinyl compounds.

There are several parameters that should be controlled carefully in order to maximize the yield of stars and prevent star–star coupling reactions. Some detailed studies have been carried out on the coupling of monofunctional polystyrenes and polyacrylates with divinylbenzene (DVB) and di(meth)acrylates (as shown in Scheme 2-2) to prepare star polymers and the following guidelines have been developed: [13, 18, 19]

— The ratio of difunctional reagent to growing chains seems to be optimal in the range of 10–20.

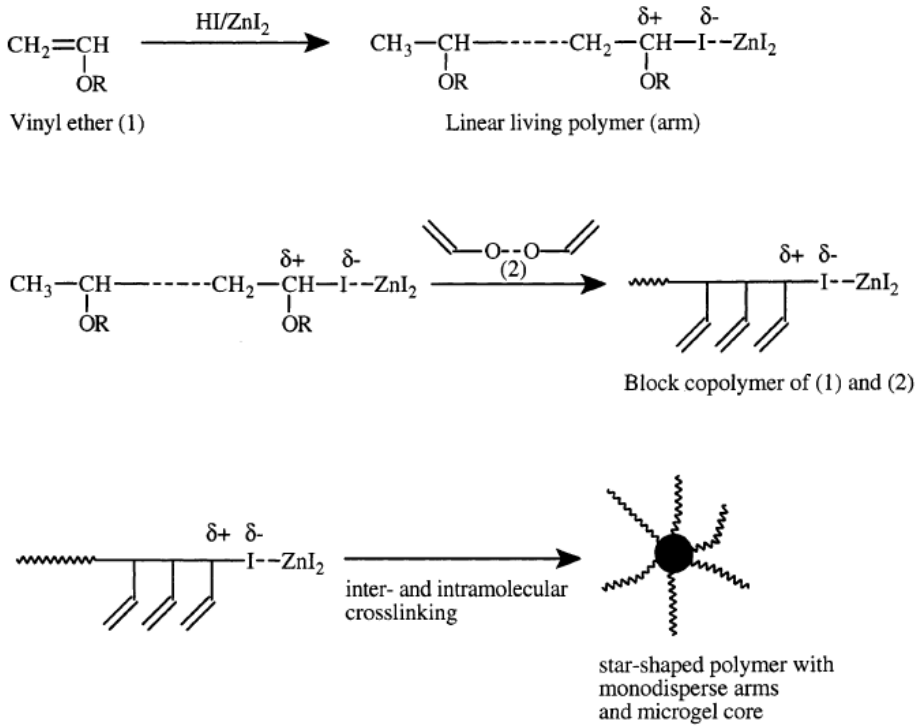

Scheme 2-2. Procedure of *arm-first* approach to synthesize star polymers

— Monomer conversion (or reaction time) has to be carefully controlled and stopped before star–star coupling occurs. It appears that ~5% of arms are still unreacted under typical conditions.

— Higher yields of stars are observed for polyacrylates than for polystyrenes. This may be attributed to a higher proportion of terminated chains (due to slower propagation and higher concentration of radicals) in styrene polymerization.

— The choice of the difunctional reagent is important and reactivity should be similar to, or lower than that of the arm-building monomers.[13]

The drawback of linking reactions of living polymers with a small amount of bifunctional vinyl compounds lies on that it will generate star polymers with a random distribution of arms per macromolecule

(2) the *core-first* approach: living polymerization on the basis of a multifunctional initiator-core using a core with a certain number of functional groups as a multiple initiator, for example, hexakis (chloromethyl) benzene was used as the initiator for styrene polymerization.[21] Subsequently, stars with 3, 4, 6 and 8 arms were prepared using various initiators based on inorganic cores,[22] and various organic structures including core-functional initiators based on natural products like sucrose[23] (8 arms，as shown in scheme 2-3), cyclodextrin (21arms)[24] as cores.

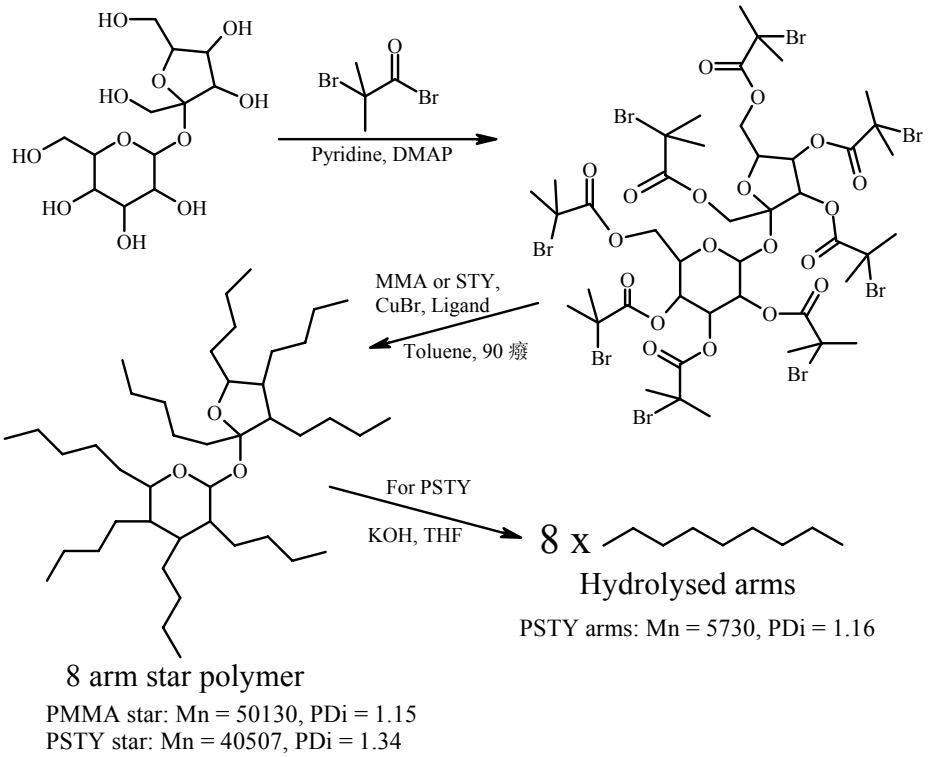

Scheme 2-3. *Core-first* synthesis approach with sucrose as core for star polymers

This polymerization with a multifunctional initiator leads to star polymers with predetermined numbers of arms.

Since well-defined star polymers cannot be prepared by means of conventional free radical polymerization, a large variety of star polymers have been synthesized by ionic polymerization procedures.[25-27] Unfortunately, these approaches are only applicable for a limited number of monomers and are very sensitive to impurities as well as functional groups. So, the "living" polymerizations mentioned above are of great usefulness, especially the ATRP, since it is of considerable efficiency for star polymer preparation.

2.1.3. Hyperbranched polymers as core for multi-arm star polymers

For the preparation of star polymers with a larger number of arms, dendrimers and hyperbranched polymers with compact and highly functional structures are attractive compounds as macroinitiators or coupling agent. For example, Xi et al reported the synthesis of star poly(*tert*-butyl acrylate) (P*t*BA) with dendritic poly(benzyl alcohol) as core, a well-defined star polymer with up to 24 arms could be obtained. (Scheme 2-4) .[28]

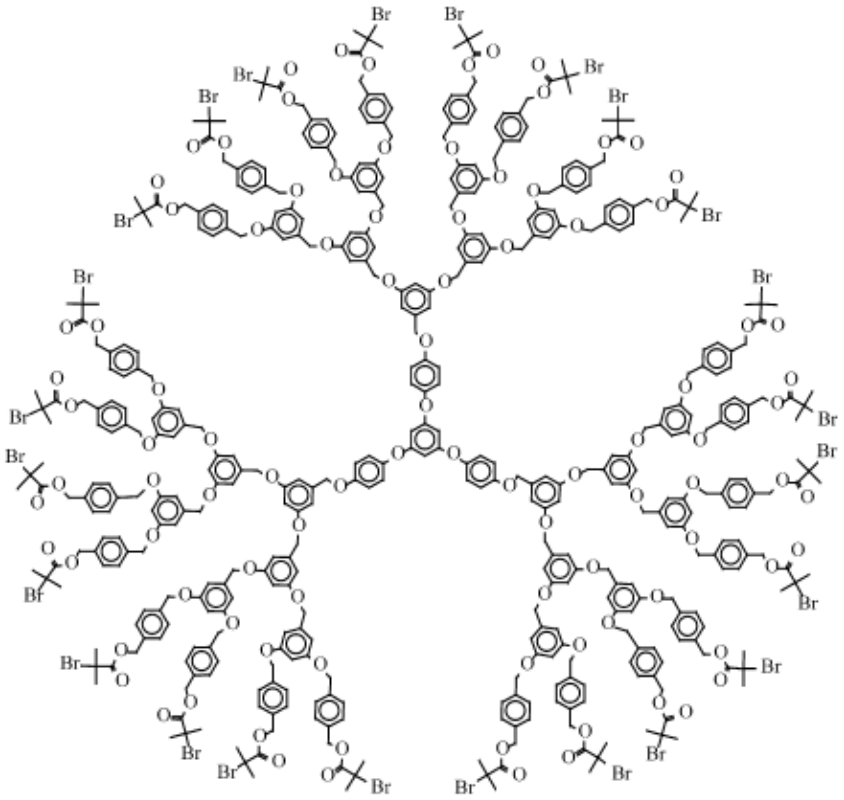

Scheme 2-4. Dendritic benzyl alcohol as multiple initiator with 24 arms

Unfortunately, the time-consuming synthesis and high cost of the structure-perfect dendrimers currently limit their practical use to laboratory scale. For that reason the imperfect and low cost hyperbranched polymers prepared from AB_m-type monomers in a one step process have gained increasing interest.[29, 30] Until now, many different kinds of hyperbranched polymers based on the AB_m-type monomers have been utilized as cores for the construction of multi-arm star polymers.

For example, hyperbranched polyoxetane polyol, hyperbranched polyester polyol derived from 2,2-bis(hydroxymethyl) propionic acid (bis-MPA), hyperbranched polymers obtained from SCVP of suitable inimers, hyperbranched polyphenylene polymers terminated with bromo functional groups and hyperbranched polyglycerol polyols can all be used as cores for multi-arm star polymers.[31]

Here is one example. Hyperbranched polyoxetane polyols with large number of hydroxyl end groups obtained from the cationic ring-opening polymerization of 3-ethyl-3-hydroxymethyloxetane (EHO) or 3-methyl-3-hydroxymethyloxetane (MHO) have been systematically studied by several groups.[32-38] The molecular weights of the obtained hyperbranched polyoxetane polyols were in the range of 1,000- 5,000 g/mol with polydispersities between 1.2-1.8, however, the degree branching (DB) of

the polymers can be controlled from 9-42% by adjusting the reaction conditions,[34-36] such as monomer-to-catalyst ratio, reaction temperature, etc.

Once nearly 100% of monomer conversion was achieved for the synthesis of hyperbranched PEHO by cationic ring-opening polymerization of EHO, the direct addition of an appropriate amount of EO to the reaction mixture could result in star block copolymers PEHO-*b*-PEO.[39] The average DP_n of the PEO arms was 10.6, however, the arm number is uncertain. The obtained star copolymer was mixed with β-cyclodextrin (β-CD) in saturated water, leading to a star polymer with channel-type polyrotaxane arms due to the formation of crystalline inclusion complexes originating from the noncovalent interactions between the linear PEG arms and the β-CDs.

Indeed, both cationic[40, 41] and anionic ring-opening multi-branching polymerization of glycidol [42-44] can lead to hyperbranched polyglycerol (PG) with a multitude of hydroxyl end groups. These polymers, however, process rather broad molecular weight distribution, usually in the range of 3-5. To prepare well-defined multi-arm stars, hyperbranched polymers must possess narrow polydispersity and predictable molecular weight.

Well-defined hyperbranched polyglycerol can be obtained by the anionic ring-opening multi-branching polymerization of glycidol with the core-dilution/slow addition technology.[43] The latent AB_2-monomer is dropwise added to a partially deprotonated 1,1,1-tris(hydroxymethyl)propane (TMP), representing a trifunctional core-initiator for the polymerization. Due to fast proton exchange during the polymerization the different chain ends (secondary and primary alcohols) are able to grow simultaneously into a branched structure as shown in Figure 1-1. The materials obtained are transparent pale yellow and viscous liquids. The molecular weight of PG can be controlled in the range of 1,000-30,000 g/mol, with the polydispersity in the range of 1.2-3. The polymers with masses between 1,200 and 6,300 g/mol exhibit a degree of branching (DB) between 0.53 and 0.59.[42] These hyperbranched polyglycerols are commercially available from the company Hyperpolymers.

In subsequent work, we have been able to demonstrate that the solubility and flexibility of the hyperbranched polyether polyols can be tailored by the attachment of different side chains, using procedures based on core-first strategies. A number of well-defined PG derived star branched polymers with different kinds of polymer arms can be thus prepared from our well-defined hyperbranched polyglycerols. (As listed in

Table 1)

Multi-arm star polymers via anionic polymerization of various epoxides have been achieved for PEO, PPO and allyl glycidyl ether.

Due to the high density of hydroxyl groups, polyglycerol is insoluble in most common organic solvents. The few exceptions besides water are typically lower alcohols and dipolar aprotic media, such as pyridine, DMF, DMSO, or NMP, that are rather limited in preparative use. In order to reduce the high polarity of the polyglycerol, propylene oxide (PPO) was directly polymerized via anionic polymerization onto the living polyglycerol chain ends without altering the total number of hydroxyl end groups (Figure 2).[45] The resulting multi-arm block copolymers with average number of arms in the range of 26-55 possessed up to five propylene oxide units per end group and showed narrow molecular weight distributions ($M_w/M_n < 1.7$). Furthermore, by variation of the block lengths between 1 and 5, the flexibility of the hyperbranched scaffold can be varied in such manner that the range of glass transitions was found to be between that of polyglycerol and linear PPO.

Table 2-1. Multi-Arm Star Polymers Based on Hyperbranched Polyglycerol Core

Monomer	Catalyst	$N_{(arm)}$ [d]	$DP_{n(arm)}$ [e]	M_w/M_n
Propylene oxide	alkoxide	26-55	1-5	< 1.7
Ethylene oxide	alkoxide	26-55	20-180	1.4- 2.2
Ethylene oxide	alkoxide	10-30	10-20	1.02-1.34
allyl glycidyl ether	alkoxide	52-76	1-3	< 1.5
ε-caprolactone	Sn $(Oct)_2$	52	10-50	1.16-1.33
Lactide	Sn $(Oct)_2$	28-68	2-20	1.2-1.9
Methyl acrylate	CuBr/PMDETA [a]	45-55	6-90	1.25-2.5
2-Hydroxyethyl methacrylate	CuCl/bipy [b]	56-90	2-94	1.1-1.8
Tert-butyl acrylate	CuBr/PMDETA	6-90	2-34	1.2-1.4
2-Dimethylaminoethyl methacrylate	CuBr/HMTETA [c]	36	2-40	1.4-1.7

[a] PMDETA: pentamethyldiethylenetriamine; [b] bipy: 2,2'-bipyridyl; [c] HMTETA: hexamethyltriethylenetetraamine; [d] $N_{(arm)}$: the number of arms; [e] $DP_{n(arm)}$: degree of polymerization per arm

The first synthesis of poly(ethylene oxide)-based multi-arm star polymers with M_n values in the range of 34,000-180,000 g/mol, arm numbers in the range of 26-55 and narrow polydispersity (M_w/M_n=1.4-2.2) has been accomplished via anionic polymerization on the basis of the PPO-terminated polyglycerols (Figure 2).[46] The novel multi-arm star architectures consist of polyether structures only and therefore possess interesting potential for biomedical applications, e.g., in hydrogels or amphiphilic networks. Because of the hydrophilic nature of the polyglycerol core, no aggregation in aqueous media or methanol was observed. This is a main advantage in comparison with the traditional DVB-core route, since the latter synthetic approach leads to a large fraction of apolar hydrocarbon material that makes the materials problematic for biomedical application. Furthermore, the PPO-capped polyglycerols, prepared in a one-pot, two-step synthesis, are easily accessible in multi-gram quantities. The use of the novel multi-arm stars for the preparation of structured hydrogels has also been addressed. Hence, the multi-arm stars based on EO were used for the preparation of structured hydrogels via partial functionalization with methacrylate end groups and radical copolymerization with linear telechelics in aqueous media.[47] The materials obtained show excellent form-stability, seen in the high compression moduli, and possess a large number of hydroxyl groups that can be further modified, e.g., with cell-growth factors.

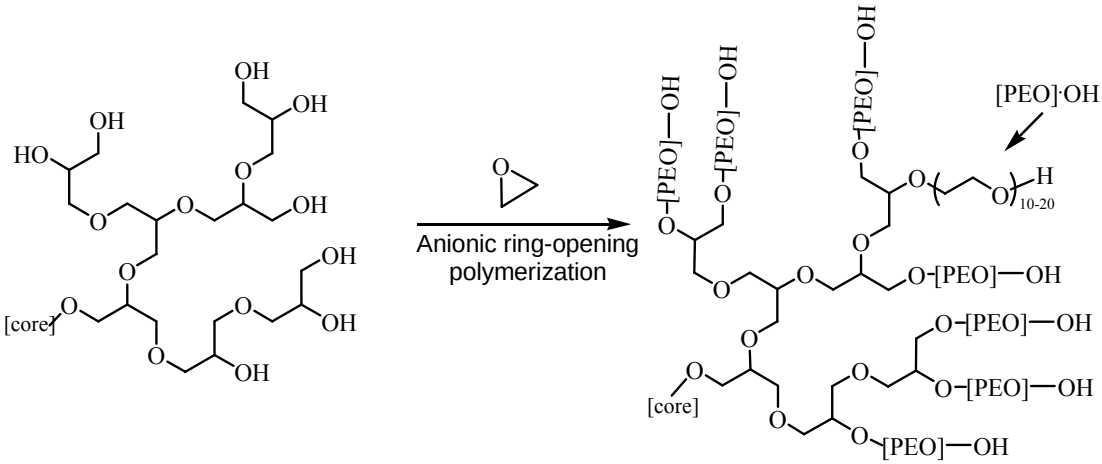

Scheme 2-5. Syntheses of multi-arm star PG-*b*-PEO, with polyether polyols (polyglycerol) as core

These star PG-PPO-PEO polymers possessed narrow polydispersity and high functionality, but they are not suitable for biomedical applications or as solid polymer electrolytes because of the presence of hydrophobic PPO. For these purposes, new

PG-PEO star polymers without PPO segment were also synthesized via anionic polymerization, PG was first deprotonated with CsOH or potassium naphthalide, EO was added subsequently and PG-star-PEO was obtained, (as shown in Scheme 2-5). The polymer was characterized with MALDI-TOF MS, confirming low polydispersity and structure of the multi-arm star PEO. For the first time it was confirmed in a detailed MALDI-TOF study that all hydroxyl groups of the multifunctional initiator had reacted, all arms possessing similar length.

Besides PO and EO, a functional epoxide monomer, allyl glycidyl ether (AGE), has also been directly polymerized onto the living polyglycerol or PPO-terminated polyglycerol chain ends, and well defined multi-arm star polymers were obtained.[48] Since the multi-arm star polymers contain a large number of vinyl groups, they have been tentatively utilized as toughening agent for a vinylester–urethane hybrid resin.[49]

Apart from anionic polymerization, we can also build multi-arm star polymers via ring-opening polymerization of cyclic ester directly. A well-known pathway to well-defined star PG copolymers is the ring-opening polymerization of ε-caprolactone catalyzed by $Sn(Oct)_2$. The polymerization of ε-caprolactone was carried out in bulk and proceeded smoothly, yielding star copolymer with approximately 52 arm biodegradable poly(ε-CL) arms ($DP_{n(arm)}$=10-50) and narrow polydispersity (M_w/M_n =1.16-1.33) (The pathway was shown in Figure 2).[50] Using a similar strategy, we can also polymerize lactone using PG as the core with $Sn(Oct)_2$ as catalyst. The obtained polymer can have either 28 or 68 arms, with each arm verified from 2 to 20 lactic acid unit. The polydispersity index is in the range of 1.2-1.9 (structure shown in Figure 9).

Apart from the above-described methods, we could also build multi-arm star polymers via controlled radical polymerization, namely ATRP.

The use of hyperbranched polyglycerol as a macroinitiator for ATRP relies on attaching a suitable initiator moiety to the hydroxyl end groups of PG.[51] Analogous approaches have been reported by Haddleton et al.,[52] using carbohydrates, as well as by Hedrick et al., [53-55] relying on hydroxyfunctional dendrimers to prepare star polymers, respectively. The dendritic macroinitiators were used in the presence of CuBr/pentamethyldiethylenetriamine (PMDETA) to initiate methyl acrylate (MA) polymerization, resulting in multi-arm block copolymers with polyether core and 45–55 PMA arms.[56] For this system, conversion represented a limiting factor, since gelation occurred when the reaction was continued to conversions exceeding 35%.[56]

2-Hydroxyethyl methacrylate (HEMA) is an important functional monomer that represents a major component in contact lenses, drug delivery, and biocompatible hydrogels used for a variety of applications. The ATRP of HEMA, initiated by a polyglycerol-based macroinitiator, was conducted in methanol at room temperature with CuCl/2,2'-bipyridyl catalyst system,[57] leading to a series of multi-arm star block copolymers with approximate 56, 66 and 90 PHEMA arms, respectively, and M_w/M_n in the range of 1.1-1.8. With the addition of some amount of $CuBr_2$, the polymerization conversion has been found to be driven to maximum values of 79%. Since both PHEMA and PG are biocompatible polymers, the obtained multi-arm copolymers with a large number of hydroxyl groups are promising with respect to biomedical application. Based on the well-defined multi-arm star block copolymers PG-*b*-PHEMA, inverted and aqueous micelle-type nanocapsules have been prepared by partially transforming the hydroxyl groups into apolar or highly polar groups and their respective capacities of guest encapsulation were studied. (This work, which has in part been carried out by the author of the thesis, will be shown in the appendix)

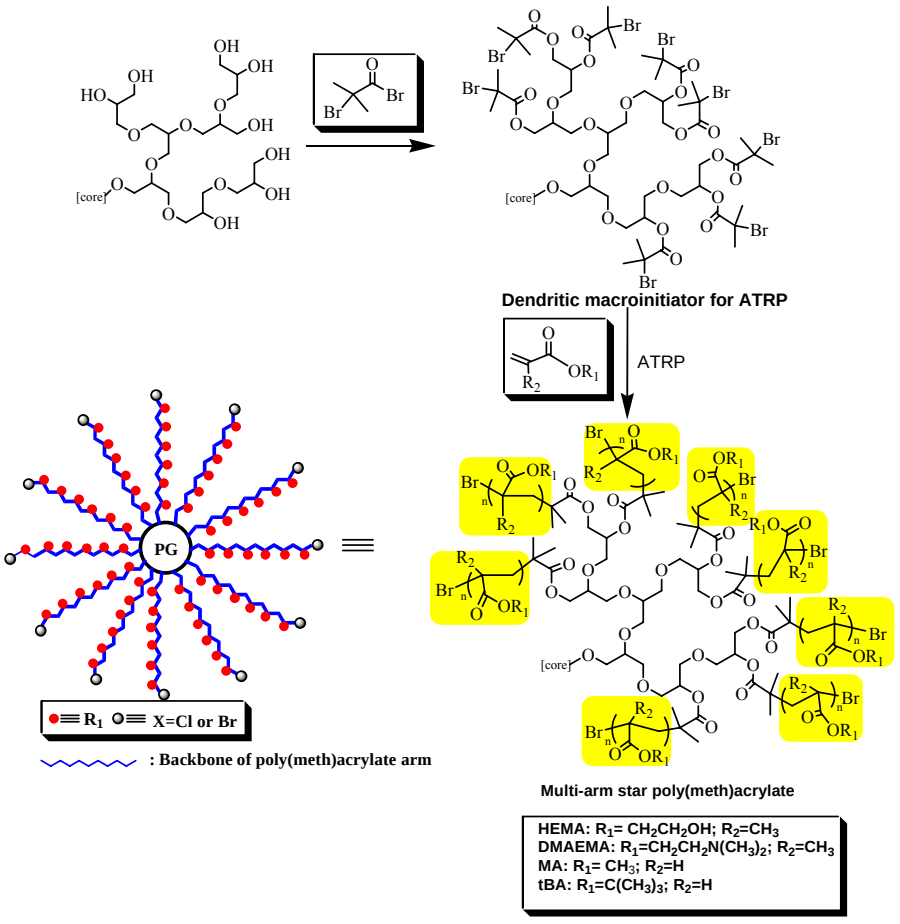

Scheme 2-6. Syntheses of multi-arm star poly(meth)acrylate based on Polyglycerol Polymer-core under ATRP conditions

Both *tert*-butyl acrylate (*t*BA) and 2-dimethylamino ethyl methacrylate (DMAEMA) are widely used functional monomers for the synthesis of polyelectrolytes. With the same methodology as HEMA and MA, well defined star-shaped multi-arm PG-*b*-P*t*BA and PG-*b*-PDMAEMA with 27-66 arms with M_w/M_n in the range of 1.2-1.4 and 1.4-1.7, respectively, have been obtained on the basis of hyperbranched polyglycerol as core macroinitiator for the ATRP of *t*BA and DMAEMA.

In chapter 2, we will discuss the respective work on PG-*b*-P*t*BA, while for PG-*b*-DMAEMA there is a detailed description in chapter 4 of this thesis.

Tert-butyl acrylate (*t*BA) is a widely used monomer for the preparation of poly(acrylic acid), since the *tert*-butyl ester groups can be easily transformed into carbonic acid groups by acidic hydrolysis. Matyjaszewski's group reported the synthesis of multi-arm star *t*BA based on an arm-first strategy, and the polydispersity of the obtained multi-arm star P*t*BA was reported to be 1.4,[58] however, the arm numbers per polymer remained uncertain. Heise et al[21] reported synthesis of well defined star P*t*BA polymers with 12 arms, using dendrimers as core-initiator. Very recently another group reported P*t*BA star polymers with up to 24 arms, synthesized by the ATRP method, again using a dendrimer as core-initiator.[28] However, the synthesis of well-defined multi-arm star polymers with arm number exceeding 30 by living radical polymerization still represents a challenge, since the probability of radical-radical coupling during the polymerization increases dramatically with increasing arm number. Moreover, to date no systematic study has addressed the relationship of arm numbers with the control of the ATRP polymerization.

In this chapter, we will describe the systematic study of the ATRP of *t*BA, initiated by a series of polyglycerol-based macroinitiators, leading to well-defined multi-arm star P(*t*BA)s. Furthermore, the limitations of the arm number in the context of the ATRP polymerization of *t*BA has been investigated and will be addressed. Hydrolysis of the P*t*BA star-polymers and the properties of the resulting multi-arm star PAA polyelectrolytes will also be discussed.[59] The multi-arm star PAA represents one kind of unusual polyelectrolytes.

2.2. Results and Discussion

2.2.1. Synthesis of multi-initiator

Hyperbranched polyglycerol samples PG_{17}, PG_{27}, PG_{36}, PG_{66}, PG_{90} and PG_{108} were prepared by anionic polymerization in the presence of trimethylolpropane as initiator- core, as previously described.[42] Subsequently, the esterification was carried out in pyridine, using 1.2 eq. of 2-bromo-isobutyryl bromide to ensure that all the hydroxyl groups reacted with bromide (as shown in Scheme 2-7). Since a stoichiometry of 1.2 was used, traces of low molecular weight initiator not attached to PG might exist. Thus, the initiators were additionally purified by dialysis in chloroform for 2 days using to completely remove low molecular weight impurities, using a benzoylated cellulose membrane (molecular weight cut-off 1000 g/mol).

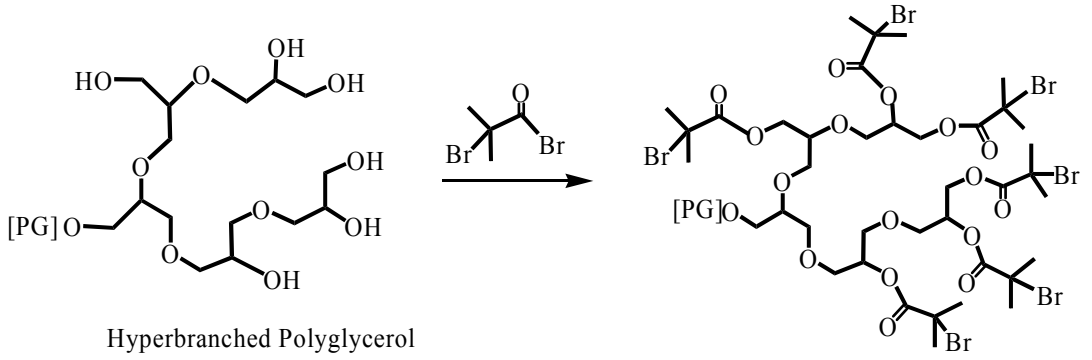

Scheme 2-7. Synthesis of PG-based ATRP macroinitiator

Six ATRP macroinitiator samples with average 17, 27, 36, 66, 90 and 108 initiating sites, respectively, have been prepared, namely **$P(G_{17}In_{17})$**, **$P(G_{27}In_{27})$,** **$P(G_{36}In_{36})$**, **$P(G_{66}In_{66})$**, **$P(G_{90}In_{90})$**, **$P(G_{108}In_{108})$**. Macroinitiator **In_6** with 6 arms was also prepared for comparison purpose. The reaction procedure is the same as that described for PG macroinitiators.

^{1}H NMR spectroscopy supports the formation of the macroinitiator, manifested by a low field shift of the PG scaffold hydrogen upon esterification.(Figure 2). The degree of esterification can be calculated from NMR for each case. The functionality always reached 100%.

The initiators were examined by both NMR and GPC. (Figure 2-3 and 2-4) Although GPC cannot afford the real molecular weight of dendritic initiators, it is convenient to evaluate the purity by determining the molecular weight distribution. The GPC traces are unimodal and the molecular weight distribution is similar with that from pure PG. No detectable signal was found for low molecular weight impurities, verifying the purity of the dendritic initiators.

Table 2-2. Polyglycerols and corresponding macroinitiators

PG	$\overline{M_n}$ [a] ($\times 10^{-3}$)	M_w/M_n [a]	Initiator	M_n [a] ($\times 10^{-3}$)	M_n [b] ($\times 10^{-3}$)	M_w/M_n [a]	Average arm numbers
			P(G_6In_6)	1.1		1.00	6
PG_{17}	1.2	1.51	**P($G_{17}In_{17}$)**	3.5	4.3	1.45	17
PG_{27}	2.0	1.54	**P($G_{27}In_{27}$)**	3.7	6.0	1.46	27
PG_{36}	2.6	1.44	**P($G_{36}In_{36}$)**	3.5	8.0	1.37	36
PG_{66}	4.8	1.51	**P($G_{66}In_{66}$)**	4.3	14.8	1.49	66
PG_{90}	6.6	1.55	**P($G_{90}In_{90}$)**	5.2	20.0	1.71	90
PG_{108}	8.0	1.64	**P($G_{108}In_{108}$)**	8.6	25.2	1.55	108

[a] M_n and M_w/M_n were obtained from GPC equipped with RI detector.

[b] M_n was calculated from NMR

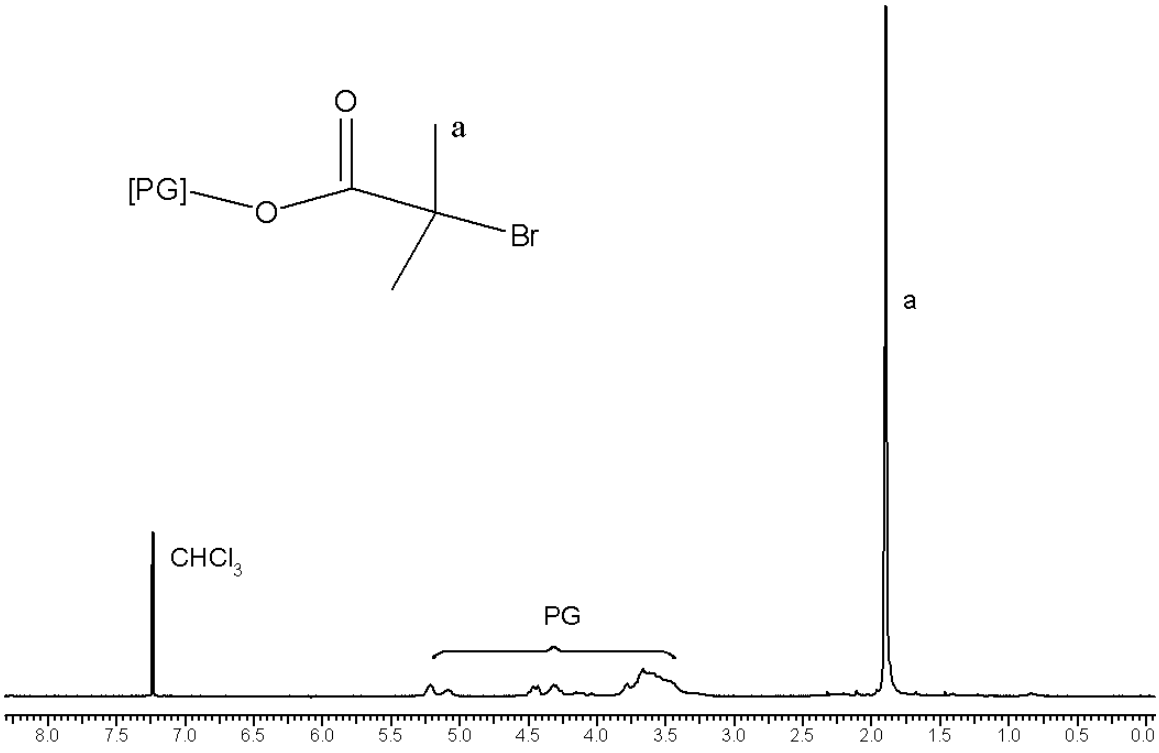

Figure 2-3. ^{1}NMR of the PG based macroinitiator with 36 arms

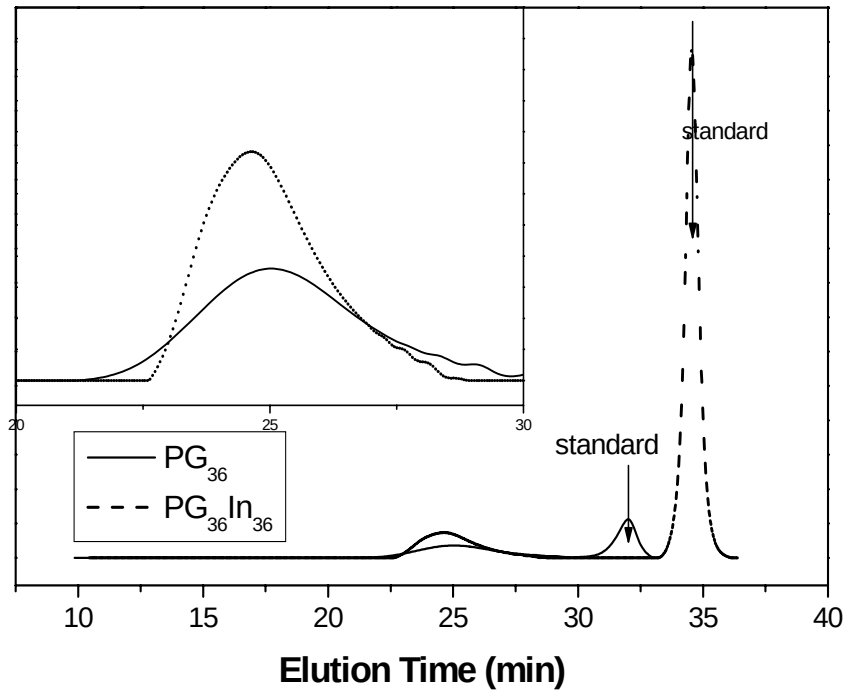

Figure 2-4. GPC traces of initiator with 36 arms P($G_{36}In_{36}$) and corresponding precursor

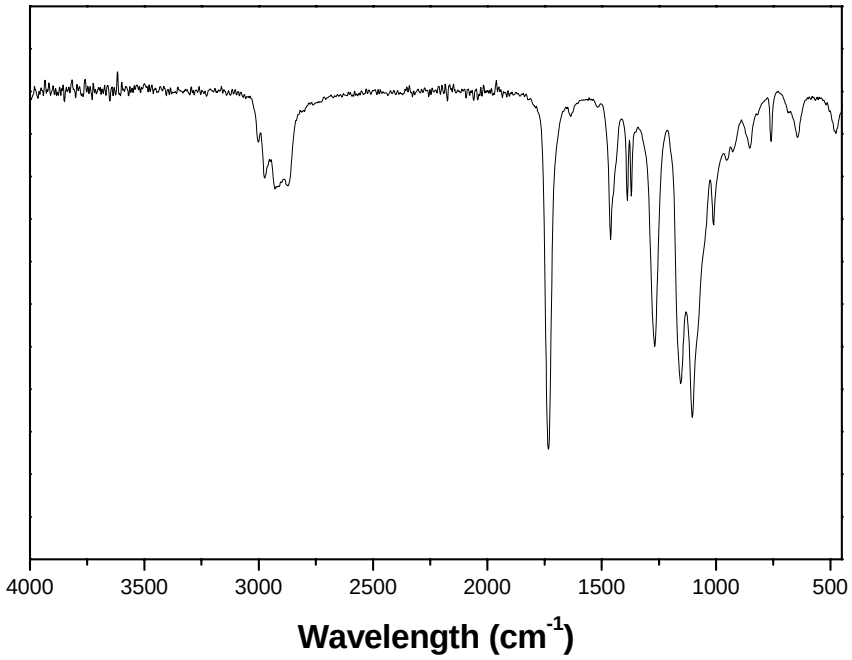

Figure 2-5. FTIR of initiator with 36 arms P($G_{36}In_{36}$)

2.2.2. Synthesis of well-defined multi-arm star P*t*BA.

2.2.2.1. Synthesis of well-defined multi-arm star P*t*BA with 36 arms.

Well-defined linear P*t*BA has been obtained via ATRP of *t*BA in acetone at 60 °C, using the CuBr/PMDTA catalytic system. The same procedure was also applied to prepare the star polymers. (Scheme 2-8)

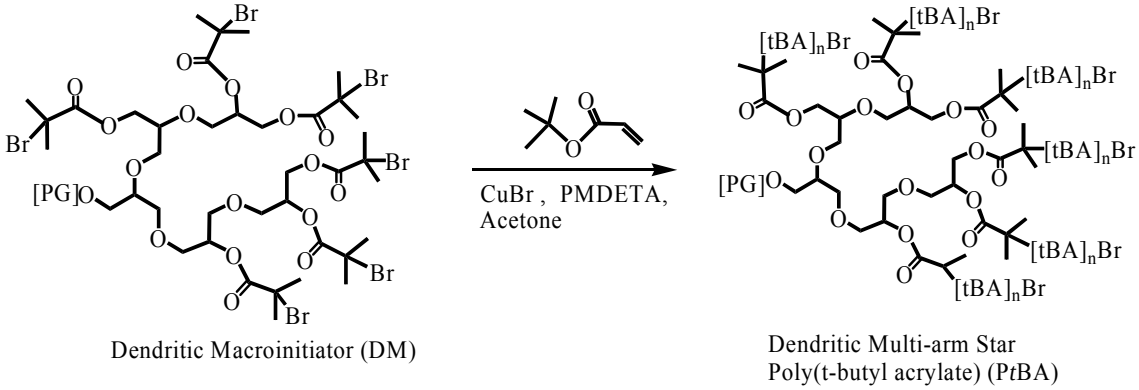

Scheme 2-8. Synthesis of multi-arm star PG-*b*-P*t*BA and PG-*b*-PAA

However, when the same reaction conditions with CuBr/initiating sites (1:1) were adopted for the synthesis of 36 arm star polymers, the obtained materials is difficult to pass through the 0.45um filter for GPC and show very broad polydispersity ($\overline{M}_w/\overline{M}_n$ = 13, Table 2-3, run no. 1). As shown in Figure 2-6, there is an obvious broad shoulder peak appear at high molecular weight, indicating that the star-star radical coupling side reaction dominated under these reaction.

Xi et al.[59] adopted a 1:1 ratio for: [In]:[CuBr] and obtained monodisperse star polymers with 24 arms at the [Acetone]:[tBA] ratio 1:4 using a dendrimer core. For our case, that might be due to the fact that the PG core is much smaller than their dendrimer core, as we can predict, the local chain end density (i.e. propagating radicals) is much more higher than their case. Also the branching PG-core also possesses certain distribution, this might also made star-star coupling easier to occur.

To suppress the side reaction, the concentration of reactant was lowered. The ratio [Acetone]:[*t*BA] = 1:1 and 2:1 were tried, however, the obtained polymer still showed broad polydispersity. This might due to the high local density of the initiation sites. Within the range of the initiator radius, all the initiation sites are chemically connected to one core. The radical concentration can not be reduced significantly by only lowering the reactant concentration.

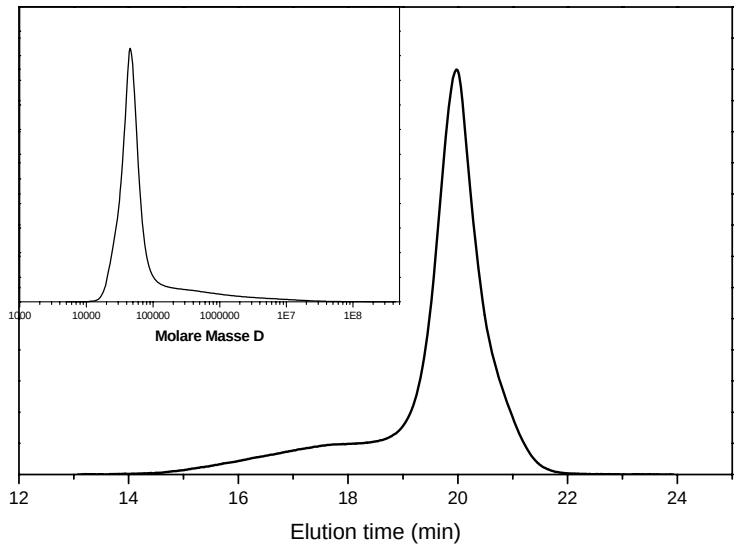

Figure 2-6. GPC traces of the crosslinked multi-arm star PG-*b*-P*t*BA using [*t*BA]:[$PG_{36}In_{36}$-Br]:[CuBr]:[PMDETA] = 50:1:1:1

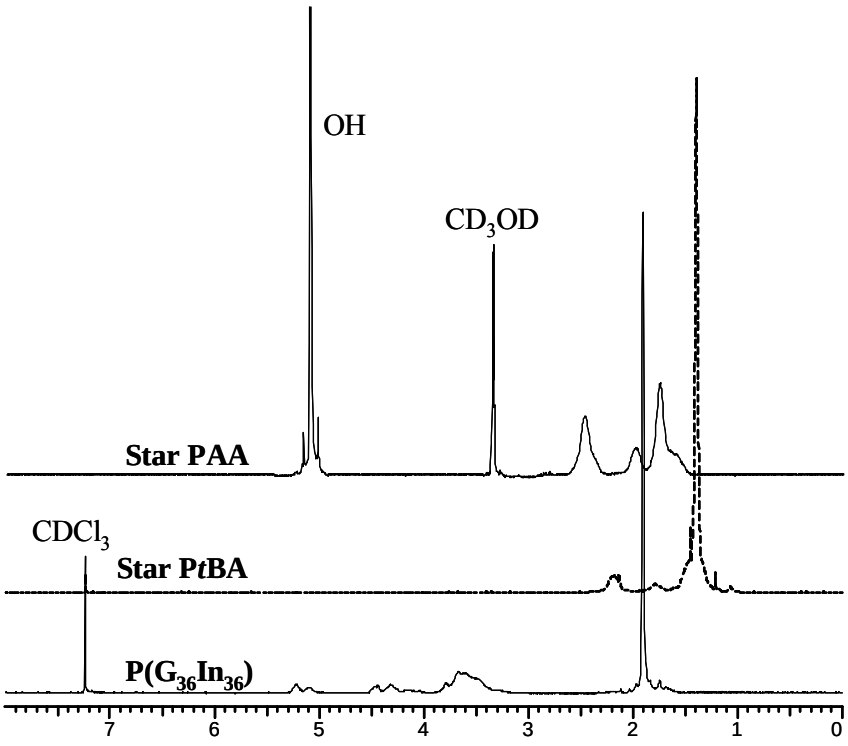

Figure 2-7. Comparison of the ^{1}H NMR spectra of macroinitiator $P(G_{36}In_{36})$ (in $CDCl_3$), multi-arm star P*t*BA (No. 3 in Table 2 in $CDCl_3$) and multi-arm star PAA (in CD_3OD)

Table 2-3. Preparation of multi-arms star P*t*BAs, based on P($G_{36}In_{36}$) macroinitiators

No.	[M]:[I]:[CuBr]	Time (h)	Conv.[a] (%)	$M_{n\,(gpc)}$[b] ($\times10^{-4}$)	M_w/M_n[b]	$M_{n\,(calc)}$[a] ($\times10^{-4}$)	$M_{n\,(abs)}$[c] ($\times10^{-4}$)
P($G_{36}In_{36}$)				0.35	1.37	0.8	
1	50: 1: 1	3	21.2	6.47	13	-	-
2	50: 1: 0.5	1	5.8	1.32	1.25	2.14	2.51
3	50: 1: 0.5	2	8.7	1.46	1.20	2.81	3.35
4	50: 1: 0.5	3	12.5	1.57	1.23	3.68	4.13
5	50: 1: 0.5	4	14.7	1.76	1.20	4.17	5.05
6	50: 1: 0.5	5	18.8	1.85	1.30	5.13	5.66
7	50: 1: 0.5	6	24.4	2.14	1.18	6.41	6.63
8	50: 1: 0.5	8	30.3	2.33	1.31	7.78	7.87
9	50: 1: 0.5	10	39	4.13	13	9.06	10.7
10	100: 1: 0.5	16	34	5.2	1.26	16.5	-
11	200: 1: 0.5	16	13	3.78	1.2	12.8	-
12	50: 1: 0.4	48	42.5	4.61	1.36	10.6	10.1
13	50: 1: 0.2	8	4.1	0.83	1.33	1.75	-

ATRP conditions: L = PMDETA, [CuBr] : [L] = 1:1, volume ratio of tBA to acetone 2:1, the polymerization was conducted in acetone at 60 ^{o}C. [a] The conversion was calculated from ^{1}H NMR, $M_{n\,(calc)}$ = [M]/[I]×$M_{(tBA)}$×conversion ×number of initiating sites per macroinitiator + $M_{n\,(initiator)}$. [b] $M_{n\,(gpc)}$ and M_w/M_n were obtained from GPC equipped with RI detector, calibrated with linear polystyrene standard [c] Measured by GPC coupled with LS in THF.

Thus, alternative way was adopted to suppress the radical-radical coupling side reaction. The amount of CuBr catalyst was lowered (Table 2-3, run no. 2-11) to reduce the concentration of propagating radicals. With half molar ratio of CuBr to initiating sites ([P$G_{36}In_{36}$-Br]:[CuBr]: [PMDETA] = 2:1:1, [acetone]:[*t*BA] = 1:2), ATRP of *t*BA using PG-based macroinitiators in acetone can be controlled.. The obtained polymers possess polydispersities in the range of 1.2-1.3 up to 30% conversion. The conversion was calculated from ^{1}H NMR spectra, using the ratio of the integral of the peak assigned a and b. Typical NMR spectra are shown in Figures 2-7. At higher conversion of 39% (run no 11), gelation was observed, which is in agreement with literature for analogous systems[60] and the previous report on ATRP for methyl

acrylate using PG initiators.[51]

When the molar ratio of CuBr to initiating sites was lowered slightly to 0.4:1 (Table 2-3, run no. 12), a monomer conversion of 42% was achieved, while still maintaining narrow polydispersity (M_w/M_n = 1.36), however, the polymerization time increased considerably (compare no.9 with no.12 in Table 2-3). For a ratio of CuBr/initiating sites of 0.2:1, the polymerization became very slow. Only 4% conversion was achieved within 8 hours.

CuCl was also used to see if it would have an obvious effect on the distribution of the star polymers obtained. For the cases examined, no detectable improvement has been achieved.

Table 2-4. Preparation of multi-arms star P*t*BAs, based on P($G_{36}In_{36}$) macroinitiators

No.	solvents	Temp (^oC)	Conv.[a] (%)	$M_{n\ (gpc)}$ [b] ($\times10^{-4}$)	M_w/M_n [b]
P($G_{36}In_{36}$)				0.35	1.37
1	Acetone	30	48	4.36	1.21
2	Ethanol	30	56	5.26	1.22
3	EtAc	30	50	4.80	1.29
4	Anisole	30	51	4.83	1.25
5	Methanol	30	59	5.47	1.31

ATRP conditions: L = Me_6TREN, [M]:[I]:[CuBr]: [L] = 50:1:0.4:0.4, Volume ratio of tBA to solvent 2:1, reaction time is 3 hours. [a] The conversion was calculated from ^{1}H NMR, [b] $M_{n\ (gpc)}$ and M_w/M_n were obtained from GPC equipped with RI detector, without counting the shoulder peak

Instead of PMDETA, we also attempted to employ Me_6TREN as ligand for polymerization, which is suitable for controlling the ATRP of acrylates.[43] However, the ATRP of *t*BA initiated by P($G_{36}In_{36}$) macroinitiators with Me_6TREN as ligand was much faster than that with PMDETA as ligand. It took about 3 hours to reach 56% monomer conversion with Me_6TREN as ligand in ethanol, compared to only 42.5% monomer conversion after 48 hours with the PMDETA ligand (compare entry no.12 in Table 2-3 and run no.14 in Table 2-4). Unfortunately, bimodal GPC curves were observed for all ATRP reactions of *t*BA with Me_6TREN in different solvents, such as acetone, methanol, ethanol, ethyl acetate and anisole. A shoulder peak was observed at the same position of the macroinitiators, (as shown in Figure 2-8) indicating that

under these reaction conditions the chain propagation rate was very high, exceeding the rate of initiation. This results in a low initiation-efficiency for the ATRP of *t*BA. Changing the catalyst to CuCl and verifying reaction temperature did not obviously diminish the mode from unreacted initiators. Thus, in the following work only PMDETA was used as a ligand.

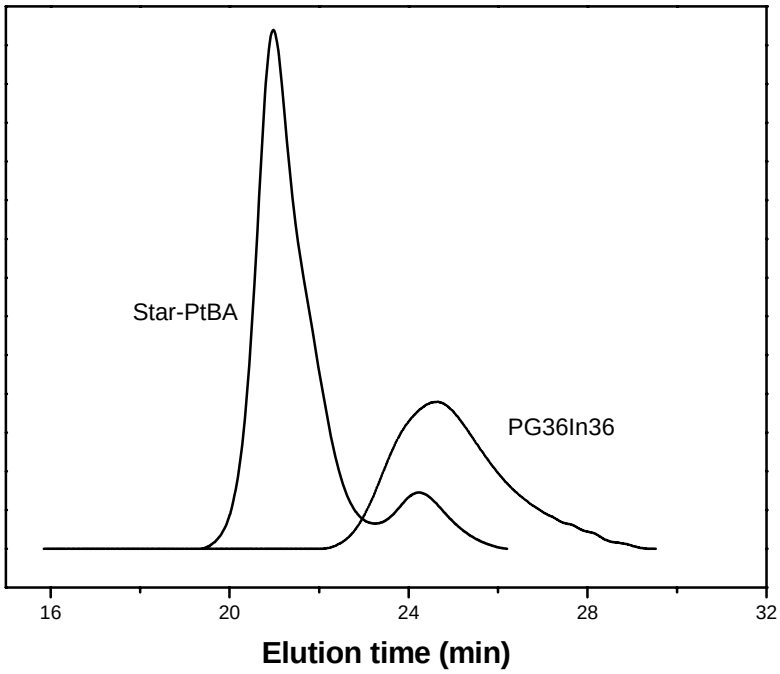

Figure 2-8. GPC elution traces of the multi-arm star PG-b-P*t*BA using [*t*BA]: [PG36In36-Br]:[CuBr]:[Me_6TREN] = 50:1:0.5:0.5 in acetone and $PG_{36}In_{36}$

2.2.2.2. Synthesis of well-defined multi-arm star P*t*BA with 6, 17 and 27 arms

For comparison, we have also carried out the ATRP of *t*BA initiated by multifunctional initiators having less than 30 initiating sites at similar reaction conditions, resulting in star polymers with average 6, 17 and 27 arms, respectively (Table 2-5).

From the data in Table 2-5, it can be seen that the fewer arms the desired star polymers have, the more easily the ATRP of *t*BA can be handled, i.e., higher conversion can be reached, while still maintaining a narrow distribution of the obtained polymers. For example, star polymer P*t*BA with 27 arms can be controlled with up to 45% conversion while the star with 36 arms can be controlled with only 30% conversion. Polymerization of the star with 17 and 6 arms can be carried out up

to 64 and 76 conversions while still in a controlled mode, respectively. Moreover, the polymerization kinetics for the star polymers with lower arm number was considerably faster. For stars with 36 arms, 8 hours reaction can afford 30% conversion while for stars with 6 arms, 8 hours enabled the reaction to reach 76% conversion.

Table 2-5. Syntheses of multi-arm star P*t*BA based on In_6, $P(G_{17}In_{17})$, and $P(G_{27}In_{27})$ macroinitiators

No.	[M]:[I]:[CuBr]	Time (h)	Conv. (%)	$M_{n\,(gpc)}$ [a] ($\times10^{-4}$)	M_w/M_n [a]	$M_{n\,(calc)}$ [b] ($\times10^{-4}$)	$M_{n\,(abs)}$ [c] ($\times10^{-4}$)
In_6				-	-	1148	-
1	50:1:0.5	8	76	2.78	1.07	3.04	3.22
$P(G_{17}In_{17})$				0.35	1.45	0.43	-
2	50:1:0.5	12	64	2.35	1.33	7.39	-
3	50:1:0.4	16	65	2.36	1.25	7.50	8.22
$P(G_{27}In_{27})$				0.37	1.46	0.60	-
4	50: 1: 0.5	5	17	1.92	1.26	3.54	3.70
5	50: 1: 0.5	10	45	3.72	1.13	8.37	9.22
6	50: 1: 0.5	15	65	4.20	7.21	11.83	-

ATRP conditions: L = PMDETA, [CuBr]:[L] = 1:1, volume ratio of tBA to acetone 2:1, polymerization was conducted in acetone at 60 °C. [a] $M_{n\,(gpc)}$ and M_w/M_n were obtained from GPC equipped with RI detector, calibrated with linear polystyrene standard. [b] $M_{n\,(calc)}$ = [M]/[I]×$M_{(tBA)}$×conversion ×number of initiating sites per macroinitiator + $M_{n\,(initiator)}$. [c] $M_{n\,(abs)}$ was obtained from GPC equipped with light scattering detector.

2.2.2.3. Synthesis of well-defined multi-arm star P*t*BA with 66, 90 and 27 arms

When the desired arm number per macromolecule was increased to 66, control of the polymerization became more difficult than in the case of stars with lower arm numbers. Using identical reaction conditions as for the 36-arm star polymer, an insoluble gel was formed (Table 2-6, run no 1). This is due to polymer coupling side reactions, which occur to an increasing extent, since the initiation sites per molecule almost doubled compared with the case of stars with 36 arms. Cu(II) was introduced into the system in order to reducing the concentration of propagating radicals. The

obtained polymer possesses low molecular weight distribution (1.35) with up to 31% monomer conversion. When the [Cu(I)] : [In] concentration was lowered to 0.3:1, narrowly distributed star polymers can be obtained at low monomer conversion 20%. (Table 2-6, runs no 3 and 4). Extended reaction times resulted in crosslinked materials with polydispersity of 8.31.

Table 2-6. Syntheses of multi-arm star P*t*BAs, based on $P(G_{66}In_{66})$, $P(G_{90}In_{90})$, and $P(G_{108}In_{108})$ macroinitiators

No.	[M]:[I]:[CuBr]	Time (h)	Conv. (%)	$M_{n\,(gpc)}$ [a] ($\times10^{-4}$)	M_w/M_n [a]	$M_{n\,(calc)}$ [b] ($\times10^{-4}$)	$M_{n\,(abs)}$ [c] ($\times10^{-4}$)
$P(G_{66}In_{66})$				0.43	1.49	1.48	-
1	50:1: 0.5	6		gel			
2 [d]	50:1: 0.5	10	31	4.54	1.35	14.5	16.9
3	50:1: 0.3	24	20	2.32	1.37	9.9	11.3-
4	50:1: 0.3	48	60	4.00	8.31	-	-
$P(G_{90}In_{90})$				0.52	1.71	2.00	
5	50:1: 0.2	24	14	1.39	1.37	10.6	12.4
6	50:1: 0.2	48	32	4.54	4.8	20.4	-
7[d]	50:1: 0.4	10	20	Micro-gel			
$P(G_{108}In_{108})$				0.86	1.55	2.52	
7	50:1:0.2	48	15	6.73	4.38	11.2	-
8	50:1:0.1	48	8	4.21	3.2	6.33	-

ATRP conditions: L = PMDETA, [CuBr]:[L] = 1:1, volume ratio of tBA to acetone is 2:1, polymerization was conducted in acetone at 60 °C. [a] $M_{n\,(gpc)}$ and M_w/M_n were obtained from GPC equipped with RI detector, calibrated with linear polystyrene standard. [b] $M_{n\,(calc)} = [M]/[I]\times M_{(tBA)}\times$conversion $\times$number of initiating sites per macroinitiator + $M_{n\,(initiator)}$. [c] $M_{n\,(abs)}$ was obtained from GPC equipped with light scattering detector. [d] [CuBr]: [$CuBr_2$] = 10:1.

For the synthesis of star polymers with 90 arms, control of the polymerization becomes even more difficult. Narrowly distributed star polymers can only be obtained at low monomer conversion (14%), using even lower copper concentration [Cu(I)] : [In] to 0.2:1. (Table 2-6, run no 5, 6). Cu(II) was also introduced for the preparation of stars with 90 arms, however, at the ratio [M]:[I]:[CuBr]:[Cu(II)] = 50:1:0.4:0.04, the

reaction system formed gel within 10 hours. The obtained polymer could not pass through the 0.45 μM filter for GPC measurements. When the ratio was lower down to [M]:[I]:[CuBr]:[Cu(II)] = 50:1:0.2:0.02, no polymer was obtained within 48 hours.

Finally, for star polymers with 108 arms, crosslinking occurred already at quite low conversion, even if less catalyst was used ([M]:[I]:[CuBr] = 50:1:0.2 and 0.1, Table 2-6, run no 7, 8). Cu(II) was also introduced at the ratio [M]:[I]:[CuBr]:[Cu(II)] = 50:1:0.2:0.02, however, no polymer was obtained within 48 hours.

2.2.2.4. Plausible relationship for PG-*star*-P*t*BA with different arms limiting conversion of the polymerization

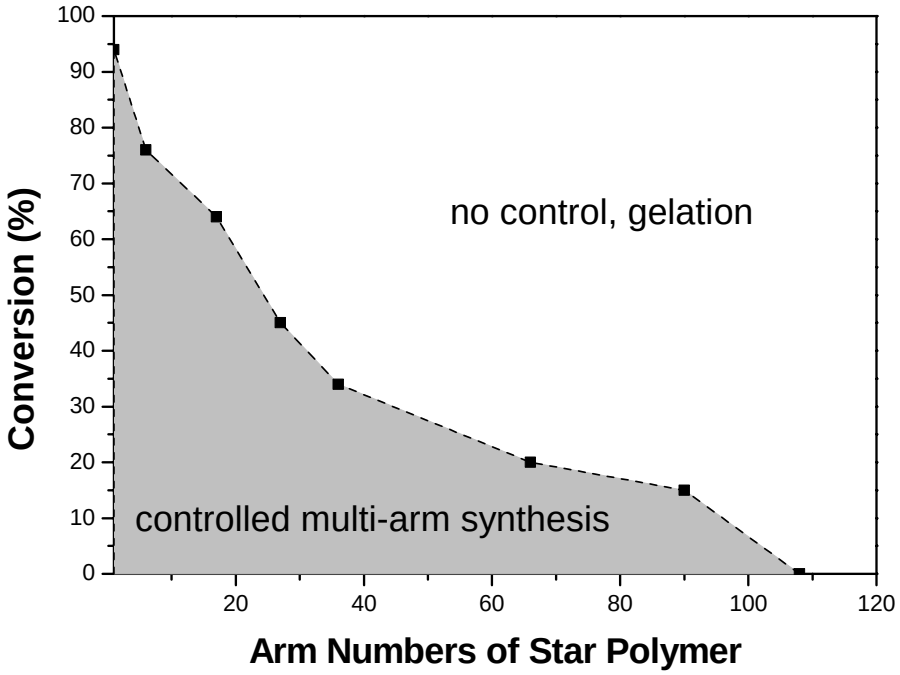

Figure 2-9. Relationship between arm numbers of the multi-arm stars and maximum conversion achieved, applying the respective optimized conditions for controlled polymerization in each case (instead of using the same ratio [Cu]/[I]).

Based on experimental data for various cores, the basic relationship of the conversion *vs* arm numbers of star polymers under the polymerization conditions employed (from the best conditions when the polymerization can be controlled instead of from the same [Cu]/[I] ratio) is summarized in Figure 2-9. With an increase of the arm number of the polymers the reaction has to be conducted at lower monomer

conversion to get control of the polymerization. As it is clear from the figure, there is a transition between 17 and 36 arms since the maximum conversion we can get controlled polymerization for the tBA system drops from 65% (17 arms) to 40% (36arms), after that they changed relatively slower until 90 arms, i.e., once the arm numbers exceed around 36 chains per polymer, polymerizations become much more difficult to control. This is in agreement with an analysis from Matyjaszewski concerning multi-arm star polymerization. [60]

2.2.3. Characterization of star polymers by GPC

All samples have been characterized by GPC with RI detector using linear polystyrene as standard. Figure 2-10 shows the typical GPC traces of the uncrosslinked star copolymers with 36 arms, demonstrating that all distributions are unimodal. Also it can be seen clearly that with increasing molecular weight, the GPC peak appears at shorter elution time. However, molecular weights obtained by this method clearly do not reflect the actual molecular weight of the star copolymers since the relation between the molecular weight and hydrodynamic volume of branched polymers differs substantially from that of the linear ones. Although GPC can only afford the apparent molecular weight of star polymers, it is convenient to estimate the molecular weight distribution. In addition, the bulky side group in P*t*BA may lead to a different hydrodynamic volume compared to that of standard PS.

Some of the samples were measured by GPC coupled with light scattering (MALLS) detector to determine absolute molecular weight values. For all these polymers calculated the theoretical molecular weight has been calculated. The calculated molecular weights can be obtained according to the following Equation 2-9:

$$\overline{M}_{n\ (calc)} = [M]/[I]\times M_{(tBA)}\times \text{conversion} \times (\text{number of Initiating sites per macroinitiator}) + \overline{M}_{n\ (initiator)}. \qquad (2\text{-}9)$$

Here the conversion was determined from NMR.

From Table 2-3 and Figure 2-11 it is obvious that molecular weights from GPC with RI detector are considerably lower than both the predicted and the absolute molecular weights.

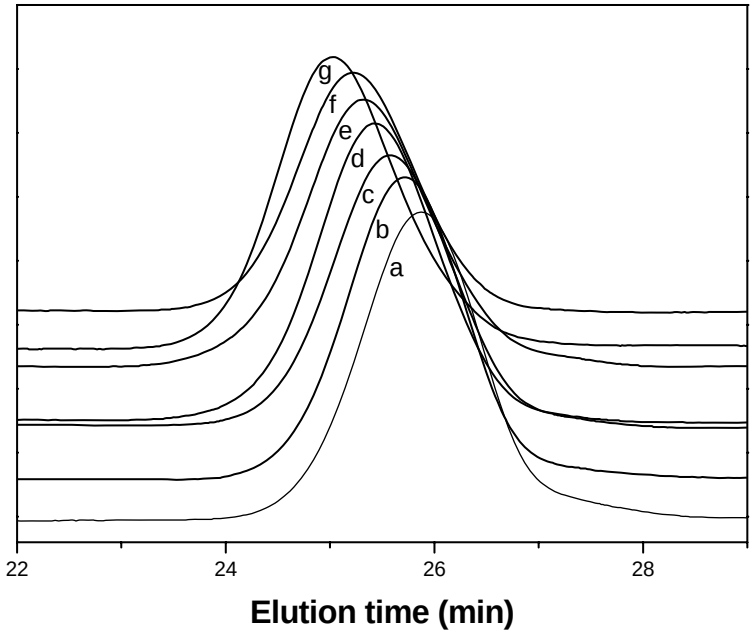

Figure 2-10. GPC traces of multi-arm PG_{36}-*b*-P*t*BA star copolymers, (a) M_n = 2.51x10^4, M_w/M_n = 1.25; (b) M_n = 3.35x10^4, M_w/M_n = 1.20; (c) M_n = 4.13x10^4, M_w/M_n = 1.23; (d) M_n = 5.05x10^4, M_w/M_n = 1.20; (e) M_n = 5.66x10^4, M_w/M_n = 1.30; (f) M_n = 6.63x10^4, M_w/M_n = 1.18; (g) M_n = 7.87x10^4, M_w/M_n = 1.31, polymerization conditions see Table 2-3.

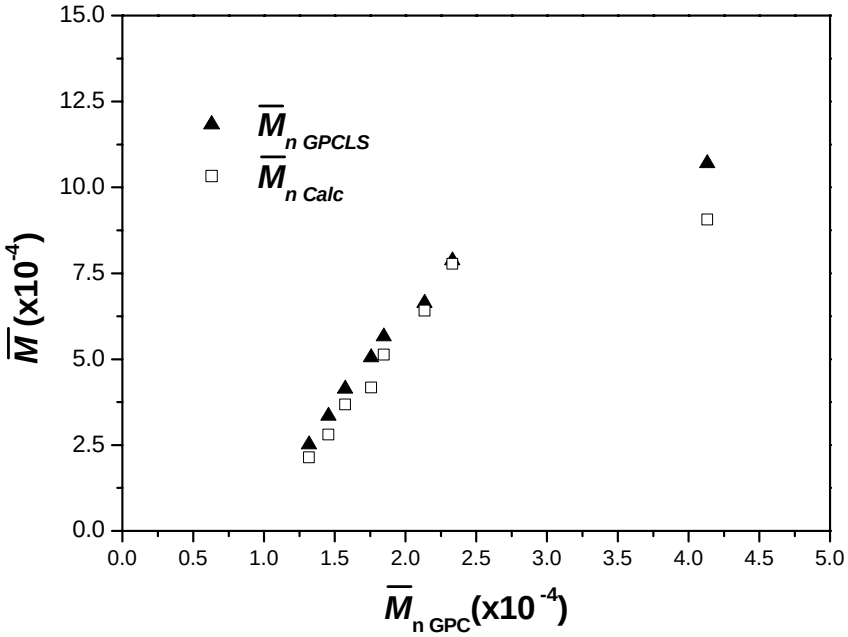

Figure 2-11. The relationship between $M_{n\ (GPC)}$, $M_{n\ (calc.)}$ and $M_{n\ (GPCLS)}$ for the multi-arm star PG_{36}-*b*-P*t*BA

This is explained by the more compact nature of the multi-arm stars in comparison with linear polymer chains, which leads to lower hydrodynamic volume.[60] Similar observations have also been found for star PHEMA.[57] Absolute molecular weights from GPC with MALLS-detector were similar to the calculated ones. This translates to good control of the polymerization in this molecular weight range and high initiation activity of the polyglycerol-based dendritic initiators. In addition, calculated M_n values showed a linear correlation with the data obtained under standard GPC conditions.

2.2.4. Kinetic studies of the ATRP of *tert*-butyl acrylate

Kinetic studies have been carried out using the following ratios: [M]:[$PG_{36}In_{36}$]:[CuBr]:[PMDETA] = 50:1:0.5:0.5. Samples were taken from the reaction mixture via syringes at certain time intervals for conversion measurements (^{1}H-NMR) and molecular weight determination (GPC). The results, depicted in Figure 2-12, show the conversion increase with time and a linear dependence of $\ln([M]_0/[M]_t)$ on time (first order polymerization kinetics), indicating a constant number of propagating species throughout the reaction.

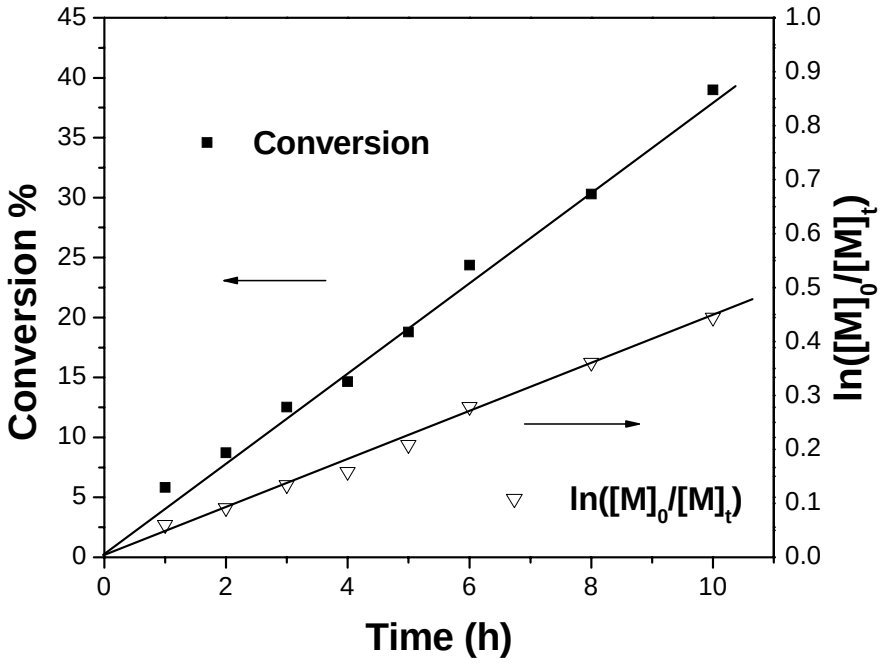

Figure 2-12. Dependence of monomer conversion and $\ln([M]_0/[M]_t)$ on time for the polymerization of tBA in acetone, using hyperbranched **$P(G_{36}In_{36})$** as macroinitiator at 60 °C. [M]:[I]:[CuBr]: [L] = 50:1:0.5:0.5, $V_{tBA}/V_{Acetone} = 2$

Figure 2-13 indicates the effect of monomer conversion on the number average molecular weight and molecular weight distribution. It can be seen that the plots of Mn $_{GPCLS}$ versus polymerization conversion are linear and approximately consistent with the theoretical, calculated values when conversion is lower than 30%. This indicates that the anticipated average molecular weight of the resulting star polymer can be manipulated by controlling polymerization conversion.

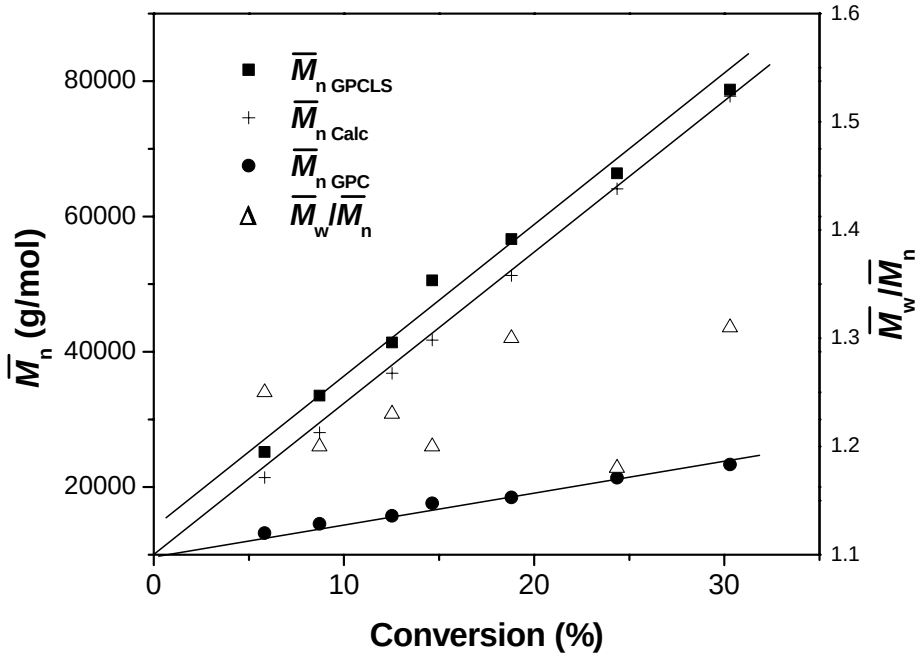

Figure 2-13. Molecular weight vs. conversion for PG_{36}-*b*-P*t*BA

Meanwhile, it is also worthwhile to note once more that the molecular weights determined by GPC, as discussed in the above part, are lower than the calculated results. In such cases, both the calculated M_n and M_{nGPCLS} are more reliable to estimate the actual molecular weight.

From Figure 2-13, we also find that the obtained star polymers possess narrow polydispersities, ($\overline{M}_w/\overline{M}_n$ = 1.2-1.35) and symmetrical and monomodal GPC traces, as shown in Figure 2-10, which suggests that the contribution of chain breaking and transfer 0as well as termination reaction during polymerization can be neglected up to 30% conversion. The above results indicate that the polymerization of *t*BA initiated with $PG_{36}In_{36}$ in acetone is controlled and "living". This agrees with the findings of other groups[60] for star P*t*BA with only 4 to 8 and in one case 24 arms with a perfect dendrimer core.

2.2.5. Building star block co-polymers using P*t*BA macroinitiator

In some polymerization systems, such as in the ATRP of acrylates, it was reported that the structure of end group was rather complex. With increasing reaction time or conversion, the polymers obtained may progressively lose functionality. To evaluate whether all arms of star PtBA synthesized via ATRP are terminally brominated, the star P*t*BA with 36 arms was used as macroinitiator for the subsequent polymerization of other monomers. In this case it is expected that star-like block copolymers can be synthesized. Three different monomers, BA, MMA and styrene were employed, using similar reaction conditions. Data from GPC and ^{1}H NMR characterization are listed in the following Table 2-7.

Table 2-7. Preparation of P*t*BA-PBA

Run	Polymer	*Time (h)*	*Conversion*	$M_{n(GPC)}$ [a] ($\times 10^{-4}$)	M_w/M_n [a]	*tBA/BA* [b]	$M_{n(calc)}$ [c] ($\times 10^{-4}$)
1	P*t*BA			3.7	1.23	22	7.8
2	P*t*BA-PBA	12	20	7.0	1.70	22:20	14.3
3	P*t*BA-PBA	24	44	12.3	3.00	22:45	23.5[d]
4	P*t*BA-PMMA	0.5	-	gel	-		
5[e]	P*t*BA-PSt	3	14	5.6	3.80	22:14	

ATRP conditions: [PMDTEA]:[CuBr] = 1:1, polymerization was conducted in acetone at 60^{o}C. [Monomer]:[Initiator] = 100:1. [a] GPC was measured in $CHCl_3$ [b] the composition of block copolymer was calculated on the basis of the ratio of the area for -O-CH_2- in BA block and all protons. [c] calculated M_n was determined from both GPC and ^{1}HNMR. [e] Polymerization was conducted in bulk at 100 ^{o}C.

Copolymerization of BA was carried out under the ratio [BA]:[P*t*BAIn$_{36}$]:[PMDATA]:[CuBr]= 100:1:0.4:0.4 in acetone. Their GPC curves are shown in Figure 2-14. It can be seen that the GPC curves for run 2 and 3 actually show two peaks, with the one at lower molecular weight corresponding to uninitiated P*t*BA, which might be caused by initiators without terminal bromines, since longer reaction time may cause loss of the initiation sites. Star-star coupling happened when the reaction lasted for 24 hours, which broadened the GPC curve considerably (run 2). The coupling can be suppressed by shortening the reaction time to 12 hours (run 3). A relatively narrow-distributed P*t*BA–*b*-PBA (PDI 1.7) was obtained under very low conversion (20%) for this case.

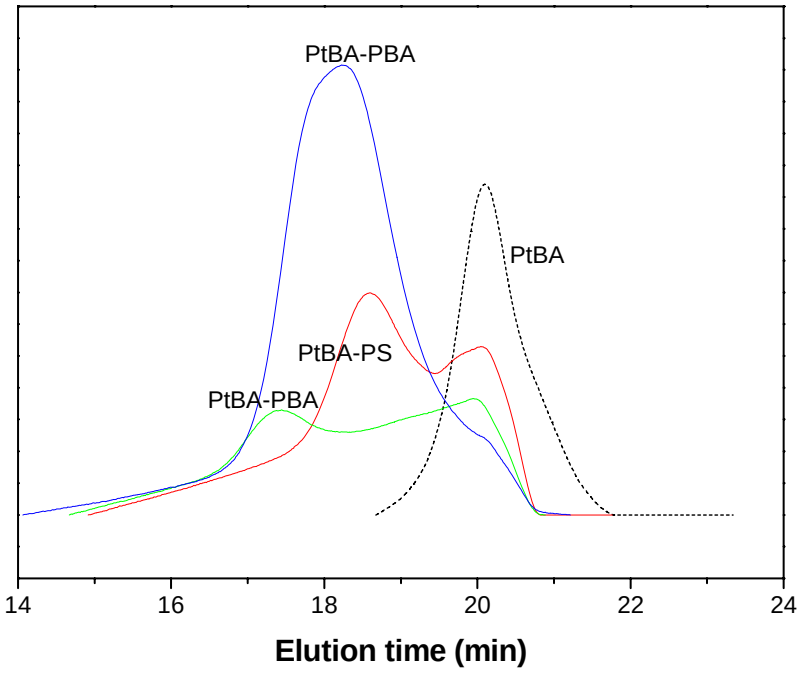

Figure 2-14. GPC traces of multi-arm PG_{36}-*b*-P*t*BA star copolymers, P*t*BA: M_n = 3.7x10^4, M_w/M_n = 1.23; P*t*BA-PS: M_n = 5.6x10^4, M_w/M_n = 3.80; P*t*BA–PBA (green): M_n = 12.3x10^4, M_w/M_n = 3.00; P*t*BA-PBA (blue): 7.0x10^4, M_w/M_n = 1.70; polymerization conditions see Table 2-7.

When the same reaction conditions were employed for block polymerization with MMA, gelation occurred within 30 min, which indicates that coupling reactions dominate after initiation. Using similar conditions, styrene was also employed. For this case (styrene), we could obtain 14% monomer conversion within 3 hours, but the obtained polymer showed 2 peaks in the GPC elugram. One is at the same position as the initiator.

From the above results, it is clear that all the GPC elugrams show two peaks with one of them appear at the same position as the original star P*t*BA initiator. This is corresponding with the star polymers lost terminal bromines that cannot start initiation once more.

We did not carry out further optimization of the reaction conditions to synthesis well defined star block copolymers since the functionality was lost in the course of polymerization. However, the experiments show that the synthesis of block copolymers with multi-arm star structure is in principle possible.

2.2.6. Hydrolysis of PG-*b*-P*t*BA to get star PAA.

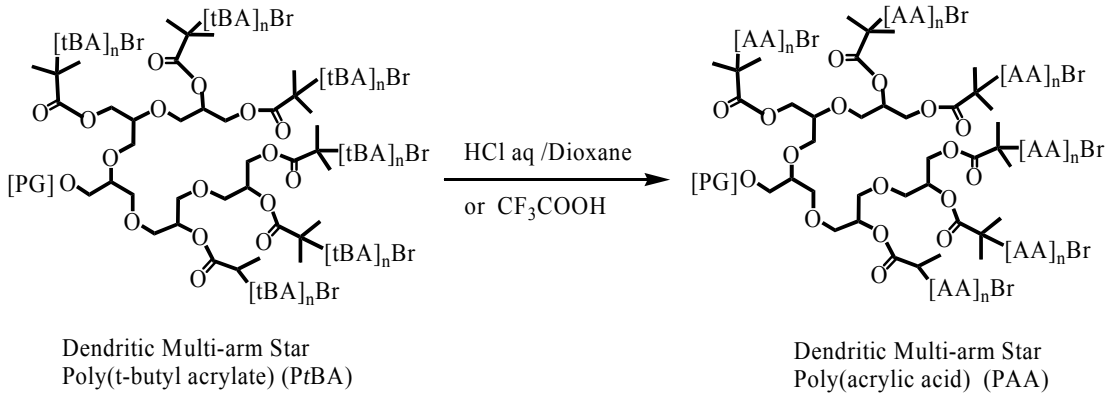

Scheme 2-9. Hydrolysis and characterization of PG-*block*-P*t*BA

PAA is an important commercial super-absorbent and a prototypical pH-responsive polyelectrolyte, representing a unique class of polyelectrolytes.[61] The typical properties of polyelectrolytes depend on molecular architecture, which is related to the formation of H-bonds as well as hydrophobic interactions. This plays a major role in several issues of current scientific interest and practical importance. The synthesis of a series of well defined star PAA polyelectrolytes with different arm number thus helps to improve the current knowledge on polyelectrolyte behavior.

To this end, the *tert*-butyl ester groups on star P*t*BA have been hydrolyzed, using excess HCl in refluxing dioxane for 8 h. ^{1}H NMR in CD_3OD confirms the disappearance of the *tert*-butyl resonance at 1.4 ppm (see Figure 2-7). FTIR analysis has been used to support the presence of the acidic group, as shown in Figure 2-15. The broad absorbance characteristic of a carboxylic acid group is seen at 2800-3600 cm^{-1} and the carbonyl stretch has shifted from 1726 to 1700 cm^{-1}. According to Matyjaszewski's results, together with our data we can assume that all the *tert*-butyl groups have been successfully cleaved. Furthermore, it should be pointed out that the backbone of PG, which is polyether, did not show detectable chain cleavage under the same acidic condition. Thus, it is reasonable to assume that during hydrolysis the backbone of the star polymers remains unchanged.

An alternative method to hydrolyze star P*t*BA with CF_3COOH has also been studied. In this case, star PAA can be obtained at room temperature. The final products show similar NMR and FTIR spectra. However, according to a report by Müller et al., this method will cause 5% loss of arm cleavage, for all the further use of PAA, we didn't use this method.

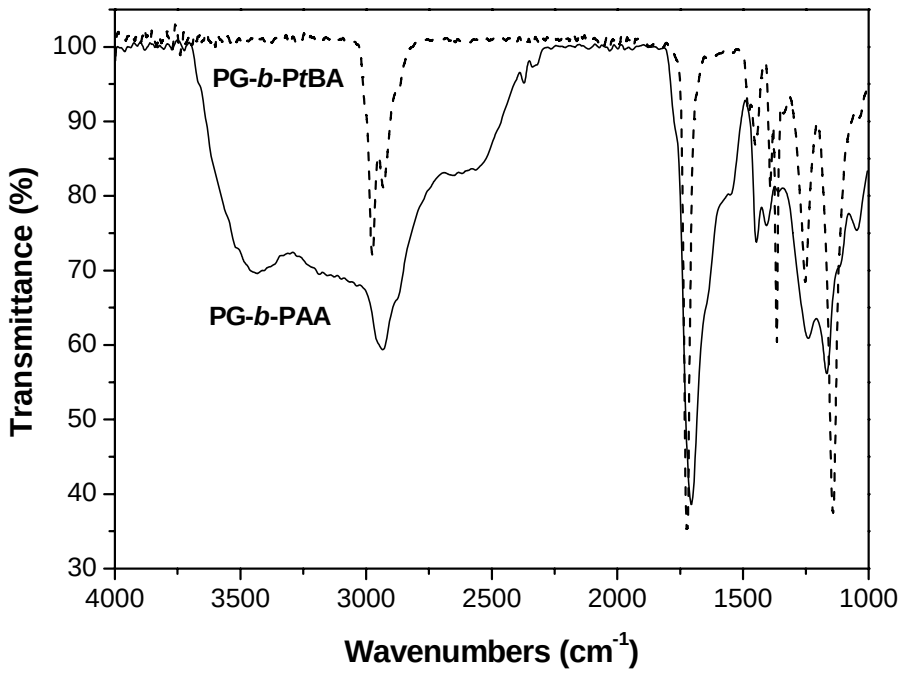

Figure 2-15. FT-IR spectra of star block PG-*b*-PtBA and PG-*b*-PAA

2.3. Conclusion

Well-defined multi-arm star block copolymer polyglycerol-*b*-poly(*tert*-butyl acrylate) (PG-*b*-P*t*BA) with average 17, 27, 36, 66 and 90 arms have been prepared via a *core-first* strategy. The hyperbranched macroinitiators employed were prepared on the basis of hyperbranched polyglycerol by esterification with 2-bromo-isobutyryl bromide. The arms were grafted by atom transfer radical polymerization (ATRP) of *t*BA in acetone. Under optimized conditions, the absolute M_n values of the obtained multi-arm-star polymers were similar to the calculated ones. Molecular weight range of the star P*t*BAs are roughly in the scope from 1×10^4 to 1×10^5. The polydispersities of the new multi-arm stars were mainly in the range of 1.22 to 1.4. Kinetic data characterized by ^{1}H NMR show a linear dependence of $\ln([M]_0/[M]_t)$ on time and molecular weights, which increase linearly with conversion, confirming that the polymerizations are controlled.

Furthermore, we have demonstrated the relationship of to which degree we can control the polymerization *vs* arm numbers of star polymers for the first time experimentally. This is due to the easy preparation of polyglycerol with different

molecular weights and end group functionality.

Both CuBr/Pentamethyldiethylenetriamine (PMDETA) and CuBr/Me_6TREN systems are effective ligands for the ATRP of *t*BA only the later show too fast initiation.

It has also been established in preliminary experiments that the star polymers can be used for further copolymerization to generate star block copolymers, even though a fraction of the initiation sites is lost during the polymerization process.

Applying the obtained PG-*b*-P*t*BA with excess concentrated HCl in refluxing dioxane, full hydrolysis of the *tert*-butyl ester groups was achieved, resulting in multi-arm star polyelectrolytes, polyglycerol-*b*-poly(acrylic acid) (PG-*b*-PAA).

2.4. Experimental Part

2.4.1. Materials

Copper(I) bromide (98%, Acros) was purified by stirring overnight over CH_3CO_2H at room temperature, followed by washing the solid with ethanol, diethyl ether and acetone prior to drying at 40^{o}C in vacuum for one day.[62] *Tert*-butyl acrylate (*t*BA, Aldrich, 98%) was distilled under reduced pressure, stored in the refrigerator and degassed with argon for 1 hr prior to use. Styrene (St, Aldrich, 99%) and methyl methacrylate (MMA, Aldrich, 99%) were washed with 5% aqueous NaOH solution to remove inhibitor, then with water, dried over $MgSO_4$ and distilled twice over CaH_2 under reduced pressure before using. N,N,N',N',N"-Pentamethyl- diethylene-triamine (PMDETA, Aldrich, 99%) was distilled under reduced pressure and degassed with argon for 30 min prior to use. Tris(2-aminoethyl)amine (96%) were purchased from Acros. Pyridine was dried over KOH and distilled under argon. 2-Bromo-isobutyryl bromide (Aldrich, 98%), Dipentaerythritol (Acros, 90%), anisole, acetone were used as received.

PG_{17}, PG_{27}, PG_{36}, PG_{66}, PG_{90}, PG_{108} (data listed in Table 2-2) were prepared as reported previously[42] and dried under vacuum.

2.4.2. Synthesis of macroinitiators for ATRP

The macroinitiators P(G_nIn_n) (n = 17, 27, 36, 66, 90, 108) for ATRP were prepared as reported previously by esterification of hyperbranched PG with 2-bromo-isobutyryl bromide in pyridine.[51] All initiators were additionally purified by

dialysis against chloroform for 2 days to completely remove low molecular weight impurities, using a benzoylated cellulose membrane (MWCO 1000 g/mol).

$P(G_nIn_n)$: The initiator functionality was 100% (with respect to the number of hydroxyl end groups of the PG), which is calculated from the ^1H NMR spectrum (see Figure 2-3). The average number of initiating sites **In** per polymer was 17, 27, 36, 66, 90, 108, respectively. ^1H NMR ($CDCl_3$): = 5.15–5.0 ppm, 4.64-3.14 ppm, 1.92. ^{13}C NMR ($CDCl_3$) δ = 171 ppm, 79 ppm, 74.5-64 ppm, 55.5 ppm, 30.5 ppm. Molecular weight and distribution data of $P(G_nIn_n)$ are listed in table 1.

Macroinitiator $\mathbf{In_6}$ with 6 arms was prepared by esterification of dipentaerythritol with 2-bromo-isobutyryl bromide in pyridine according to the procedure described above. The product was washed with water and dried in vacuo. The dried samples were dissolved in acetone and precipitated from methanol. ^1H NMR ($CDCl_3$): δ = 4.27 ppm; 3.57 ppm; 1.91 ppm. ^{13}C NMR ($CDCl_3$): δ = 170 ppm; 75 ppm; 72 ppm; 55.8 ppm; 45 ppm; 31 ppm. MS: m/z = 1145.6 (M^+), 1147.5(M^+).

2.4.3. Synthesis Me_6TREN

Tris(2-dimethylaminoethyl)amine (Me_6TREN) was synthesized as reported. First Tris(2-aminoethyl)amine react with HCl and generate hydrochloride salt. A mixture of 62g of this hydrochloride, 30 ml. of water, 200 ml. of 85% formic acid, and 170 ml. of 30% formaldehyde was heated at 120 ^oC until the evolution of carbon dioxide stopped (more than. 6 hr.). All the volatile fractions were then removed by vacuum distillation. The product was treated with 400 ml. of 10% NaOH. An oily layer formed which was extracted into ether. The ethereal extract was dried over potassium hydroxide. After removal of the ether the compound tris(2-dimethy-laminoethyl) amine distilled as a colorless oil, b.p. 70-71 ^oC (0.5 mm.); yield 55 g. (88%).

2.4.4. Synthesis of PG-b-PtBA multi-arm star copolymer

In a typical experiment, 121.7 mg (0.546 mmol of initiating sites) of the initiator $P(G_{36}In_{36})$, 4 ml of *t*BA (27.3 mmol), 39.1 mg of CuBr (0.273 mmol) and 2 ml of acetone were placed in a flask with a magnetic stir bar. The flask was sealed with a rubber septum and degassed by three freeze-pump-thaw cycles. Then 57 μl of PMDETA (0.273 mmol) was introduced into the flask by an argon-purged syringe. The flask was then immersed in an oil bath thermostated at 60 ^oC. After a certain time,

the flask was immersed into liquid nitrogen to quench the reaction. Samples were taken, diluted with deuterated chloroform and subsequently analyzed by ^{1}H NMR spectroscopy to determine the polymerization conversion. The residual sample was diluted with acetone and passed through a silica gel column to remove the copper complex. The samples were precipitated in 10 fold excess methanol/water (1:1) and dried at 40 ^{o}C in *vacuo* for 2 days. ^{1}H NMR($CDCl_3$): δ = 2.20 ppm, 1.78 ppm (backbone protons), 1.41-1.48 ppm (*tert*-butyl).

2.4.5. Synthesis of PtBA-PBA multi-arm star co-polymer

In a typical experiment, 500 mg (0.362 mmol of initiating sites) of the initiator P(tBAIn$_{36}$), 2.7 ml of BA (54.6 mmol), 20.8mg of CuBr (0.145 mmol) and 1.4 ml of acetone were placed in a flask with a magnetic stir bar. The flask was sealed with a rubber septum and degassed by three freeze-pump-thaw cycles. Then 30.20 μl of PMDETA (0.145 mmol) were introduced into the flask by an argon-purged syringe. The flask was then immersed in an oil bath thermostated at 60 ^{o}C. After 12 h, the flask was immersed into liquid nitrogen to quench the reaction. It was diluted with acetone and passed through a silica gel column to remove the copper complex. The samples were precipitated in 10 fold excess methanol and dried at 40 ^{o}C in vacuo for 2 days.

2.4.6. Hydrolysis and analysis of PG-b-PtBA

The *tert*-butyl ester groups on P*t*BA were hydrolyzed by using excess HCl in refluxing dioxane for 8 h. All volatiles were removed under reduced pressure, and the residue was dried at 40^{o}C under vacuum for 2 days. ^{1}H NMR (CD_3OD): δ = 1.45-2.7 ppm; FTIR: ν = 1700 cm^{-1}(C=O), 2800-3600 cm^{-1}(OH).

An alternative method is to dissolve PtBA in dichloromethane. Subsequently, trifluoroacetic acid was added (8 fold excess). The color of the mixture turned dark, and after 24 h stirring at room temperature PAA precipitated. The white precipitate was collected and dissolved in dioxane and methanol. Finally, drying enabled to remove the trifluoroacetic acid. ^{1}H NMR (CD_3OD): δ = 1.45-2.7 ppm; FTIR: ν =1700 cm^{-1}(C=O), 2800-3600 cm^{-1}(OH).

2.5. References

[1] Gaynor, S. G.; Matyjaszewski, K. *ACS Symp. Ser.* **1998,** 685, 396.
[2] Malmström, E. E.; Hawker, C. J. *Macromol. Chem. Phys.* **1998,** 199, 923.

[3] Chiefari, J.; Chong, F. E. Y. K.; Kristina, J.; Jeffery, J.; Le, T. P. T.; Mayadunne, R. T. A.; Meijs, G. F.; Moad, C. L.; Moad, G.; Rizzardo, E.; Thang, S. H. *Macromolecules* **1998,** 31, 5559.
[4] Odian, G., *Principles of Polymerization*. 4th Edition ed.; John Wiley & Sons, Inc.: 2004.
[5] Matyjaszewski, K.; Xia, J. *Chem. Rev.* **2001,** 101, 2921.
[6] Kamigaito, M.; Ando, T.; Sawamoto, M. *Chem. Rev.* **2001,** 101, 3689.
[7] Hawker, C. J. *Acc. Chem. Res.* **1997,** 30, 373.
[8] Hawker, C. J.; Bosman, A. W.; Harth, E. *Chem. Rev.* **2001,** 101, 3661.
[9] Barner-Kowollik, C.; Quinn, J. F.; Morsley, D. R. *J. Polym. Sci. Polym. Chem.* **2001,** 39, 1353.
[10] Matyjaszewski, K.; Davis, T. P., *Handbook of Radical Polymerization*. Wiley: New York, 2002.
[11] Matyjaszewski, K.; Patten, T. E.; Xia, J. *J. Am. Chem. Soc.* **1997,** 119, 674.
[12] Flory, P. J. *J. Am. Chem. Soc.* **1940,** 62, 1561.
[13] Matyjaszewski, K. *Polym. Int.* **2003,** 52, 1559.
[14] Roovers, J.; Zhou, L.-L.; Toporowski, P. M.; Zwan, M. v. d.; Iatrou, H.; Hadjichristidis, N. *Macromolecules* **1993,** 26, 4324.
[15] Vlassopoulos, D. *J. Polym. Sci. Polym. Phy.* **2004,** 42, 2931.
[16] Vlassopoulos, D.; Fytas, G.; Pakula, T.; Roovers, J. *J. Phys.: Condens. Matter* **2001,** 13, 855.
[17] Baek, K. Y.; Kamigaito, M.; Sawamoto, M. *Macromolecules* **2001,** 34, 215.
[18] Xia, J.; Zhang, X.; Matyjaszewski, K. *Macromolecules* **1999,** 32, 4482.
[19] Zhang, X.; Xia, J.; Matyjaszewski, K. *Macromolecules* **2000,** 33, 2340.
[20] Rein, D.; Rempp, P., ;; Lutz, P. J. *Macromol. Symp.* **1993,** 67, 237.
[21] Heise, A.; Hedrick, J. L.; Frank, C. W.; Miller, R. D. *J. Am. Chem. Soc.* **1999,** 121, 8647.
[22] Matyjaszewski, K.; Miller, P. J.; Pyun, J.; Kickelbick, G.; Diamanti, S. *Macromolecules* **1999,** 32, 6526.
[23] Stenzel-Rosenbaum, M. H.; Davis, T. P.; Chen, V.; Fane, A. G. *Macromolecules* **2001,** 34, 5433.
[24] Plamper, F. A.; Becker, H.; Lanzendoerfer, M.; Patel, M.; Wittermann, A.; Ballauff, M.; Müller, A. H. E. *Macromol. Chem. Phys.* **2005,** 206, 1813.
[25] Charleux, B., Faust, R. *Adv. Polym. Sci.* **1999,** 142, 1.
[26] Hirao, A.; Hayashi, M.; Loykulnant, S.; Sugiyama, K.; Ryu, S. W.; Haraguchi, N.; Matsuo, A.; Higashihara, T. *Pro. Polym. Sci.* **2005,** 30, 111.
[27] Webster, O. *Science* **1991,** 251, 887.
[28] Zhao, Z.; Chen, Y.; Chen, C.; Xi, F. *Polymer* **2005,** 46, 5808.
[29] Sunder, A.; Heinemann, J.; Frey, H. *Chem. Eur. J.* **2000,** 6, 2499.
[30] Jikei, M.; Kakimoto, M. *Prog. Polym. Sci.* **2001,** 26, 1233.
[31] Chen, Y.; Frey, H., *Hyperbranched Star Polymers. Wiley Science*: In press.
[32] Magnusson, H.; Malmstrom, E.; Hult, A. *Macromol. Rapid Comm.* **1999,** 20, 453.
[33] Bednarek, M.; Biedron, T.; Helinski, J.; Kaluzynski, K.; Kubisa, P.; Penczek, S. *Macromol. Rapid Comm.* **1999,** 20, 369.
[34] Yan, D. Y.; Hou, J.; Zhu, X. U.; Kosman, J. J.; Wu, H. S. *Macromol. Rapid Comm.* **2000,** 21, 557.
[35] Magnusson, H.; Malmstrom, E.; Hult, A. *Macromolecules* **2001,** 34, 5786.
[36] Mai, Y. Y.; Zhou, Y. F.; Yan, D. Y.; Lu, H. W. *Macromolecules* **2003,** 36, 9667.
[37] Kubisa, P. *J. Polym. Sci. Polym. Chem.* **2003,** 41, 457.

[38] Bednarek, M.; Kubisa, P. *J. Polym. Sci. Polym. Chem.* **2004,** 42, 245.
[39] Zhu, X. Y.; Chen, L.; Yan, D. Y.; Chen, Q.; Yao, Y. F.; Xiao, Y.; Hou, J.; Li, J. Y. *Langmuir* **2004,** 20, 484.
[40] Tokar, R.; Kubisa, P.; Penczek, S.; Dworak, A. *Macromolecules* **1994,** 27, 320.
[41] Dworak, A.; Walach, W.; Trzebicka, B. *Macro. Chem. Phys.* **1995,** 196, 1963.
[42] Sunder, A.; Hanselmann, R.; Frey, H.; Mülhaupt, R. *Macromolecules* **1999,** 32, 4240.
[43] Sunder, A.; Frey, H.; Mülhaupt, R. *Macromol. Symp.* **2000,** 153, 187.
[44] Sunder, A.; Mülhaupt, R.; Haag, R.; Frey, H. *Adv. Mater.* **2000,** 12, 235.
[45] Sunder, A.; Mülhaupt, R.; Frey, H. *Macromolecules* **2000,** 33, 309.
[46] Knischka, R.; Lutz, P. J.; Sunder, A.; Mülhaupt, R.; Frey, H. *Macromolecules* **2000,** 33, 315.
[47] Chen, Y.; Frey, H., *Hyperbranched Star Polymers*, Wiley Science: In press.
[48] Sunder, A.; Turk, H.; Haag, R.; Frey, H. *Macromolecules* **2000,** 33, 7682.
[49] Karger-Kocsis, J.; Fröhlich, J.; Gryshchuk, O.; Kautz, H.; Frey, H.; Mülhaupt, R. *Polymer* **2004,** 45, 1185.
[50] Burgath, A.; Sunder, A.; Neuner, I.; Mülhaupt, R.; Frey, H. *Macromol. Chem. Phys.* **2000,** 201, 792.
[51] Maier, S.; Sunder, A.; Frey, H.; Mülhaupt, R. *Macromol. Rapid Commun.* **2000,** 21, 226.
[52] Haddleton, D. M.; Kukulj, D.; Kelly, E. J.; Waterson, C. *Prog. Polym. Sci.* **1999,** 80, 145.
[53] Heise, A.; Hedrick, J. L.; Frank, C. W.; Miller, R. D. *J. Am. Chem. Soc.* **1999,** 121, 8647.
[54] Hedrick, J. L.; Atthoff, B.; Boduch, K. A.; Hawker, C. J.; Mecerreyes, D.; Miller, R. D.; Trollsås, M. *Prog. Polym. Sci.* **1999,** 80, 104.
[55] Hedrick, J. L.; Trollsås, M.; Hawker, C. J.; Atthoff, B.; Claesson, H.; Heise, A.; Miller, R. D.; Mecerreyes, D.; Jérome, R.; Dubois, P. *Macromolecules* **1998,** 31, 8691.
[56] Maier, S.; Sunder, A.; Frey, H.; Mülhaupt, R. *Macromol. Rapid Comm.* **2000,** 21, 226.
[57] Chen, Y.; Shen, Z.; Barriau, E.; Kautz, H.; Frey, H. *Biomacromolecules* **2006,** 7, 919.
[58] Zhang, X.; Xia, J.; Matyjaszewski, K. *Macromolecules* **2000,** 33, 2340.
[59] Davis, K. A.; Matyjaszewski, K. *Macromolecules* **2000,** 33, 4039.
[60] Nanda, A. K.; Matyjaszewski, K. *Macromolecules* **2003,** 36, 599.
[61] Förster, S.; Müller, A. H. E. *Adv. Poly. Sci.* **2004,** 166, 173.
[62] Keller, R. N.; Wycoff, H. D. *Inorg. Synth.* **1946,** 2, 1.

Chapter 3. Viscosity of Star PAA in water and use as a template to prepare water-soluble silver nanoparticles and fluorescent Ag nanoclusters

3.1. Introduction

Star polymers have attracted much attention due to their unique shape and possible processing advantages derived from their spherical, compact structure.[1] In Chapter 2, the synthesis of star P*t*BA has been presented. *Tert*-butyl acrylate (*t*BA) is a widely used monomer for the preparation of poly(acrylic acid) since the *tert*-butyl ester groups can be easily transformed into carboxylic acid groups by acidic hydrolysis. A well-defined multi-arm star PAA polyelectrolyte was obtained after the hydrolysis. (the structure is shown in Scheme 3-1)

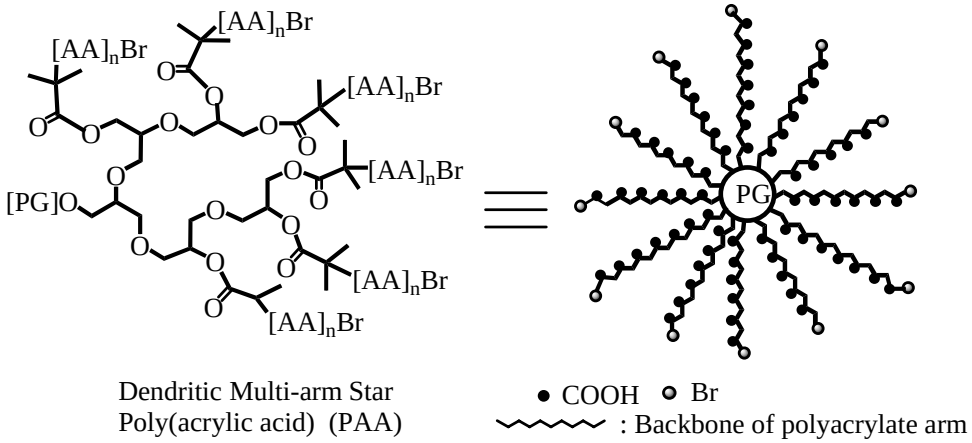

Scheme 3-1. Schematic illustration of multi-arm star branched PG-*b*-PAA

PAA is a commercial super-absorbent and a prototypical pH-responsive polyelectrolyte.[2] Polyelectrolytes play a major part in Nature and find manifold application in industrial processes and daily life. Because they are both macromolecules and electrolytes they represent a unique class of polymer.[2] The special properties of these polymers are determined by their electrochemical and macromolecular parameters and their chemical structure. Charge density and charge strength result in variable long-range electrostatic interactions, which are mainly responsible for the physicochemical properties and the peculiarities of polyelectrolytes in aqueous solution. These interactions and the formation of

complexes driven by attractive Coulomb forces between charged macromolecules and oppositely charged macroions, surfactants, colloid particles, or solid surfaces are of central importance in life sciences and in most technical applications.[2] However, the typical properties of polyelectrolytes do not depend exclusively on electrostatic forces. Differences between the flexibility of the polymer chain and, especially, a molecular architecture[2] supporting the formation of H-bonds or hydrophobic interactions also play a major role in questions of scientific interest and practical importance. The synthesis of a series of well-defined star PAA polyelectrolytes with different arm length will help to better understand the polyelectrolyte behavior.

In this chapter, a study of solution behavior using viscometry will be presented. It must be emphasized that viscometry represents probably the most widely[3, 4] used experimental method to assess conformational transitions of polyelectrolytes in solution. Indeed, the viscosity behavior is related not only to the chemical structure of the polyanion, its size and charge density but also to the environmental properties such as ionic strength, pH and addition of salts.[5-7]

To date, only a very limited number of studies on the viscosimetric behaviors of star polyelectrolytes have been published due to the difficult synthesis.[8, 9] In this chapter, the viscosity properties of well-defined star PAA with 36 arms in salt-free solution and buffer solutions have been investigated. Due to the poor yield of the star PAA polymers with more than 36 arms, here only the viscosity properties of star PAA with 36 arms will be presented. The influence of the macromolecular parameters such as composition and molar mass will also be analyzed. In order to avoid the limitations induced by the partial protonation of PAA chains in water, additional experiments to measure the viscosity behavior of PAA in buffered solution were also carried out.

Ionic star polymers in aqueous solution represent a family of special polyelectrolytes. Their application potential in water has been explored by using these ionic star polymers as templates for the preparation of silver nanoparticles (NPs) or fluorescent nanoclusters.

3.2. Results and Discussion

3.2.1 Viscosity properties

3.2.1.1. Potentiometric titrations of the stars PAA

As a first task, potentiometric titrations of the star PAAs with 36 arms were carried out. Linear PAA with molecular weight of 2000 g/mol was also used for comparison. In all the cases, PAAs were not further purified prior to titration. Samples are listed in Table 3-1.

Table 3-1. Apparent values of pK_a of star PAA samples

Sample name	Length of Arms [a]	$M_{n\ GPC}$ ($x10^{-4}$ g/mol) [b]	PDI [b]	$pK_{a,app}$
$PG_{36}(PAA_{10})_{36}$	10	2.98	1.28	6.73
$PG_{36}(PAA_{22})_{36}$	22	4.61	1.30	6.66
$PG_{36}(PAA_{35})_{36}$	35	6.60	1.36	6.63
$PG_{36}(PAA_{43})_{36}$	43	7.87	1.42	6.58
$PG_{17}(PAA_{33})_{17}$	33	2.36	1.33	6.55
LPAA[c]	27	0.20	-	6.23

[a)] Calculated from ^{1}H NMR, [b)] determined from P*t*BA precursors by GPC, [c)] commercial sample.

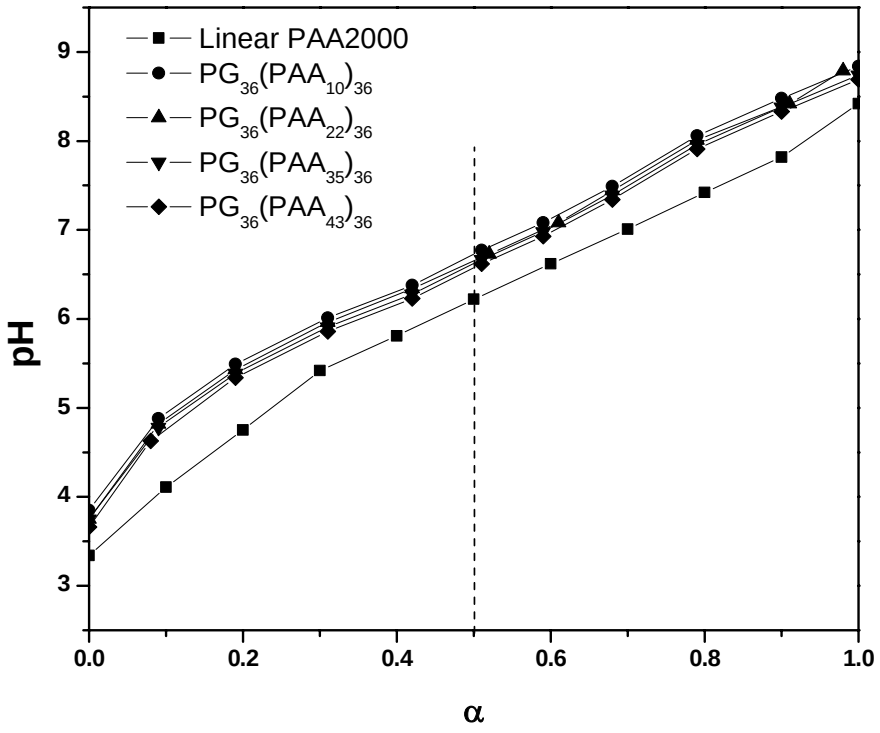

Figure 3-1. Potentiometric titration curves for $PG_{36}(PAA_{10})_{36}$, $PG_{36}(PAA_{22})_{36}$, $PG_{36}(PAA_{35})_{36}$, $PG_{36}(PAA_{43})_{36}$ and linear PAA.

The pH dependence on the degree of neutralization, $\alpha = [Na^+]/[COOH]_0$, where $[COOH]_0$ is the total concentration of carboxyl and carboxylate groups and $[Na^+]$ assigns the amount of added NaOH, is presented in Figure 3-1.

As seen in Figure 3-1, the shape of the titration curves is as expected for linear and star PAAs,[3-5] and does not change significantly with arm length and topology. The titration curves of the star polymers shift slightly to higher pH values and show higher pK_a. Here, the apparent values of pK_a are taken as the pH at 50% neutralization according to qualitative theory. The pK_a results are listed in Table 3-1.

According to Müller's report,[10] the shift of titration curves is due to the higher osmotic pressure inside the stars, caused by counterion confinement. This will lead to a partial reversal of the acid-base reaction, the formation of uncharged -COOH groups within the polyelectrolyte star. As a consequence of this process, the pH value will increase outside. Their conclusion was further confirmed by osmometry measuremenst.[10] Current results of us show a similar tendency and are in agreement with theory.

According to theory,[11, 12] this effect (titration curve shift) is believed to be more pronounced for higher arm numbers, as the osmotic pressure inside the star increases with segment density. The star PAA with more than 36 arms was not subjected to titration measurements due to the low yields; star PAA with 17 arms was used instead to test this. The obtained *pKa* of $PG_{17}(PAA_{33})_{17}$ is 6.55, as listed in Table 3-1. This is lower than 6.63, *pKa* of $PG_{36}(PAA_{35})_{36}$, and in agreement with the theoretical predictions.

It is also noticed that stars with different arm lengths show different pK_a: the apparent pK_a values decrease very slightly with increasing arm length. A similar tendency is also observed for star PAA with 21 arms.[10] This can be explained by the fact that increasing arm length leads to a decrease of the mean segment density within the star polymer and less NaOH is expelled due to the lowered osmotic pressure.

3.2.1.1. Viscosity of PAA in salt-free solution

Salt-free solutions of linear chain polyelectrolytes show characteristic viscosity behavior, i.e., the reduced viscosity η_{sp}/C increases drastically with decreasing polymer concentration c and it shows a maximum at a very dilute concentration C_{max}.[5] This behavior deserves to be considered anomalous, when it is compared with

that of neutral polymer solutions; however, the phenomenon is qualitatively common to almost all linear chain polyelectrolytes, regardless of the degree of polymerization or the type of backbone.[5]

However, according to the literature,[7, 12, 13] in the case of aqueous suspensions of charged spherical particles, the reduced viscosity shows quite a variety of characteristics, although the shape of the particles is much more simple than that of linear chain polyelectrolytes and the size of the particle does not vary with dilution.

The viscosities of the star PAAs (36 arms) with different arm length in salt-free solution (water) have been measured. Figure 3-2 shows the reduced viscosity of the four star polymers as a function of their concentration.

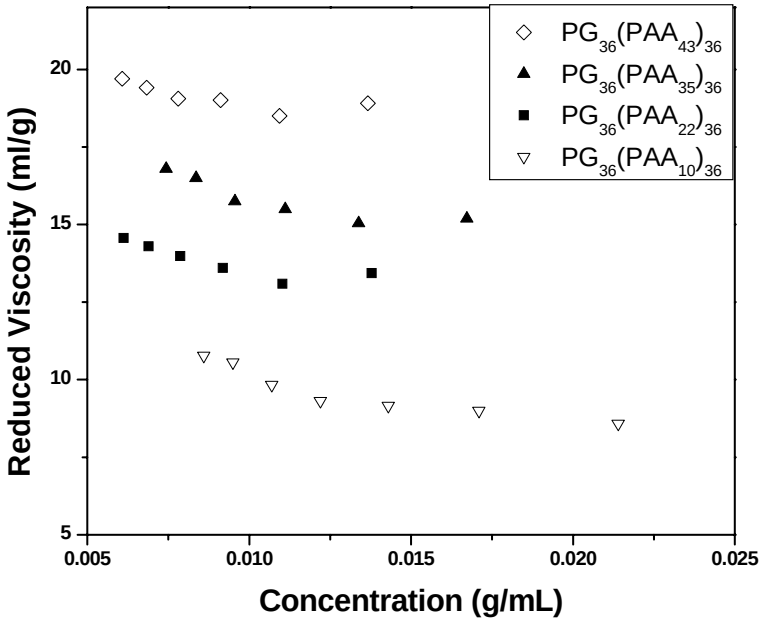

Figure 3-2. Concentration dependence of the reduced viscosities of various star-PAA with 36 arms in salt free aqueous solution at 30 ^{o}C

Normally for non-ionized or poorly ionized polymer solutions, the reduced viscosity profile follows the Huggins relationship (Equation 3-1), i.e., no polyelectrolyte effect can be detected but η_{sp}/C can slightly increase with both polymer concentration and molar mass. Equation 3-1 reflects the net contribution of the hydrodynamic effect of a single polymer molecule and the extrapolation to zero concentration that corresponds to intrinsic viscosity.

$$\frac{\eta_{sp}}{C} = [\eta] + k'[\eta]^2 C \qquad (3\text{-}1)$$

Where η_{sp}, C, [η] and k' are the specific viscosity, the concentration of the polymer, the intrinsic viscosity and the Huggins constant, respectively.

However, from Figure 3-2, it is clear that all the four star PAAs show typical polyelectrolyte behavior characterized by an increase of the reduced viscosity at low concentration range. Under this situation, extrapolation to zero concentration will not correspond to intrinsic viscosity.

Here, the polyelectrolyte effect is due to an expansion of the polyionic side chain, which is caused by the progressively enhanced dissociation of ionizable AA groups as concentration decrease and therefore intensification of intra-star repulsive interactions between ionized AA groups at the surface of the star. It is worth to mention that for linear polyelectrolytes, a minimum apparent molar mass is needed to display a polyelectrolyte effect.[6] However, the current results indicated that no minimum arm length is necessary for the star PAAs (the DP of AA is in the range of 10 to 43) to display polyelectrolyte effects. The lack of a minimum arm length might be due to that although the dissolution of star PAA in pure water only provides partial deprotonation (the pKa value of star PAA in water is within a narrow range 6.58-6.73) of the AA groups, however, due to the geometrical confinement of the star, these ionized AA groups will nevertheless be localized preferentially at the surface of the spherical stars and enable them to display a polyelectrolyte effect.[14]

The curve shown in Figure 3-2 can be fit into the empirical Fuoss equation.[5, 15] (Equation 3-2)

$$\frac{\eta_{sp}}{C} = \frac{[\eta]}{1 + kC^{0,5}} \qquad (3\text{-}2)$$

Where η_{sp}, C, [η] and k are the specific viscosity, the concentration of the polymer, the intrinsic viscosity and the Fuoss constant, respectively.

Figure 3-3 shows the straight lines obtained using Fuoss equations. This made the calculation of intrinsic viscosity values (empirical one) of the star PAAs possible. The calculated results are listed in Table 3-2. The overlap concentration [C*] can be obtained from the reciprocal of the intrinsic viscosity. ([C*] = 1/[η])

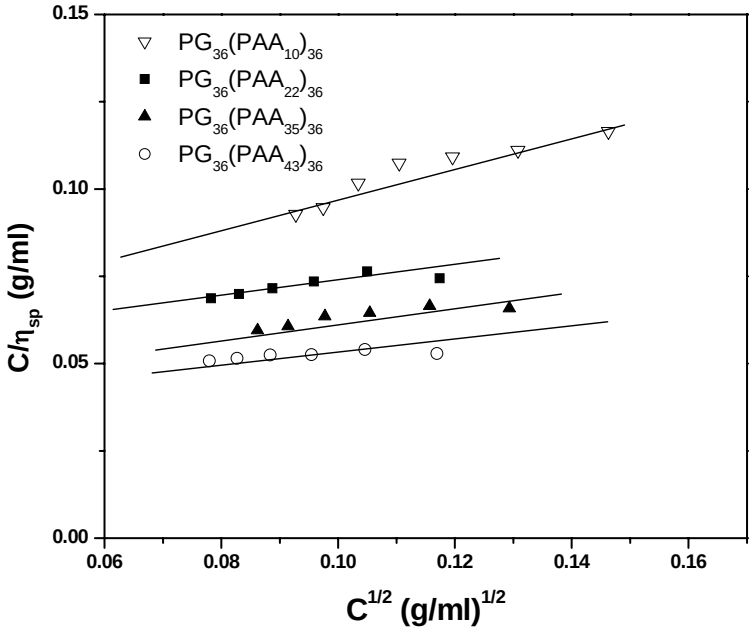

Figure 3-3. Representation of the Fuoss equation of the star-PAA

Table 3-2. Fuoss viscosity and overlap concentrations of star PAA with 36 arms

Sample name	[η] (ml/g)	[C*][a] (g/ml)
$PG_{36}(PAA_{10})_{36}$	14.40	0.0694
$PG_{36}(PAA_{22})_{36}$	20.20	0.0495
$PG_{36}(PAA_{35})_{36}$	24.21	0.0413
$PG_{36}(PAA_{43})_{36}$	26.60	0.0376

[a] Overlap concentration [C*] can be approached from 1/[η].

The Fuoss intrinsic viscosity (Figure 3-4) shows a linear dependence on the arm length of AA units: the larger the size of the star polymer, the higher the viscosity. This is reasonable since the viscosity reflects the polymer size.[5] The Coulomb repulsion forces between the carboxyl groups lead to a more rigid PAA arm and to a expanded star whose size is determined by the arm length. The calculated overlap concentration, C*, (a relative empirical measure of coil expansion) at which star polymers begin to overlap with each other, is in the range of 37.6 mg/ml and 69.4 mg/ml.

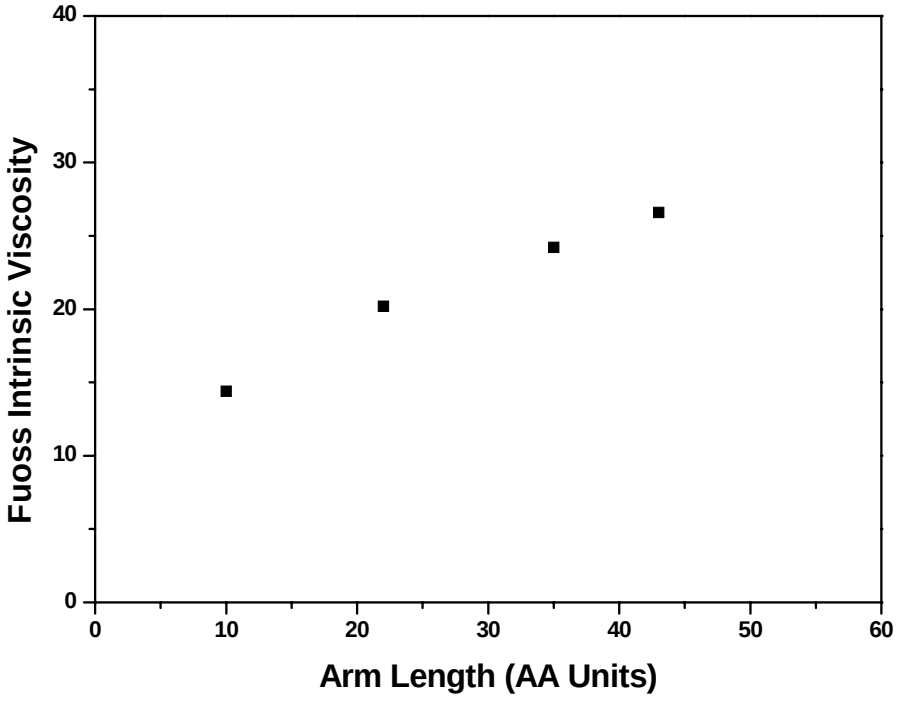

Figure 3-4. Relationship between the Fuoss intrinsic viscosity and arm length of PAA units

3.2.1.3. Viscosity of PAA at different pH

In order to avoid limitations induced by the partial deprotonation of PAA chains in water, additional measurements were made. The conformation of a polyelectrolyte in solution depends on several factors, among which the charge density and the salt concentration are most important. Viscosity of the star $PG_{36}(PAA_{22})_{36}$ and $PG_{36}(PAA_{35})_{36}$ were measured in buffer solutions at pH 7, 8 and 9 to monitor the charge density effects and in 1M NaCl solution to study the salt effects.

Figure 3-5 shows reduced viscosities of the star $PG_{36}(PAA_{22})_{36}$ and $PG_{36}(PAA_{35})_{36}$ in buffer solutions at pH 7, 8 and 9. It is clear that star PAAs show typical polyelectrolyte behavior characterized by an increase of the reduced viscosity at low concentration range. Compared with the situation in water, the increase of the reduced viscosity is more pronounced. The curve of reduced viscosity slightly shifts to higher position with increasing pH. For the case of pH 8 and 9, they show similarly reduced viscosity curves. This can be explained by the following proposed models. PAA is a weak polyelectrolyte, the dissolution of star PAAs in pure water could only provide partial deprotonation (Scheme 3-2, a), most of those ionized AA groups are

localized at the surface of the star polymers. When measured at pH 7, from Figure 3-1 and *pKa*, we know that star PAAs reach around 60 % deprotonation, the ionized AA groups are distributed not only at the surface of the star polymers, but also along the arms of the star polymer, (Scheme 3-2, b), turned the star PAA into a charged spherical colloid; therefore, they could display a more pronounced polyelectrolyte effects.[16-18]

When the pH increased to 8 or 9, the degree of deprotonation are 80%, 100%, respectively. (refer to the potentiometric titration curve for the degree of deprotonation) For both cases, charge density per star is high, i.e., the undeprotonated AA groups do not have an obvious influence on the dimensions of charged spherical colloids. They could thus possess similar size and display almost identical viscosity behavior.[19, 20] The experimental results show that the viscosity data are quite similar at pH 8 and 9 for $PG_{36}(PAA_{22})_{36}$ and $PG_{36}(PAA_{35})_{36}$.

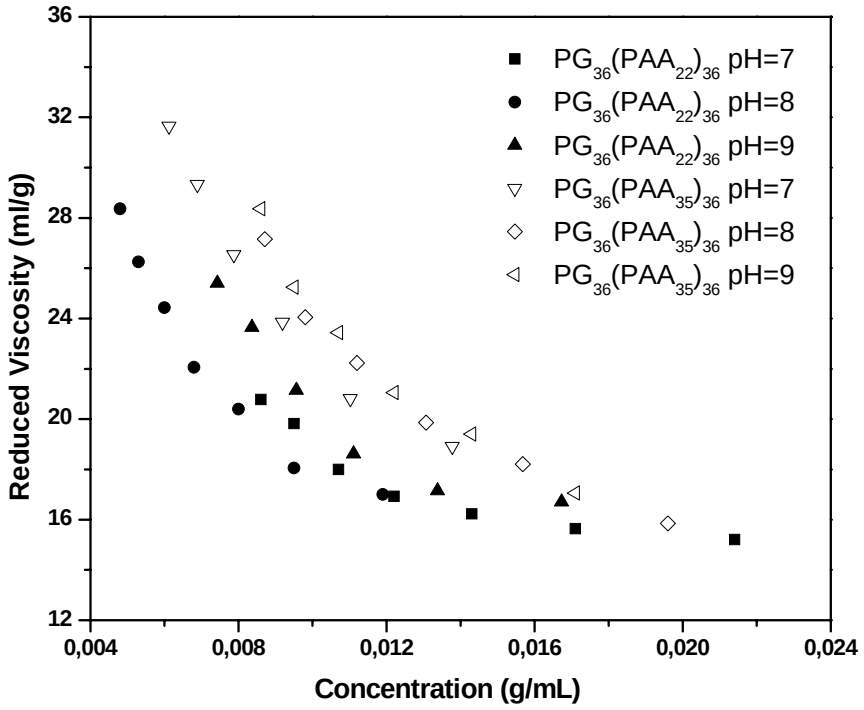

Figure 3-5. Concentration dependence of the reduced viscosities of $PG_{36}(PAA_{22})_{36}$ and $PG_{36}(PAA_{35})_{36}$ at different pH, 30 ^{o}C

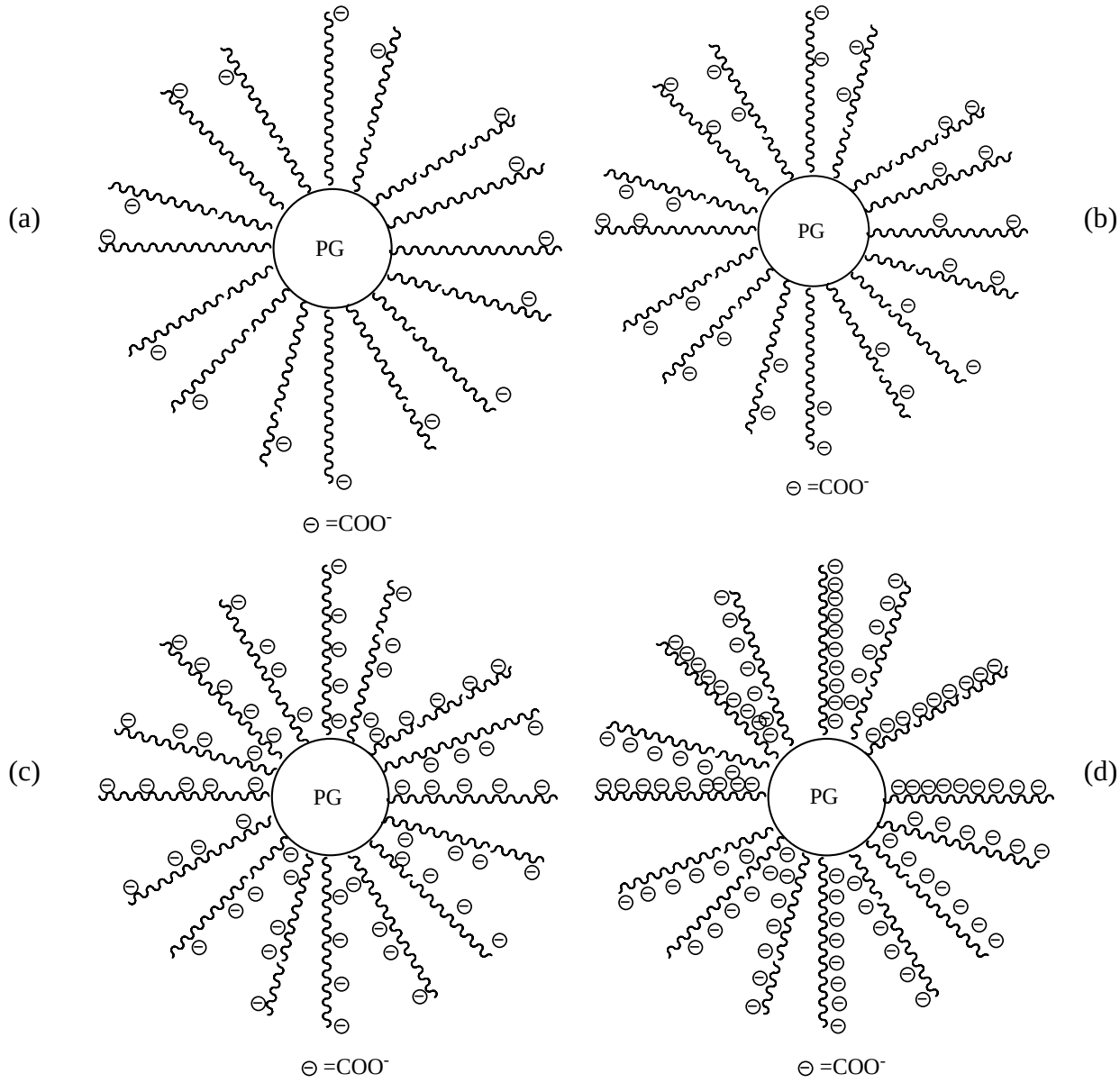

Scheme 3-2. Possible conformation of star PAA in water, different degree of ionization (a) in pure water (b) pH = 7 (c) pH = 8 (d) pH = 9

AFM measurements were carried out for star $PG_{36}(PAA_{35})_{36}$ under soft tapping mode at r.t. The aqueous solution of the sample was first filtered through a 0.45 μm PTFE syringe filter. Samples were prepared by dropcasting 5 μL of the dilute solution onto freshly cleaved mica.

The results of AFM measurements provide support for the formation of charged, spherical colloid-like particles. AFM photographs are shown in Figure 3-6. The top image represents $PG_{36}(PAA_{35})_{36}$ measured at a concentration of 1 mg/ml. From the image it is can be seen that the star PAAs possess approximately spherical shapes.

When the solution is diluted to 0.01 mg/ml, single spheres could be observed (bottom photograph). The average size of the deposited species is around 20-40 nm (Figure 3-7).

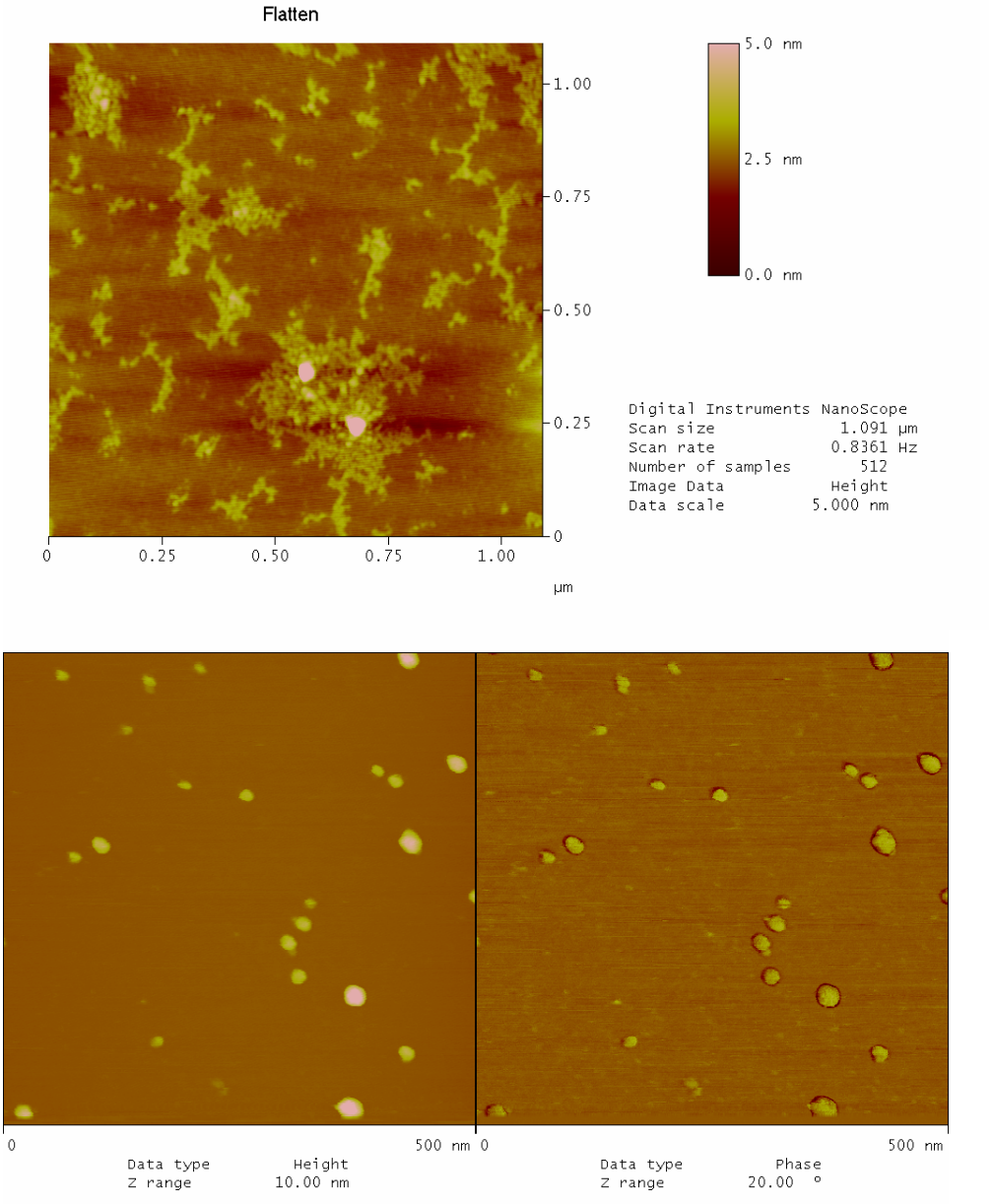

Figure 3-6. AFM micrographs of the star $PG_{36}(PAA_{35})_{36}$ (Sodium Salt, pH of the solution is around 8) on a mica surface (tapping mode) at the concentration of 1 mg/ml (top one) and 0.01 mg/ml (bottom one).

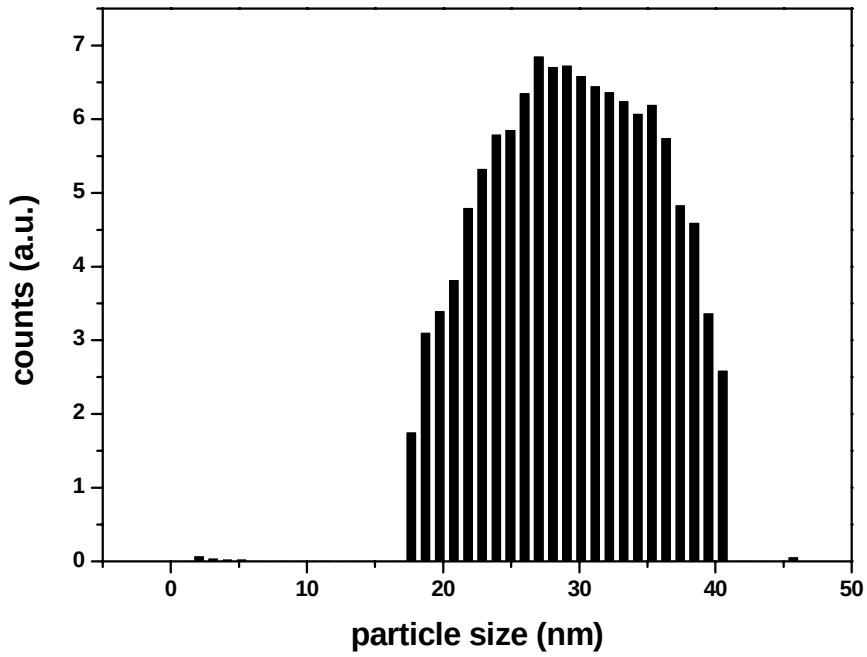

Figure 3-7. Particles count from AFM measurement for the star $PG_{36}(PAA_{35})_{36}$

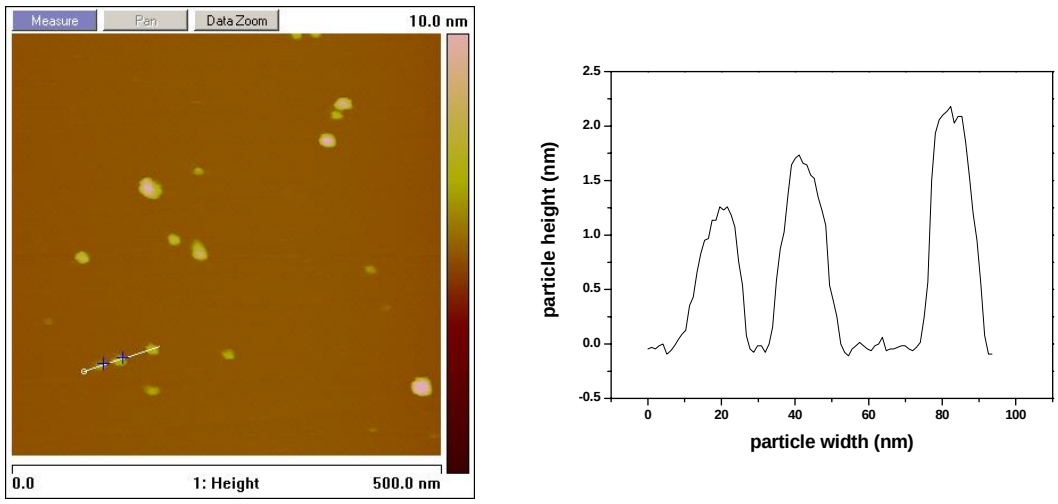

Figure 3-8. AFM micrograph (left) with corresponding height profile (right) of star $PG_{36}(PAA_{35})_{36}$ (Sodium Salt, pH of the solution is around 8) on a mica surface at the concentration of 0.01 mg/ml (tapping mode)

The height images represent the true surface topography.[21] As can be seen from the height profile of the polymers on the mica surface presented in Figure 3-8, (also

from the first height image in Figure 3-6) the star polymers are 2-3 nm in height which indicates the molecules of the star polymer under a flattening process upon deposition on the mica surface.[22]

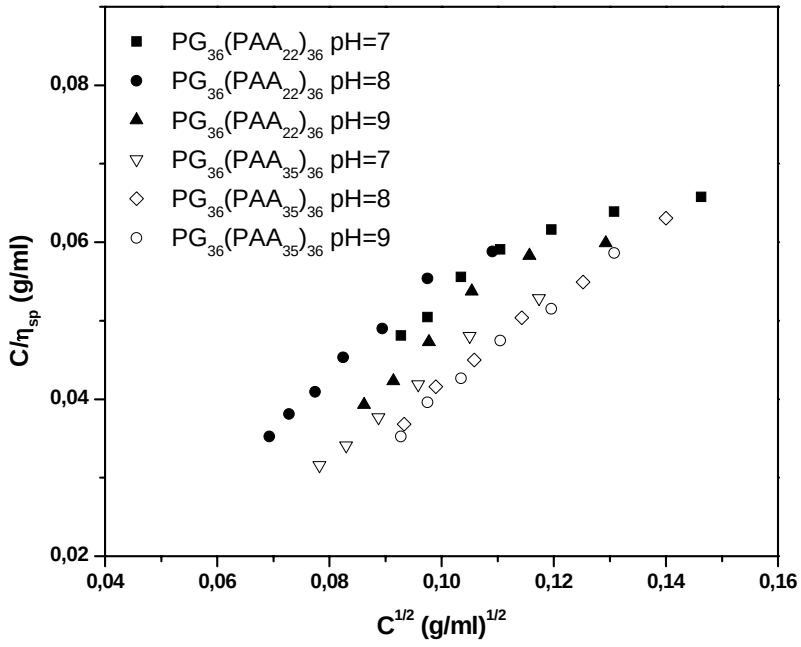

Figure 3-9. Representation of the Fuoss equation of $PG_{36}(PAA_{22})_{36}$ and $PG_{36}(PAA_{35})_{36}$ at different pH, 30 ^{o}C

The curves shown in Figure 3-5 were also fit into the Fuoss equation. As can be seen from Figure 3-9, pseudo straight lines were obtained for all the cases. However, the intersection of the fit with the y-axis can not be used to calculate intrinsic viscosity since the intersections give negative values. Elias also pointed similar tendency.[23] This problem can be ascribed to the limitations of the empirical equation when applied to polymer with non-linear topology.

As already mentioned, the salt concentration will have a pronounced effect on the solution properties of the star polyelectrolytes. The viscosities of $PG_{36}(PAA_{22})_{36}$ and $PG_{36}(PAA_{35})$ were measured in 1 M NaCl solution to test the effect. Both samples were first neutralized with a stoichiometric equivalent of NaOH. The viscosity curves are shown in Figure 3-10. It can be seen that with the presence of NaCl, electrostatic effects are suppressed due to neutralization of the charged groups of the PAA side chains. In this case, the polymers adopt the behavior of neutral, i.e., uncharged

chains.[5, 12, 20] Since the polymer is a multiarm star, the dimensions of the polymer do not change upon dilution, and the viscosity curve displays an almost linear function, allowing one to determine [η] by the extrapolation of η to $C_{polymer}$ = 0. In this case, [η] for $PG_{36}(PAA_{22})_{36}$ and $PG_{36}(PAA_{35})_{36}$ is around 12 and 15, respectively. This implies that the side PAA chains collapse with the presence of NaCl and the star polymer displays a lower intrinsic viscosity, compared with the case of star PAA in water, where [η] are 20.2 and 24.2 (Table 3-2), respectively.

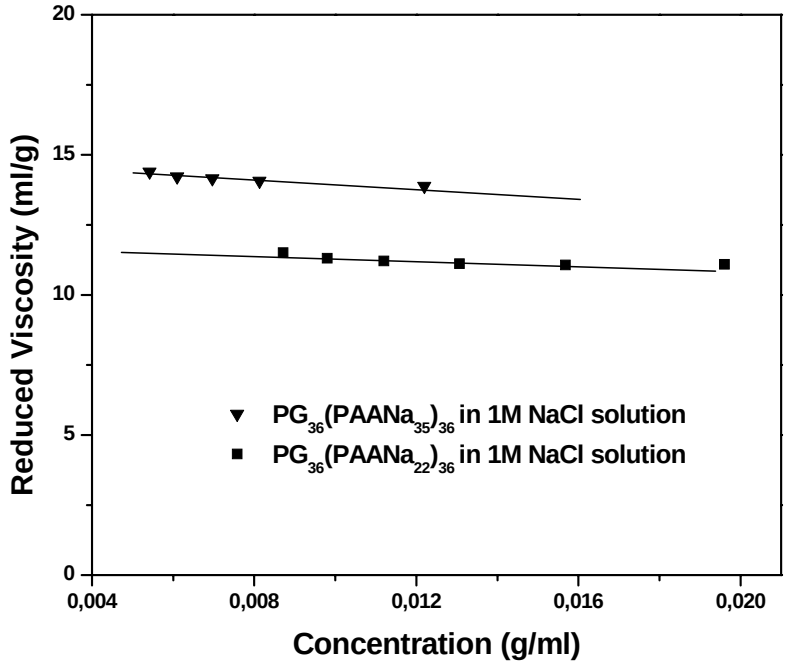

Figure 3-10. Concentration dependence of the reduced viscosities for $PG_{36}(PAA_{22})_{36}$ and $PG_{36}(PAA_{35})_{36}$ in 1 M NaCl solution

3.2.2. Use of star PAA as a template for the synthesis of silver nanoparticles

As discussed above, the charged star PAA can be viewed as tiny core-shell particles in solution: the PG core was covered by ionic polyelectrolytes, which leads to a net negative charge that will attract much smaller particles bearing positive charges.

This property of star PAA can be utilized to prepare nanoparticles (NPs). The remarkable size- and shape-dependence of physical, optical, and electronic properties of metal and semiconductor nanocrystals make them compelling components of

modern materials chemistry.[24-27] Fabrication of these materials is useful not only for understanding fundamental phenomena such as quantum confinement, but also for obtaining "building blocks" featuring optical and electronic properties that are desirable for advanced applications in photovoltaic solar cells, light-emitting diodes, and biological diagnostics.[25] The formation of metal NPs in a polymeric matrix such as dendrimers, latex particles, microgels, or other polymers has fascinated scientists because of the importance such systems may have in nanotechnology. Colloid chemists have recently made considerable progress in preparing spherical nanocrystals via ambient temperature wet-chemical routes or organometallic methods.[28-30] Although the synthesis of spherical nanocrystals is well developed for many materials, systematic manipulation of the shapes of nanocrystals is still a significant challenge.

Nanometer size silver particles attached to colloidal spheres have been a field of intense research during the recent years.[27] Dendrimers have been used to prepare silver NPs,[31] and, more recently Kumacheva and co-workers[32] introduced polymer microgels as templates and carrier systems for NPs. Thus, dendrimers or microgels may be viewed as "nanoreactors" in which metal NPs can be immobilized and handled in an easier fashion. All the studies utilized polymer matrix as suitable support for the metal NPs and prevented them from aggregation.

There is always considerable interest in developing new templates for making NPs with control over shape and size. Here the work of using PAA as template to prepare silver NPs (section 3.3.2) and nanoclusters (section 3.3.3) will be presented since silver ions possess positive charge and have great affinity.[33]

Silver samples were first prepared as described in the following: fresh Ag^+ solution was mixed with an aqueous solution of star $PG_{36}(PAA_{22})_{36}$. The mixing conditions are listed in Table 3-3. To this mixture, aged N,N-dimethylformamide (DMF) was added. The solution was then heated under stirring at 40 ^oC. Within 8-12 min, the solution color changed from yellow through red to purple. After further aging time, some of the nanoparticle solutions turned into dark blue due to aggregation. (cf. Figure 3-10) The product was kept in the fridge at 4 ^oC.

The binding behavior of Ag^+ with the star PAA samples was first examined by FTIR since a ligation can be formed between the high electronic density of the oxygen atoms and the Ag^+ ion. Figure 3-11 presents the IR spectra of PAA and PAA- Ag^+.

The OH band remains unchanged (not shown), while the C=O band changed very slightly. It seems the more Ag^+ interacts with carboxylic groups, the more obvious is the shift of the C=O band. The C-O band (in the structure O=C-O-) cannot be detected, which may be due to strong solution effects.[34] Some changes can be observed in the fingerprint area which could be attributed to the interaction between Ag^+ and COO^-.

Table 3-3. Conditions for Preparing Ag Nanoparticles

No.	Polymer : Ag^+	Aging time	Color
Ag1	1 : 0.8	2 hr	Yellow ppt
Ag2	1 : 0.4	24hr	Dark Red
Ag3	1 : 0.3	24hr	Dark Red
Ag4	1 : 0.2	24hr	Dark Red
Ag5 [a]	1 : 0.4	24hr	Green/Blue
Ag6 [b]	1 : 0.4	24hr	Violet
Ag7 [c]	1 : 0.4	24hr	Blue/Green

The reduction of silver was carried out at 40 ^oC. The polymer used for the experiments is $PG_{36}(PAA_{22})_{36}$. Ag^+ The solution contains 10 wt% $AgNO_3$ and 6% ammonium hydroxide. [a] $PG_{36}(PAA_{16})_{36}$ was used. [b] pH was adjusted to 9. [c] Sodium salt was used.

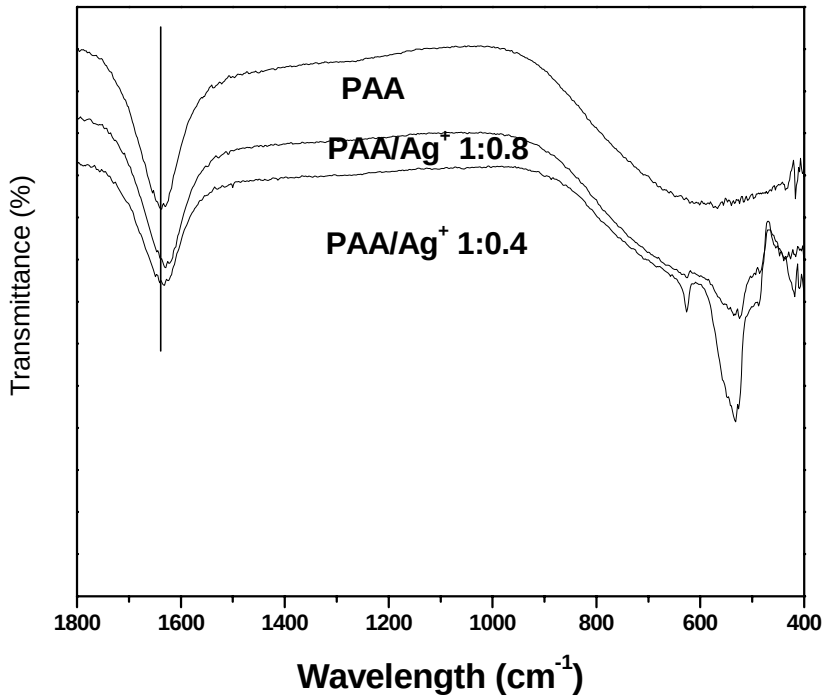

Figure 3-11. FTIR spectra of Poly(acrlic acid)-Ag^+ complex

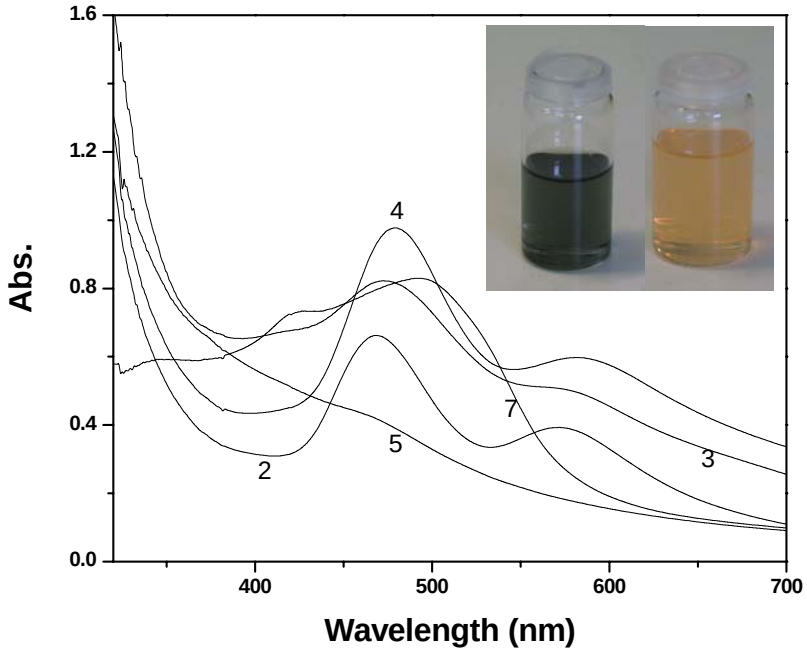

Figure 3-12. UV-Vis spectra of the obtained silver solutions (Inserts are photos of samples after mixing, yellow, and after aggregation, dark blue/green)

Figure 3-12 shows the UV spectra of the solution after reduction. It can be seen for the current reaction pairs that all the obtained UV spectra display several absorption bands. For most cases an absorption band at 415 nm, which is typical for DMF-reduced Ag cannot be observed,[35, 36] due to overlap with the other absorptions.

Figure 3-13 shows the transmission electron micrographs (TEM) of the silver samples. It is obvious that silver NPs can be successfully produced using star PAAs as templates. For most cases, both individual particles and the aggregation of particles are present. As can be seen from Ag 3 (Figure 3-13 c,d), the obtained Ag particles show good contrast for particles with different orientation and a clear diffraction pattern can be obtained.

Interestingly, we noticed that Ag sample 4 (Figure 3-13 e), for which very low [COOH]:[Ag^+] ratio were used, 5:1, some nanosize core-shell structures could be observed. We assume that at low silver concentration, the small silver NPs formed are attached to one star polymer and do not cause the further collapse of the star polymer support and thus form this nanosized core-shell structure (necklace like). The magnified photos (Figure 3-13 f, g, h) show that the cyclic structures are composed of

many smaller silver particles. The sizes of the rings are around 20-30 nm, which corresponds with the size of the star PAA obtained from AFM.

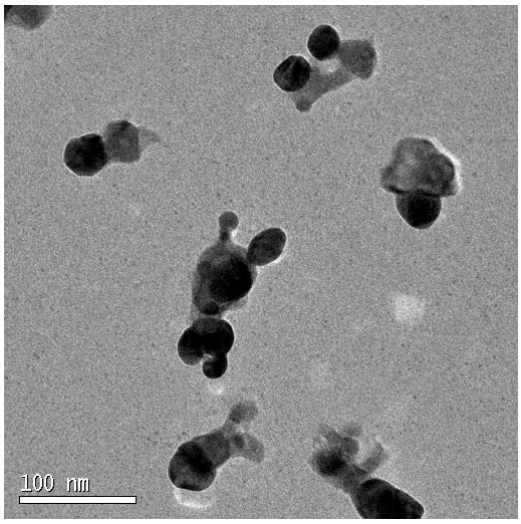

(a) Ag 2

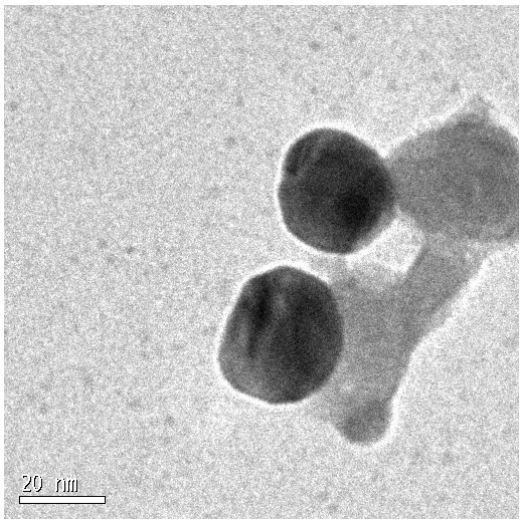

(b) Ag 2

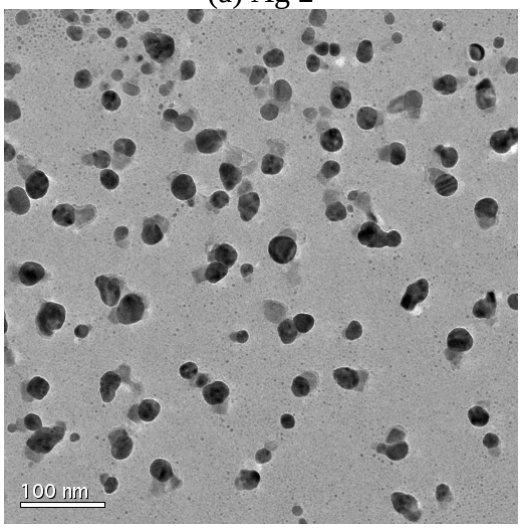

(c) Ag 3

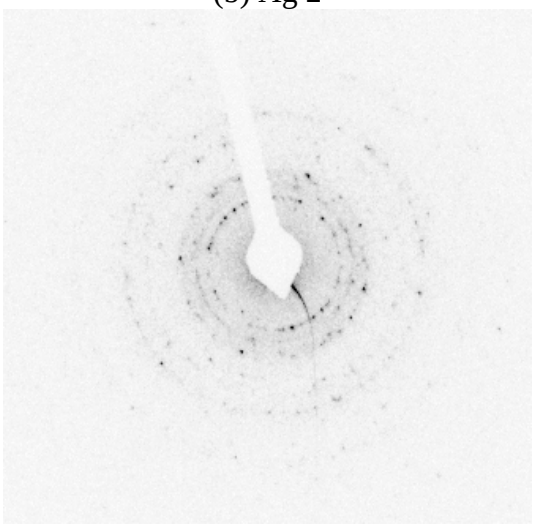

(d) Diffraction of Ag 3

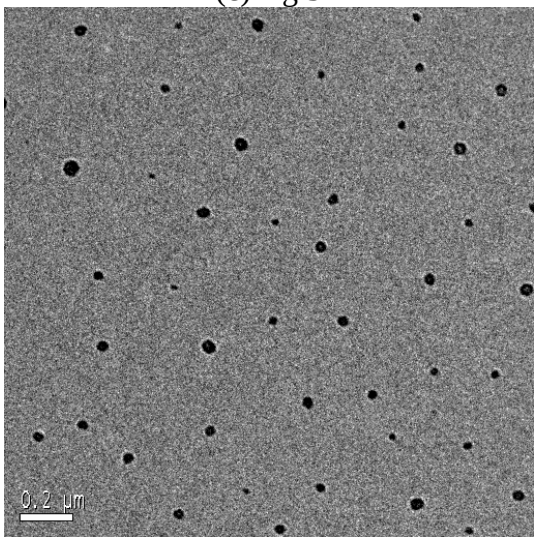

(e) Ag 4

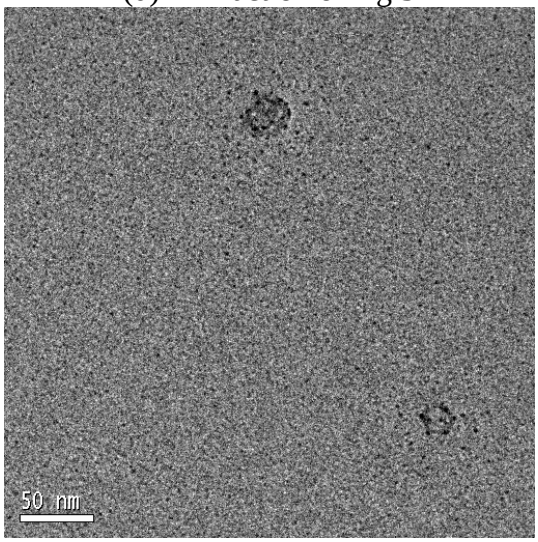

(f) Ag 4

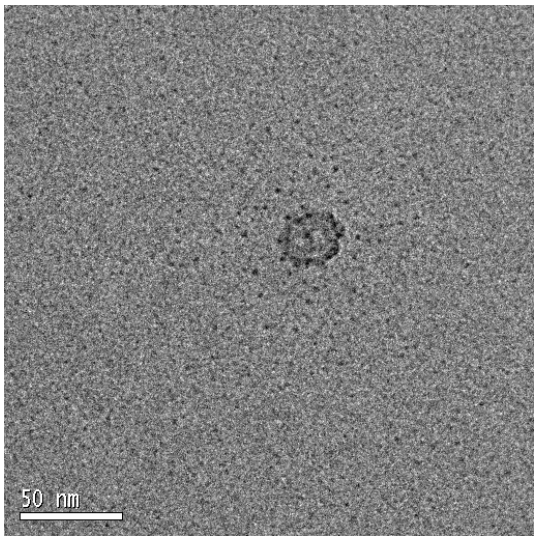

(g) Ag 4

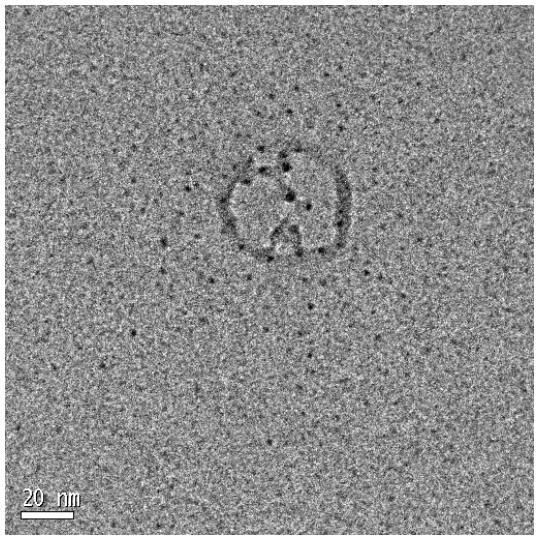

(h) Ag 4

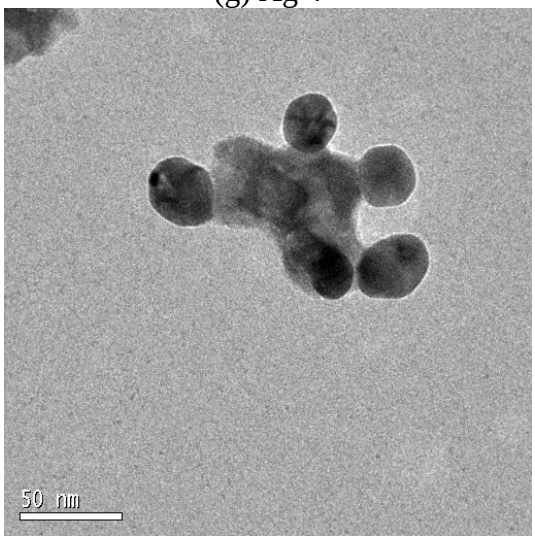

(i) Ag 5

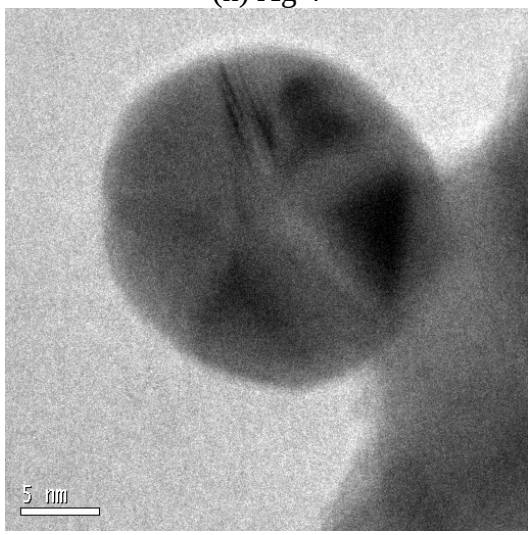

(j) Ag 5

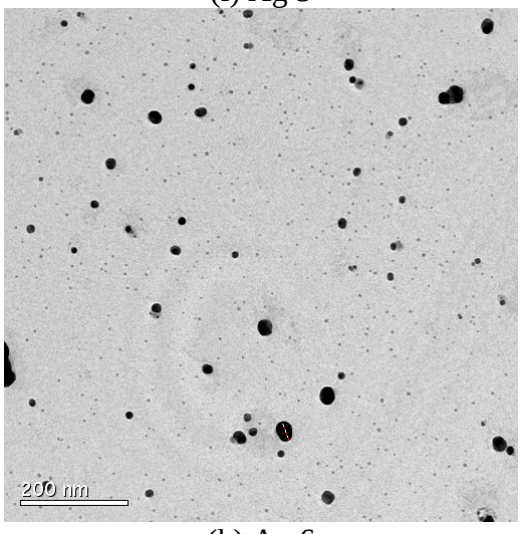

(k) Ag 6

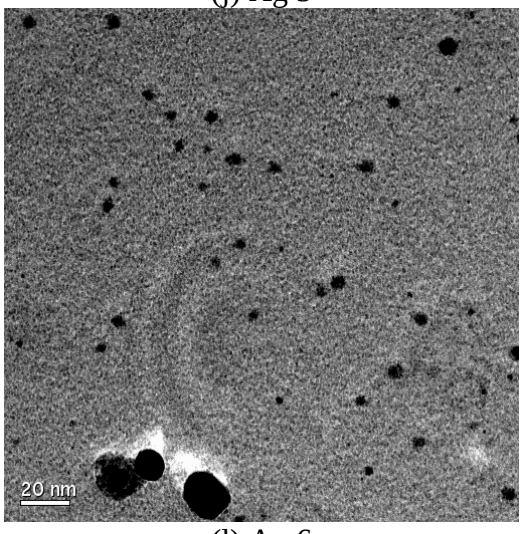

(l) Ag 6

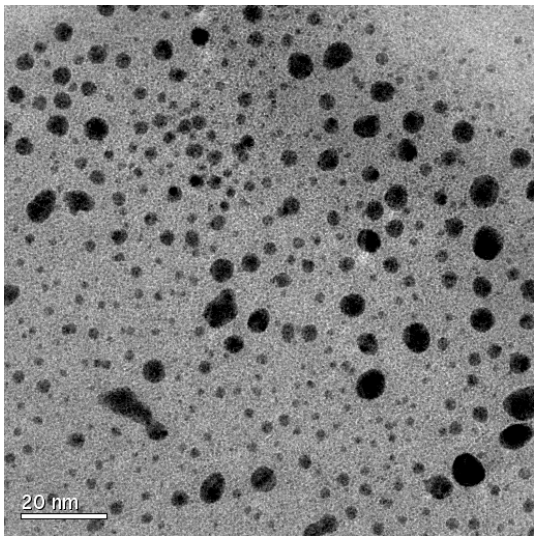

(m) Ag 7

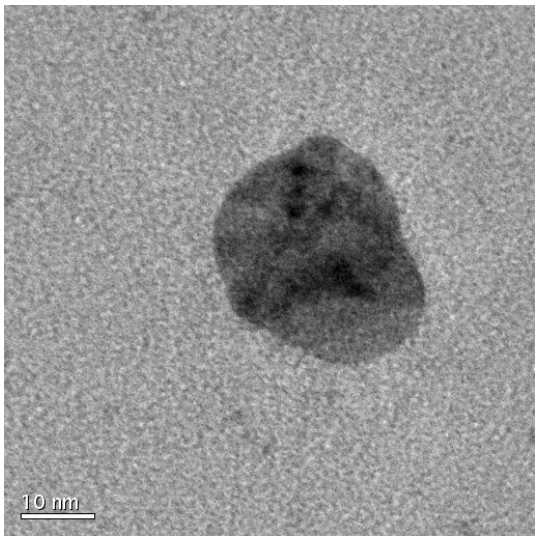

(n) Ag 7

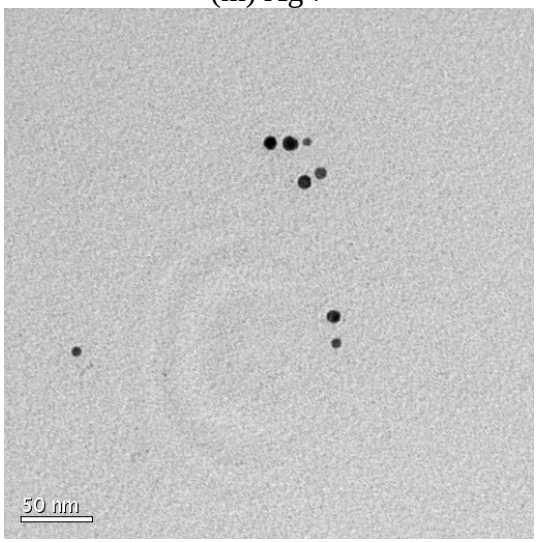

(o) Ag 7, after centrifugation

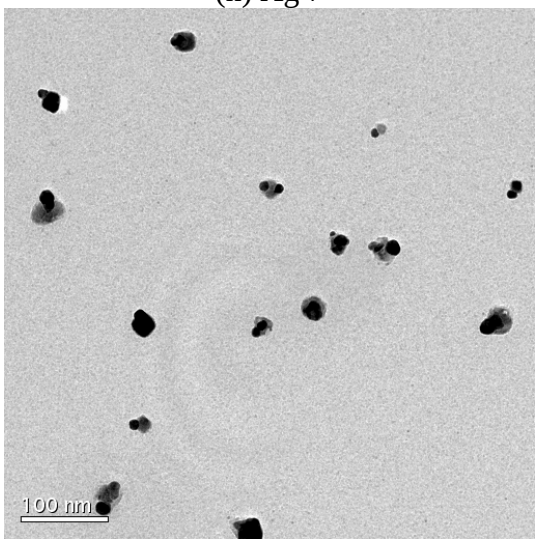

(p) PAA in MeOH and reduced with $NaBH_4$ at r. t.

Figure 3-13. TEM of the silver nanoparticles

Silver NPs obtained from $PG_{36}(PAA_{16})_{16}$ (Figure 3-13, i, j) show a smaller size compared with Ag 2 (Figure 3-13, a, b). This indicates that the size of the generated silver nanoparticles depends on the size, i.e., the molecular weight of the polymer.

For sample 7, AFM was also used to observe the particle sizes. It can be seen clearly that two distributions are present from Figure 3-14. Very small particles from DMF reduction are also present. Gradient ultra-centrifugation (Mr. Jianjun Wang from MPI-P Mainz was highly appreciated for the helping of ultra-centrifugation) was used to remove those smaller particles.[35] The TEM-image of the sample after ultra-centrifugation is shown in Figure 3-13, o. Compared with Figure 3-13, m, it can

be seen that the particles with smaller size have been successfully separated from the bigger ones.

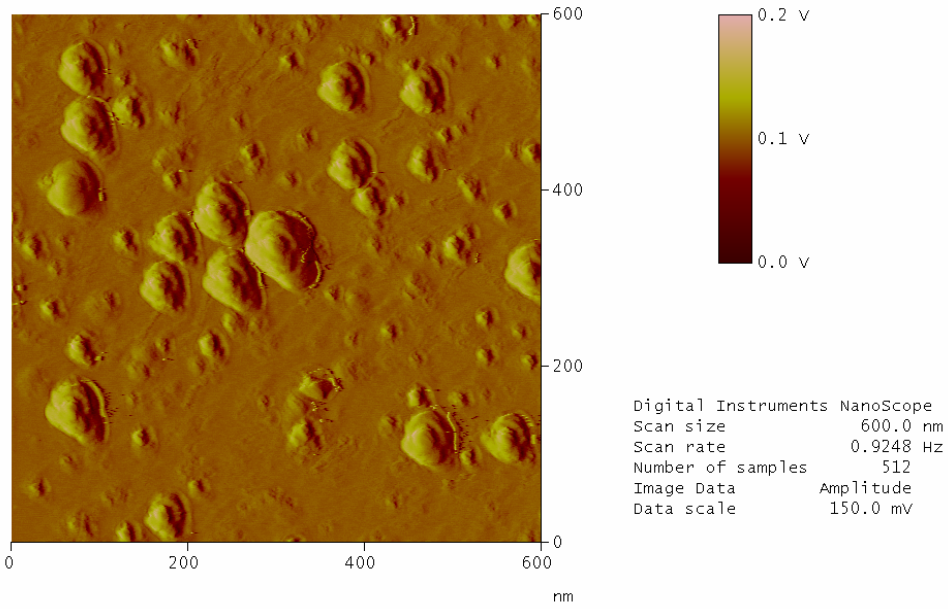

Figure 3-14. AFM image of the silver nanoparticles for sample Ag 7

Apart from DMF, $NaBH_4$ was also used as reducing agent to reduce Ag^+ and generate silver NPs. According to literature,[26] it is believed that NPs with small size can be obtained from this system. However, we did not observe a different size of the NPs prepared by this method. The obtained particles are in a similar size range (20-30 nm) as those particles produced by DMF reduction, which indicates the sizes of the generated particles depend on the size of the star PAA used, rather than the reduction method used. Moreover, an obvious difference can also be observed: the smaller size silver NPs generated in DMF reduction were not observed here. (See Figure 3-13, p)

3.2.3. Using star PAA as template for synthesizing silver nanoclusters

Metal nanoclusters, consisting of several to some tens of atoms, typically possess sizes less than two nanometers. The space confinement of free electrons in metal nanoclusters results in size-dependent discrete energy levels, thus causing molecular-like properties, such as strong fluorescence.[24, 25] The extremely small size and fluorescence properties have made metal nanoclusters excellent candidates as bio-imaging labels.[37] The catalytic activity of metal nanoclusters has also been

extensively investigated.[24] Recently, Dickson and coworkers demonstrated that Ag nanoclusters can significantly enhance the Raman scattering of scaffold molecules, which opened new application possibilities for metal nanoclusters.[38] Motivated by their broad application perspectives, research efforts dedicated to metal nanoclusters[32, 39-43] have gone beyond the early focus on gas-phase based preparation methods and mere characterization.[44, 45] Recent advances in the template-based synthesis of metal nanoclusters have led to highly fluorescent, water-soluble metal nanoclusters.[32, 39-41] Using poly(amidoamine) (PAMAM) dendrimers and DNA as templates, Dickson et. al. prepared photostable and water-soluble Ag or Au nanoclusters.[39, 40] Taking advantage of the same concept, Kumacheva and coworkers recently reported the successful generation of fluorescent Ag nanoclusters in hydrogel-microspheres by photoreduction.[32] These developments are crucial both for fundamental studies and eventual technical application of metal nanoclusters in biological environments. However, the demands to further define the structure-property relationships and applications in complex environments necessitate new synthetic methods to create such materials.

In this section, we present a novel approach towards water-soluble fluorescent Ag nanoclusters, which relies on multiarm star polyglycerol-*b*-poly(acrylic acid) (PG-b-PAA) as templates. Such unusual polymers represent in fact the single macromolecular analog of nanosize hydrogel particles. The narrowly distributed multi-arm star branched PG-*b*-PAAs (M_w/M_n = 1.20-1.30) are synthesized as describe in Chapter 2, followed by hydrolysis of the *t*-butyl group using CF_3COOH as cleaving agent.[10] The relevant structure parameters of the PG-b-PAA samples used in this chapter are summarized in Table 3-4.

Table 3-4. Star PAA and Linear PAA

Sample	Arm numbers	Arm Length [a]	PDI [b]
S1	36	35	1.20
S2	36	21	1.30
S3	6	38	1.18
L4	1	28	-

[a] Calculated from ^{1}H-NMR, [b] Calculated from precursor

It is well-known that charged carboxyl groups exhibit a strong affinity to Ag ions. Our results in the previous section also support this. This concept has been widely used to immobilize Ag-ions on carboxyl group-rich materials to serve as Ag source for further reduction reactions.[35, 46] For example, Kumacheva et al[32] reported that the uptake of Ag ions by the PAA moiety in microgels is critical for the successful preparation of Ag nanoclusters. Our work described in section 3.2.2 also leads to this result.

On the other hand, the core-shell structure of the PAMAM dendrimers has been suggested to result in a "cage effect", which provides enhanced stability for metal nanoclusters and prevents continuing growth of nanoclusters to larger NPs.[39] The multi-arm PG-b-PAA polymers (Scheme 3-1) exhibit a core-shell structure with dense PAA grafts, and the local density of carboxyl group may be viewed to gradually decrease from core to shell, which is likely to lead to a "cage effect". Based on the analysis above, it is obvious that the structure of PG-b-PAA may be useful as a template for Ag nanoclusters synthesis as a "molecular hydrogel".

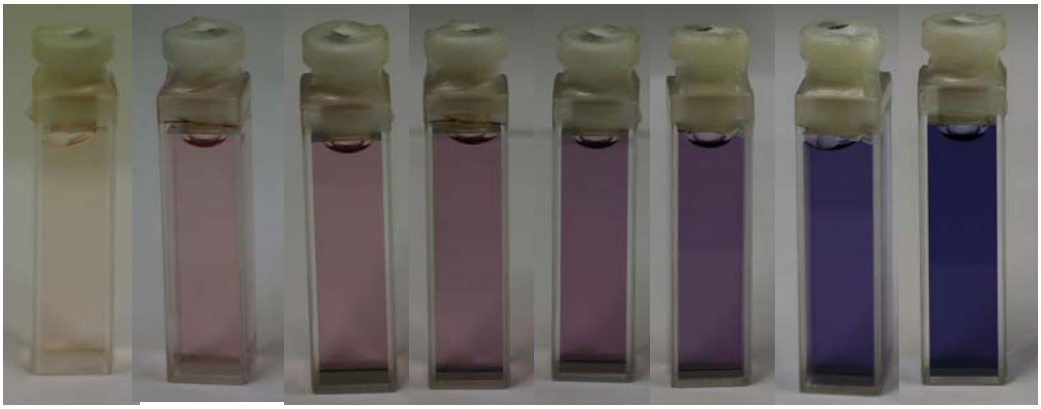

Figure 3-15. Photograph of the solutions after UV exposure, from left to right are 30, 100, 120, 160, 200, 300, 440, 540 min, respectively.

To prepare Ag-nanoclusters, a freshly prepared aqueous 0.1 M $AgNO_3$ solution was dropwise added into a solution of polymer S1 (0.1 M) under stirring. The molar ratio of AA groups to Ag^+ ions was 2:1. The system was mixed for half an hour and then dialyzed against Millipore water to remove traces of free ions. The subsequent photo-reduction was carried out under UV-irradiation at λ = 365 nm for various time intervals. In the course of nine hours irradiation time, the solution color gradually changed from colorless to light pink, then to purple and finally to dark violet (as shown

in Figure 3-15). Figure 3-16 shows absorption spectra of the solution of polymer S1 with Ag^+ ions after UV irradiation for different periods of time. Before irradiation, the initial S1-Ag^+ solution showed no absorption in the range of 300-700 nm. After 10 min UV-irradiation, a peak centered at 500-520 nm appeared, and further irradiation led to an increase of peak intensity. However, no obvious peak shift was observed, until UV-irradiated for 200 min. The absorption peak at 500-520 nm is associated with Ag_n nanoclusters with n from 2 to 8 atoms, and has also been observed in Ag nanoclusters prepared by templating with DNA[41] and hydrogel microspheres[32]. After 200 min, the absorption peak shifted to longer wavelength (560-580 nm), which should result from the complexation of acrylate acid residues with Ag nanoclusters.[32, 46] This increase in adsorption intensity and red-shift of the absorption peak indicate the generation of Ag nanoclusters under prolonged illumination.

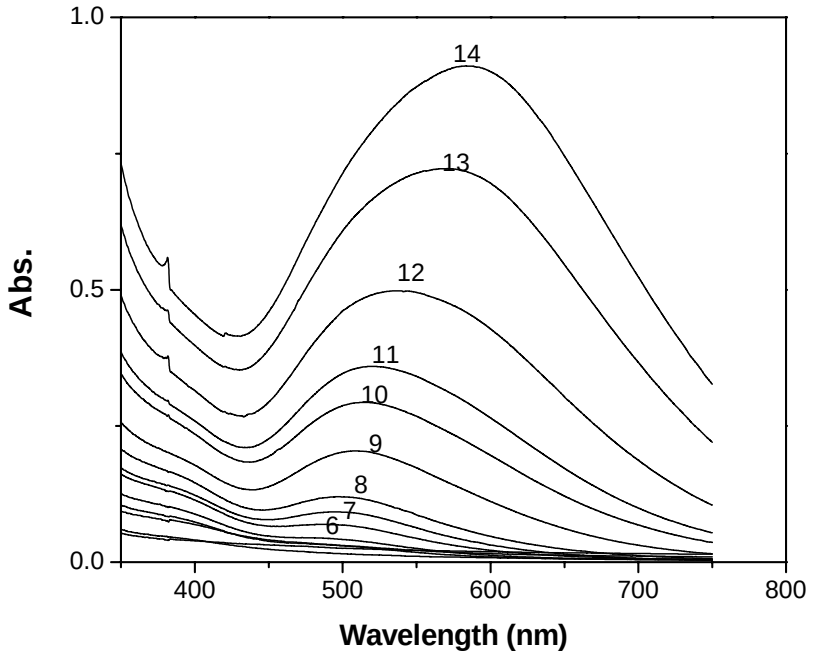

Figure 3-16. UV-Vis spectra of the S1-Ag nanocluster solution after different periods of UV irradiation, in minutes: 1) 0; 2) 5; 3) 10; 4) 15; 5) 20; 6) 30; 7) 40; 8)60; 9)100; 10) 160; 11) 200;12) 300; 13) 440; 14) 540;

We noticed that after 10 min irradiation the reaction mixture of the polymer S1 and Ag^+ ions became photoluminescent (Figure 3-17 and 3-20). 10-200 min irradiation led to an emission peak centering at about 590 nm, spanning the wavelength range of 450-750 nm. The emission spectra of the Ag nanoclusters formed are similar to the

Ag_2-Ag_8 nanoclusters obtained in hydrogel microspheres,[32] agreeing well with our analysis on absorption spectra of corresponding nanoclusters. All of these spectra exhibit a shoulder peak at about 690 nm, which indicates the presence of a distribution of Ag nanoclusters with different association numbers.

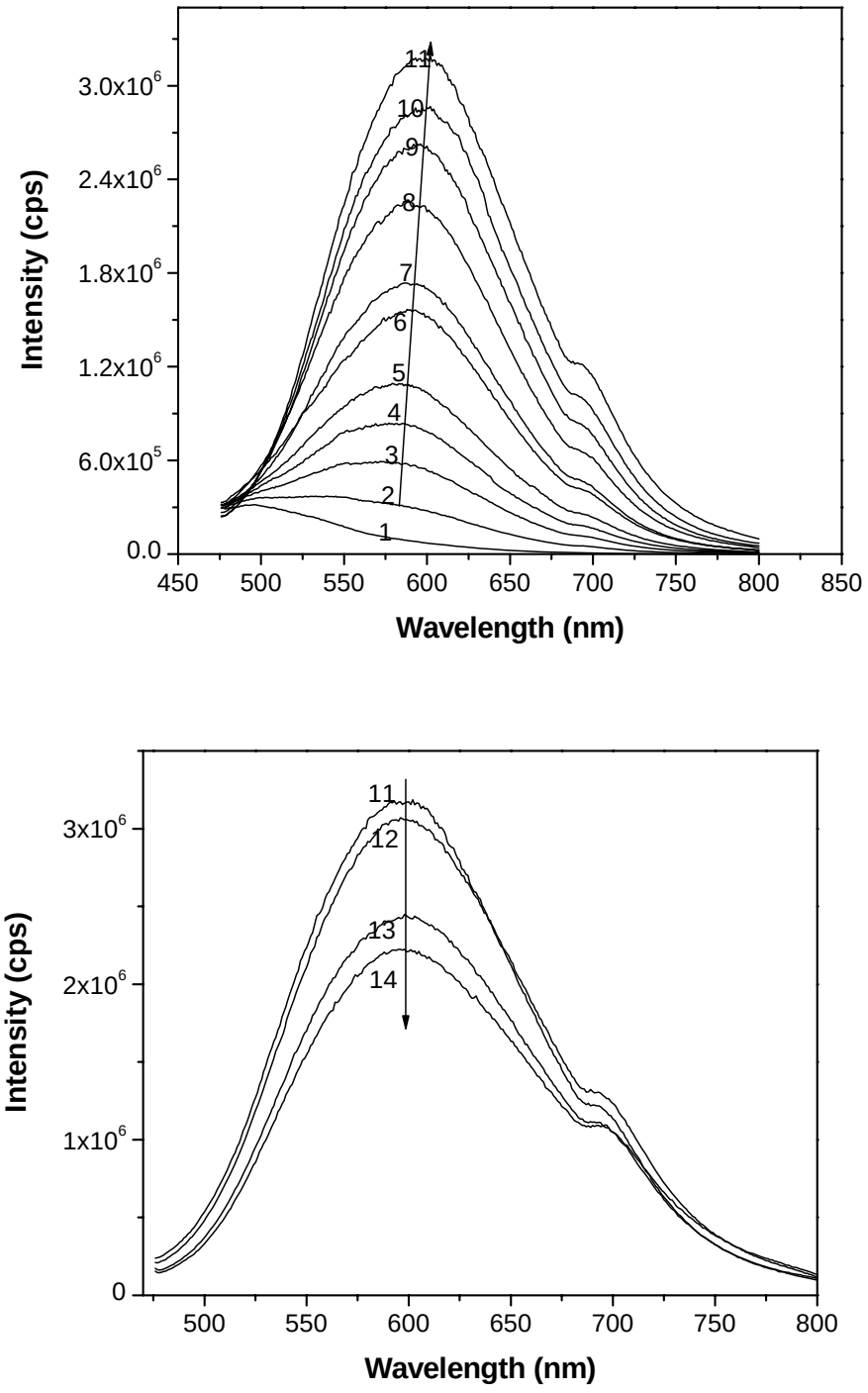

Figure 3-17. Fluorescence spectra of the S1-Ag nanocluster solutions after different periods of UV irradiation, in minutes: 1) 0; 2) 5; 3) 10; 4) 15; 5) 20; 6) 30; 7) 40; 8)60; 9)100; 10) 160; 11) 200;12) 300; 13) 440; 14) 540;

Note that extending the irradiation time up to 200 min gave rise to a gradual increase of the fluorescence intensity, which is consistent with Figure 1a on the sustaining generation of Ag nanoclusters in that time range. In our study, 200 min irradiation time led to the maximum photoluminescence intensity, as shown in Figure 3-18, however, additional 100 min illumination only slightly diminished the emission of the Ag nanoclusters, suggesting excellent photostability of the nanoclusters. It is worth mentioning that even exhaustive UV irradiation (up to nine hours) did not lead to complete disappearance of the fluorescence of the hybrid system in our experiments.

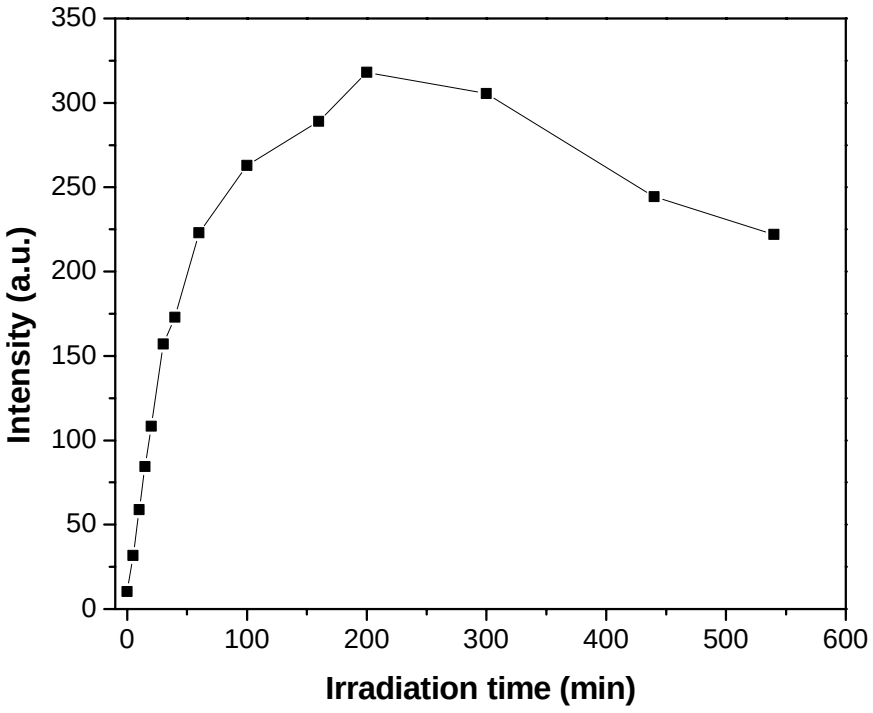

Figure 3-18. Fluorescence intensity of the S1-Ag nanoclusters *vs* UV-irradiation time.

In contrast, the fluorescence of Ag nanoclusters in hydrogel microspheres has been reported to disappear completely after 100 min illumination, which resulted in large Ag NPs (>2 nm), exhibiting a strong plasmon band adsorption around 400 nm.[32] The improved photostability of the Ag nanoclusters is tentatively explained by the higher AA segment density of the multi-arm star PG-*b*-PAA in comparison to the less dense hydrogel networks, which leads to a more pronounced “cage effect” and thereby provides better protection of the nanoclusters against quenching in solution, but also appears to prevent further growth of nanoclusters by confining the nanoclusters generated in the “cages”.

Transmission electron microscopy (TEM) (Figure 3-19, a) shows that Ag NPs of 2-3 nm in diameter are present in the as-prepared nanocluster solution after 60 min irradiation. Further UV exposure will lead to aggregates (Figure 3-19, b) and silver dendrites. (Figure 3-19, c, d)

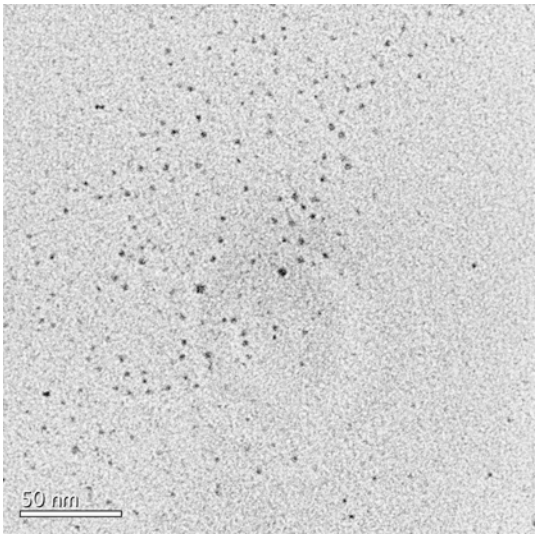

(a) 60 min

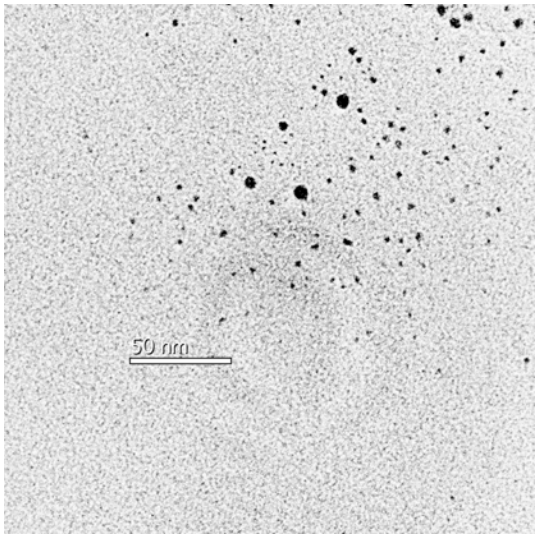

(b) 100 min

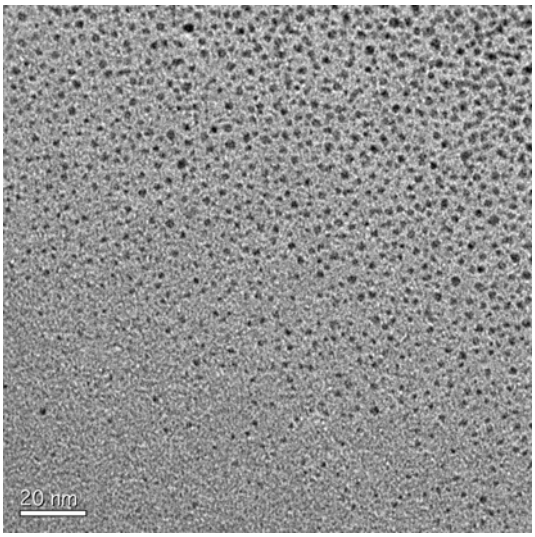

(c) 200 min

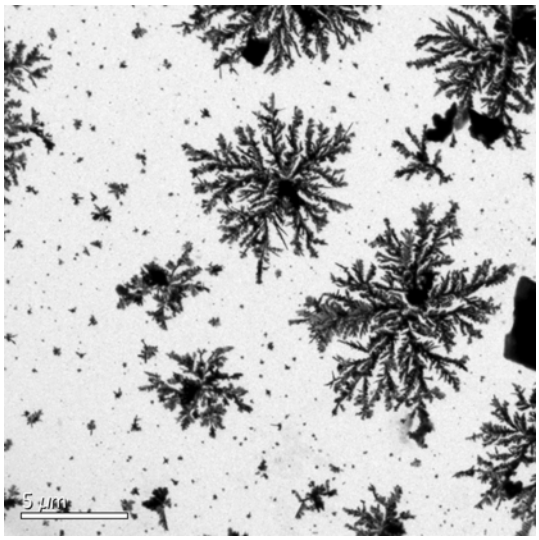

(d) 440 min

Figure 3-19. TEM-image of S1-Ag nanoparticles formed after irradiation.

However, as addressed above (Figure 3-18), the fluorescence of the reaction solution keeps increasing in the time range of 60-200 min of irradiation, indicating that the larger NPs (2-3 nm) do not have an obvious quenching effect on the fluorescence of the nanoclusters, which further supports our assumption concerning the stronger “cage effect” of multiarm star PG-*b*-PAA templates. It is important to mention that Ag

nanoclusters prepared in our studies remained luminescent over three months storage time. The photostability of such nanoclusters is a key issue for future application as bio-imaging labels, especially when long-term tracking becomes necessary.

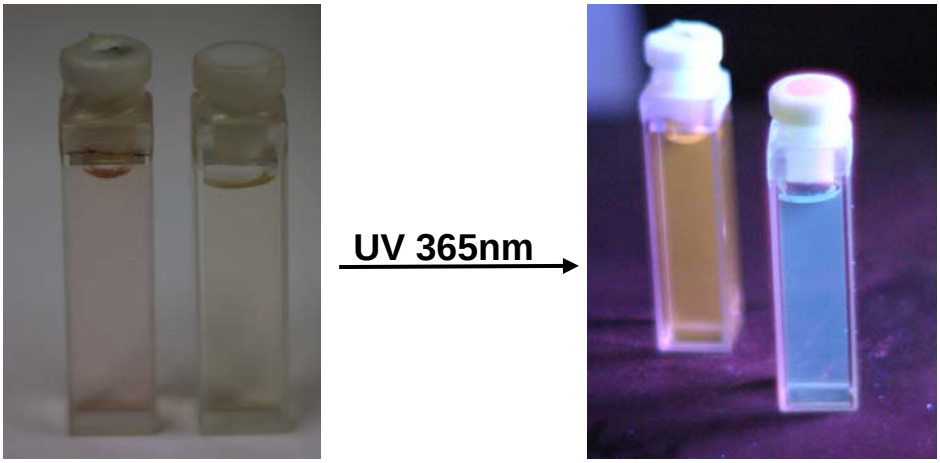

Figure 3-20. Photograph of the solution after 30 min UV exposure, and a photograph of the solution (excited at 365nm), in each photo, left is S1-Ag, right S2-Ag.

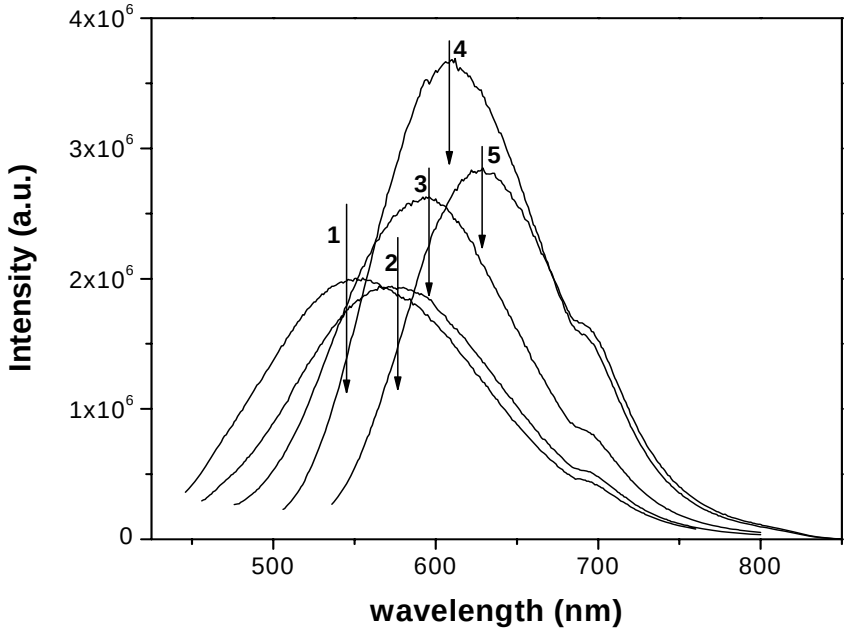

Figure 3-21. Fluorescence spectra of S1-Ag nanocluster-solution excited at different wavelengths (1) 410 nm, (2) 430 nm, (3) 450 nm, (4) 480 nm, (5) 510 nm.

Figure 3-21 shows the emission spectra of S1-Ag nanocluster solutions at various excitation wavelengths. In cases of excitations between 410 and 510 nm, the maximum emission is observed at an excitation wavelength of 480 nm. An increase of

the excitation wavelength gives rise to a red-shift of the emission maximum, which further confirms the presence of a distribution of nanoclusters with different numbers of Ag atoms in the star branched PG-*b*-PAA polymer structure. Dickson and coworkers also observed the same trends in a recent work, when using DNA as templates for Ag nanocluster synthesis.[41]

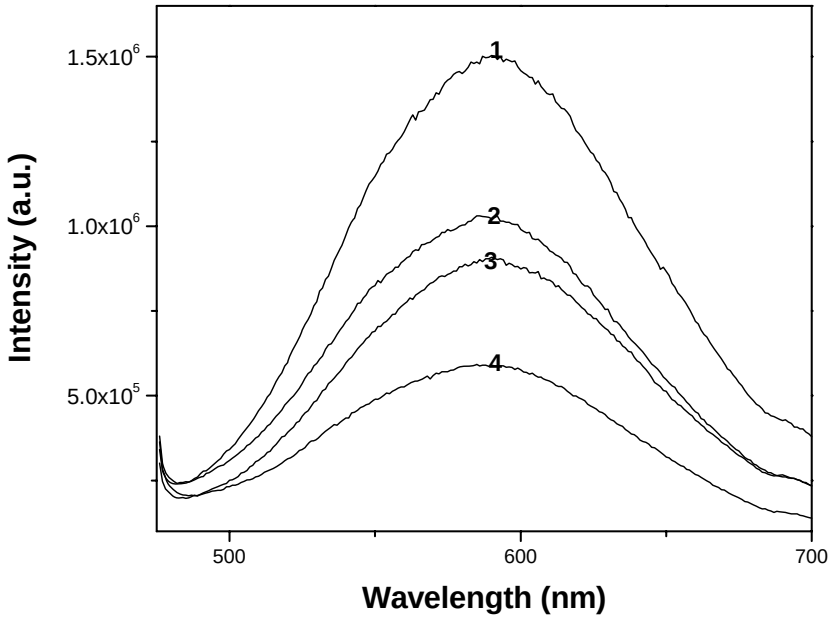

Figure 3-22. Fluorescence spectra of S1-Ag nanoclusters prepared at different $AgNO_3$ concentration and various irradiation time: (1) $[Ag^+]/[AA]$ = 1:2 at 90 min, (2) $[Ag^+]/[AA]$ = 2:1 at 60 min, (3) $[Ag^+]/[AA]$ = 1:4 at 90 min, (4) $[Ag^+]/[AA]$ = 1:4 at 60 min.

The initial stoichiometry of Ag^+: AA has a strong influence on the generation rate of Ag nanoclusters. When the concentration of Ag^+ was reduced from $1Ag^+$:2AA to $1Ag^+$:4AA, the fluorescence intensity of an Ag nanocluster solution decreased to 50% after the same irradiation time (60 and 90 min), as shown in Figure 3-22. However, the emission spectra of the resulting nanoclusters remained unchanged, which suggests that the structure of S1 is in favor of Ag nanoclusters with a defined stoichiometry. This actually is a strong evidence of the presence of "cage" structures of a certain size in this template. This point is further confirmed, when one uses PAA S2, which possesses the same arm numbers, but shorter arm length to produce Ag nanoclusters. Under the exact same conditions, the shorter-armed PAA (S2) template results in nanoclusters with a

maximum emission at ca. 500 nm (Figure 3-23), which obviously are of smaller size compared to the nanocluster prepared in the S1 template.

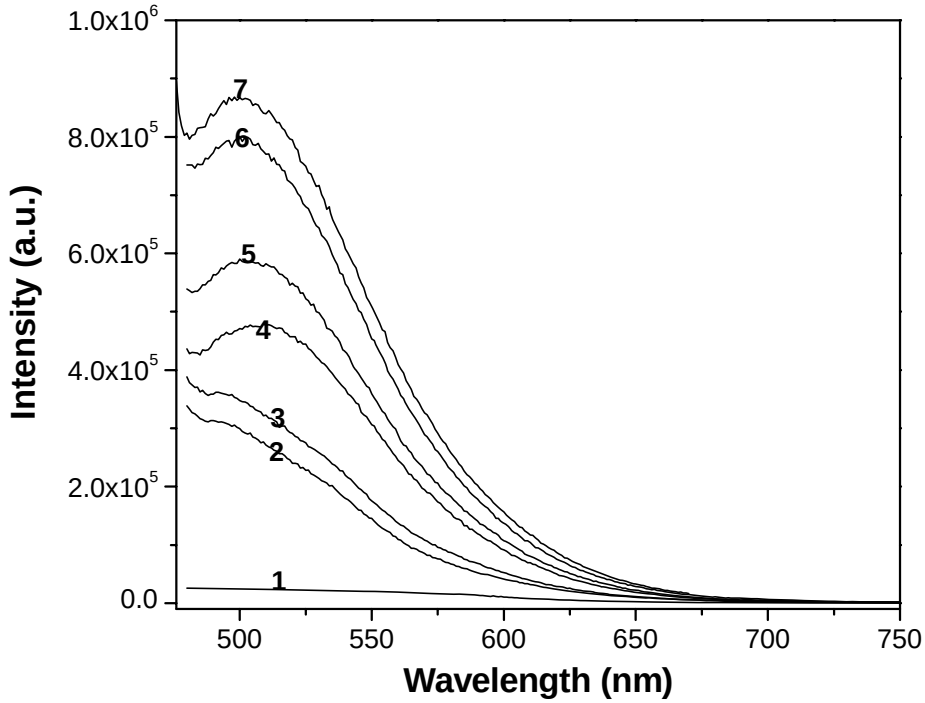

Figure 3-23. Fluorescence spectra of the S2-Ag nanocluster solution after UV-irradiation for different time intervals: (1) 0, (2) 1, (3) 20, (4) 120, (5) 220, (6) 310, (7) 400 min.

Further efforts will be devoted to the elucidation of a correlation between the central structure parameters (e.g., arm number and arm length) of the multi-arm star PG-*b*-PAA and the size and properties of the nanoclusters formed. Preliminary results show that the model star polymers PAA S3 with 6 arms and linear PAA L4 did not lead to fluorescent nanoclusters, thus confirming the importance of high AA segment density for the successful generation of fluorescent Ag nanoclusters.

3.3. Conclusion

Solution viscosity measurements in water demonstrate that the star PAAs show typical polyelectrolyte behavior characterized by an increase of the reduced viscosity at low concentration range, and no minimum apparent molar mass is needed to display a polyelectrolyte effect.

An empirical intrinsic viscosity was calculated using the Fuoss equations. The calculated intrinsic viscosity is in the range of 14.40 and 26.60 ml/g. The overlap concentration [C*] can also be obtained in the range of 37.6 mg/ml to 69.4 mg/ml.

The viscosity of the star PAAs measured in buffer solutions also shows typical polyelectrolyte behavior. Under this situation, star PAA is a charged spherical colloid. AFM measurements provided support for the formation of charged spherical colloids. The average size of these structures is around 30 nm. The polyelectrolyte behavior was suppressed in 1 M NaCl solution.

Silver nanoparticles can be obtained using star PAA as template, reducing with either DMF or $NaBH_4$. The size of the obtained NPs depends on the size of the star PAA used.

The nanoclusters obtained from star PAA template via UV-reduction show fluorescent properties. The "cage effect" associated with densely grafted PAA and strong binding of protonated AA groups with Ag^+ are two essential factors for the formation of the fluorescent nanoclusters. The fluorescent properties show both arm-density dependence and arm length dependence. It can be expected that stable fluorescent nanoclusters will represent an interesting alternative to quantum dots as a new class of fluorescent labels,[30, 47, 48] favored by the extremely small size,[37] stability and biocompatibility of these materials.

3.4. Experimental

3.4.1. Materials

Linear PAA was purchased from Aldrich (molecular weight 2000). Star PAAs are synthesized as described in Chapter 2. All other materials were purchased from common suppliers and used as received, unless otherwise stated.

3.4.2. Potentiometric Titration

Potentiometric titrations of PAA stars were carried out at crude mass concentrations of 0.5 g /L in order to determine the degree of neutralization at room temperature. The titration was carried out with 0.05 M NaOH. The volume change does not exceed 20%. An EcoScan hand-held series pH meter was used to determine the pH of the solution, and was calibrated by buffer solutions at pH = 7.00 and 4.00. The α-value, which is imprecise, since it is difficult to obtain completely water-free

star PAA, was calculated according to the NaOH added. Adsorbed water can reduce the molar carboxyl concentration by up to 20% according to literature.

3.4.2. Preparation of the buffer solutions

PH = 7: Dissolve 0.12 g NaH_2PO_4 in approx. 90 ml of Milipore water, titrate to pH 7.02 at r.t, with 0.01M NaOH or HCl solution. The solution was then dilute to 100 ml.

PH = 8: Dissolve 0.121 g of Tris base (Tris(Hydroxymethyl)aminomethane) in approx. 90 ml of Milipore water. Titrate to pH 8.28 with NaOH or HCl. The solution was then dilute to 100 ml.

PH = 9: Dissolve 0.121 g of Tris base (M = 121.14) in approx. 90 ml of pure water. Titrate to pH 9.28 at room temperature with NaOH or HCl. The solution was then dilute to 100 ml.

3.4.3. Preparation of Ag NPs using DMF as reducing agent

An aqueous solution of PAA was prepared. A fresh Ag^+ solution containing 10 wt% $AgNO_3$ and 6% ammonium hydroxide was also prepared. Then the two solutions were mixed according to different [AA]:[Ag^+] ratios. Briefly, 100 mg $PG_{36}(PAA_{22})_{36}$ and 80 mg $AgNO_3$ (1:0.4) solution were mixed. Afterwards, 60 ml of DMF were introduced. The solution was kept in an oil bath at 40 ^oC with stirring. Within 8-12 min, the solution color changed from yellow through red to purple, after further aging for 24 hours, some of the sample solutions turned into dark blue due to aggregation while others did not change color. The products were kept at 4 ^oC.

3.4.4. Preparation of Ag NPs using $NaBH_4$ as reducing agent

MeOH solution of $PG_{36}(PAA_{22})_{36}$ was first prepared, [AA] = 0.1 M, then mixed with freshly prepared aqueous $AgNO_3$ solution, 0.1 M. ([AA]:[Ag^+] = 1:0.4), fresh $NaBH_4$ solution in MeOH 0.1 M was quickly introduced. (must be very quick) The solution was kept at room temperature with vigorous stirring and aged for 24 hours.

3.4.5. Prepare Ag nanocluster under UV reduction

The obtained star PAAs were neutralized with equivalent NaOH (adjust the PH to around 8) and dialyzed against de-ionized water to remove traces of low molecular

weight impurities. The typical procedure to prepare the photoluminescent Ag nanoclusters includes the following steps: Preparation of 2 ml of PG-*b*-PAA-Ag^+ solution with different [AA]:[Ag^+] ratio (2:1, 4:1), by mixing $AgNO_3$ (0.1 M) and PG-*b*-PAA (AA unit 0.1 M) solutions under stirring. The solution was kept for 30 min first, then it was dialyzed for 2 days against de-ionized water. The solution was then diluted to 4 ml and transferred into a fluorescence cuvette with a PTFE lid, the solutions are subject to UV exposure (Vilber Lourmat, France, Model VL-6.LC, 6 W, an average UV intensity of 0.5 mW cm^{-2}) to produce Ag nanoclusters.

3.5. References

[1] Roovers, J.; Zhou, L.-L.; Toporowski, P. M.; Zwan, M. v. d.; Iatrou, H.; Hadjichristidis, N. *Macromolecules* **1993,** 26, 4324.
[2] Förster, V. A. S.; Müller, A., H. E. *Adv. Polym. Sci.* **2004,** 166, 173.
[3] Förster, S.; Schmidt, M. *Adv. Polym. Sci.* **1995,** 120, 51.
[4] Park, I. H.; Choi, E., J. *Polymer* **1996,** 37, 313.
[5] Clasen, C., *Viscosimetry of Polymers and Polyelectrolytes, Chap. 6*. Springer-Verlag: Berlin-Heidelberg, 2004.
[6] Ydens, I.; Moins, S.; Degee, P.; Dubois, P. *Eur. Polym. J.* **2005,** 41, 1502.
[7] Okubo, T. *J. Chem. Phys.* **1987,** 87, 6733.
[8] Moinard, D.; Borsali, R.; Taton, D.; Gnanou, Y. *Macromolecules* **2005,** 38, 7105.
[9] Furukawa, T.; Ishiyu, K. *Macromolecules* **2005,** 38, 2911.
[10] Plamper, F. A.; Becker, H.; Lanzendoerfer, M.; Patel, M.; Wittermann, A.; Ballauff, M.; Müller, A. H. E. *Macromol. Chem. Phys.* **2005,** 206, 1813.
[11] Klein Wolterink, J.; van Male, J.; Cohen Stuart, M. A.; Koopal, L. K.; Zhulina, E. B.; Borisov, O. V. *Macromolecules* **2002,** 35, 9176.
[12] Antoneietti, M.; Briel, A.; Foester, S. *J. Chem. Phys.* **1996,** 105, 7795.
[13] Nishida, K.; Kiriyama, K.; Kanaya, T.; Kaji, K.; Okubo, T. *J. Polym. Sci. Polym. Phy.* **2004,** 42, 1068.
[14] de Robillard, Q.; Guo, X.; Ballauff, M.; Narayanan, T. *Macromolecules* **2000,** 33, 9109.
[15] Fuoss, R. M.; Strauss, U. P. *J. Polym. Sci.* **1948,** 3, 246.
[16] Lauw, Y.; Leermakers, F. A. M.; Cohen Stuart, M. A.; Borisov, O. V.; Zhulina, E. B. *Macromolecules* **2006,** 39, 3628.
[17] Miura, N.; Dubin, P. L.; Moorefield, C. N.; Newkome, G. R. *Langmuir* **1999,** 15, 4245.
[18] van Duijvenbode, R. C.; Rajanayagam, A.; Koper, G. J. M.; Baars, M. W. P. L.; de Waal, B. F. M.; Meijer, E. W.; Borkovec, M. *Macromolecules* **2000,** 33, 46.
[19] Guo, X.; Ballauff, M. *Langmuir* **2000,** 16, 8719.
[20] Hariharan, R.; Biver, C.; May, J.; Russel, W. B. *Macromolecules* **1998,** 31, 7506.
[21] Magonov, S. N. *Encyclopedia of Analytical Chemistry* **2000**, 7432.
[22] Schnitter, M.; Engelking, J.; Heise, A.; Miller, R. D.; Menzel, H. *Macromol. Chem. Phys.* **2000,** 201, 1504.
[23] Elias, H. G., *Makromoleküle:physikalische Strukturen und Eigenschaften*. Wiley: New York, Weinheim, 2001.
[24] Schmid, G. *Chem. Rev.* **1992,** 92, 1709.

[25] Lee, T. H.; Gonzalez, J. I.; Zheng, J.; Dickson, R. M. *Acc. Chem. Res.* **2005,** 38, 534.
[26] Bönnemann, H.; Richards, M. R. *Eur. J. Inorg. Chem.* **2001**, 2455.
[27] Xia, Y.; Yang, P.; Sun, Y.; Wu, Y.; Mayers, B.; Gates, B.; Yin, Y.; Kim, F.; Yan, H. *Adv. Mater.* **2003,** 15, 353.
[28] Daniel, M. C.; Astruc, D. *Chem. Rev.* **2004,** 104, 293.
[29] Cushing, B. L.; Kolesnichenko, V. L.; O'Connor, C. J. *Chem. Rev.* **2004,** 104, 3893.
[30] Chan, W. C. W.; Nie, S. M. *Science* **1998,** 281, 2016.
[31] Crooks, R. M.; Zhao, M.; Sun, L.; Chechik, V.; Yeung, L. K. *Acc. Chem. Res.* **2001,** 34, 181.
[32] Zhang, J.; Xu, S.; Kumacheva, E. *Adv. Mater.* **2005,** 17, 2336.
[33] Chen, S.; Fan, Z.; Carroll, D. L. *J. Phys. Chem. B* **2002,** 106, 10777.
[34] Kang, S. W.; Kim, J. H.; Ko, D. K.; Kim, C. K.; Won, J. *J. Polym. Sci. Polym. Phy.* **2004,** 42, 3344.
[35] Hao, E. C.; Kelly, K. L.; Hupp, J. T.; Schatz, G. C. *J. Am. Chem. Soc.* **2002,** 124, 15182.
[36] Pastoriza-Santos, I.; Liz-Marzan, L. M. *Langmuir* **1999,** 15, 948.
[37] Lesniak, W.; Bielinska, A. U.; Sun, K.; Janczak, K. W.; Shi, X. Y.; Baker, J. R.; Balogh, L. P. *Nano Lett.* **2005,** 2, 2123.
[38] Capadona, L. P.; Zheng, J.; Gonzalez, J. I.; Lee, T. H.; Patel, S. A.; Dickson, R. M. *Phys. Rev. Lett.* **2005,** 94, 058301.
[39] Zheng, J.; Dickson, R. M. *J. Am. Chem. Soc.* **2002,** 124, 13982.
[40] Zheng, J.; Petty, J. T.; Dickson, R. M. *J. Am. Chem. Soc.* **2003,** 125, 7780.
[41] Petty, J. T.; Zheng, J.; Hud, N. V.; Dickson, R. M. *J. Am. Chem. Soc.* **2004,** 2004, 5207.
[42] Jin, R. C.; Egusa, S.; Scherer, N. F. *J. Am. Chem. Soc.* **2004,** 126, 9900.
[43] Negishi, Y.; Tsukuda, T. *J. Am. Chem. Soc.* **2003,** 125, 4046.
[44] Ozin, G. A.; Mitchell, S. A. *Angew. Chem. Int. Ed.* **1983,** 22, 674.
[45] Morse, M. D. *Chem. Rev.* **1986,** 86, 1049.
[46] Henglein, A.; Giersig, M. *J. Phys. Chem. B* **1999,** 103, 9533.
[47] Bruchez, M.; Moronne, M.; Gin, P.; Weiss, S.; Alivisatos, A. P. *Science* **1998,** 281, 2013.
[48] Michalet, X.; Pinaud, F. F.; Bentolila, L. A.; Tsay, J. M.; Doose, S.; Li, J. J.; Sundaresan, G.; Wu, A. M.; Gambhir, S. S.; Weiss, S. *Science* **2005,** 307, 538.

Chapter 4. Synthesis of Multi-Arm Star Polyglycerol-*b*-Poly-2-(dimethylamino) ethyl methacrylate

4.1. Introduction

Multi-arm star polymers have evoked much interest because of their lower bulk and solution viscosities than their linear counterparts with the same molecular weight, [1-6] in addition to special functionality based on their core-shell structure.[7] Compared with micelles obtained from self-assembly of amphiphilic block copolymers, they are structurally stable against temperature, solvent and concentration variations.[8] In chapter 2, the routes to synthesize multi-arm star polymers have been summarized, either by core-first or arm-first methods. Following this introduction, the works using hyperbranched polyglycerol as the core molecule to generate multi-arm star branched PG-*b*-P*t*BA and PG-b-PAA polymers using the ATRP method were presented. As described in chapter 3, PAA is a polyelectrolyte. Here the work to generate cationic multi-arm star polymers using the ATRP method will be presented. The monomer used for polymerization is 2-(dimethylamino)-ethyl methacrylate (DMAEMA), a hydrophilic, positively ionizable monomer.

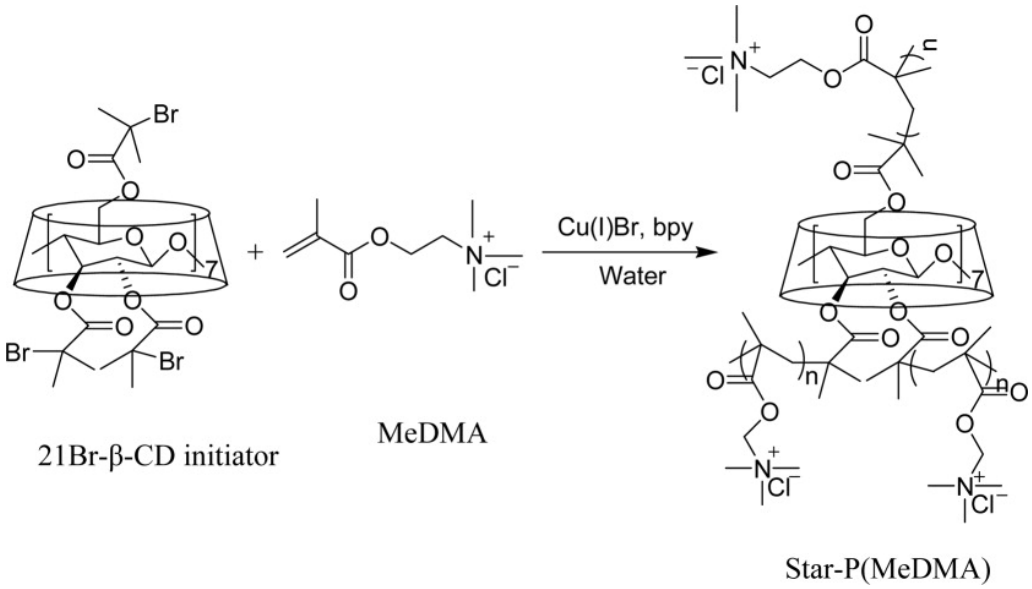

Scheme 4-1. A synthetic route of β-CD based star PDMAEMA

Matyjaszewski's group has reported the synthesis of linear PDMAEMA using ATRP and investigated the effects of ligands, solvents and temperature.[9] Their results show that the reaction in anisole at a relatively low temperature with HMTETA as

ligand can be well controlled. The obtained polymers possess a molecular weight distribution of 1.4.[9] Haddleton et al reported the synthesis of star PDMAEMA with 21 arms using β-cyclodextrin (β-CD) as core molecules,[10-12] where they obtained star polymers with rather narrow molecular weight distributions, 1.05 at low conversion. (below 29%) However, they did not look into the details of the polymerization control. Xiao et al later used the same β-CD based procedure to synthesize quaternized star PDMAEMA (as shown in Scheme 4-1), and they studied the control of polymerization in much more detail.[13] For most polymers they obtained, the distribution is around 1.3 at 60% conversion. The drawback of using β-CD as a core is that, in some cases, polymers with β-CD as core were more or less considered as brush polymers rather than star polymers (as shown in Scheme 4-2).

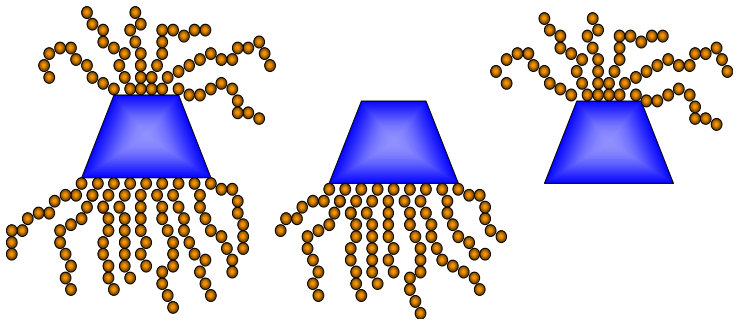

Scheme 4-2. β-CD based star polymers, from left to right, β-CD with 21, 14, 7 arms

In this chapter, the efforts dedicated to the synthesis of cationic multi-arm star polymers with more than 21 arms by the ATRP method will be discussed. As we described in chapter 2, using living radical polymerization to synthesize well-defined multi-arm star polymers with arm numbers exceeding 30 still represents a challenge, because the probability of radical-radical coupling during the polymerization increases dramatically with the increase in arm numbers.

Preliminary experiments related to possible applications of the obtained catonic star polymer will also be described.

4.2. Results and Discussion

4.2.1. Monomer/copper coordination

Haddleton recently reported the reactivities of a number of small monomers that would be expected to coordinate with the copper catalyst during ATRP.[14] They found

that the coordination between monomers or propagating radicals and the copper catalyst may affect the monomer reactivity by altering the electronic structure of the double bond, or simply through a "mass effect".[14] Trends in reactivities within the monomers appear to support this explanation, as the secondary amine shows the greatest deviation from free-radical reactivity ratios, while the most sterically hindered tertiary amine shows the least, suggesting that the extent of deviation is correlated with decreasing congestion around the nitrogen. Nevertheless, the interaction between the amines and copper will alter the monomer reactivity, which can be seen in Scheme 4-3.

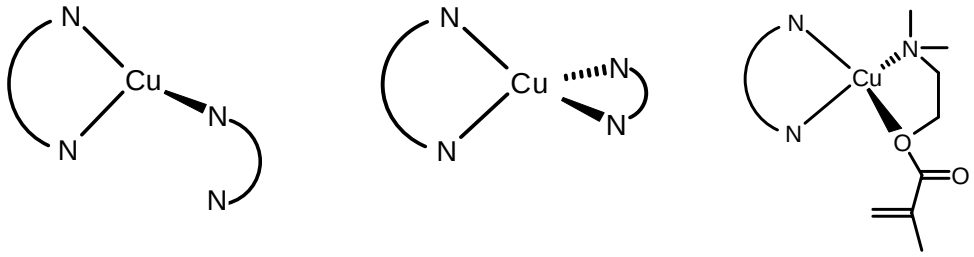

Scheme 4-3. Coordination between monomer and the copper catalyst

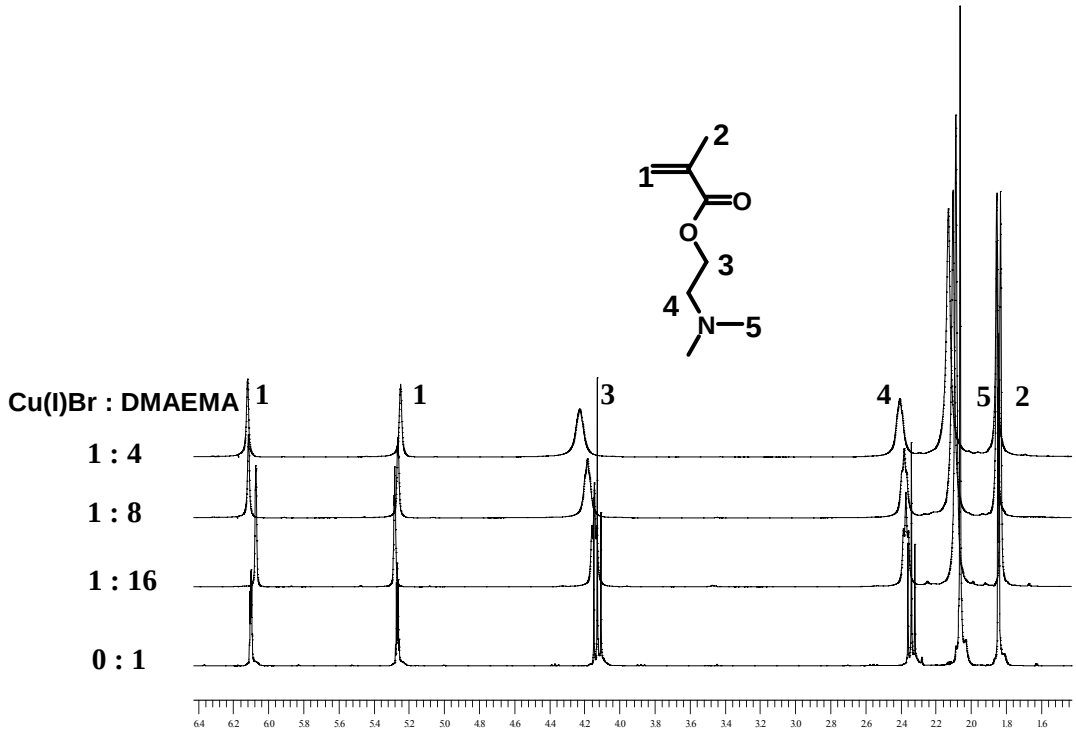

Figure 4-1. Chemical shifts with varying concentration of DMAEMA. (in d_8-toluene, 25 °C) from bottom to top: 1) free DMAEMA; 2) DMAEMA/CuBr 16:1; 3) DMAEMA/CuBr 8:1; 4) DMAEMA/CuBr 4:1, respectively.

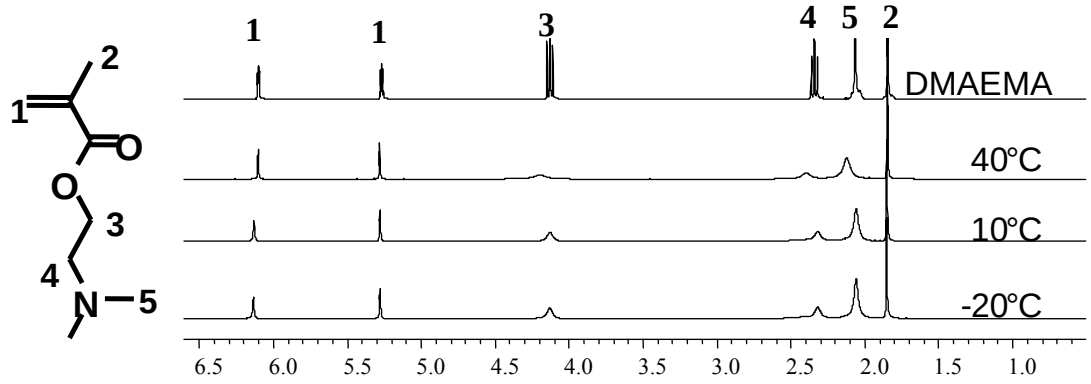

Figure 4-2. Chemical shifts of the complex DMAEMA /Cu(I)Br (4:1) in d_8-toluene at different temperatures.

NMR studies of the complex DMAEMA/Cu(I)Br at various ratios (Figure 4-1) and different temperatures (Figure 4-2) show a clear chemical shift: for DMAEMA/ Cu(I)Br at 16:1. One can observe that the chemical shift of the double bond hydrogen and the chemical shift of the complex display detail at lower temperature and show less information at 40 ^{o}C. This coordination effect cannot be observed with regard to the position of the IR absorptions of the carbonyl groups of the aminomethyl methacrylates in the presence of copper(I) bromide.

4.2.2. Synthesis of well-defined multi-arm star PDMAEMA

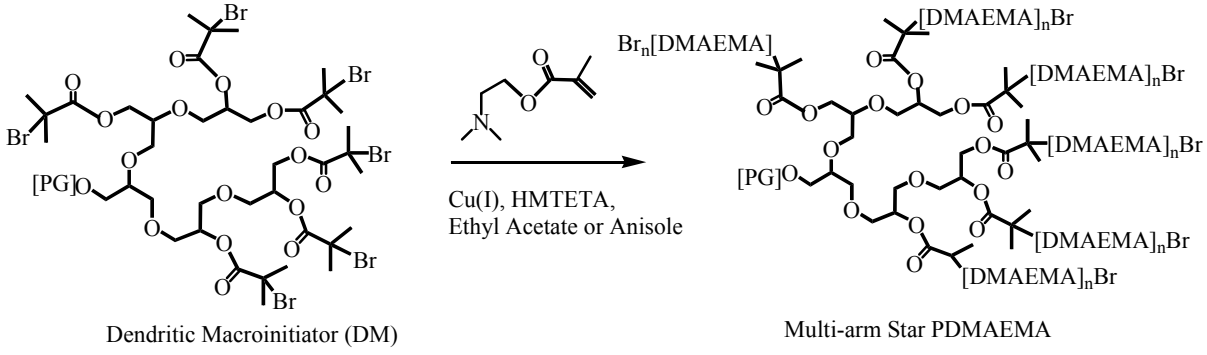

Scheme 4-4. Synthesis of multi-arm star PG-b-PDMAEMA

Well-defined multi-arm star P(DMAEMA) with 36 arms has been synthesized as described in Scheme 4-4, using P($G_{36}In_{36}$) as the initiator in either ethyl acetate or anisole, with CuBr/HMDETA as catalyst/ligand.

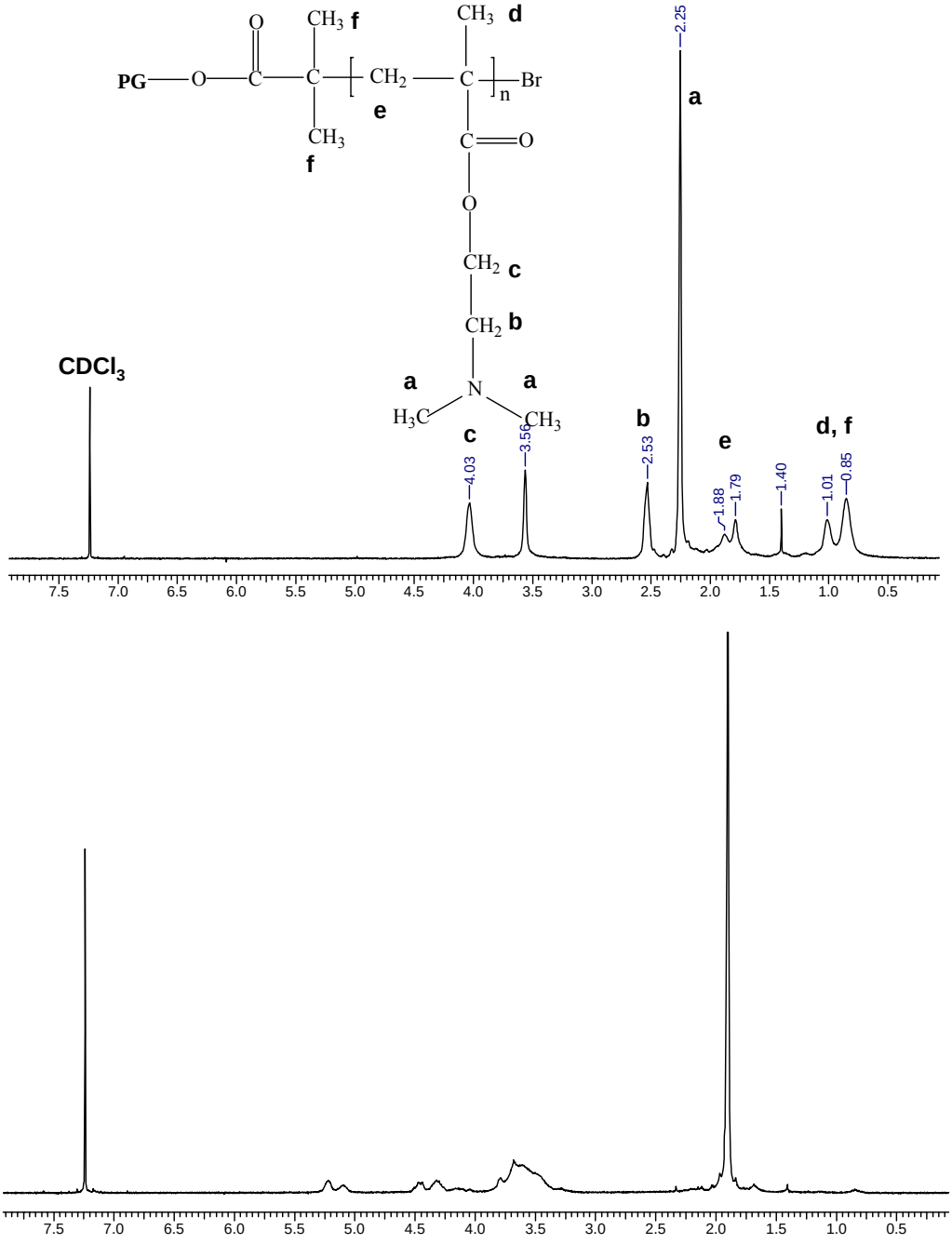

Figure 4-3. Comparison of the ^{1}H NMR spectra of macroinitiator P($G_{36}In_{36}$) (bottom) in $CDCl_3$ and multi-arm star PDMAEMA (top)

Figure 4-3 shows a comparison of the ^{1}H NMR spectra of macroinitiator P($G_{36}In_{36}$) and multi-arm star PDMAEMA and the respective peak assignments. From the spectra it can be seen that the resonance peaks of the PG core can not be detected after the polymerization. This is the same as in the case of the synthesis of P*t*BA (Refer to Figure 2-7) and PHEMA.[15]

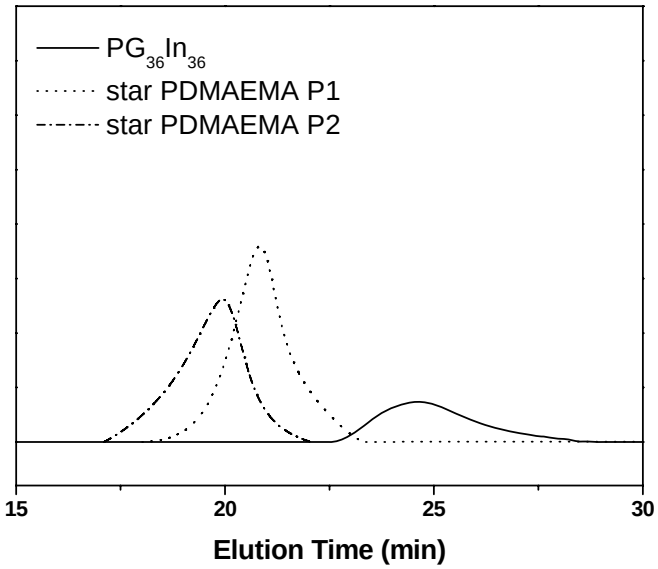

Figure 4-4. Comparison of the GPC traces in $CHCl_3$ of macroinitiator $P(G_{36}In_{36})$ multi-arm star PDMAEMA with 36 arms. ($M_{P1} = 3.82\times10^4$, PDI = 1.81; $M_{P2} = 7.26\times10^4$, PDI=1.91)

For GPC characterization, the samples were first measured in DMF. However, due to the strong interaction between the polymer and the column, there is a tail present in the GPC elution curve. In the literature, it was reported that PDMAEMA can be measured in DMF with additional TEA as eluent to eliminate the tail.[9, 16] Since we could not apply this method to our GPC, all the samples were measured in $CHCl_3$ instead. Figure 4-4 shows the typical GPC curves in chloroform of the obtained star polymers and a comparison with the initiator. The resulting data are listed in Table 4-1.

As discussed above, the monomer DMAEMA can coordinate with the Cu(I) catalyst, which would increase the local concentration of the co-monomer. To diminish this effect, a stronger ligand (compared with PMDETA), 1,1,4,7,10,10 hexamethyl triethylene tetraamine (HMTETA, structure is shown in Scheme 4-5),[9, 17] has been used for the ATRP of DMAEMA.

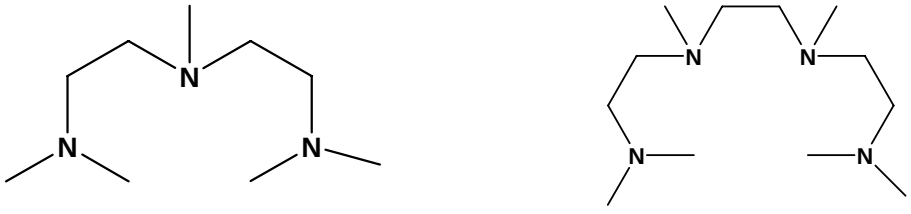

Scheme 4-5. Structure of PMDETA (left) and HMTETA (right)

Table 4-1. Preparation of multi-arms star PDMAEMA based on $P(G_{36}In_{36})$ macroinitiators in EtAc

No.	[M]:[I]:[Cu(I)]	*Temp* (^oC)	Time (min)	Conv.[a] (%)	$M_{n\ (gpc)}$[b] ($\times10^{-4}$)	M_w/M_n[b]	$M_{n\ (calc)}$[a] ($\times10^{-4}$)
$P(G_{36}In_{36})$					0.35	1.37	0.8
1	50: 1: 1	40	60	67	gel	-	-
2	50: 1: 0.4	40	30	9	-	-	3.34
3	50: 1: 0.4	40	40	14	1.79	1.7	4.77
4	50: 1: 0.4	40	50	28	2.89	1.55	8.66
5	50: 1: 0.4	40	60	47	4.86	1.43	14.09
6	50: 1: 0.4	40	90	62	7.53	3.00	18.34
7[c]	50: 1: 0.4	40	90	58	6.00	2.60	17.21
8[d]	50: 1: 0.4	40	90	43	4.26	1.90	12.97
9[e]	50: 1: 0.4	40	60	38	3.77	1.61	11.55
10	50: 1: 0.2	50	60	53	5.23	1.47	15.79
11	50: 1: 0.4	60	60	62	7.26	1.91	18.34
12[f]	50: 1: 0.4	40	40	25	2.65	2.12	7.87

ATRP conditions: polymerization in ethyl acetate. L = HMTETA. [CuBr] : [L] = 1:1, volume ratio of DMAEMA to solvent is 2:1, [a] The conversion was calculated from ^{1}H NMR, $\overline{M}_{n\ (calc)}$ = [M]/[I]×$M_{(DMAEMA)}$×conversion ×36 (number of initiating sites per macroinitiator) + 8000($M_{n\ (initiator)}$). [b] M_n and M_w/M_n were obtained from GPC equipped with RI detector in $CHCl_3$. [c] CuCl as ligand. [c] With 5% $CuBr_2$. [e] DMAEMA to solvent is 1:1. [f] Ligand is PMDETA.

As we expected from the experience with the synthesis of P*t*BA, the same reaction conditions at 40 ^{o}C with CuBr/initiating sites (1:1) did not work for the preparation of star PDMAEMA with 36 arms, because the obtained material is not soluble. (Table 4-1, run 1) From the discussion in Chapter 2 we know this arises from the coupling side reaction and finally leads to gelation of the reaction system. Therefore, the same strategy as used for the preparation of P*t*BA was adopted, i.e., the amount of CuBr catalyst was lowered to reduce the concentration of propagating radicals. With 40% molar ratio of CuBr to initiating sites, ATRP of DMAEMA using PG-based macroinitiator in EtAc can be controlled, with polydispersities in the range of 1.43-3. (Table 4-1, run 2-6) The molecular weight distribution was fairly narrow at

the beginning of the polymerization, but it broadened with increasing conversion. This tendency of the PDI was also observed for star DMAEMA using β-CD as core.[13]

A comparison reaction using PMDETA as ligand has also been carried out (Table 4-1, run 12). The reaction showed insufficient control (broader distribution) of the polymerization than when using HMTETA as a ligand.

Since the obtained PDMAEMAs show a polydispersity in the range of 1.43-3, many efforts have been dedicated at a better control of the polymerization. For example, CuCl was used to substitute CuBr for the ATRP, (Table 4-1, run 7). Usually, using CuCl will lower the reaction rate and enable better control of the polymerization, but for the current case, it can be seen that using CuCl did not help to improve the distribution of the obtained polymer. Thus, only CuBr was used in the following works. We also tried to introduce Cu(II) in the reaction system to reduce the concentration of active species in order to obtain better control. As it can be seen from Table 4-1, run 8, the introduction of Cu(II) did not help to obtain a polymer with narrow polydispersity. Besides, carrying out the reaction under a more diluted solution (Table 4-1, run 9) or at higher temperature (Table 4-1, run 11) also did not help to improve the control over the polymerization.

Well-defined linear PDMAEMA has been obtained via ATRP of DMAEMA in anisole at 90 ^{o}C, using the CuBr/ HMDETA catalytic system.[9, 17] So here, the reaction was also carried out in anisole, demonstrating that the use of CuCl as catalyst can yield better control of the polymerization than CuBr. (Compare Table 4-2, run 1 and run 3) For this reason, CuCl was used for all reactions in anisole. Surprisingly, the reaction in anisole can be well controlled until 72% conversion. Introducing Cu(II) into the reaction system did not show an obvious improvement of the control. (Table 4-2, run 8, 9, 10).

The polymerization of DMAEMA was also carried out in MeOH. (Table 4-2, run 11, 12, 13) Here the materials obtained show quite narrow distribution 1.4, when using CuCl compared with the case using CuBr (compare run 11 and 12). Introducing Cu(II) can help to improve control of the polymerization. For the polymerization of DMAEMA in MeOH, it was reported that trans-esterification might take place, however, for the current cases, no transesterification was observed from their ^{1}H NMR. This is reasonable because the reactions were carried out at 40 ^{o}C for quite a short time (90 min), while the side reaction might require longer time and higher

temperature. However, a broad study to avoid this possible side reaction in methanol has not been performed.

Table 4-2. Preparation of multi-arms star PDMAEMA based on $P(G_{36}In_{36})$ macroinitiators in anisole or MeOH

No.	[M]:[I]:[CuCl]	*Temp* (^oC)	Time (min)	Conv.[a] (%)	$M_{n\ (gpc)}$[b] ($\times10^{-4}$)	M_w/M_n[b]	$M_{n\ (calc)}$[a] ($\times10^{-4}$)
1[c]	50: 1: 0.4	50	30	45	5.88	2.40	13.53
2	50: 1: 0.4	50	15	14	1.70	1.72	4.76
3	50: 1: 0.4	50	30	32.9	6.09	1.61	10.10
4	50: 1: 0.4	50	45	49.5	6.73	1.48	14.80
5	50: 1: 0.4	50	60	63.2	7.63	1.58	18.68
6	50: 1: 0.4	50	75	72.1	9.09	1.72	21.20
7	50: 1: 0.4	50	90	80	6.00	2.60	23.43
8[d]	50: 1: 0.4	50	90	46.5	4.26	1.90	13.95
9[d]	50: 1: 0.4	40	90	39	3.82	1.81	11.83
10[d]	50: 1: 0.4	30	90	27.4	2.96	1.67	8.55
11[c, e]	50: 1: 0.4	40	40	62	7.38	2.70	18.34
12[e]	50: 1: 0.4	40	40	25	4.48	1.40	7.87
13[c, d, e]	50: 1: 0.4	40	40	19	3.19	1.90	6.17

ATRP conditions: polymerization conducted in anisole. L = HMTETA. [CuCl] : [L] = 1:1, volume ratio of DMAEMA to solvent was 2:1, [a] The conversion was calculated from ^1H NMR, $\overline{M}_{n\ (calc)}$ = [M]/[I]×$M_{(DMAEMA)}$×conversion ×36 (number of initiating sites per macroinitiator) + 8000($M_{n\ (initiator)}$). [b] M_n and M_w/M_n were obtained from GPC equipped with RI detector in $CHCl_3$. [c] CuBr as ligand. [d] With 5% $CuBr_2$. [e] in MeOH.

4.2.3. Kinetic studies of the ATRP of DMAEMA

Kinetic studies have been carried out first in ethyl acetate, using the following ratios: [M]:[In]:[CuBr]:[HMDETA] = 50:1:0.5:0.5. Samples were taken from the reaction mixture via syringes at certain time intervals for conversion measurements (^1H NMR) and molecular weight (GPC) determination. The results, depicted in Figure 4-5, show a 2-stage linear dependence of $\ln([M]_0/[M]_t)$ on time, indicating that the concentration of propagating species changed during the reaction.

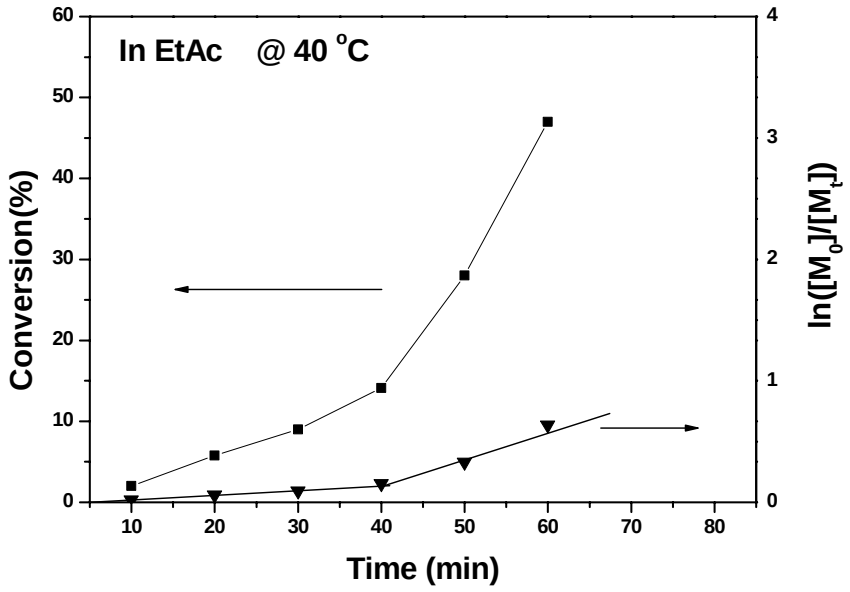

Figure 4-5. Dependence of the monomer conversion and $\ln([M]_0/[M]_t)$ on time for the polymerization of DMAEMA in EtAc, using hyperbranched **P($G_{36}In_{36}$)** as macroinitiator at 40°C. [M]:[I]:[CuBr]: [L] = 50:1:0.5:0.5, $V_{DMAEMA}/V_{EtAc} = 2$

As can be seen from Figure 4-6, molecular weights increase linearly with conversion. (lower than 50%) The molecular weight distributions are in the range of 1.43-1.70, demonstrating the polymerizations are not well controlled, as typical for conventional ATRP. This phenomenon was also observed by other groups for star PDMAEMA using beta-CD as core.[13] Samples obtained at higher conversion than 60% could not pass through the 0.4 μm filter for GPC measurement. This is probably due to the fact that star-star coupling dominated and the polymer formed a gel at higher monomer conversion, as also described in Chapter 2. Apparent molecular weights obtained from conventional GPC show a linear dependence, but are much smaller than the theoretical values. This could be due to two reasons: 1) the compact structure of the star polymers enables them to show a relatively smaller hydrodynamic volume compared with linear polymer of the same molecular weight; 2) the interaction of the polymer with the column results in a tail for the GPC measurement (the GPC curves can be seen in Figure 4-9). This would on one hand broaden the molecular weight distribution and on the other hand make the apparent molecular weight smaller than the real one. A similar result can also be found in Haddleton's papers.[10]

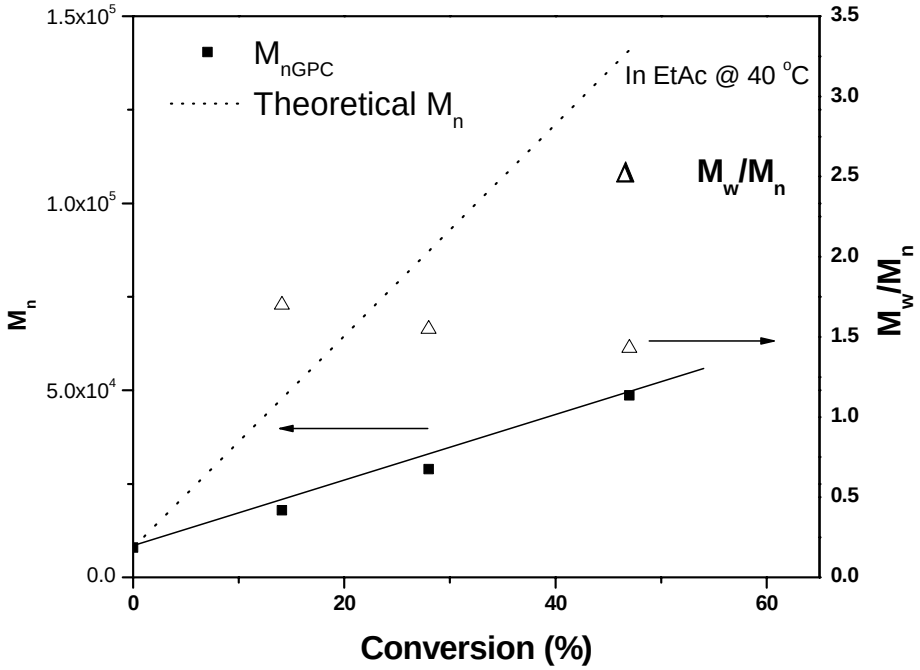

Figure 4-6. Molecular weights and distributions vs. conversion for PG_{36}-*b*-PDMAMEA

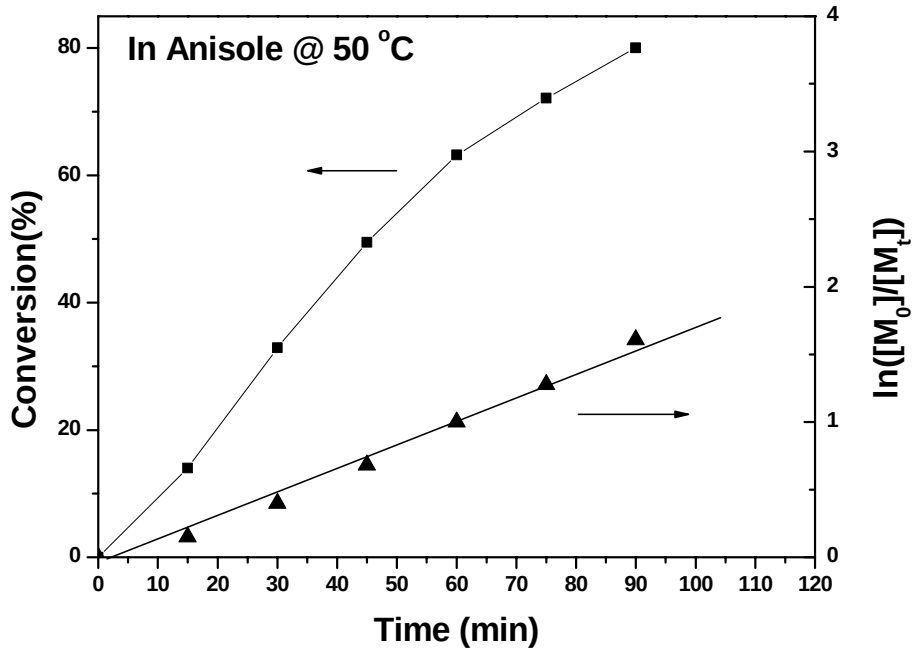

Figure 4-7. Dependence of monomer conversion and $\ln([M]_0/[M]_t)$ on time for the polymerization of DMAEMA in anisole, using hyperbranched **$P(G_{36}In_{36})$** as the macroinitiator at 50°C. [M]:[I]:[CuCl]: [L] = 50:1:0.4:0.4, $V_{DMAEMA}/V_{Anisole} = 2$

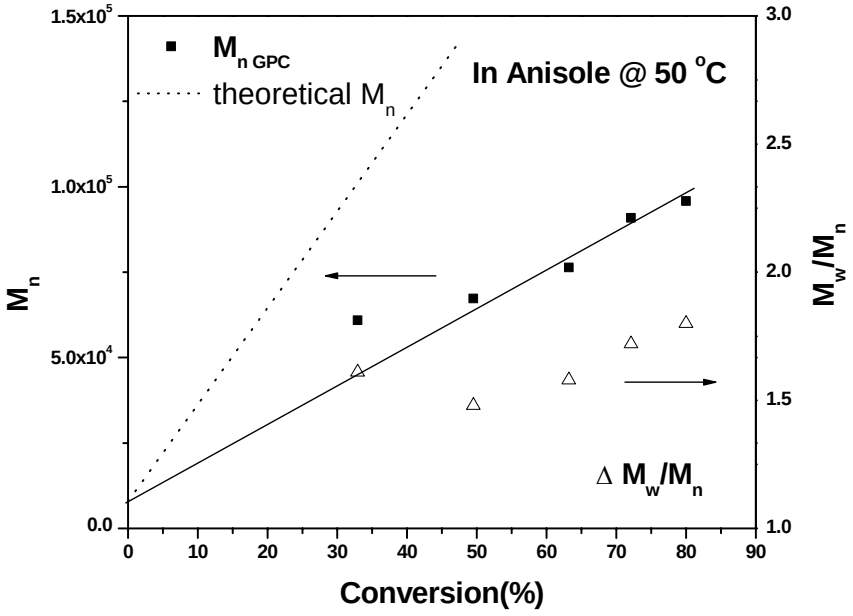

Figure 4-6. Molecular weights and distributions vs. conversion for PG_{36}-*b*-PDMAMEA

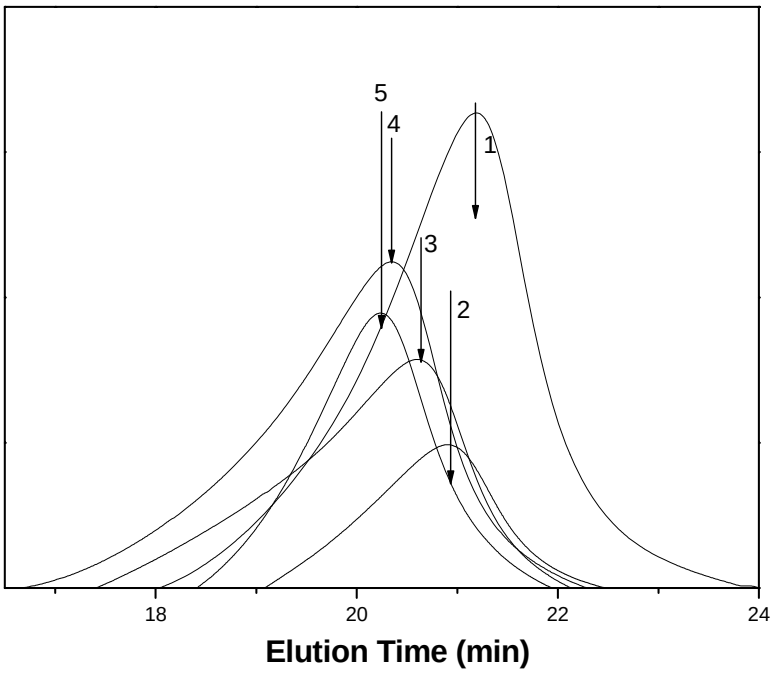

Figure 4-9. GPC traces of multi-arm PG_{36}-*b*-PDMAEMA star copolymers, (1) M_n = 2.51x10^4, M_w/M_n = 1.25; (2) M_n = 3.35x10^4, M_w/M_n = 1.20; (3) M_n = 4.13x10^4, M_w/M_n = 1.23; (4) M_n = 5.05x10^4, M_w/M_n = 1.20; (5) M_n = 5.66x10^4, M_w/M_n = 1.30; polymerization conditions see Figure 4-8.

Kinetic studies were also carried out in anisole at 50 °C using the same [M]:[In]:[CuCl]:[HMDETA] ratio as above. The results, as depicted in Figure 4-7, show a linear dependence of $\ln([M]_0/[M]_t)$, indicating a constant number of propagating species throughout the reaction. Apparent molecular weights obtained from conventional GPC show a linear dependence, but they are off linearity at the beginning of the reaction. The molecular weights are also much smaller than the theoretical values, possibly due to the reasons described above.

4.2.4. Syntheses of inverted unimolecular micelles and their encapsulation behavior

Multi-arm star copolymers PG-*b*-PDMAEMA possess a large number of tertiary amine groups along the side chain of PDMAEMA arms, which can be easily modified via quaternization. Herein, $PG_{36}(DMAEMA_{31})_{36}$ (PG with average 36 functionalities as core, average PDMAEMA arm number is 36, $\overline{DP}_{n(arm)}$ =31) was used to synthesize unimolecular micelles.

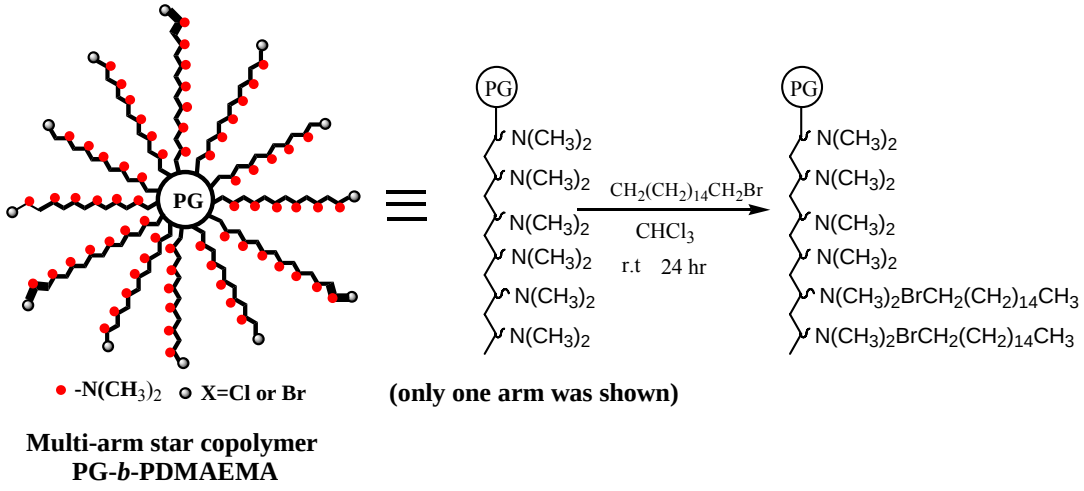

Scheme 4-6. Synthesis of inverted unimolecular micelles (only one arm is shown schematically, cf. above) and schematic image of the unimolecular micelles (bottom)

$PG_{36}(DMAEMA_{31})_{36}$ was first quaternized with $C_{16}H_{33}Br$ or $C_{18}H_{37}Br$. It has been found that the interior of star polymers can become quite crowded, as the number of arms increases and the free ends of the chains are excluded from the core region simply by steric effects.[18] Thus, we can expect that the tertiary amine groups located in the outer part of PG-*b*-PDMAEMA are more reactive than those amine groups in the inner part, and the modification reaction by aliphatic bromide will

mainly take place in the outer periphery of PG-*b*-PDMAEMA, particularly considering the long aliphatic chains. (as shown in Scheme 4-6) The degree of modification can be calculated from the respective ^{1}H NMR spectra. (Figure 4-10) The residual tertiary amine groups can be further quaternized with CH_3I to give nanocapsule structures, as illustrated in Scheme 4-7, following the synthetic procedure shown in Scheme 4-6.

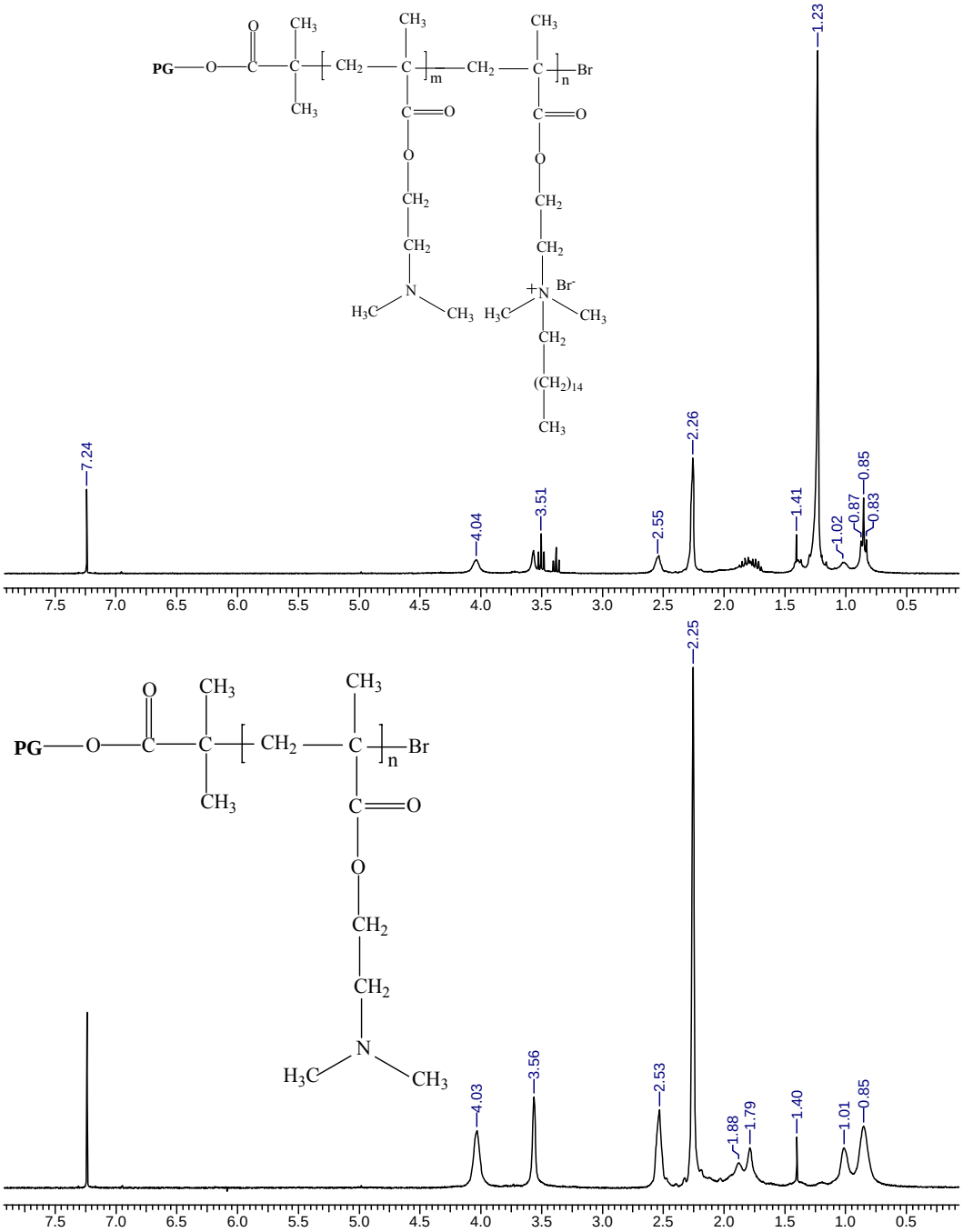

Figure 4-10. ^{1}H NMR comparison of the star PDMAEMA and aliphatic bromide modified PDMAEMA "capsules"

After partial modification of the tertiary amine groups of star PDMAEMA, the outer part of the arms became hydrophobic, and the inner part of the arms was still hydrophilic, turning the macromolecule into a core-shell structure. Here the inner and outer blocks of the arms are regarded as the core and shell, respectively. Thus, the resulting polymers are expected to display an inverted micellar behavior. Compared with the analogous species derived from dendrimers,[19, 20] the core size of the current capsule can be increased much more conveniently by increasing the degree of polymerization of the inner blocks of the arms.[21]

Unimolecular micelles with hydrophobic outer shell and hydrophilic inner shell may favorably serve for the extraction and irreversible encapsulation of water-soluble molecules.[22, 23] To date, two kinds of star polymers with amphiphilic core-shell structure, a prerequisite for guest molecule encapsulation, have been designed as unimolecular micelles. In the first one, the homopolymer arms are linked together by linking agents, such as microgels[24] and dendrimers.[19, 20] The homopolymer arms are used as the shell for stabilizing the star polymers in solution, and the linking agents represent the core, i.e., the environment for the guest molecules. In the second case, the amphiphilic block copolymers are used as arms, being linked together by linking agents.

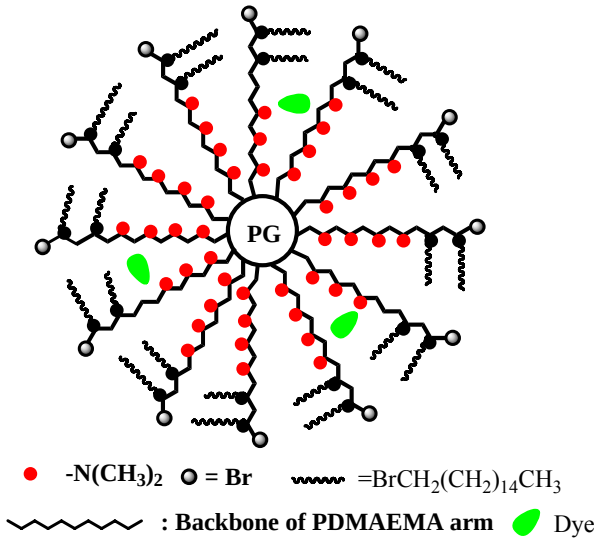

Scheme 4-7. Schematic image of the unimolecular micelle from modified star PDMAEMA

To test the micellar properties of these modified star PDMAEMAs, their capacity for polar guest encapsulation was evaluated by transfer of the water-soluble dye Methyl Orange (MO) into the organic phase. The procedure is shown in Figure 4-11.

The dye loading capacity per polymer was estimated from the UV-vis spectra (detailed procedure can be found in Chapter 7), and the results are summarized in Table 4-3.

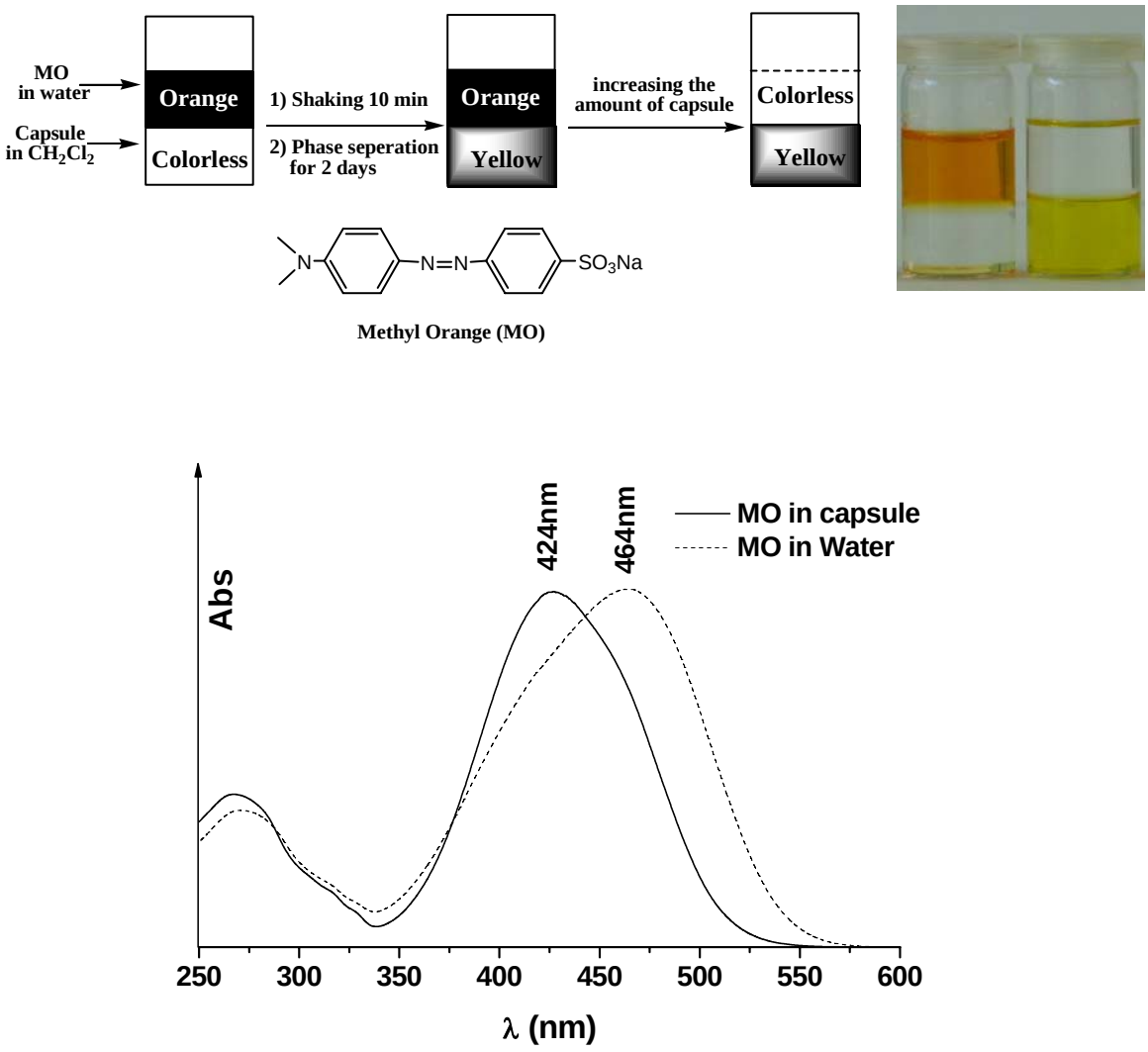

Figure. 4-12 Illustration of the water soluble dye extraction from water to the chloroform solution of nanocapsules, and its UV-vis spectra in different phases

From Table 4-3, it is clear that all the modified star polymers can transfer water soluble dye into the organic phase. Surprisingly, both core-quaternized (4, 5, 7) and non-quaternized samples (2, 3, 6) can efficiently encapsulate the dye molecules, although further quaternization of the inner tertiary amines (increasing the polarity of the core) can enhance the encapsulation capacity compared with non-quaternized samples: 35-37 dye molecules per polymer capsule for 2, 3, and 6, while 54-70 dye molecules for samples 4, 5 and 7). Besides that, both the length of the aliphatic chains

(C16 and C18) and the degree of modification (30% and 40%) show no significant influence on the dye encapsulation capability. Increasing the degree of modification from 30% to 40%, only a slightly decrease of the concentration of dye encapsulated was observed. This tentatively ascribed to the effect that the dye shows more difficulty to pass through the C16 periphery. Alternatively, the higher degree of modification decreases the available space inside the capsules. Samples with 20% of modification caused serious emulsion. Since no further test has been made for different modification degrees, we cannot simply attribute the ability to transfer dyes to the size of the star polymers.

Table 4-3. Inverted unimolecular micelles based on multi-arm star polymers and their hydrophilic dye encapsulation capacities

No.	Samples [a)]	DM (%) [b)]	Dye loading [c)]
1	$PG_{66}(H_{22})_{66}$	0	—
2	$[PG_{36}(DMAEMA_{31})_{36}]\ C16_{0.3}$	30%	34.6
3	$[PG_{36}(DMAEMA_{31})_{36}]C16_{0.4}$	40%	32.2
4	$[PG_{36}(DMAEMA_{31})_{36}]C16_{0.3}Qm_{0.7}$	30%	56.7
5	$[PG_{36}(DMAEMA_{31})_{36}]C16_{0.4}Qm_{0.6}$	40%	54.3
6	$[PG_{36}(DMAEMA_{31})_{36}]C18_{0.4}$	38%	37.2
7	$[PG_{36}(DMAEMA_{31})_{36}]C18_{0.4}Qm_{0.6}$	38%	59.6

[a)] $[PG_{36}(DMAEMA_{31})_{36}]C18_{0.4}Qm_{0.6}$: 36 arm star PDMAEMA based on PG_{36} core; average DP of each arm is 31; C16, C18 are hexadecanoate, octadecanoate; Qm: quaternized core. Qm degree was not calculated from NMR, since here we suppose all tertiary amines groups were quaternized by using an excess of CH_3I.

[b)] DM%: degree of aliphatic chain modification.

[c)] Loading number of methyl orange molecules per amphiphilic star macromolecule; determined from UV-vis spectra.

4.3. Conclusions

Well-defined multi-arm star block copolymers polyglycerol-*b*-poly(DMAEMA) with an average 36 arms have been prepared via a *core-first* strategy. The arms were grafted by atom transfer radical polymerization (ATRP) of DMAEMA in either ethyl acetate or anisole. The polydispersities of the new multi-arm stars can be controlled

within the range of 1.4-1.9. The kinetic data do not show a linear dependence of $\ln([M]_0/[M]_t)$ on time, indicating that the polymerizations are only in a relative controlled mode. The star polymers can be converted to inverted micelles by further modification with aliphatic bromides. These inverted micelles can be used to transfer water soluble dyes into the organic phase.

4.4. Experimental Part

4.4.1. Materials

CuBr (98%, Acros) was purified as described in literature. 2-(dimethylamino)-ethyl methacrylate (DMAEMA, Aldrich, 98%) was distilled under reduced pressure, stored in the refrigerator and degassed with argon for 1 hr prior to use. N,N,N',N',N"-Pentamethyldiethylene-triamine (PMDETA, Aldrich, 99%) were distilled under reduced pressure and degassed with argon prior to use. Anisole, acetone, dioxane, ethyl acetate, 1,1,4,7,10,10-hexamethyletrethylenetetramine (HMTETA), methanol, ethanol, chloroform, 1-bromohexadecane (97%, Aldrich) were used as received. **$P(G_{36}In_{36})$** was prepared as described in chapter 2.

4.4.2. Synthesis of PG-b-PDMAEMA multi-arm star copolymer

In a typical experiment, 105.4 mg (0.4732 mmol of initiating sites) of the initiator $P(G_{36}In_{36})$, 4 ml of DMAEMA (23.66 mmol), 27.3 mg of CuBr (0.19 mmol) and 2ml of solvent were placed in a flask with a magnetic stir bar. The flask was sealed with a rubber septum and degassed by three freeze-pump-thaw cycles. Then 51.7 μl of HMTETA (0.19 mmol) was introduced into the flask by an argon-purged syringe. The flask was then immersed in an oil bath thermostated at 50 ^{o}C. After a certain time, the flask was immersed into liquid nitrogen to quench the reaction. Samples were taken, diluted with deuterated chloroform and subsequently analyzed by ^{1}H NMR spectroscopy to obtain the polymerization conversion. The residual sample was diluted with acetone and passed through a silica gel column to remove the copper complex. The samples were precipitated in a 10 fold excess of hexane and dried at 40 ^{o}C in vacuo for 2 days.

4.4.3. Synthesis of bromohexadecane modified PDMAEMA star

In a typical experiment, 0.50 g PDMAEMA (3.00 mmol) and 0.36 ml 1-bromohexadecane (1.18 mmol, 40% of DMAEMA units) dissolved in 10 ml of

$CHCl_3$, reflux for 44 hours, the product were dialyzed against chloroform (MWCO 1000 g/mol) to remove traces of small molecules. The sample was further quaternized with 5 fold excess of CH_3I by refluxing in $CHCl_3$ overnight.

4.4.4. Methodology for dye extraction in phase transfer processes using the multi-arm star polymers

4 ml of the $CHCl_3$ solution of multi-arm star polymer was added to 4 ml of MO in water. The solution was shaken for 10 minutes and kept at room temperature in the dark overnight prior to the measurements. The concentration of MO in water was fixed ($[MO]_0 = 6.78x10^{-5}$ M), but the concentrations of the modified star polymer in $CHCl_3$ was adjusted, until only part of the dye in water was transferred into the $CHCl_3$ phase. The water phase was studied by UV-vis spectroscopy, and the remaining dye in water can be calculated according to Lambert-Beer´s law (The molar extinction coefficients (ε) of MO in water at 464 nm was measured to be $2.16x10^4$ L/mol.cm). Subsequently, the number of dye molecules transferred into $CHCl_3$ phase was obtained.

4.5. References

[1] Hawker, C. J.; Farrington, P.; Mackay, M.; Fréchet, J. M. J.; Wooley, K. L. *J. Am. Chem. Soc.* **1995,** 117, 4409.
[2] Roovers, J.; Zhou, L.-L.; Toporowski, P. M.; Zwan, M. v. d.; Iatrou, H.; Hadjichristidis, N. *Macromolecules* **1993,** 26, 4324.
[3] Mourey, T. H.; Turner, S. R.; Rubenstein, M.; Frechet, J. M. J.; Hawker, C. J.; Wooley, K. L. *Macromolecules* **1992,** 25, 2401.
[4] Jansen, J. F.; Brabander van den Berg, E. M.; Meijer, E. W. *Science* **1994,** 266, 1226.
[5] Pakula, T.; Vlassopoulos, D.; Fytas, G.; Roovers, J. *Macromolecules* **1998,** 31, 8931.
[6] Islam, M. T.; Juliani; Archer, L. A.; Varshney, S. K. *Macromolecules* **2001,** 34, 6438.
[7] Stiriba, S. E.; Kautz, H.; Frey, H. *J. Am. Chem. Soc.* **2002,** 124, 9698.
[8] Vlassopoulos, D.; Fytas, G.; Pakula, T.; Roovers, J. *J. Phys.: Condens. Matter* **2001,** 13, 855.
[9] Teodorescu, M.; Matyjaszewski, K. *Macromol. Rapid Comm.* **2000,** 21, 190.
[10] Ohno, K.; Wong, B.; Haddleton, D. M. *J. Polym. Sci. Polym. Chem,* **2001,** 39, 2206.
[11] Haddleton, D. M.; Edmonds, R.; Heming, A. M.; Kelly, E. J.; Kukulj, D. *New J. Chem.* **1999,** 23, 477.
[12] Narrainen, A. P.; Pascual, S.; Haddleton, D. M. *J. Polym. Sci. Polym. Chem,* **2002,** 40, 439

[13] Li, J.; Xiao, H.; Kim, Y. S.; Lowe, T. L. *J. Polym. Sci. Polym. Chem,* **2005,** 43, 6345.
[14] Lad, J.; Harrisson, S.; Mantovani, G.; Haddleton, D. M. *Dalton Trans.* **2003**, 4175.
[15] Chen, Y.; Shen, Z.; Barriau, E.; Kautz, H.; Frey, H. *Biomacromolecules* **2006,** 7, 919.
[16] Mori, H.; Walther, A.; Andre, X.; Lanzendorfer, M. G.; Muller, A. H. E. *Macromolecules* **2004,** 37, 2054.
[17] Xia, J.; Matyjaszewski, K. *Macromolecules* **1997,** 30, 7697.
[18] Grest, G. S. *Macromolecules* **1994,** 27, 3493.
[19] Liu, M.; Kono, K.; Fréchet, J. M. J. *J. Controlled Release* **2000,** 65, 121.
[20] Kojima, C.; Kono, K.; Maruyama, K.; Takagishi, T. *Bioconjugate Chem.* **2000,** 11, 910.
[21] Wang, F.; Bronich, T. K.; Kabanov, A. V.; Rauh, R. D.; Roovers, J. *Bioconjugate Chem.* **2005,** 16, 397.
[22] Georgiou, T. K.; Vamvakaki, M.; Patrickios, C. S.; Yamasaki, E. N.; Phylactou, L. A. *Biomacromolecules* **2004,** 5, 2221.
[23] Meier, M. A. R.; Gohy, J. F.; Fustin, C. A.; Schubert, U. S. *J. Am. Chem. Soc.* **2004,** 126, 11517.
[24] Baek, K.-Y.; Kamigaito, M.; Sawamoto, M. *Macromolecules* **2002,** 35, 1493.

Chapter 5. Complex of Modified Hyperbranched Polyethylenimine with Cuprous Halide as Recoverable Homogeneous Catalyst for the Atom Transfer Radical Polymerization of Methyl Methacrylate

5.1. Introduction

During the past couple of years, several procedures for controlled or "living" radical polymerizations have been developed and used to prepare various well-defined polymers and polymers with complex architectures.[1-6] Among these methods, atom transfer radical polymerization (ATRP), a living radical polymerization technique based on a reversible activation/deactivation equilibrium between the active and dormant species mediated by transition metal complexes, (as shown in Scheme 5-1) is a very versatile tool for the synthesis of well-defined polymers and complex macromolecular architectures[7, 8] like block,[9] star,[10, 11] and hyperbranched (co)-polymers.[12]

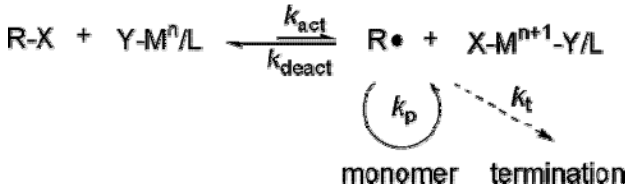

Scheme 5-1. General mechanism of ATRP

Various systems based on Cu, Ru, Fe, Ni and Rh have been developed for the ATRP of styrenic, acrylic, and methacrylic monomers.[7, 8] (We have already summarized the scopes of ligand, monomer and catalyst for ATRP in detail in Chapter 2, no further description will be given here) Among them the complexes of Cu(I) with nitrogen-based ligands have been widely used because of their good catalytic efficiency for the polymerization of most common monomers and their low cost.[7, 8] However, the high amount of catalyst required to realize reasonable rates of polymerization leads to deeply colored polymerization solutions and polymer products contaminated with toxic heavy metals. (The colored, i.e., transition metal contaminated polymer system can be seen from Figure 5-1, a)

(a) *(b)*

Figure 5-1. Copper contamination of ATRP (a) reactant solution, (b) conventional way of removing copper from polymers via column filtration

Additional purification steps are required to remove those copper catalyst from the product, usually by passing the solution over silica[13, 14] or alumina[2, 15, 16] gel after the polymerization, (see Figure 5-1b) which is only possible on lab scale. Biphase separation from ionic liquid, fluorous biphases, and emulsion have also been used to directly remove the catalyst residue. However, these treatments are expensive and not applicable to large industrial scales. In addition, these methods cannot recycle and reuse the catalysts. For industrial application of ATRP more efficient removal of the catalyst from the polymer is a crucial issue.

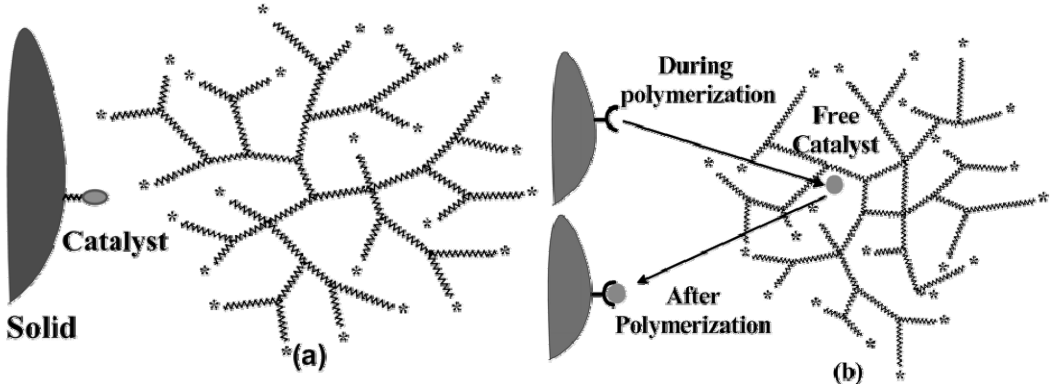

Scheme 5-2. Illustrations of (a) a covalently solid-supported catalyst and (b) a reversibly supported catalyst in the synthesis of polymer architectures

To date, research efforts have been directed at the use of heterogeneous catalysts immobilized onto inorganic (Scheme 5-2) or organic polymer supports[17-21], (Scheme 5-3) since these materials can be removed from the final polymer products by simple filtration or sedimentation and reused several times. By these ways, the cost can be reduced.

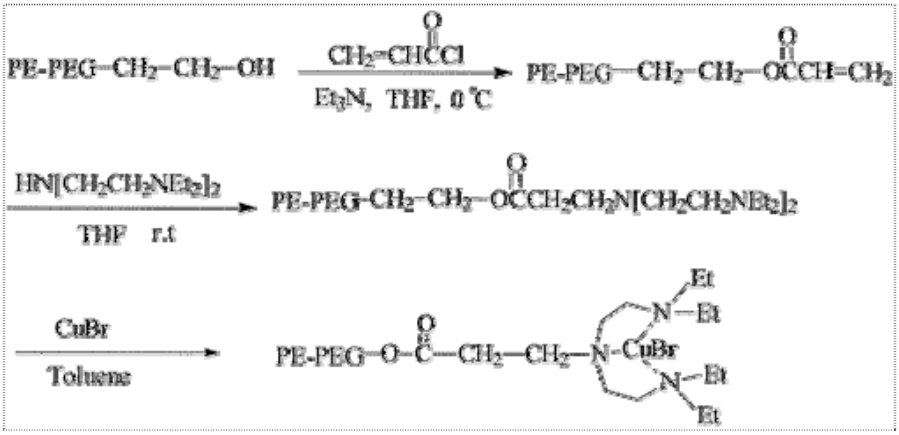

Scheme 5-3. Supporting CuBr onto poly(ethylene-b-ethylene glycol) or polyethylene via tetraethyldiethylenetriamine (TEDETA).

However, heterogeneous catalysts show reduced efficiency for the control of the polymerization, producing polymers with higher molecular weights than the theoretical values and broader molecular weight distributions due to a reduction of the radical deactivation rate, resulting in radical termination reactions and uncontrolled chain growth.

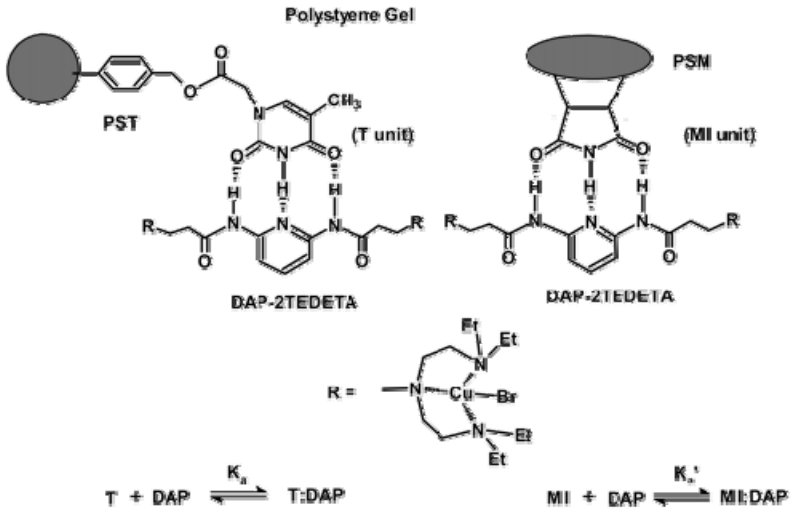

Scheme 5-4. Tetraethyldiethylenetriamine (TEDETA)-CuBr reversibly supported onto polystyrene gel via a triple hydrogen bond array of the thymine-diaminopyridine or maleimide-diaminopyridine

More efficient heterogeneous catalyst systems like reversibly supported catalyst (Scheme 5-2b and Scheme 5-4) are also being explored at present.[22-25] Addition of a small amount of soluble catalyst to the heterogeneous system enhances the deactivation rate, affording polymers with controlled molecular weights and low polydispersity;[26-29] however, obviously the soluble catalyst remains in the final polymer, if no additional purification step is applied.

Due to the problems encountered with heterogeneous ATRP catalysts, the interest in recoverable homogeneous catalysts is growing, since catalyst molecules can diffuse freely and take part effectively in the activation-deactivation cycle. To date, recoverable homogeneous catalysts can be classified into the following three categories.

(i) Thermo-responsive catalyst complexes: the formed catalyst-complex is soluble under reaction conditions, permitting a homogeneous transformation, but precipitates under work-up conditions to render catalyst recycling possible. In this case good control of both polydispersities and molecular weights of the polymers was obtained.[22, 30-33] (as that shown in Scheme 5-5) The drawback of this kind of catalyst system is that only specific apolar solvents, such as toluene and 1,4-dioxane can be used, which limits the monomers to apolar structures.

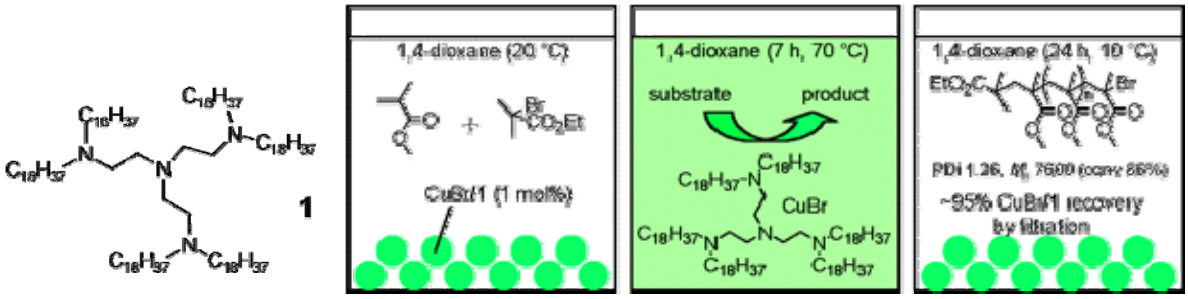

Scheme 5-5. The separation process for a thermo-responsive complex

(ii) Catalyst complexes conjugated with a second component that can be isomerized after the catalyzed transformation and thereby precipitated.[34] Stilbene-bound ligands (as shown in Scheme 5-6) successfully mediate the ATRP of methyl methacrylate (MMA) and allow for facile and fast removal of the copper catalyst by exposure of the solution to a UV light source. However, in this case the recovered catalyst complex loses its catalytic activity.[34]

(iii) Catalyst-complexes with good solubility in both polar and apolar solvents can be employed. [35] For the ATRP of apolar monomers, separation of the final products from the catalyst complex was achieved by pouring the solution into polar solvents[35]. The catalyst complex in the solution can be recovered by ultrafiltration[36, 37] or simple evaporation of the volatiles.

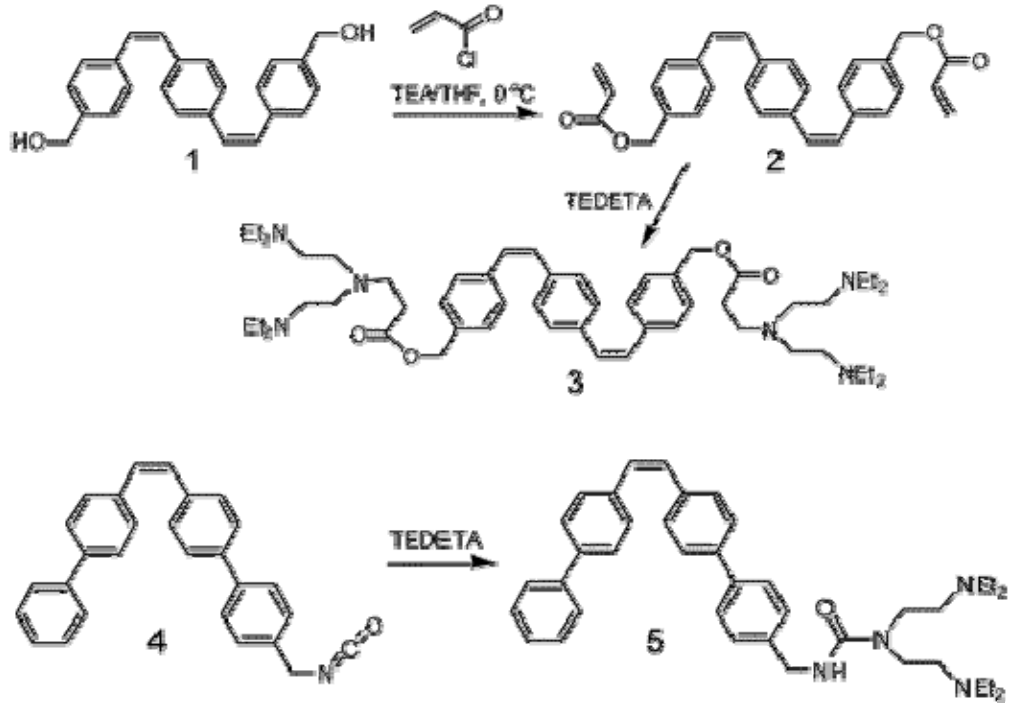

Scheme 5-6. Synthesis of Stilbene-bound ligands from Diol and Isocyanate

Dendrimers and their less-defined hyperbranched analogues are attracting tremendous interest at present due to their specific shape and multi-functionality, which are powerful motifs in the design of new molecular and supramolecular structures.[38-42] Both dendrimers and hyperbranched polymers covalently or non-covalently functionalized with catalytically active transition-metal complexes are promising scaffolds with respect to catalyst recovery.[35-37], [43-48] Whilst the preparation of structurally perfect dendrimers suffers from its tedious multi-step nature, hyperbranched polymers made from AB_m type monomer in one step have emerged as excellent alternatives. To date, catalysis using hyperbranched macromolecules functionalized covalently or non-covalently with catalytic sites has received surprisingly limited attention.[35],[44-48] Except for hyperbranched polycarbosilanes modified with aryldiamine palladium (II)-complexes,[44] the well-

defined hyperbranched polyglycerol represents the only hyperbranched material used as polymeric support for the catalyst complexes.[35],[45-48]

In this chapter, the use of one-step modified hyperbranched polyethylenimine (HPEI) as support and macromolecular ligands ("macroligands") for the Cu(I) catalyzed ATRP of MMA will be described. The use of HPEI possesses the following advantages: (i) simple one-step modified HPEI can be used directly as macroligand to form a complex with the Cu(I) catalyst for ATRP, however, as for other hyperbranched polymers, low molecular weight ligands have to be attached by multi-step reactions; (ii) HPEIs possess low toxicity and are used widely in gene transfection,[49-51] while low molecular weight ligands for ATRP, such as 2,2-bipyridines and their derivatives as well as multidentate amines, are toxic for humans as described by Aldrich; (iii) in addition, various molecular weight HPEIs are commercially available and considerably cheaper than other hyperbranched or dendrimer polymer supports.

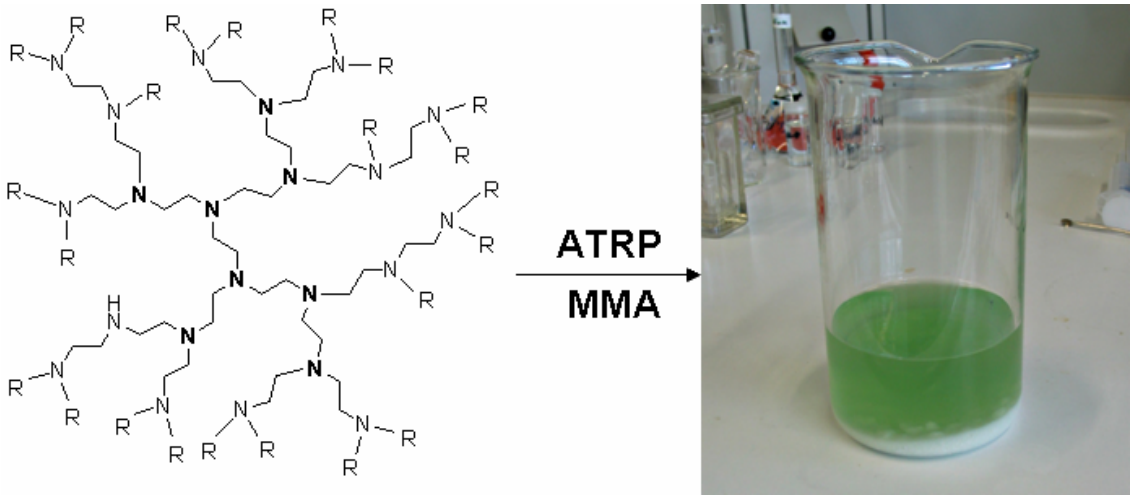

Scheme 5-7. Schematic show of the work in Chapter 5

5.2. Results and Discussion

5.2.1. Synthesis of the Hyperbranched PEI-Based Macroligands

Efficient ligands for copper-mediated ATRP are usually composed of pyridine, tertiary amines or Schiff bases.[7, 8] Commercially available hyperbranched polyethylenimines consist of primary, secondary and tertiary amine groups, and their structures are similar to tris(2-aminoethyl)amine (TREN), which is the precursor of the efficient ligands for copper-mediated ATRP, tris (2-dimethylaminoethyl) amine

(Me_6-TREN)[7, 52] and acrylate-TRENs[15] derived from Michael addition of TREN with acrylates. Compared with Me_6-TREN, the properties of acrylated TRENs can be tailored conveniently, and a broader range of monomers can be polymerized in a controlled manner with acrylate-based TRENs as the ligand for the copper-mediated ATRP.[15] Thus, we modified HPEI with EA or BA via Michael addition reaction to generate the macroligands for the copper-mediated ATRP (Scheme 5-7).

The resulting polymers were characterized by ^1H and ^{13}C NMR spectroscopy. All signals can be assigned, as shown in Figure 5-2 and Figure 5-3. The ratio of EA or BA moieties (R groups in Scheme 5-7) relative to amine groups of HPEI ([R]/[amine]) can also be calculated from their corresponding integration (I) in the ^1H-NMR spectra (Figure 5-2) according to Equation 5-1.

$$\frac{[R]}{[amine]} = \frac{2I_{(b)}}{I_{(c+d+e)} - 2I_{(b)}} \qquad (5\text{-}1)$$

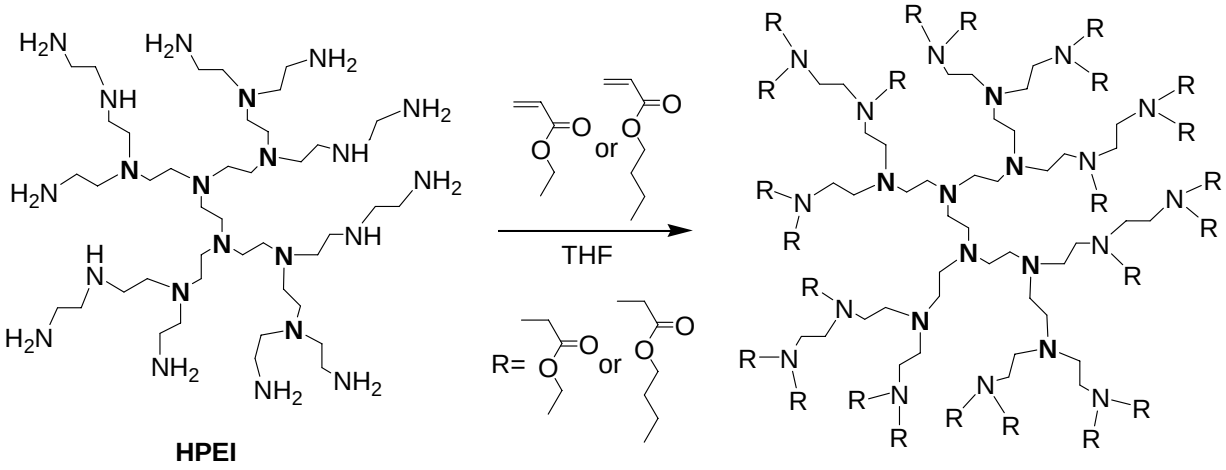

Scheme 5-7. Syntheses of hyperbranched macroligands via Michael addition reaction of acrylates with hyperbranched polyethylenimine (HPEI)

$I_{(b)}$ is the integration of protons of methylene units attached to ester groups ($CH_3C\underline{H_2}OOC$-); $I_{(c+d+e)}$ is the integration of protons of ethylene groups adjacent to carbonyl groups and amine groups, and ethylene units from HPEI (-$NCH_2C\underline{H_2}COO$-, -$NC\underline{H_2}CH_2COO$-, -$NC\underline{H_2}C\underline{H_2}N$- of PEI).

Clearly, one primary amine can react with two EA or BA molecules, one secondary amine can only react with one EA or BA molecule and tertiary amines

usually do not react with EA or BA by Michael addition reaction.[53] Thus, based on the mole ratio of primary, secondary and tertiary amine groups (NH_2 : NH : N) of HPEIs, the theoretical maximum ratio of EA or BA moieties relative to amine groups of HPEI can be calculated according to Equation 5-2.

$$\left(\frac{[R]}{[amine]}\right)_{max} = \frac{2[NH_2]+[NH]}{[NH_2]+[NH]+[N]} \qquad (5\text{-}2)$$

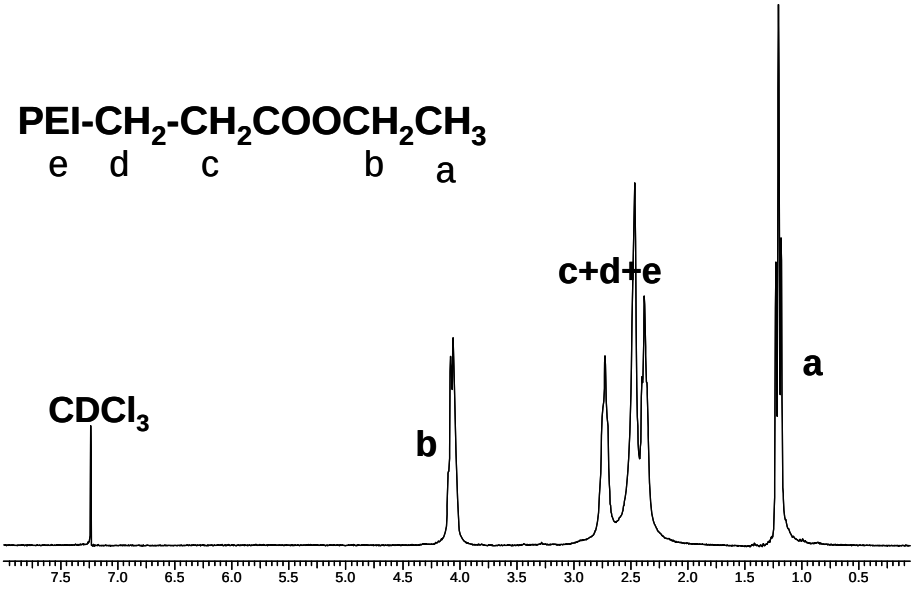

Figure 5-2. ^{1}H spectra (operated at 300 MHz) of hyperbranched macroligands obtained from the Michael addition of hyperbranched PEI with ethyl acrylate (HPEI25k-$EA_{1.01}$)

The mole ratio of primary, secondary and tertiary amine groups (NH_2 : NH : N) for HPEI1.2k, HPEI1.8k, HPEI10k and HPEI25k has been obtained from their inverted gate ^{13}C NMR spectra to be 37:35:28, 37:35:28, 33:40:27 and 33:35:32, respectively. Since the amount of primary amines is higher than that of tertiary amines for all the employed HPEIs, the maximum ratio [R]/[amine] should exceed 1, i.e. 1.09, 1.09, 1.06 and 1.01 for HPEI1.2k, HPEI1.8k, HPEI10K and HPEI25k, respectively.

Table 5-1. Hyperbranched polyethylenimine (HPEI)-based macroligands

Ligand Name [a]	$M_{n\text{-HPEI}} \times 10^{-3}$	[R]/[amine][b]	$M_n \times 10^{-4}$ [c]
HPEI1.2k-$EA_{0.73}$	1.2	0.73	0.32
HPEI1.8k-$EA_{0.87}$	1.8	0.87	0.55
HPEI10k-$EA_{1.06}$	10	1.06	3.46
HPEI10k-$EA_{0.77}$	10	0.77	2.79
HPEI10k-$BA_{0.76}$	10	0.76	3.27
HPEI25k-$EA_{1.01}$	25	1.01	8.38
HPEI25k-$EA_{0.79}$	25	0.79	7.09
HPEI25k-$BA_{1.01}$	25	1.01	10.0
HPEI25k-$BA_{0.76}$	25	0.76	8.17

[a] Nomenclature: HPEIX-Y_z: HPEI, hyperbranched polyethylenimine scaffold; X, M_n of HPEI; Y, BA or EA; z, ratio of EA or BA moieties relative to amine groups of HPEI; [b] Ratio of EA or BA moieties relative to amine groups of HPEI, [R]/[amine] = $2I_{(b)}/[I_{(c+d+e)}\text{-}2\ I_{(b)}]$ according to the typical ^{1}H NMR in Figure 1; [c] Calculated from ^{1}H NMR operated at 300 MHz.

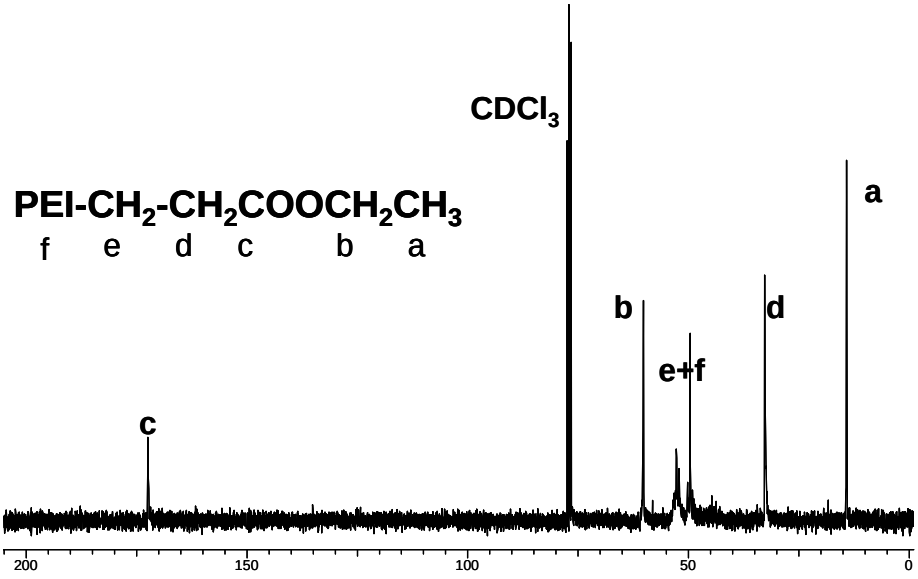

Figure 5-3. ^{13}C NMR spectra (operated at 75.4 MHz) of hyperbranched macroligands obtained from the Michael addition of hyperbranched PEI with ethyl acrylate (HPEI25k-$EA_{1.01}$)

Syntheses of hyperbranched macroligands with maximum ratio [R]/[amine] were time-consuming (more than 10 days) and a considerable excess of EA or BA was required, which would increase the cost dramatically. For comparison, we also prepared the more easily available hyperbranched macroligands with ratio [R]/[amine] less than maximum, which can be obtained in a one-pot procedure within 2 days. All obtained hyperbranched macroligands are listed in Table 5-1.

5.2.2. ATRP of MMA with the New HPEI Based Macroligands

All hyperbranched macroligands can complex with Cu(I) and the complexes are fully soluble in toluene, acetone, 1,4-dioxane, tetrahydrofuran (THF), and methanol. For the copper-mediated ATRP with Me_6-TREN or acrylate-TREN as a ligand, the ratio of amine groups of the ligands to copper were usually set to be 4:1. The structure of the obtained macroligands is similar to acrylate-TREN, thus, the lowest ratio of amine groups of macroligands to copper should be 4:1. In the first experiments the ratio of amine groups of macroligands to copper was set to 4:1. Detailed polymerization conditions for the ATRP of MMA are described in the experimental part. Ethyl 2-bromoisobutyrate (EBIB) was used as initiator. However, after purification by precipitating the polymerization mixture into methanol, the resulting polymer was greenish, indicating that the material was still contaminated with large amounts of copper. Increasing the ratio of amine groups of the macroligands to copper to 5:1, the same phenomenon was observed. From the typical structure of hyperbranched macroligands shown in Scheme 5-7, it is obvious that the amine groups of the macroligands are also present in the interior. The interior amine groups may not coordinate well with copper due to steric effects, resulting in a fraction of uncomplexed copper ions in the polymerization system, when the ratio of amine groups of macroligands to copper is chosen to be 4:1 or 5:1.

The greenish color of the resulting polymer is therefore ascribed to trapped free copper ions during precipitation of PMMA. In order to reduce the concentration of free copper ions in the polymerization system, the ratio of amine groups of the macroligand to copper was raised to 10:1. After polymerization and purification, a colorless material was obtained, indicating that nearly no free copper ions were present in the polymerization system, when the ratio of amine groups of macroligands to copper was set to be approximately 10:1 or higher. Therefore, in all subsequent

polymerization runs, the ratio of amine groups of macroligands to copper was fixed to 10:1.

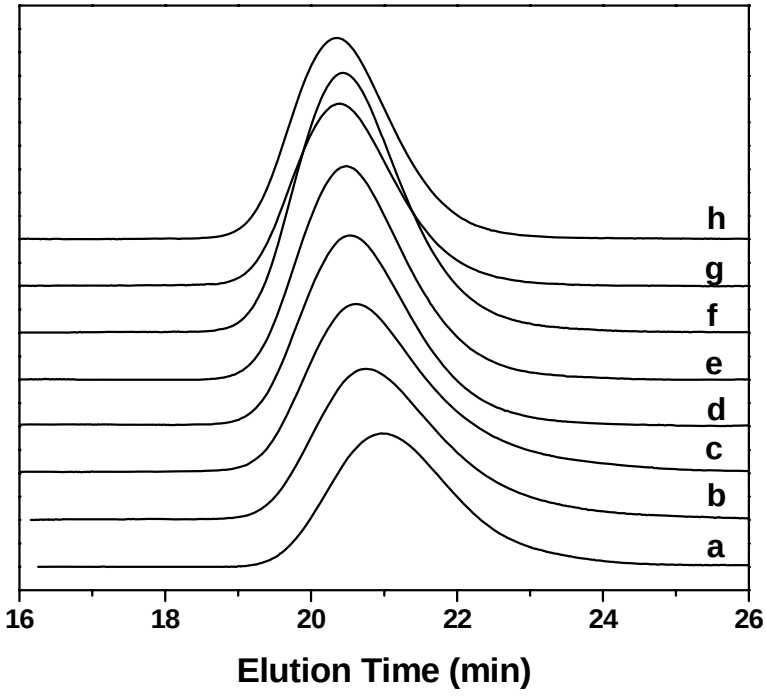

Figure 5-4. Typical Size Exclusion Chromatography (SEC) traces of poly(methyl methacrylate) (PMMA) prepared with HPEI25k-$EA_{0.79}$ as macroligand, polymerization conditions: [M]:[I]:[CuCl]:[amine groups of ligands]=254:1:1:10, ethyl 2-bromoisobutyrate (EBIB) as initiator, $V_{MMA}/V_{Solvent}$=2, at 80 °C in 1,4-dioxane. M_n was measured by SEC in $CHCl_3$ at 30°C. (a) $M_n = 1.50x10^4$, Polydispersity Index (PDI) = 1.31; (b) $M_n = 1.83x10^4$, PDI = 1.40; (c) $M_n = 1.95x10^4$, PDI = 1.37; (d) $M_n = 2.30x10^4$, PDI = 1.30; (e) $M_n = 2.54x10^4$, PDI = 1.28; (f) $M_n = 2.63x10^4$, PDI = 1.27; (g) $M_n = 2.72x10^4$, PDI = 1.25. (h) $M_n = 2.89x10^4$, PDI = 1.24.

All of the ligands were used for polymerization and lead to the formation of polymers. This demonstrates that they can in principle be used as ligand for ATRP.

Molecular weights ($M_{n(SEC)}$) and polydispersities of the resulting poly(methyl methacrylate) samples were measured by SEC equipped with a RI-detector. Figure 5-4 shows typical SEC traces for the polymers obtained. All molecular weight distributions are unimodal and the polydispersity index (PDI) values are in the range of 1.2-1.4 (Table 5-2), indicating that EA- or BA-modified HPEIs are suitable macroligands for the copper mediated ATRP of MMA.

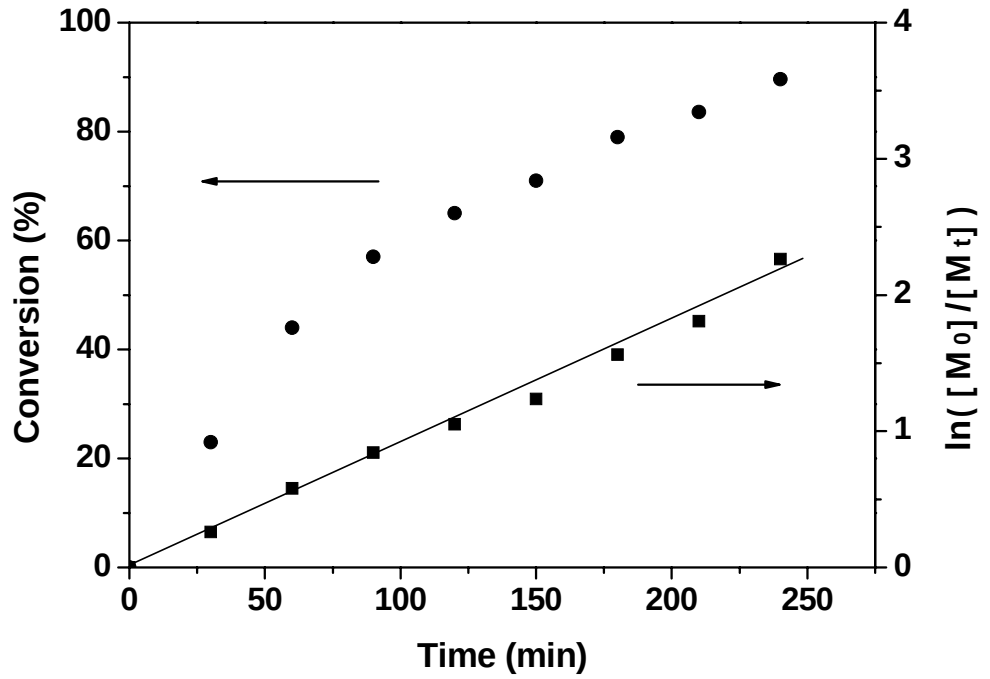

Figure 5-5. Dependence of monomer conversion and $\ln([M]_0/[M]_t)$ on time for the polymerization of methyl methacrylate in 1,4-dioxane, using HPEI25k-$EA_{0.79}$/CuCl as homogenous catalyst at 80°C. Ethyl 2-bromoisobutyrate (EBIB) was used as initiator, [M]:[I]:[CuCl]: [amine groups of HPEI25k-$EA_{0.79}$]=254:1:1:10, $V_{MMA}/V_{Dioxane}$=2 (volume ratio of MMA to 1,4-dioxane)

Kinetic studies have been carried out using the following ratios: [M]:[I]:[CuCl]:[amine of ligands] = 254:1:1:10, $V_{MMA}/V_{Dioxane}$ = 2 (volume ratio of MMA to 1,4-dioxane). Samples were taken from the reaction mixture via syringes at certain time intervals for conversion measurements (^{1}H NMR) and molecular weight determination (SEC). The respective first order kinetic plot is depicted in Figure 5-5. $\mathrm{Ln}([M]_0/[M]_t)$ shows a linear dependence on time, indicating a constant concentration of propagating species throughout the reaction. Molecular weights increase linearly with conversion, and the molecular weight distributions are fairly narrow (M_w/M_n<1.4) (Figure 5-6), demonstrating that the ATRP of MMA with macroligands derived from HPEI represents a controlled process.

Table 5-2. Atom transfer radical polymerization (ATRP) of methyl methacrylate (MMA) using hyperbranched polyethylenimine (HPEI)-based macroligands [a]

Entry	Ligands	Time (h)	Conv. (%)	$M_{n(calc)}$ $\times 10^{-4}$	$M_{n(SEC)}$ $\times 10^{-4}$	Initiation efficiency [b]	PDI
1	HPEI25k-$EA_{1.01}$	3	76	1.95	2.70	0.72	1.26
2	HPEI25k-$EA_{0.79}$	3	79	2.03	2.63	0.77	1.27
3	HPEI25k-$BA_{1.01}$	3	79	2.03	2.61	0.78	1.32
4	HPEI25k-$BA_{0.76}$	3	82	2.10	2.63	0.80	1.29
5	HPEI10k-$EA_{1.06}$	2.5	68	1.75	2.30	0.76	1.31
6	HPEI10k-$EA_{0.77}$	2.5	71	1.83	2.48	0.74	1.27
7	HPEI10k-$BA_{0.76}$	2.5	73	1.88	2.59	0.73	1.29
8	HPEI1.8k-$EA_{0.87}$	3	89	2.28	3.87	0.59	1.27
9	HPEI1.2k-$EA_{0.73}$	3	92	2.36	4.06	0.58	1.33

[a] ATRP conditions: [M]:[I]:[CuCl]:[amine of ligands] = 254:1:1:10, ethyl 2-bromoisobutyrate (EBIB) as initiator, $V_{MMA}/V_{Solvent} = 2$ (volume ratio of MMA to 1,4-dioxane), at 80 ^{o}C in 1,4-dioxane. The conversion was calculated from ^{1}H NMR, $M_{n(calc)}$ was calculated from conversion. [b] Initiation efficiency = $M_{n(calc)}/M_{n(SEC)}$.

The preparation of hyperbranched PEI-macroligands with maximum [R]/[amine] value was time-consuming and laborious. Thus, it is important to clarify whether application of the maximum [R]/[amine] value is a necessary precondition. It is obvious from Table 5-2 that the polymerization results using hyperbranched macroligands with maximum and lower [R]/[amine] values are similar (Entries 1-6 in Table 5-2), indicating that the extent of control over the polymerization does not critically depend on full acrylate substitution of the macroligand. The effect of the nature of the alkyl group (EA or BA) at the hyperbranched macroligands on the ATRP of MMA has also been studied, and also this parameter does not lead to obvious differences in the catalytic activities for the polymerization or the quality of the resulting polymers (Entries 1-4, 6, 7 in Table 5-2). However, variation of the molecular weight of the HPEI scaffold showed obvious effects on the catalytic

activity (Entries 2, 6, 8, 9 in Table 5-2). Upon lowering the molecular weight of HPEI the polymerization rate increased.

The M_n values of PMMA obtained from SEC using polystyrene calibration standards can be taken as absolute molecular weights, since they have been demonstrated to exhibit very little difference with those from SEC using PMMA standards for calibration.[17, 32, 33] In order to confirm this, the viscosity of several PMMA samples has been measured and their respective absolute molecular weights were calculated on the basis of their respective viscosities according to the following equation:

$$[\eta] = \kappa[M]^{\alpha} \qquad (5\text{-}3)$$

Here $k = 4.8 \times 10^{-3}$, $\alpha = 0.8$ in $CHCl_3$ at 25°C. As shown in Table 5-3, they were found to be very similar to the values obtained from SEC using polystyrene standards for calibration.

Table 5-3. Comparison: molecular weights obtained from GPC and viscosimetry

Sample	$M_{n(SEC)}$ x10^{-4}	M_{η} [a] x10^{-4}
1	1.50	1.45
2	2.90	2.41
3	3.97	3.86
4	2.49	1.96

[a] Calculated according to $[\eta] = k[M]^{\alpha}$, where $k = 4.8 \times 10^{-3}$, $\alpha = 0.8$.

Thus, in this chapter the $M_{n(SEC)}$ of the obtained PMMA samples was also regarded as absolute M_n. This is important, since by comparing the molecular weights obtained from theoretical calculations ($M_{n(cacl)}$) with $M_{n(SEC)}$, the polymerization initiation efficiency ($M_{n(cacl)}/M_{n(SEC)}$) can be calculated. The initiation efficiencies for the polymerization with the hyperbranched macroligands from HPEI1.2k and HPEI1.8k are obviously lower than those from the macroligands with higher molecular weights, indicating that the control of polymerization with the hyperbranched macroligands from low molecular weight HPEI is limited. In addition, the separation of the low molecular weight macroligand complex with copper from the resulting PMMA by a precipitation procedure is difficult, i.e., thsse PMMA

products still show greenish color after the precipitation purification, confirming that the products are contaminated with copper.

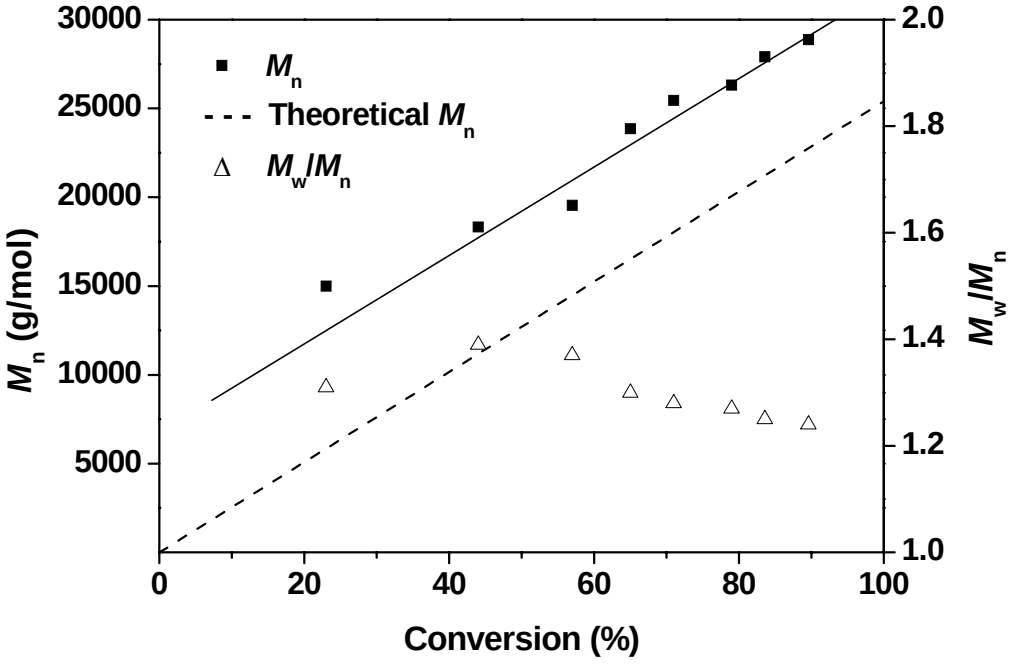

Figure 5-6. Dependence of molecular weight and polydispersity on conversion for poly(methyl methacrylate) obtained from atom transfer radical polymerization of methyl methacrylate, using HPEI25k-$EA_{0.79}$/CuCl as homogeneous catalyst at 80 ^{o}C

From Table 5-4 it is obvious that all initiation efficiencies of the ATRP of MMA with hyperbranched macroligands are below 100%. Similar phenomena have also been observed by other groups. For example, Brooks et al.[35] observed reduced initiation efficiency when using multiamines supported on hyperbranched polyglycerol as a ligand.

The lower initiation efficiency might be attributed to the very high activation ability of the CuX-macroligand catalyst system, leading to a high concentration of primary radical species from the sacrificial initiators at the beginning of the polymerization, which result in a loss of initiator due to termination reactions, just as in the ATRP of MMA using the low molecular weight analogue of HPEI, Me_6-TREN, as a ligand.[7, 52]

For an additional improvement of the initiation efficiencies and the polydispersity of the polymers, the conveniently available hyperbranched macroligand, HPEI25k-

$EA_{0.79}$, showing better control of the ATRP of MMA and purification of the products, was chosen. The results are listed in Table 5-4. A fast and reversible transition between the activating agent CuX (X = Cl or Br) and the deactivating agent CuX_2 is the key parameter in ATRP systems to assure a controlled radical polymerization process. CuX_2 can deactivate most of the active propagating radical species into dormant ones, suppressing radical coupling side reactions.[7, 8]

Table 5-4. Atom transfer radical polymerization of methyl methacrylate using HPEI25k-$EA_{0.79}$ as macroligand [a]

Entry	Solvent	T (^oC)	Time (h)	Conv. (%)	$M_{n(calc)}$ $\times 10^{-4}$	$M_{n(SEC)}$ $\times 10^{-4}$	Initiation efficiency [g]	PDI
1	1,4-dioxane	80	0.5	23	0.61	1.50	0.41	1.31
2	1,4-dioxane	80	1	44	1.14	1.83	0.62	1.40
3	1,4-dioxane	80	2	65	1.67	2.30	0.73	1.30
4	1,4-dioxane	80	3	79	2.03	2.63	0.77	1.27
5	1,4-dioxane	80	3.5	84	2.16	2.72	0.80	1.25
6	1,4-dioxane	80	4	90	2.31	2.89	0.83	1.24
7[b]	1,4-dioxane	80	4	71	1.83	2.90	0.63	1.23
8[c]	1,4-dioxane	80	7	45	1.20	3.56	0.34	1.29
9[d]	1,4-dioxane	80	3	91	2.33	3.97	0.59	1.31
10[e]	1,4-dioxane	80	2.5	68	1.75	2.48	0.71	1.23
11	toluene	80	2.5	62	1.60	2.49	0.64	1.25
12	acetone	60	20	67	1.73	2.22	0.78	1.39
13[f]	acetone	60	48	72	1.85	2.76	0.67	1.26

[a] ATRP conditions: [M]:[I]:[CuCl]:[amine groups of ligands] = 254:1:1:10, ethyl 2-bromoisobutyrate (EBIB) as initiator, $V_{MMA}/V_{Solvent} = 2$, the conversion was calculated from ^1H NMR, operated at 300MHz, $M_{n(calc)}$ was calculated from conversion. [b] with 5% $CuBr_2$; [c] with 10% $CuCl_2$; [d] using CuBr as catalyst. [e] $V_{MMA}/V_{Solvent} = 0.5$; [f] [M]:[I]:[CuCl]:[amine groups of ligands] = 254:1:1:20; [g] Initiation efficiency = $M_{n(calc)}/M_{n(SEC)}$,

Since the lower initiation efficiency for the Cu(I)-HPEI macroligand catalyst system might be attributed to the very high concentration of primary radical species from the sacrificial initiators activated by CuX at the beginning of the polymerization, ATRP experiments of MMA with additional CuX_2 pre-introduced into the polymerization mixture have been carried out. To our surprise, the introduction of an excess amount CuX_2 did not improve the polymerization, but contrarily reduced the initiation efficiency (Comparing entries 7 with 3; entries 8 with 2 in Table 5-4). The cause for this phenomenon is still not clear.

When CuBr was used as a catalyst, the initiation efficiency was much lower than using CuCl as a catalyst (Comparing entries 9 with 6 in Table 5-4), which may be due to the higher activity of CuBr,[7, 8] resulting in a considerably higher concentration of primary radical species at the beginning of the polymerization. Other parameters, such as the ratio of CuCl to macroligand and the type or amount of solvent, have also been tested in this context; however, the initiation efficiency could not be improved significantly.

The polymerizations were carried out also in toluene and acetone, (Entries 11, 12 and 13 in Table 5-4) from the results we can see, the polarity of the solvents does not have obvious influence on the polymerization or alter the PDI of the obtained polymer.

5.2.3. Separation of the hyperbranched macroligand/copper complex from PMMA

Usually silica or alumina gels have to be used to separate low molecular weight copper complexes from the polymers. However, in this case large amounts of waste are produced and the catalyst complex can usually not be recovered and reused. In our case, the hyperbranched macroligand-copper complex can be separated from the PMMA product by simple precipitation of the polymerization mixture into methanol, which is due to the large solubility difference between the macroligand and the polymer. As we described before, all hyperbranched macroligands can complex with Cu(I) and the complexes are fully soluble in solvents with a range of different polarities, such as toluene, acetone, dioxane, THF, and methanol, while PMMA is not soluble in the polar solvent methanol.

After filtration, the precipitated PMMA polymers are obtained as white materials, while the solution is green (Figure 5-7), indicating that the copper had been

effectively transferred into the methanol phase in a complexation form with the hyperbranched macroligand. The catalyst complex could be recovered by removing the volatiles under vacuum. Moreover, a control experiment with PMDETA as ligand has also been conducted and the resulting polymer was obtained as an intensely green material (Figure 5-8), indicating that the complex of copper with low molecular weight ligands can not be efficiently separated from PMMA by simple precipitation in methanol.

Figure 5-7. Separation of the complex of HPEI25K-$EA_{0.79}$/CuCl from the polymerization mixture. Left: after precipitation; Right: after filtration.

Figure 5-8. PMMA polymers after purification by precipitation in methanol (A) with HPEI25K-$EA_{0.79}$ as macroligand; (B) with PMDETA as ligand

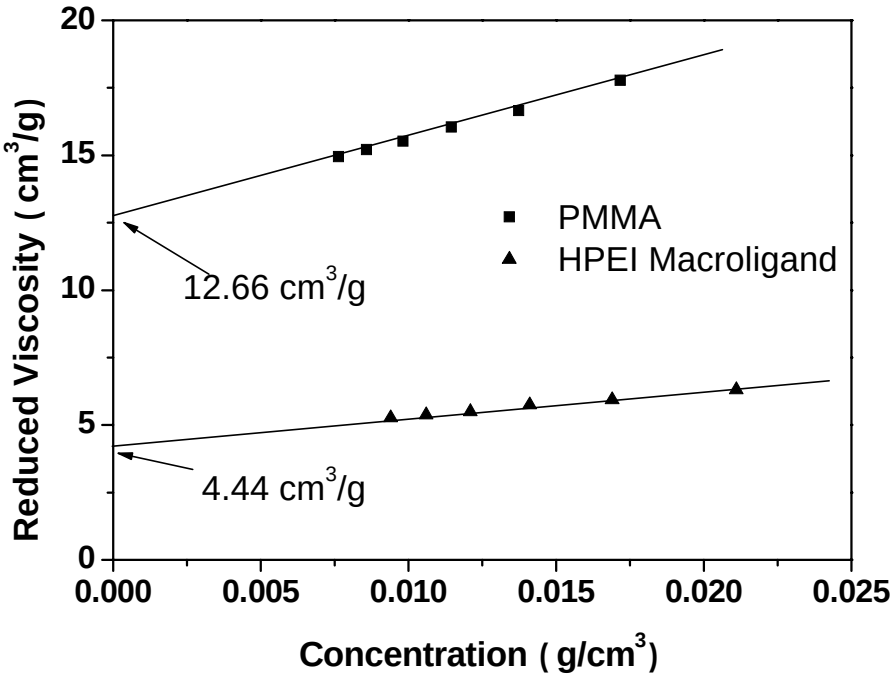

Figure 5-9. Viscosity of (■) poly(methyl methacrylate) (PMMA) (M_n = 2.49x10^4, PDI = 1.25) and (▲) HPEI macroligand: HPEI25K-EA$_{0.79}$ (M_n = 7.09x10^4) in $CHCl_3$ at 25 ^oC

Figure 5-9 shows the viscosity of HPEI25k-EA$_{0.79}$ and the corresponding PMMA synthesized with this hyperbranched macroligand using the ATRP method. As expected, the hyperbranched macroligand possesses much lower viscosity than the final PMMA due to its compact structure. Therefore, it can be deduced that the presence of a hyperbranched macroligand will not lead to a problematic contribution to the final viscosity of the reaction system. This may represent an additional advantage besides the solubility issue. Modified linear PEI has not been used as a macroligand, since it possesses higher viscosity as reported elsewhere,[54, 55] (This will be discussed in Chapter 6 and 7) which is comparable to that of the obtained linear PMMA product. Moreover, chain entanglement or interaction between linear polymers might prevent efficient transfer of the copper complex into methanol during the precipitation process, resulting in Cu-contaminated PMMA.

5.2.4. Residual copper

Atomic absorption spectroscopy (AAS) was used to determine the residual copper content in the PMMA with THF as solvent. According to AAS, 16.5 ppm of Cu

remained in the final PMMA products after the first precipitation from methanol. The copper concentration can be reduced to 12 ppm via a second precipitation step, which is still higher than the value of 5 ppm achieved with a heterogeneous catalyst system,[17] but is comparable to the value of 15 ppm with a heterogeneous catalyst system combined with a small amount of soluble catalyst,[26] and considerably better than the value of 200 ppm reported for thermo-responsive catalyst complexes.[33]

5.2.5. Recycling the hyperbranched macroligand-Cu complex

After recovering the complex of the hyperbranched macroligand with copper, it was reused for the ATRP of MMA. The polymers obtained using recycled catalyst systems during the second cycle and the third cycle still possess similarly narrow molecular weight distributions at high conversion (Table 5-5) as the product from the first run.

Table 5-5. Atom transfer radical polymerization of methyl methacrylate with recycled catalyst system [a]

Run	Time (h)	Conversion (%)	$M_{n(SEC)}$ $\times 10^{-4}$	$M_{n(calc)}$ $\times 10^{-4}$	PDI
1st cycle with fresh catalyst	6	95	2.83	2.44	1.23
2nd cycle with recycled catalyst	9	96	2.82	2.46	1.29
3rd cycle with recycled catalyst	15	94	2.73	2.41	1.25

[a] ATRP conditions: [M]:[I]:[CuCl]:[amine groups of ligands] = 254:1:1:10, ethyl 2-bromoisobutyrate (EBIB) as initiator, $V_{MMA}/V_{Solvent} = 2$, at 80 °C, 1,4-dioxane as solvent, HPEI25K-$EA_{0.79}$/CuCl as catalyst system.

Kinetic studies for the fresh and the reused catalyst system have also been carried out. All the curves of $\ln([M]_0/[M]_t)$ versus time are linear (Figure 5-10), indicating a constant number of propagating species throughout the reaction. Molecular weights increase in a linear fashion with conversion, and the molecular weight distributions are fairly narrow in all cases ($M_w/M_n<1.4$) (Figure 5-11), demonstrating that the

recycled catalysts are still active for the ATRP of MMA. Clearly, the polymerizations can still be controlled until the third cycle.

However, the concentration of propagating species in the polymerization decreased and consequently the reaction time required for the same conversion had to be raised with increasing the number of cycles (Figure 5-10). We tentatively explain this by partial oxidation of the active Cu(I) catalyst to the deactivating Cu(II) agent. The deactivating Cu(II) agent can be formed in two ways: (i) during polymerization or (ii) during precipitation of the macroligand-Cu(I) catalyst complex, since the catalyst is inevitably exposed to air for some time, resulting in partial oxidation of the active Cu(I) catalyst.

In the reported heterogeneous catalytic system,[25, 32] due to the generation of the deactivating Cu(II) agent better control for the polymerization was observed, when recycled catalyst was used. However, in our system the generated deactivating Cu(II) agent in the second and third cycles did not aid to improve the polymerization initiation efficiency and the quality of the final products. The products obtained from different cycles at the same conversion possess similar molecular weight and polydispersity.

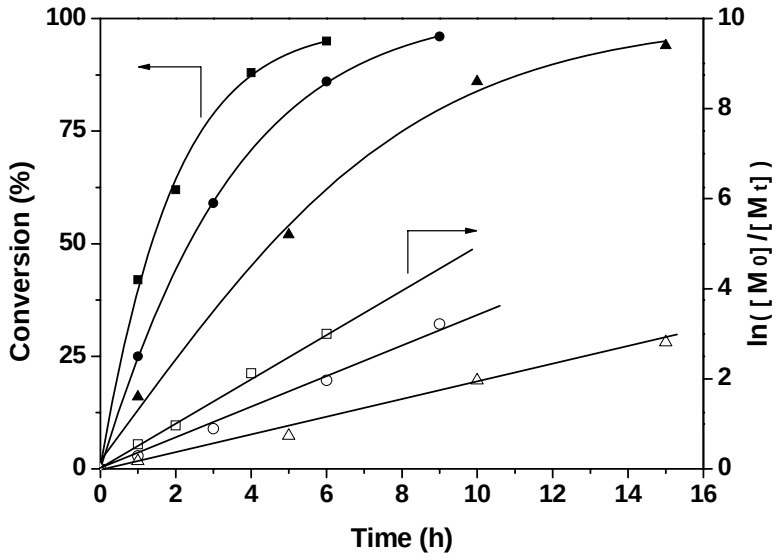

Figure 5-10. Dependence of monomer conversion and $\ln([M]_0/[M]_t)$ on time for the polymerization of methyl methacrylate in 1,4-dioxane, reusing hyperbranched HPEI25K-$EA_{0.79}$/CuCl as recoverable homogeneous catalyst at 80 °C. Reaction conditions as indicated in Table 4. (■□) first cycle, (●○) second cycle and (▲Δ) third cycle.

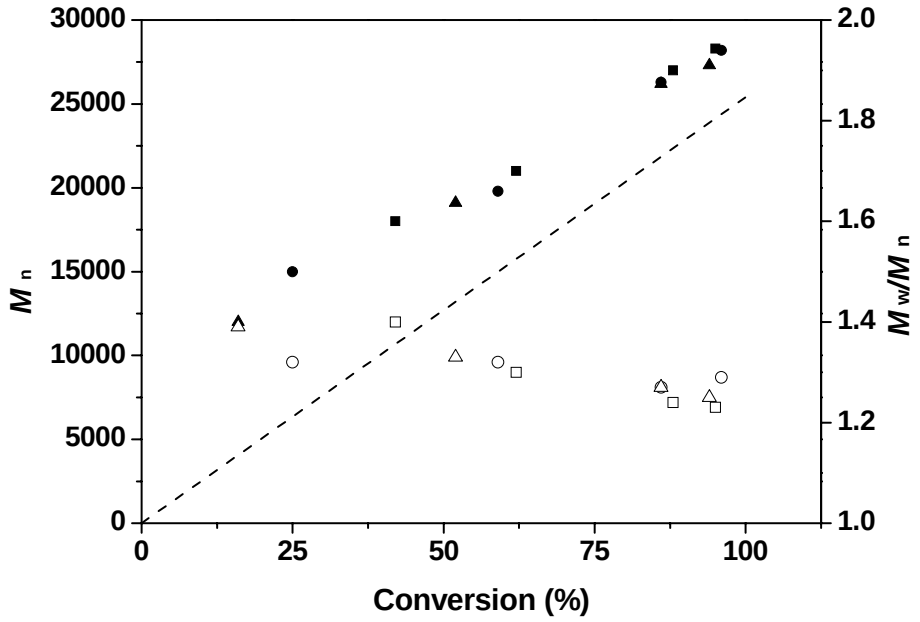

Figure 5-11. Molecular weight *vs*. conversion for poly(methyl methacrylate) obtained from recycled catalyst at 80 °C, (■□) first cycle, (●○) second cycle and (▲Δ) third cycle.

5.2.6. Tacticity of the obtained PMMA

Since in all experiments PMMA samples with narrow molecular weight distribution, was obtained, the possibility that coordination of the polymer might play a role in the polymerization has to be taken into account. Radical coupling may be reduced due to the bulky size of the HPEI ligand, i.e., the monomers might have to adopt a specific arrangement during chain growth which can be designated "coordination".

The tacticity of the obtained PMMA was measured using ^{13}C NMR (Figure 5-12) and listed in Table 5-6 for comparison.[56] Clearly, the same *mm:rr:mr* ratio as for PMMA obtained from normal free radical polymerization is observed. The tacticity of the polymer did not show any difference with the one obtained from normal radical polymerization, which indicates that the same type of active species are present in both ATRP and the conventional radical system. The PMMA samples prepared by ATRP are all predominantly syndiotactic.

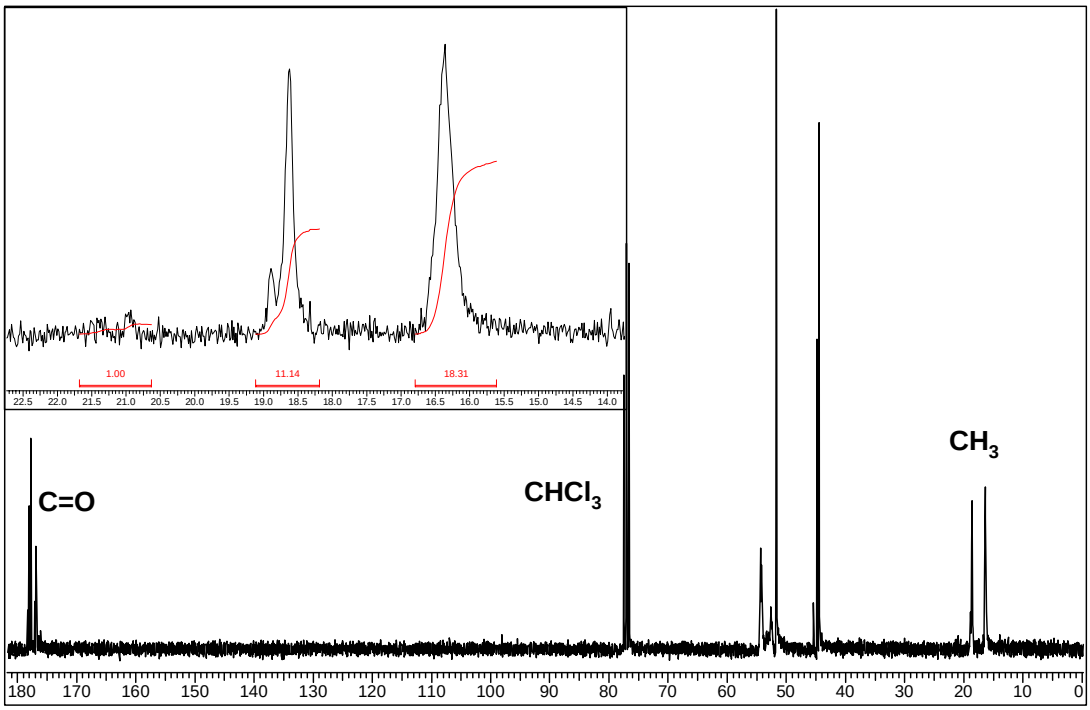

Figure 5-12. ^{13}C NMR spectrum of lab-scale PMMA from ATRP using HPEI/Cu(I) as recoverable macroligand/catalyst system

Table 5-6. Tacticity of PMMA from ATRP and conventional radical polymerization

	Tacticity [a]		
	mm (%)	*mr (%)*	*rr (%)*
PMMA from conventional radical polymerization	2	35	63
PMMA from ATRP (this work)	4	35	61

a) Calculated from ^{13}C NMR.

5.2.7. Use of the ligand for ATRP of styrene and butyl acrylate

Tests of these macroligands for the ATRP of other acrylate monomers (butyl acrylate and *tert*-butyl acrylate) and styrene have also been carried out. The results for acrylate monomers are not comparable to those for MMA, since we only obtained polymer with polydispersity around 1.5-1.6. (Runs no 1, 2 in Table 5-7)

In the case of styrene, experiments indicated that conversion increases with time, but at the beginning the obtained polystyrene samples show rather broad

polydispersity. (Run no 3, 4 in Table 5-7) Polymers with relatively narrow molecular weight distribution can only be obtained at higher conversion. (Run no. 5 in Table 5-7, 1.36 at 74% conversion). Increasing the polarity of the solvent did not lead to better control of the polymerization. (From anisole to dioxane, Table 5-7, runs no. 6 and 7) Additional optimization of the polymerization conditions is necessary to utilize modified PEI macroligands as ligand for the ATRP of either BA or styrene.

Table 5-7. Atom transfer radical polymerization of BA, *t*BA, St using HPEI25k-$EA_{0.79}$ as macroligand

Run	Monomer	Time (hr)	Solvent	*Conversion (%)*	$M_{n\ NMR}$ *x* 10^4	M_{nGPC} *x* 10^4	M_w/M_n
1 [a]	BA	4	Acetone	34	0.89	1.24	1.64
2 [a]	*t*BA	8	Acetone	73	1.88	2.34	1.50
3 [b]	St	12	Toluene	32	1.29	1.78	1.76
4 [b]	St	16	Toluene	39	1.58	2.18	1.53
5 [b]	St	32	Toluene	74	2.96	3.67	1.36
6 [b]	St	24	anisole	56	2.26	2.87	1.90
7 [b]	St	24	dioxane	69	2.78	3.38	1.70

[a] [Monomer]:[In] = 200:1, at 60°C. [b] [Monomer]:[In] = 400:1, at 100°C, ATRP conditions: [I]:[CuCl]:[amine groups of ligands] = 1:1:10, ethyl 2-bromoisobutyrate (EBIB) as initiator, $V_{Monomer}/V_{Solvent} = 2$, the conversion was calculated from ^{1}H NMR, operated at 300MHz, $M_{n(calc)}$ was calculated from conversion.

5.3. Conclusions

Hyperbranched macroligands were successfully prepared by facile Michael addition reaction of hyperbranched PEI with EA or BA. The resulting hyperbranched macroligand/Cu(I) complexes are efficient catalyst systems for the ATRP of MMA. The ATRP of MMA with hyperbranched macroligands is a controlled process, since $\ln([M]_0/[M]_t)$ is a linear function of time. Molecular weights of the resulting PMMA increase linearly with conversion and the molecular weight distributions are fairly narrow (M_w/M_n<1.4) even at very high conversion. However, the initiation efficiency of the polymerization using hyperbranched macroligands is less than 100%, usually in the range of 0.41-0.83. The compact structure not only leads to very low viscosity

compared to the synthesized linear PMMA, but also imparts facile separation from the PMMA product by precipitation of the polymerization mixture in methanol. Copper is separated together with the hyperbranched macroligands and no additional steps are required to purify the polymer from copper contamination. The hyperbranched macroligand/CuCl system can be recycled for the ATRP of MMA, keeping relatively high activity. The obtained PMMAs do not exhibit unusual tacticity.

These macroligands can also be utilized for the ATRP of BA or Styrene, however, additional optimization of the polymerization conditions is necessary.

5.4. Experimental Part

5.4.1. Materials

CuBr (98%, Acros) was purified as described in literature.[57] Methyl methacrylate (MMA, Aldrich, 99%), styrene (St, Aldrich, 99%), butyl acrylate (BA, Acros, 99%), *tert*-butyl acrylate (*t*BA, Aldrich, 98%), were distilled under reduced pressure, stored in a refrigerator and bubbled with argon for 1 hr prior to use. *N,N,N',N',N"*- Pentamethyldiethylenetriamine (PMDETA, Aldrich, 99%) were distilled under reduced pressure and degassed with argon for 30 min prior to use. Ethyl 2-bromoisobutyrate (EBIB, 98%) was used as received from Aldrich. Butyl acrylate for Micheal-addition (BA, 99+%), ethyl acrylate (EA, 99%), CuCl (99.99%) and $CuBr_2$ (99+%) were used as received from Acros.

Hyperbranched polyethylenimines, HPEI1.2k (Polysciences, M_n= 1200, M_w/M_n = 1.03,), HPEI1.8k (Polysciences, M_n = 1800, M_w/M_n = 1.04), HPEI10k (Aldrich, M_n = 10^4, M_w/M_n = 2.5), HPEI25k (Hyperpolymers GmbH, M_n = 2.5x10^4, M_w/M_n = 2.5) were dried under vacuum prior to use.

5.4.2. Synthesis of the Hyperbranched Macroligands via Michael-Addition of Ethyl Acrylate or Butyl Acrylate with HPEI

The synthetic procedure for partially EA- or BA-modified HPEI is exemplified for HPEI25k-$EA_{0.79}$: 1.00 g of HPEI25k (M_n = 2.50x10^4, 23.3 mmol amine groups) was dissolved in 5.00 ml THF, and then 2.52 ml (23.3 mmol) of EA was added. The mixture was stirred at room temperature for 24 h, and subsequently at 50 ^oC for another 24 h. The solvents were removed under vacuum, and 2.83 g yellow honey-like polymer was obtained. M_n = 7.09 x 10^4, yield = 100%. IR: ν = 1735 cm^{-1} (C=O); ^1H NMR (300 MHz, $CDCl_3$): δ = 1.20 ($C\underline{H}_3CH_2OOC$-), 2.38-2.73 (-$NCH_2C\underline{H}_2COO$-,

-NC$\underline{H}_2$CH$_2$COO-, -NC$\underline{H}_2$C$\underline{H}_2$N- of PEI), 4.08 (CH$_3$C$\underline{H}_2$OOC-); ^{13}C NMR (75.4 MHz, $CDCl_3$, 25°C): δ = 14.2 (C$\underline{H}_3$CH$_2$OOC-), 32.7 (-NCH$_2$C$\underline{H}_2$COO-), 49.7-52.7 (-N$\underline{C}$H$_2$CH$_2$COO-, -N$\underline{C}$H$_2$C$\underline{H}_2$N- of PEI), 60.3 (CH$_3$$\underline{C}H_2$OOC-), 172.4 (-NCH$_2CH_2$$\underline{C}$OO-).

The synthetic procedure for fully EA- or BA-modified HPEIs is exemplified for HPEI25k-EA$_{1.01}$: 2.50 g of HPEI25k (M_n = 2.50 x 10^4, 58.1mmol amine groups) was dissolved in 10 ml THF, and then 20 ml (184.5 mmol) of EA was added. The mixture was stirred at room temperature for 5 days. Then the solvent was removed, and the residual polymer was re-dissolved in 20 ml of EA. The mixture was stirred for another 5 days at room temperature in order to obtain full conversion. This procedure was repeated, until the reaction reached the maximum degree of conversion (followed by ^{1}H NMR). Solvents were evaporated to yield a yellow honey-like polymer (8.00 g). M_n = 8.38 x 10^4, yield = 95.5%. IR: ν = 1735 cm^{-1} (C=O); ^{1}H NMR (300 MHz, $CDCl_3$): δ = 1.20 (C$\underline{H}_3$CH$_2$OOC-), 2.38- 2.73 (-NCH$_2$C$\underline{H}_2$COO-, -NC$\underline{H}_2$CH$_2$COO-, -NC$\underline{H}_2$C$\underline{H}_2$N- of PEI), 4.08 (CH$_3$C$\underline{H}_2$OOC-); ^{13}C NMR (75.4 MHz, $CDCl_3$, 25°C): δ = 14.2 (C$\underline{H}_3$CH$_2$OOC-), 32.7 (-NCH$_2$C$\underline{H}_2$COO-), 49.7-52.7 (-N$\underline{C}$H$_2$CH$_2$COO-, -N$\underline{C}$H$_2$C$\underline{H}_2$N- of PEI), 60.3 (CH$_3$$\underline{C}H_2$OOC-), 172.4 (-NCH$_2CH_2$$\underline{C}$OO-).

All ligands were additionally purified by dialysis against chloroform for 2 days to completely remove low molecular impurities, using a benzoylated cellulose membrane (MWCO 1000 g/mol).

5.4.3. ATRP of MMA Using the New Hyperbranched Macroligand

In a typical experiment, 84.1 mg (0.690 mmol of amine groups) of macroligand HPEI25k-EA$_{0.79}$, 8.1 mg (0.082 mmol) of CuCl, 4 ml (37.4 mmol) of MMA and 2 ml of 1,4-dioxane were placed in a flask with a magnetic stir bar. The flask was sealed with a rubber septum and degassed by three freeze-pump-thaw cycles. Then 12 μl (0.082 mmol) of EBIB was introduced into the flask by an argon-purged syringe. The flask was then immersed in an oil bath thermostated at 80 ^{o}C. After 3 hours, the flask was immersed into liquid nitrogen to quench the reaction. Samples were taken, diluted with deuterated chloroform and subsequently analyzed by ^{1}H NMR spectroscopy (operated at 300 MHz). Comparing the integration of the double bonds of MMA monomers (2H, 6.06 ppm & 5.52 ppm) with that of methyl groups of monomers and polymers (3H, 0.97 ppm & 0.80 ppm), the monomer conversion was calculated. The

residue was diluted with acetone and precipitated into 10 fold methanol directly. The precipitant was collected via filtration, and then redis-solved in acetone and re-precipitated in methanol. Pure samples were obtained after drying at 40 ^{o}C in *vacuo* for 2 days. Conversion: 79%. $M_{n(SEC)}$ = 2.63x10^4, PDI = 1.27.

5.4.4. Recovery and Reuse of the Macroligand-Copper Catalyst

In a typical experiment, 84.1 mg (0.690 mmol of amine groups) of macroligand HPEI25k-EA$_{0.79}$, 8.1 mg (0.082 mmol) of CuCl, 4 ml (37.4 mmol) of MMA and 2.00ml of 1,4-dioxane were placed in a flask with a magnetic stir bar. The flask was sealed with a rubber septum and degassed by three freeze-pump-thaw cycles. Then 12 μl (0.082 mmol) of EBIB was introduced into the flask by an argon-purged syringe. The flask was then immersed in an oil bath thermostated at 80 ^{o}C. After 6 hours, the polymerization reach ca. 95 %, verified by ^{1}H NMR spectroscopy. The flask was then immersed into liquid nitrogen to quench the reaction. The mixture was diluted with acetone and precipitated into 10 fold methanol directly. The precipitant was quickly removed using a Büchner funnel under reduced pressure. After the volatile of the solution was distilled off under reduced pressure (the catalyst containing solution and filtrate were exposed to air for a short period of time), the residue was re-dissolved in 2.00 ml of 1,4-dioxane and 4.00 ml of MMA, as in the first polymerization run. After the degassing step, the same amount of initiator, 12 μl (0.082 mmol) of EBIB was introduced and the flask was immersed in an oil bath thermostated at 80 ^{o}C under stirring. After 9 h, the polymerization was stopped and the macroligand-copper catalyst was recovered as described above. The recovered macroligand-copper catalyst was reused for the third polymerization run with the same condition as the second polymerization run. First run: conversion = 95% (6 h); $M_{n(SEC)}$ = 2.83x10^4; PDI = 1.23. Second run: conversion = 96% (9 h); $M_{n(SEC)}$ = 2.82x10^4; PDI = 1.29. Third run: conversion = 94% (15 h); $M_{n(SEC)}$ = 2.73x10^4; PDI = 1.25.

5.4.5. ATRP of Styrene, BA and *t*BA Using the New Hyperbranched Macroligand

In a typical experiment, 84.1 mg (0.690 mmol of amine groups) of macroligand HPEI25k-EA$_{0.79}$, 8.1 mg (0.082 mmol) of CuCl, a certain amount of monomer and solvent were placed in a flask with a magnetic stir bar. The flask was sealed with a

rubber septum and degassed by three freeze-pump-thaw cycles. Then 12 μl (0.082 mmol) of ethyl 2-bromoisobutyrate (EBIB) was introduced into the flask by an argon-purged syringe. The flask was then immersed in an oil bath thermostated at 60 or 100 ^{o}C. After several hours, the reactant was diluted with chloroform and precipitated into 10 fold methanol directly. The precipitant was collected via filtration, and then re-dissolved in chloroform and re-precipitated in methanol. Pure samples were obtained after drying at 40 ^{o}C in *vacuo* for 2 days.

5.5. References

[1] Wang, J.-S.; Matyjaszewski, K. *J. Am. Chem. Soc.* **1995,** 117, 5614.
[2] Gaynor, S. G.; Matyjaszewski, K. *ACS Symp. Ser.* **1998,** 685, 396.
[3] Percec, V.; Barboiu, B. *Macromolecules* **1995,** 28, 7970.
[4] Kato, M.; Kamigaito, M.; Sawamoto, M.; Higashimura, T. *Macromolecules* **1995,** 28, 1721.
[5] Chiefari, J.; Chong, Y. K.; Ercole, F.; Kristina, J.; Jeffery, J.; Le, T. P. T.; Mayadunne, R. T. A.; Meijs, G. F.; Moad, C. L.; Moad, G.; Rizzardo, E.; Thang, S. H. *Macromolecules* **1998,** 31, 5559.
[6] Malmstrom, E. E.; Hawker, C. L. *Macromol. Chem. Phys.* **1998,** 199, 923.
[7] Matyjaszewski, K.; Xia, J. *Chem. Rev.* **2001,** 101, 2921.
[8] Kamigaito, M.; Ando, T.; Sawamoto, M. *Chem. Rev.* **2001,** 101, 3689.
[9] Tsarevsky, N. V.; Sarbu, T.; Gobelt, B.; Matyjaszewski, K. *Macromolecules* **2002,** 35, 6142.
[10] Matyjaszewski, K. *Polym. Int.* **2003,** 52, 1559.
[11] Shen, Z.; Chen, Y.; Barriau, E.; Frey, H. *Macromol. Chem. Phys.* **2006,** 207, 57.
[12] Matyjaszewski, K.; Gaynor, S. G.; Kulfan, A.; Podwika, M. *Macromolecules* **1997,** 30, 5192.
[13] Krishnan, R.; Srinivasan, K. S. V. *Macromolecules* **2004,** 37, 3614.
[14] Karanam, S.; Goossens, H.; Klumperman, B.; Lemstra, P. *Macromolecules* **2003,** 36, 8304.
[15] Gromada, J.; Spanswick, J.; Matyjaszewski, K. *Macromol. Chem. Phys.* **2004,** 205, 551.
[16] Matyjaszewski, K.; Nakagawa, Y.; Jasieczek, C. B. *Macromolecules* **1998,** 31, 1535.
[17] Kickelbick, G.; Paik, H. J.; Matyjaszewski, K. *Macromolecules* **1999,** 32, 2941.
[18] Haddleton, D. M.; Duncalf, D. J.; Kukulj, D.; Radigue, A. P. *Macromolecules* **1999,** 32, 4769.
[19] Haddleton, D. M.; Kukulj, D.; Radigue, A. P. *Chem. Commun.* **1999,** 1, 99.
[20] Shen, Y.; Zhu, S.; Pelton, R. *Macro. Rapid Comm.* **2000,** 21, 956.
[21] Shen, Y.; Zhu, S.; Zeng, F.; Pelton, R. *J. Polym. Sci. Polym. Chem.* **2001,** 39, 1051.
[22] Shen, Y.; Zhu, S.; Zeng, F.; Pelton, R. *Macromolecules* **2000,** 33, 5427.
[23] Shen, Y.; Zhu, S.; Zeng, F.; Pelton, R. *Macromol. Chem. Phys.* **2000,** 201, 1387.
[24] Shen, Y.; Zhu, S.; Pelton, R. *Macromolecules* **2001,** 34, 5812.
[25] Nguyen, J. V.; Jones, C. W. *Macromolecules* **2004,** 37, 1190.

[26] Hong, S. C.; Paik, H.-J.; Matyjaszewski, K. *Macromolecules* **2001,** 34, 5099.
[27] Hong, S. C.; Matyjaszewski, K. *Macromolecules* **2002,** 35, 7592.
[28] Hong, S. C.; Lutz, J. F.; Inoue, Y.; Strissel, C.; Nuyken, O.; Matyjaszewski, K. *Macromolecules* **2003,** 36, 1075.
[29] Hong, S. C.; Neugebauer, D.; Inoue, Y.; Lutz, J. F.; Matyjaszewski, K. *Macromolecules* **2003,** 36, 27.
[30] Liou, S. R., J. T.; Malaba, D.; Pallack, M. E.; Brittain, W. J. *Macromolecules* **2000,** 33, 4295.
[31] Shen, Y.; Zhu, S.; Pelton, R. *Macromolecules* **2001,** 34, 3182.
[32] Yang, J.; Ding, S.; Radosz, M.; Shen, Y. *Macromolecules* **2004,** 37, 1728.
[33] Barré, G.; Taton, D.; Lastecoueres, D.; Vincent, J. M. *J. Am. Chem. Soc.* **2004,** 126, 7764.
[34] Honigfort, M. E.; Brittain, W. J.; Bosanac, T.; Wilcox, C. S. *Macromolecules* **2002,** 35, 4849.
[35] Kumar, K. R.; Kizhakkedathu, J. N.; Brooks, D. E. *Macromol. Chem. Phys.* **2004,** 205, 567.
[36] Dijkstra, H. P.; Klink, G. P. M.; Koten, G. *Acc. Chem. Res.* **2002,** 35, 798.
[37] Heerbeek, R.; Kamer, P. C. J.; Leeuwen, P. W. N. M.; Reek, J. N. H. *Chem. Rev.* **2002,** 102, 3717.
[38] Frey, H.; Lach, C.; Lorenz, K. *Adv. Mater.* **1998,** 10, 279.
[39] Bosman, A. W.; Hanssen, H. M.; Meijer, E. W. *Chem. Rev.* **1999,** 99, 1665.
[40] Grayson, S. M.; Fréchet, J. M. J. *Chem. Rev.* **2001,** 101, 3819.
[41] Hecht, S.; Fréchet, J. M. J. *Angew. Chem. Int. Ed.* **2001,** 40, 74.
[42] Newkome, G. R.; Moorefield, C. N.; Vögtle, F. *Wiley-VCH, Weinheim* **2001**.
[43] Astruc, D.; Chardac, F. *Chem. Rev.* **2001,** 101, 2991.
[44] Schlenk, C.; Kleij, A. W.; Frey, H.; Koten, G. *Angew. Chem. Int. Ed.* **2000,** 39, 3445.
[45] Stiriba, S.-E.; Slagt, M. Q.; Kautz, H.; Gebbink, R. J. M. K.; Frey, H.; Koten, G. *Organometallics* **2004,** 23, 1525.
[46] Stiriba, S.-E.; Slagt, M. Q.; Kautz, H.; Gebbink, R. J. M. K.; Thomann, R.; Frey, H.; Koten, G. *Chem. Eur. J.* **2004,** 10, 1267.
[47] Slagt, M. Q.; Stiriba, S.-E.; Gebbink, R. J. M. K.; Kautz, H.; Frey, H.; Koten, G. *Macromolecules* **2002,** 35, 5734.
[48] Salazar, R.; Fomina, L.; Fomine, S. *Polym. Bull.* **2001,** 47, 151.
[49] Boussif, O., ;; Lezoualch, F., ;; Zanta, M. A.; Mergny, M. D.; Scherman, D.; Demeneix, B.; Behr, J. P. *Proc. Natl. Acad. Sci.* **1995,** 92, 7297.
[50] Godbey, W. T.; Wu, K. K.; Mikos, A. G. *Proc. Natl. Acad. Sci.* **1999,** 96, 5177.
[51] Godbey, W. T.; Barry, M. A.; Saggau, P.; Wu, K. K.; Mikos, A. G. *J. Biomed. Mater. Res.* **2000,** 51, 321.
[52] Queffelec, J.; Gaynor, S. G.; Matyjaszewski, K. *Macromolecules* **2000,** 33, 8629.
[53] Smith, M. B.; March, J., *March's Advanced Organic Chemistry: Reactions, Mechanisms, and Structure*. 5th ed.; Wiley-Inter Science: New York, 2001; pp.999.
[54] Chen, Y.; Shen, Z.; Perez, L. P.; Frey, H.; Stiriba, S.-E.; *Macromolecules* **2005,** 38, 227.
[55] Chen, Y.; Shen, Z.; Frey, H.; Paik, H. J.; Prieto, J. P.; Stiriba, S.-E. *Chem. Commun.* **2005,** 6, 755.
[56] Ferguson, R. C.; Ovenall, D. W. *Macromolecules* **1987,** 20, 1245.
[57] Keller, R. N.; Wycoff, H. D. *Inorg. Synth.* **1946,** 2, 1.

Chapter 6. Supramolecular Nanocapsules by Synergistic Self-Assembly of Fatty Acids and Hyperbranched Polyethylenimine

6.1. Introduction

Modern techniques of liquid-liquid phase transfer and separation involve the use of ionic liquids and polymeric supports. In this context, polymer-based materials play a more and more important role. Generally, their application range, including both solid phase and solution, can be summarized in Scheme 6-1. [1]

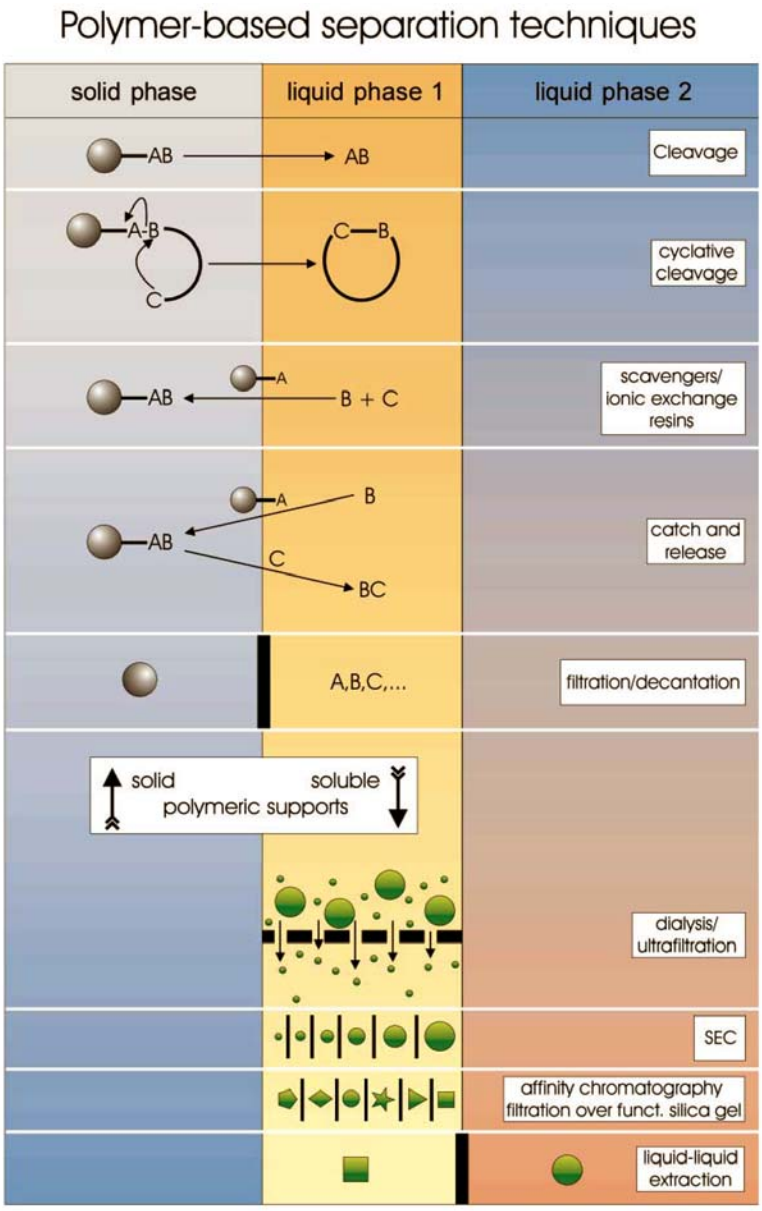

Scheme 6-1. Polymeric materials in liquid-liquid phase transfer

Polymeric supports have been used for over 50 years. Mostly, polymers are used either as solid phase (cross-linked and insoluble) or dissolved in solution (non-cross-linked). Initially ion-exchange resins dominated the field of separation, while in the last decade more specific polymeric supports and linker systems have been used. In contrast to solid-phase concepts, soluble polymeric supports permit reactions to be performed under homogenous conditions.[1] In addition, the presence of a polymer support in an organic solvent increases to a large extent the sequestration of a compound (i.e. the solute) from an immiscible solvent such as aqueous media, into the organic solvent, providing a new confined environment.[2] This is an important point for further specific application in catalysis and drug delivery.[3]

In this context, structurally precise dendrimers with their highly branched and multifunctional globular structure have been shown to exhibit topological encapsulation of various guests for catalysis, drugs and dyes.[4] Encapsulation can be achieved using the unimolecular micelle approach with core-shell structures to dissolve organic molecules in dendrimers,[5, 6] or by utilizing the organosoluble alkyl amide-modified dendrimers known as "dendritic box" to extract water soluble guests to organic solvents.[7] Unfortunately, dendrimer synthesis is usually limited to a laboratory scale due to the stepwise iterative approach. However, the less defined hyperbranched polymers can be prepared conveniently from AB_m type monomers on a large scale. When using slow monomer addition techniques, hyperbranched polymers with rather narrow polydispersity and dendrimer-like properties are obtained. The utility of hyperbranched polymers as macromolecular structures to build new materials with specific properties for further applications is illustrated by the wide use of hyperbranched polyglycerols prepared in a one-step process. For example, PG etherified with fatty acid chlorides displays an amphiphilic core-shell structure.[8] Modified PG has been successfully used to extract and irreversibly encapsulate various polar dyes from the aqueous phase (Scheme 6-2). Surprisingly, all dendrimer-based core-shell architectures for phase transfer processes have been obtained via covalent linking of hydrophobic alkyl chains to the polyfunctional core,

followed by several purification steps.

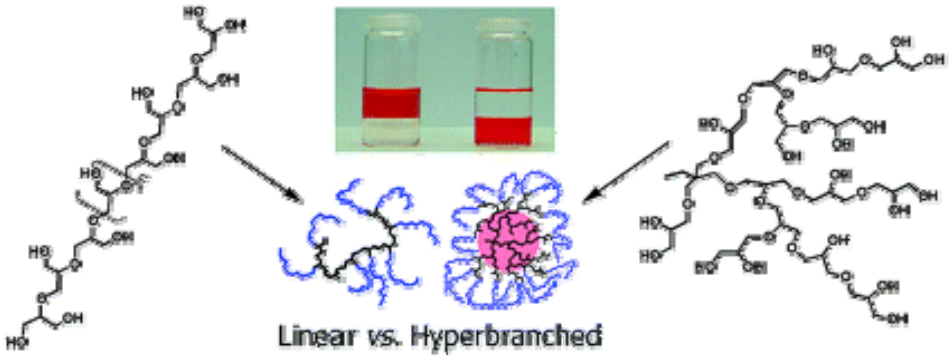

Scheme 6-2. Schematic image of the encapsulation dye into modified PG capsules.

These approaches are all based on the covalently modified dendrimer or hydperbranched polymers, however, there is only little data concerning the concept of non-covalent interaction. To date, only one report described a non-covalent concept for organosoluble, inverted micelles, prepared by self-assembly of various generations of amine-terminated poly (amidoamine) (PAMAM) dendrimers and fatty acids, relying on acid-base interaction.[9] (Scheme 6-3)

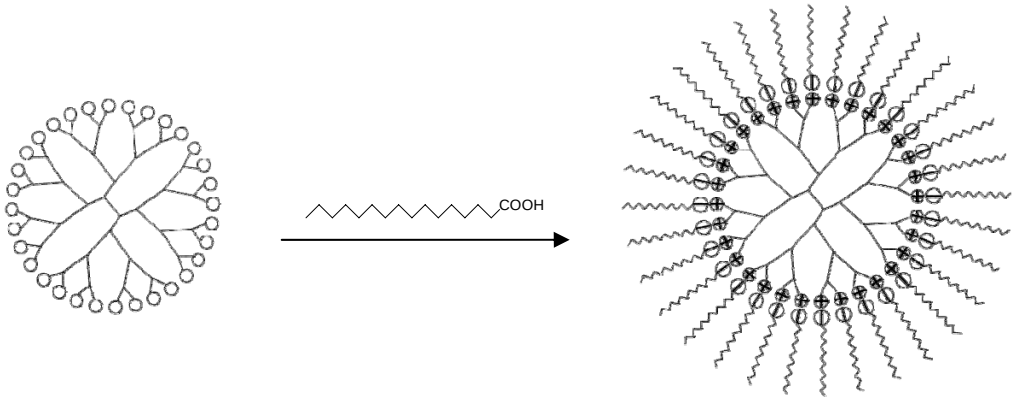

Scheme 6-3. Schematic image of the encapsulation process by non-covalent self-assembly between PAMAM dendrimers and fatty acids.

For hyperbranched polymers, however, there is no report on supramolecular nanocapsules obtained from non-covalent assembly.

In this chapter we will demonstrate that self-assembly of hyperbranched polyethylenimine (HPEI) and fatty acids leads to supramolecular inverted micellar structures that are able to irreversibly transfer water-soluble guest molecules into

organic solvents. It is a convenient one-step process for the preparation of supramolecular nanocapsules by electrostatic interaction between fatty acids and a commercially available hyperbranched polyamine, namely polyethylenimine (HPEI) (Scheme 6-4).

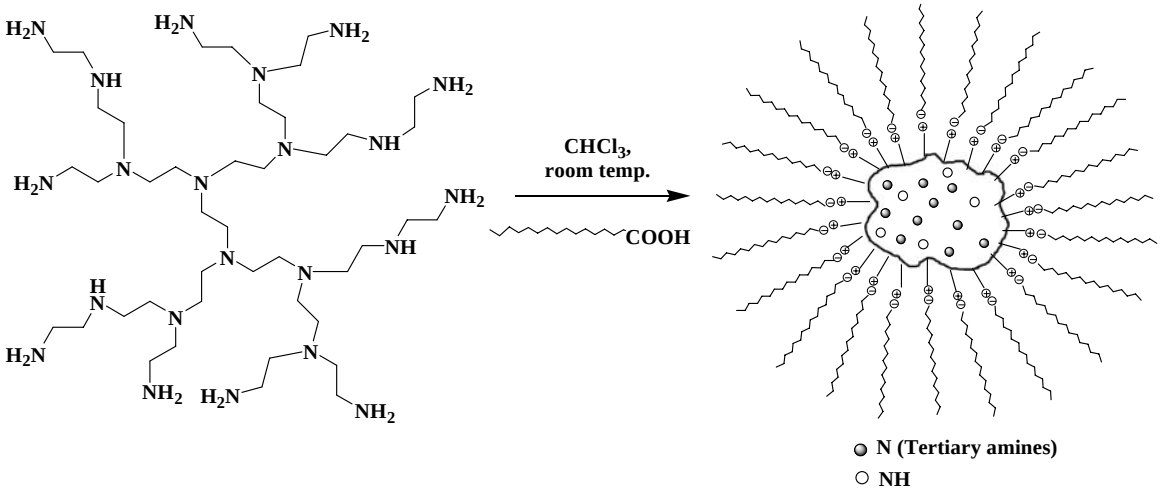

Scheme 6-4. Schematic illustration of an inverted, supramolecular micelle based on the self-assembly of HPEI and palmitic acid.

6.2. Results and Discussion

6.2.1. Determination of the Branching structure of HPEI

HPEIs with molecular weight exceeding 1000 g/mol obtained from cationic polymerization of aziridine are usually hyperbranched due to the well-known branching mechanism in the synthesis of HPEI.[10] The degree of branching of commercially available HPEIs are commonly between 60%-65%, as reported by other groups.[11]

The branching structure of HPEI was studied using inverted gate ^{13}C NMR spectra. As it can be seen from the ^{13}C NMR spectrum (Figure 6-1, the spectrum contains eight lines which were assigned) of HPEI10K, (232 repeat units), the branched structure is evident. Based on this ^{13}C NMR spectrum, we can calculate the fractions of terminal (T), linear (L) and dendritic (D) amine groups. The results are listed in Table 6-1. The degree of branching (DB) of HPEI10k can then be calculated

to be 74.7% according to the Equation 6-1.[12]

$$DB_{Frey} = \frac{2D}{2D + L} \qquad (6\text{-}1)$$

For the case of HPEI25K (^{13}C NMR spectrum is shown in Figure 6-2), the results are also calculated and listed in Table 6-1. The degree of branching (DB) of HPEI25k is 68.6 % calculated according to the Equation 6-1

Table 6-1. Degree of branching of HPEI samples

PEI	DP	M_n[a]	M_w/M_n[a]	T (%)[b]	D(%)[b]	L(%)[b]	DB(%)[b]
HPEI10K	232	10,000	2.5	33.0	40.0	27.0	74.7
HPEI25K	581	25,000	2.5	33.0	35.0	32.0	68.6

[a] Molecular weight and molecular weight distribution are determined by GPC, [b] Degree of branching and abundance of terminal (T), dendritic (D) and linear (L) amine units are calculated from inverted gate ^{13}C NMR.

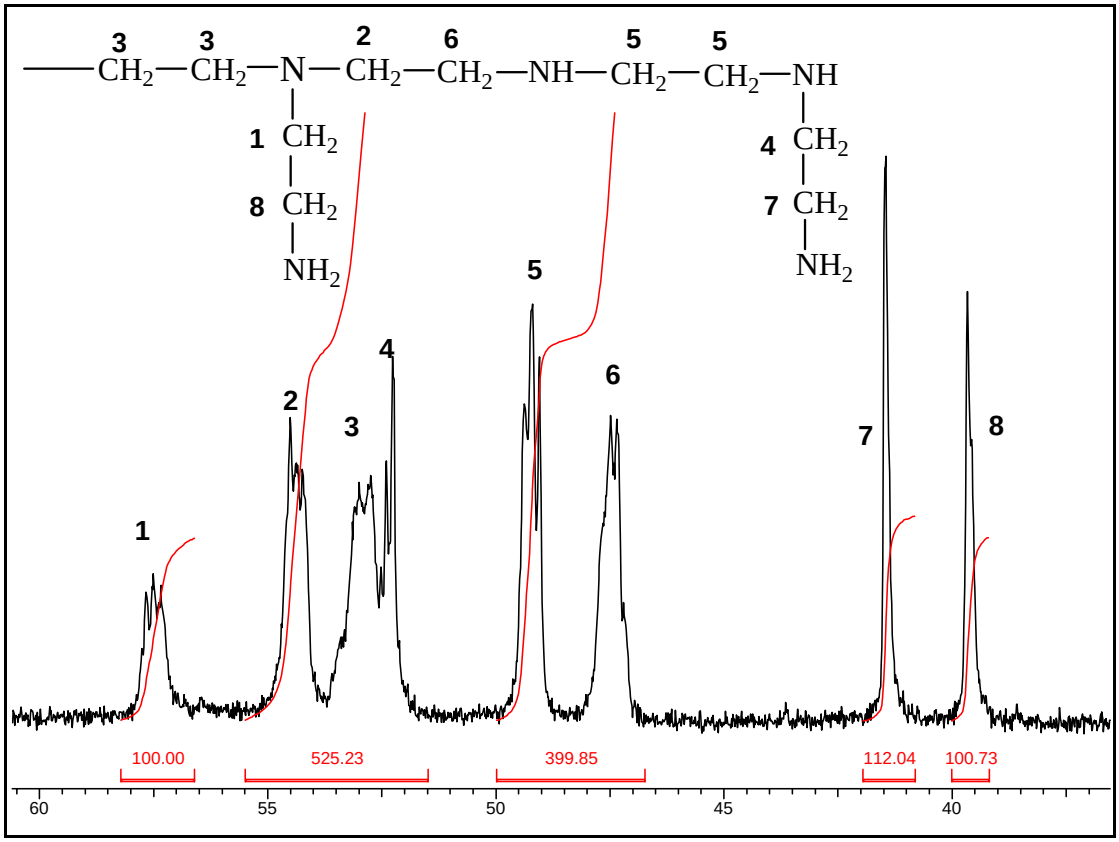

Figure 6-1. Inverted gate ^{13}C NMR of HPEI10K and chemical shift assignments.

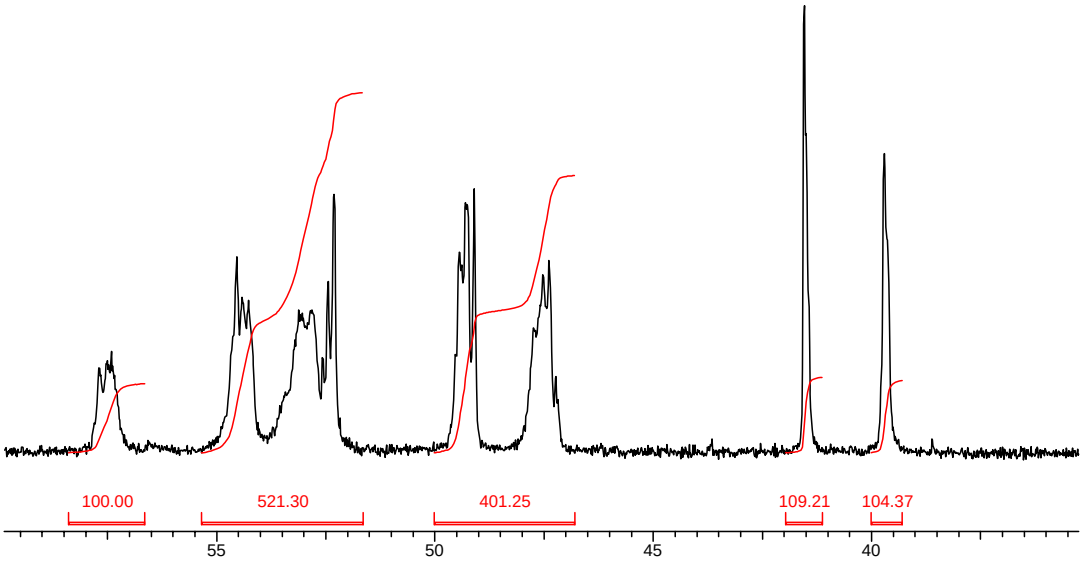

Figure 6-2. Inverted gate ^{13}C NMR of HPEI25K

6.2.2. Formation of Supramolecular Nanocapsules

The addition of fatty acids, namely lauric acid (LA, $C_{11}H_{23}COOH$) or palmitic acid (PA, $C_{15}H_{31}COOH$) to a chloroform solution of hyperbranched polyethylenimine HPEI10K (Mn = 10,000 g/mol, DB = 60 %) in 0.6 (acid groups / amine) ratio spontaneously afford the respective polyelectrolyte-surfactant complexes, i.e., LA-HPEI10K and PA-HPEI10K. This conclusion is supported by various analytical methods.

FT-IR absorbance spectra show the disappearance of the characteristic symmetric (C=O) band of the fatty acids at 1700 cm^{-1} upon addition to HPEI10K in solution, accompanied by the appearance of a sharp, asymmetric band at 1550 cm^{-1} (C=O), typical of the carboxylate salt. (Figure 6-3) This demonstrates that the fatty acid molecules are deprotonated and the terminal, primary NH_2 groups of HPEI (fraction of terminal, T-groups = 33.0%, pKa = 9.64) are protonated at first,[13] leading to ionic interaction and thus a polyelectrolyte-surfactant complex with rather hydrophilic core and hydrophobic alkyl periphery that acts as a “supramolecular nanocapsule”.

Upon addition of larger amounts of carboxylic acid, also the secondary amine groups of the linear units (fraction L = 40 %， pKa = 8.59) are protonated and interact with the alkyl carboxylates.

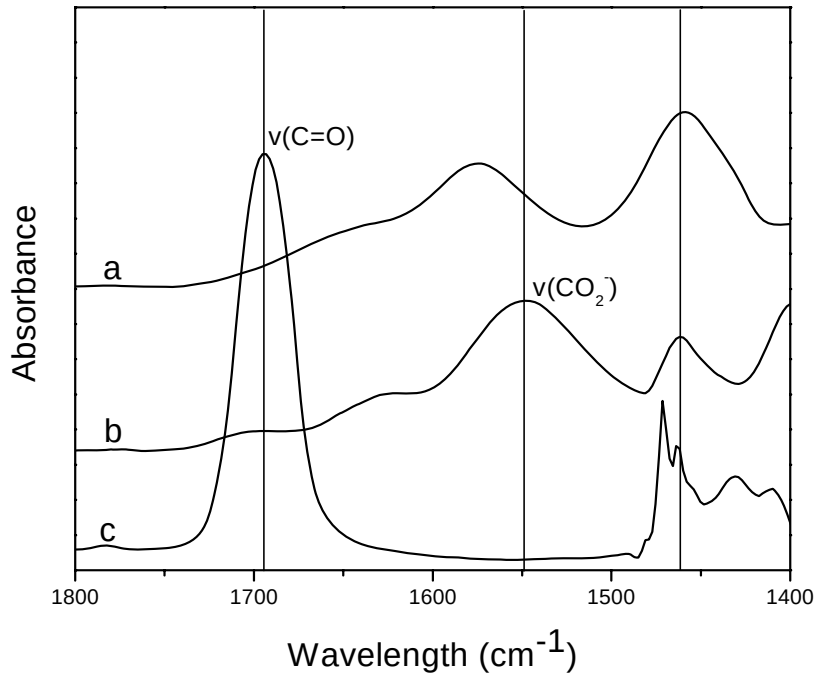

Figure 6-3. ATR-FTIR spectra of (a) neat HPEI10K, (b) palmitic acid 60% + HPEI10K, (c) neat palmitic acid

Here, it should be noted that both electrostatic interaction between charged amine groups as well as hydrophobic interaction between the sphere HPEI core and the alkyl tails are important in stabilizing the complex. Since the core molecules is sphere-like HPEI instead of linear polymer, an inverted "uni-molecular" analogous (if we consider the number of core molecules) supramolecular nanocapsule was formed, while in the case of linear polymer, micelles will be formed.

Formation of the hyperbranched polyelectrolyte-surfactant complex can be expected to lead to pronounced changes of the conformation of the hyperbranched polymer. This issue was studied by solution viscosity measurements of the mixtures LA-HPEI10K at different ratios of both components. There specific viscosity curves are shown in Figure 6-4. Interestingly, from Figure 6-4, a systematic decrease in the specific viscosity ($\eta_{spec.}$) can be seen when increasing the lauric acid proportion at fixed concentration of HPEI10K. For instance, pure HPEI10K displays an intrinsic viscosity [η] = 10.6 mL/g, while a mixture of LA and HPEI10K at LA/amine ratio of

0.6 shows clearly reduced intrinsic viscosity [η] = 6.5 mL/g, (for this case, we used the molecular weight of the capsule equal molecular weight of HPEI plus the molecular weight of LA/PA), here the intrinsic viscosities are obtained by extrapolating to c = 0 g/L. We could attribute this pronounced difference to a very compact solution structure,[14, 15] due to the supramolecular nanocapsules LA-HPEI10K and PA-HPEI10K formed in apolar solvents. A comparative study with the linear analogue $LPEI_{348}$ assembled with LA in LA/amine ratio of 0.6 also provided a polyelectrolyte complex LA-$LPEI_{348}$ (observed from FTIR), however, no similarly compact structure as in the case of hyperbranched PEI10K. This is evident from the values of the specific and particularly the intrinsic viscosity LA-$LPEI_{348}$, [η] = 13.1 mL/g.

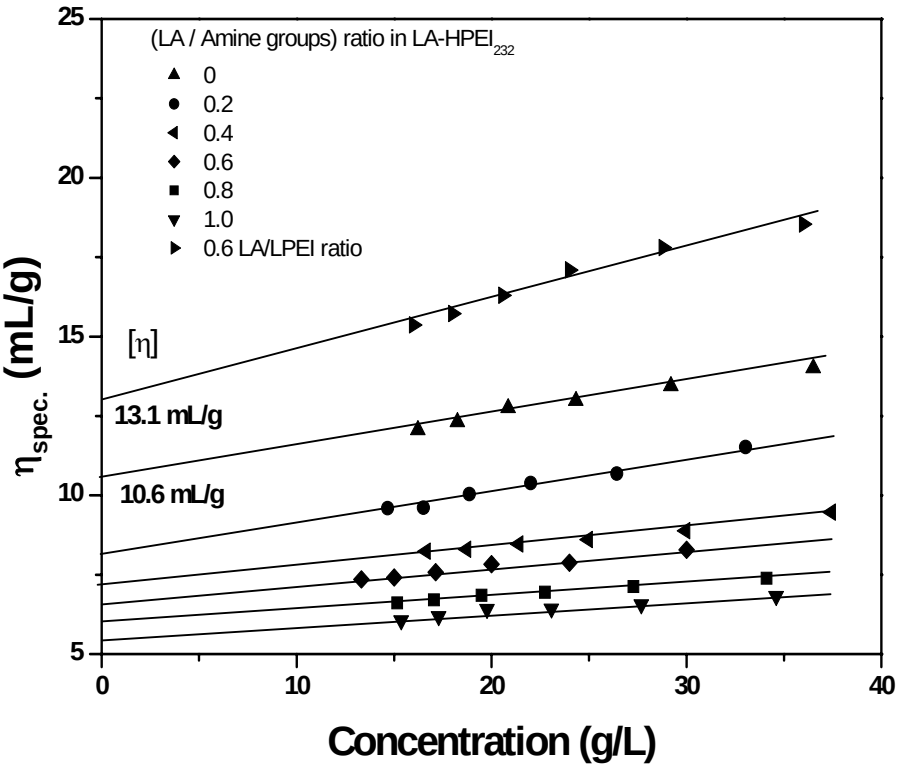

Figure 6-4. Viscosity measurements of LA-HPEI10K mixtures in chloroform at different ratios of the components， data for a linear analogue LA-HPEI10K are also shown for comparison.

Dynamic Light Scattering (DLS) showed the average size of HPEI10K (M_n = 10^4 g/mol) to be 5.1 nm at c = 10^{-4} M, whereas the size of associated LA-HPEI10K (LA/amine groups in HPEI = 60%) was 6.5 nm. These DLS values also support the conclusion that amphiphilic hyperbranched polymers with hydrophilic core and hydrophobic shell form stable and compact, hard-sphere like "supramolecular nanocapsules".

6.2.3. Encapsulation of Dyes

In order to demonstrate the phase-transfer properties of the nanocapsules, three polar dyes, i.e., Congo Red (CR), Methyl Orange (MO) and Fluorescein Sodium (FS) were dissolved in water. The aqueous phases were extracted with chloroform solutions containing either PA-HPEI10K or LA-HPEI10K capsules.

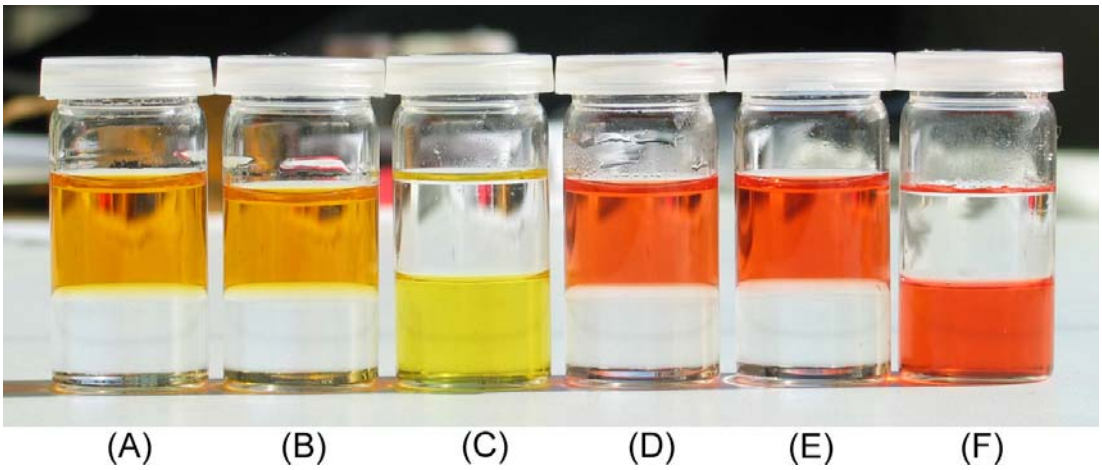

Figure 6-5. Illustration of dye extraction processes (bottom layer: chloroform, upper layer: water). (A) Congo Red; only lauric acid (LA) in organic layer; (B) Congo Red; only HPEI10K in organic layer; (C) Congo Red (CR); LA-HPEI10K nanocapsule in organic layer; (D) Methyl Orange; only LA in organic layer; (E) Methyl Orange (MO); only HPEI10K in organic layer; (F) Methyl Orange; LA-HPEI10K nanocapsule in organic layer

We can see clearly from Figure 6-5 that both water soluble dyes MO and CR can be successfully transferred into the organic phase in the presence of LA-HPEI10K. (Figure 6-5, c, and f) However, for the cases of LA or HPEI alone, no dye is transferred into chloroform phase. (Figure 6-5, a, b, d, e) These observations clearly

support the synergistic behavior of the system. Together with data from FTIR, DLS and viscosity, we can confirm that the synergistic assembly of fatty acids and HPEI lead to supramolecular nanocapsules for liquid-liquid phase transfer. For FS, hardly any encapsulation is observed.

The dye encapsulation capacity by the supramolecular nanocapsules was calculated from the UV-*vis* absorption spectra.

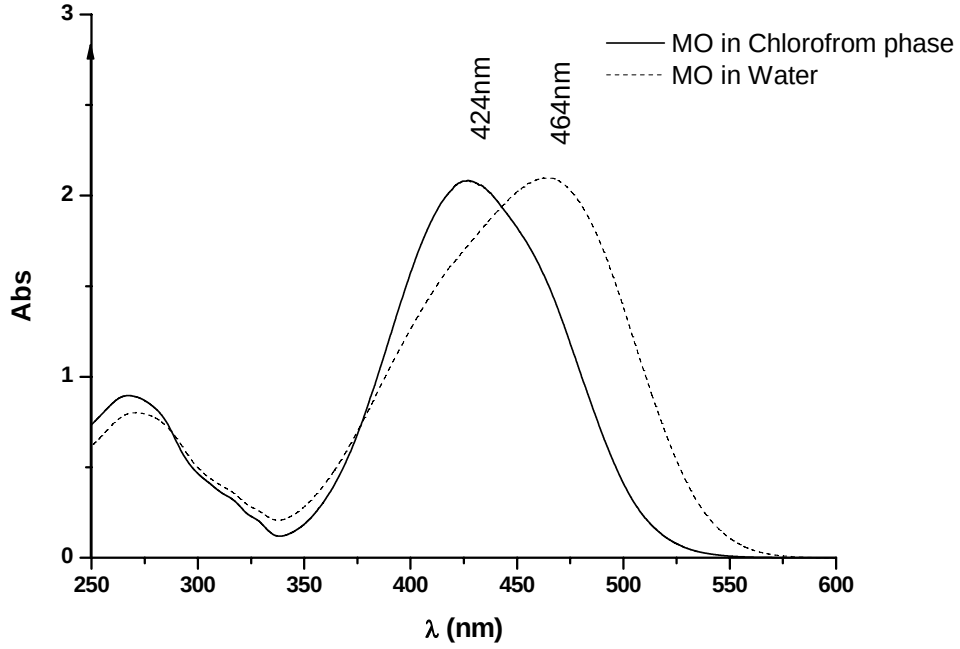

Figure 6-6. The UV-*vis* spectra of Methyl Orange in water and Methyl Orange encapsulated by LA-HPEI10K molecular nanocapsule in chloroform

Figure 6-5 shows the UV-vis spectra of MO in water (λ_{max} = 464 nm) and MO encapsulated by LA-HPEI10K molecular nanocapsules in chloroform. (λ_{max} = 424 nm) The wavelength change also shows that the dyes are in basic environment, which indicates that the inner part of the nanocapsules consists of HPEI. The number of encapsulated dye molecules per nanocapsule can be calculated according to Lambert-Beer´s Law. (Equation 6-2)

$$A = \varepsilon bc \quad (6\text{-}2)$$

ε is the molar extinction coefficient while c is the concentration of the solution.

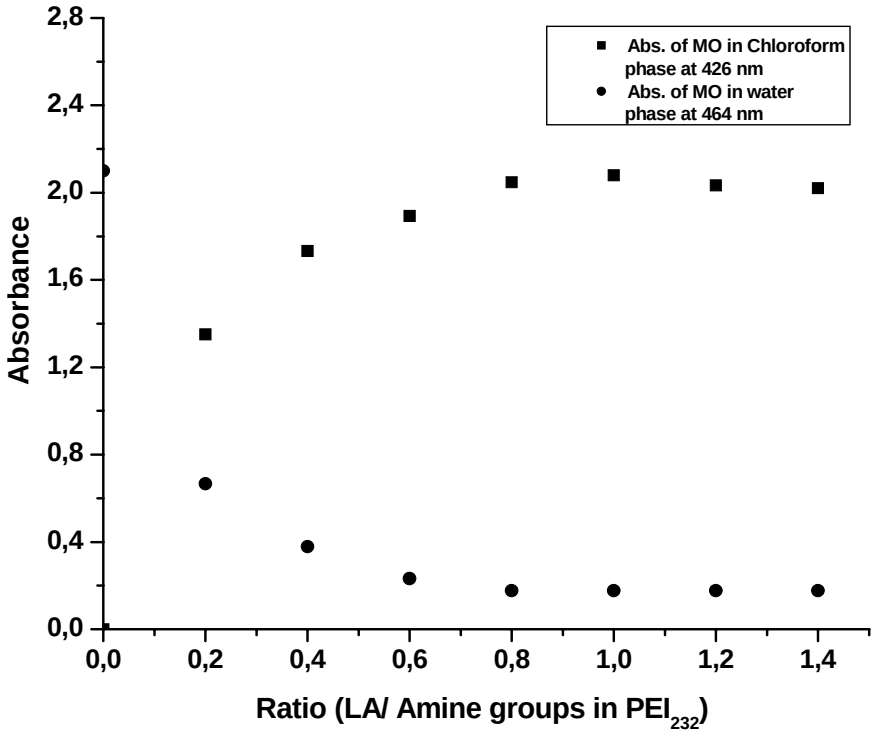

Figure 6-7. Absorbance of Methyl Orange in the chloroform layer containing inverted micelle LA-HPEI10K and its trace in the aqueous layer

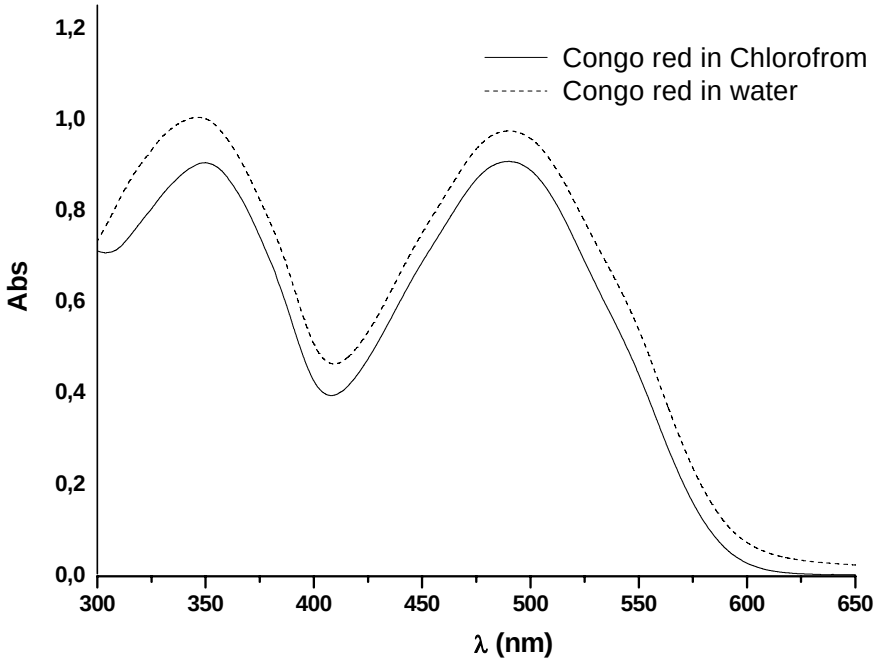

Figure 6-8. The UV-vis spectra of Congo Red in water and Congo Red encapsulated by LA- HPEI10K molecular nanocapsule in chloroform.

Figure 6-7 shows an increase in the absorbance of methyl orange in the chloroform phase (λ_{max} = 424 nm), indicating dynamic transport of the dye from the aqueous phase (λ_{max} = 464 nm) into the organic medium. Corresponding to this, a decrease in the absorbance of methyl orange in the water phase (λ_{max} = 464 nm) can also be observed.

For Congo Red, the same method was used to determine the dye content. However, both the UV-vis spectra of Congo Red in water and in chloroform show similar absorption as we can see from Figure 6-8. The calculations are based on the absorption maximum at λ_{max} = 498 nm.

The number of encapsulated dye molecules per nanocapsule was calculated for different ratios of acid/amine groups. They are listed in Table 6-2 and illustrated in Figures 6-9 and 6-10. We can see that for Methyl Orange, when the [LA]:[Amine] ratio is 0.2, the system can already encapsulate 3-4 dye molecules per HPEI capsule, when the LA ratio increases to 0.4, 6-7 dye guests can be encapsulated. Upon further increase of the ratio to 0.6-1.4, the dyes encapsulation reaches a maximum number of 8.5 remains constant. When the acid was changed to PA, the same tendency was observed. The only difference is that at low ratio of PA to amines the dye numbers can not be measured accurately due to heavy emulsification. It was observed that PA-HPEI10K can encapsulate a maximum of 8.6 MO molecules, which is the same as in the case of LA-HPEI10K. This indicates that encapsulation is independent of the length of the alkyl chain in the fatty acids.

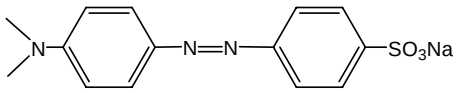

Methyl Orange (MO)

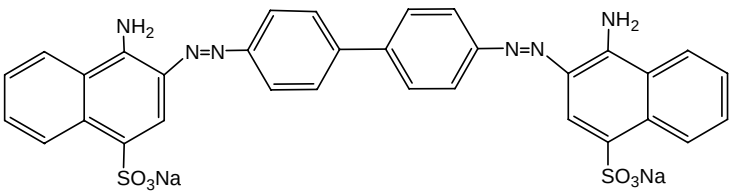

Congo Red (CR)

Scheme 6-5. Chemical structure of Methyl Orange & Congo Red

Table 6-2. Hydrophilic dye encapsulation of LA/HPEI10K, PA/HPEI10K

		pH[a]	Intrinsic Viscosity[b]	Dye loading per molecule [c]		
				N(MO)	N(CR)	N(FS)
HPEI10K		9	10.64	0	0	0
LA/HPEI	20	9	8.22	3.6	-	-
(%)	40	8	7.21	6.6	-	0.1
	60	7	6.61	7.7	1.7	0.2
	70	-	-	8.1	2.7	0.2
	80	7	6.03	8.4	3.0	0.3
	100	7	5.32	8.5	3.3	0.3
	120	-	-	8.3	3.1	0.3
	140	-	-	8.3	3.1	0.3
LA		6	-	0	0	0
PA/HPEI10K	20	9	8.05	0.5	0.3	0.02
(%)	40	8	7.09	1.7	0.4	0.03
	60	7	6.58	4.0	1.3	0.07
	70	7	-	8.2	2.3	0.09
	80	7	6.00	8.4	2.4	0.10
	100	7	5.22	8.4	2.7	0.20
	120	-	-	8.6	2.8	0.20
	140	-	-	8.4	2.8	0.20
PA		6	-	0	0	0

[a] pH was estimated by pH indication-paper prior to viscosity measurement. [b] Viscosity was measured in $CHCl_3$, the concentration of (HPEI10k +Acid) was controlled within 32-40 g/L. [c] Dye loading was calculated from UV-spectra.. N(MO): loaded number of methyl orange dye molecules; N(CR): loaded number of Congo Red molecules; N(FS): loaded number of Fluorescein Sodium molecules.

For the case of CR, it can be seen that a lower concentration of CR dye molecules is encapsulated (3.3 and 2.9 dye molecules in LA-HPEI10K and PA-HPEI10K, respectively). This is tentatively explained by the larger size of CR and limited spaces that occupied by the encapsulated dyes inside the capsules. (Scheme 6-5). We can see from Table 6-2 that the capsules almost cannot encapsulate FS.

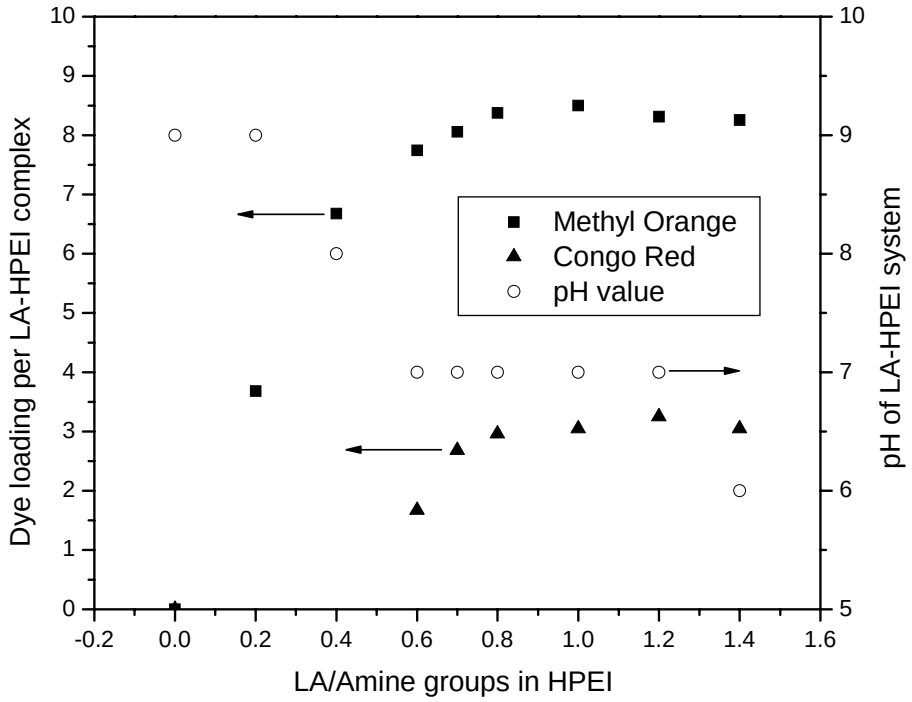

Figure 6-9. Dye loading of LA-HPEI10K complex at different ratio of LA with amines groups in HPEI10K

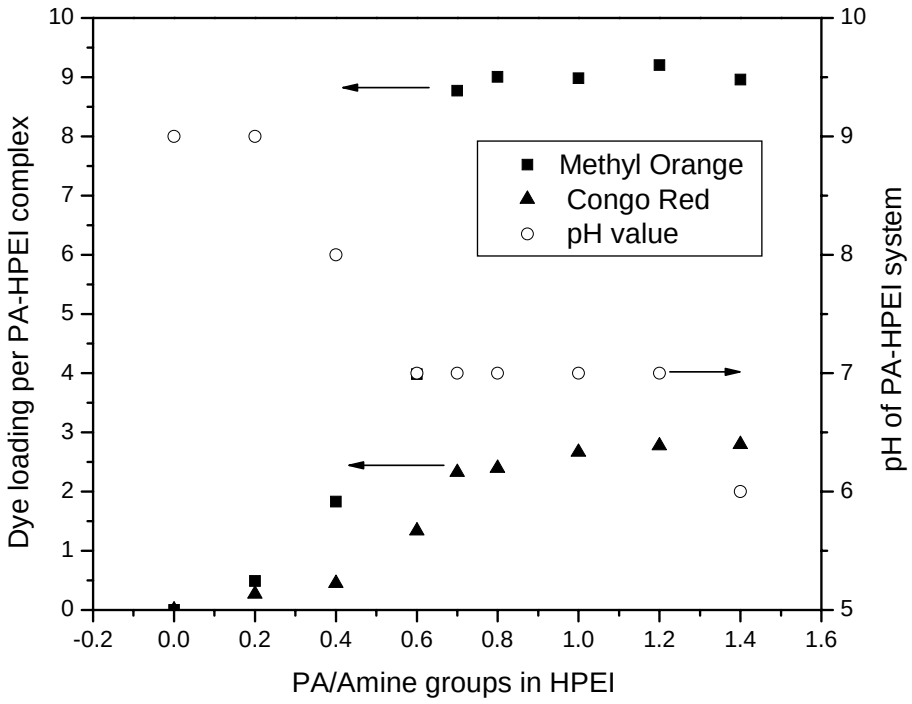

Figure 6-10. Dye loading of PA-HPEI10K complex at different ratio of PA and amine groups in HPEI10K

Table 6-3. Maximum number of hydrophilic dye molecules encapsulated by the micellar polymeric systems

Micellar structure [a]	M_n of HPEI (x 10^{-4})	Number of Methyl orange dye mol. [b]	Number of Congo Red dye mol [b]
LA-HPEI10K	1	8.5	3.3
PA-HPEI10K	1	8.6	2.9
LA–HPEI25K	2.5	21.4	7.2
LA –LPEI$_{348}$	1.5	1.2	0

[a] Samples are mixture of linear or hyperbranched PEI with LA or PA . [b] Dye loading measured at LA or PA / amine groups in HPEI = 0.6

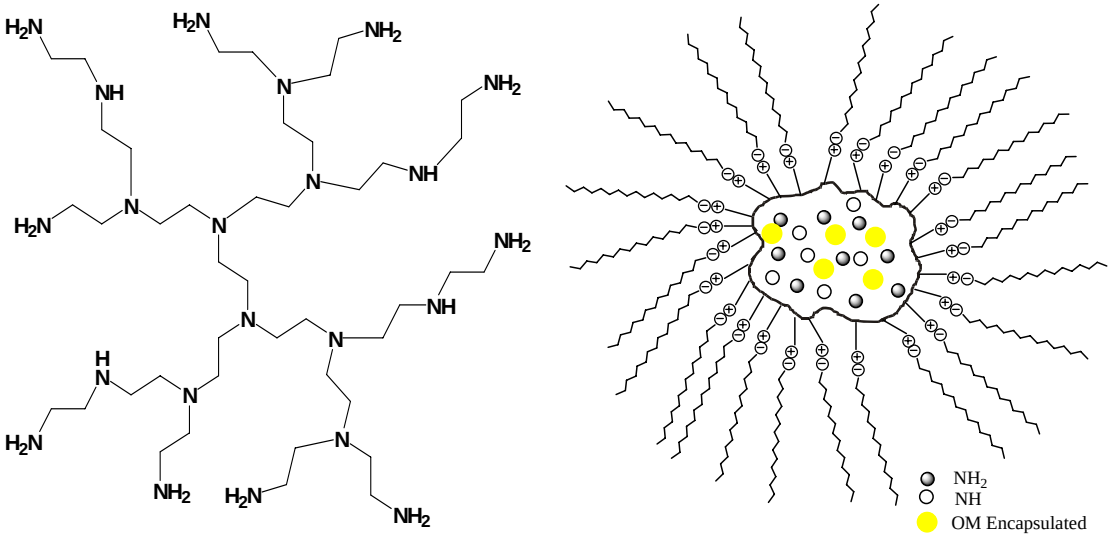

Scheme 6-6. Schematic show how dye distribute in the spaces inside the capsule

Apart from HPEI10K, for comparison, both HPEI25K (M_n = 25000 g/mol) and LPEI$_{348}$ (M_n = 15000 g/mol) have also been used to build capsules for dye encapsulation. The maximum numbers of encapsulated dye molecules (both CR and MO) by all nanocapsules are listed in Table 6-3. We can see for all the cases that the capsules are more favorable with MO than CR, which can be explained as above, the larger size of CR and limited steric possibilities of the capsules. (Scheme 6-6) Also we observed that the number of encapsulated dye molecules was HPEI core molecular weight dependent, as demonstrated using the larger HPEI25K (Table 6-3). For this

case, the capsule can encapsulate 21.4 dye molecules while the HPEI10K can only encapsulate 8.5 guest molecules.

The pH value of the organic layer was also assessed with a pH indication paper. When the acid/amine ratio was below 0.40, the pH was above 7 due to the presence of free NH_2 or NH groups, for the remaining cases, the solution is neutral, since at these times all amines are located inside the capsule. Until the acid/amine ratio reaches 1.4, there are free acid groups present and the solution turns slightly acidic.

The hyperbranched architecture of HPEI was crucial to realize dye extraction, as indicated by the incapability of the linear analogue LA-$LPEI_{348}$ to encapsulate CR and its insignificant extraction of MO dyes as well. In this case, micelles are likely to be formed and the core is composed of dense-coiled LPEI.

Upon addition of acid (pH = 2) to the organic phase containing the encapsulated dyes, the dyes can be released into the aqueous layer. This also supports the concept of solubilization by supramolecular nanocapsules.

The same strategy was also employed in order to achieve guest molecule transfer between aqueous phase and perfluorinated phase. We substituted lauric acid with $CF_3CF_2CF_2CF_2CF_2CF_2CF_2COOH$ to complex with HPEI, however, for compositions studied no stable capsules were observed in either trifluoro-toluene or hexafluoro-propanol. The reason is still not clear, although we could ascribe this to the very unfavorable formation of ionic interaction in the perfluorinated solvents as well as additional strong phase segregation between the perfluorinated compounds and the polymer.

There have been reports that amidated HPEI can be used for dye and silver encapsulation.[16, 17] In Chapter 7, the work of further quaternization of amidated HPEIs is presented. Both encapsulation of gold nanoparticles and dyes was also achieved. As it is easy to conceive, the present supramolecular nanocapsules possess several advantages over the covalent analogues: i) convenient preparation without need for further purification; ii) facile variation of the composition to fine-tune the molecular nanocapsules as a function of the acid-HPEI ratios.

6.3. Conclusion

In conclusion, the data demonstrate that supramolecular self-assembly of a well known, commercially available, inexpensive and easily accessible hyperbranched polyethylenimine (HPEI) obtained by polymerization of aziridine can be used to construct new molecular nanocapsules together with fatty acids for phase transfer processes.

An arrangement of fatty acids around the HPEI in a composite structure that resembles an inverted micelle, having a hydrophilic interior and hydrophobic shell that assures solubility for the entire new system was suggested. The synergy between both components affords phase transfer properties due to the polyelectrolyte-surfactant complexes. These self-assembled molecular nanocapsules were demonstrated to be of unimolecular nature, as evidenced from light scattering analysis. Viscosity measurements show compact structures. Proof of that arises from their comparison with linear PEI assembled with fatty acids.

The HPEI-fatty acids synergism in the self-assembled inverted micelles leads to molecular nanocapsules able to sequester polar dyes, as demonstrated by encapsulation of water-soluble dyes like Congo Red and methyl orange. Dye loading was found to be molecular weight-dependent.

6.4. Experimental Part

6.4.1. Preparation of the linear polyethylenimine $LPEI_{348}$

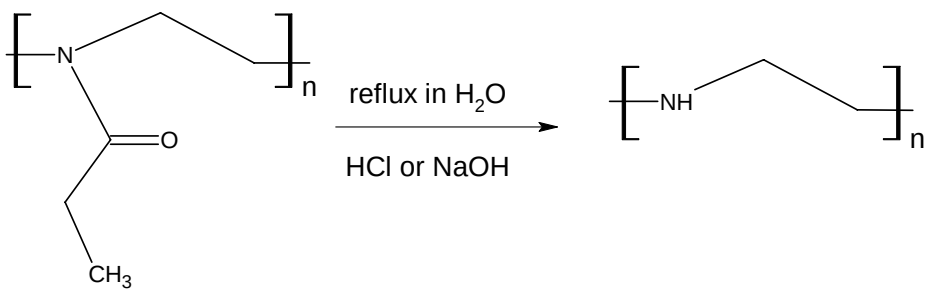

Scheme 6-7. Preparation of Linear PEI

Linear PEI was prepared from poly(2-ethyl-2-oxazoline) according to Kem's methods[18]: A solution of 25 g poly(2-ethyl-2-oxazoline) in 65 ml of deionized water was introduced into a 250 ml three-necked flask equipped with funnel, magnetic stirrer and condenser. Then 40 ml of 37% HCl was added. The mixture was refluxed for 96 hours. All the volatile was removed under reduced pressure and the resulting product was re-dissolved in deionized water. The solution was neutralized with NaOH solution and then evaporated to dryness. The opaque residue is taken up in isopropanol and the precipitated sodium chloride was filtered off. The cycle was repeated twice to remove all NaCl completely. The pure linear PEI ($LPEI_{348}$, functionality of amine is 348, M_n = 1.5x10^4 g/mol) was purified by dialysis against chloroform. ^{1}H NMR ($CDCl_3$): = 2.67 (-C<u>H</u>$_2$C<u>H</u>$_2$NH-); 1.76 (-CH$_2$CH$_2$N<u>H</u>-). IR (NaCl): = 1633 cm^{-1} (amide group)

6.4.2. Methodology for dyes (CR and MO) extraction in phase transfer processes using the molecular nanocapsules and the UV-vis spectroscopy analysis

Hyperbranched or linear PEI was mixed with lauric acid (LA) or palmitic acid (PA) in chloroform, and then 4 ml of the micellar structure PEI-fatty acid, chloroform solution was added to 4 ml of dye in water. The solutions were shaken for 10 minutes and kept at room temperature in a dark chamber overnight prior to the measurements. The concentrations of dyes in water were fixed ([MO] = 1.0x10^{-4} M, [CR] = 6.0x10^{-5} M), but the concentrations of PEI/Acid mixture were adjusted until only part of the dyes in water was transferred into the chloroform phase. The water phase was measured by UV-vis spectrum, the remaining dye in water can be calculated, and the number of dye transferred into chloroform phase could be therefore be obtained. (The mole extinction coefficients (ε) of Methyl Orange and Congo Red in water were measured and were found to be 2.16 x 10^4 L/mol cm (464 nm) and 2.50 x 10^4 L/mol cm (498 nm), respectively.

6.5. References

[1] Tzschucke, C. C.; Markert, C.; Bannwarth, W.; Roller, S.; Hebel, A.; Haag, R. *Angew. Chem. Int. Ed.* **2002,** 41, 3964.
[2] Sekine, T.; Hasegawa, Y. *Solvent Extraction Chemistry. Fundamentals and Applications, Marcel Dekker, New York* **1997**.
[3] Haag, R. *Angew. Chem. Int. Ed.* **2004,** 43, 278.
[4] Newkome, G. R.; Moorefield, C. N.; Vögtle, F. *Dendritic Molecules: Concepts, Synthesis, Perspectives, VCH, Weinheim* **2001**.
[5] Newkome, G. R.; Moorefield, C. N.; Baker, G. R.; M. J. Saunders, M. J.; Grossman, S. H. *Angew. Chem. Int. Ed.* **1991,** 30, 1178.
[6] Baars, M.; Kleppinger, R.; Koch, M. H. J.; Yeu, S. L.; Meijer, E. W. *Angew. Chem. Int. Ed.* **2000,** 39, 1285.
[7] Stevelmans, S.; van Hest, J. C. M.; Jansen, J.; van Boxtel, D.; van den Berg, E.; Meijer, E. W. *J. Am. Chem. Soc.* **1996,** 118, 7398.
[8] Stiriba, S. E.; Kautz, H.; Frey, H. *J. Am. Chem. Soc.* **2002,** 124, 9698.
[9] Chechik, V.; Zhao, M. Q.; Crooks, R. M. *J. Am. Chem. Soc.* **1999,** 121, 4910.
[10] Ivin, K. J.; Saegusa, T., *Ring-Opening Polymerization*. Elsevier: 1984.
[11] Kreamer, M.; Stumb, J.; Grimm, G.; Kaufmann, B.; Kreager, U.; Weber, M.; Haag, R. *ChemBioChem* **2004,** 5, 1081.
[12] Holter, H.; Burgath, A.; Frey, H. *Acta Polymerica* **1997,** 48, 30.
[13] Borkovec, M.; Koper, G. J. M. *Macromolecules* **1997,** 30, 2151.
[14] Lias, H.-G., *An Introduction to Polymer Science;*. Wiely VCH, Weinheim:, Germany, : 1997; p Chapter 5.8.
[15] Kulicke, W. M.; Clasen, C., *Viscosimetry of Polymers and Polyelectrolytes;* Springer: Heidelberg, Germany,: 2004.
[16] Aymonier, C.; Schlotterbeck, U.; Antonietti, L.; Zacharias, P.; Thomann, R.; Tiller, J. C.; Mecking, S. *Chem. Comm.* **2002**, 3018.
[17] Krämer, M.; Stumbe, J. F.; Turk, H.; Krause, S.; Komp, A.; Delineau, L.; Prokhorova, S.; Kautz, H.; Haag, R. *Angew. Chem. Int. Ed.* **2002,** 41, 4252.
[18] Kem, K. M. *J. Polym. Sci. Polym. Chem.* **1979,** 17, 1997.

Chapter 7. Functionalized Hyperbranched Polyethylenimines for Guest Molecule Encapsulation

7.1. Introduction

Defined micellar structures are of interest from a fundamental perspective, as well as for applications. For example, such structures can be used as hosts for the encapsulation and subsequent controlled release of guest molecules[1] or as templates for the formation of nanoscale particles.[2, 3] Block copolymer micelles can allow for a precise control of metal nanoparticle size and arrangement in thin films.[4-6] However, such self-assembled micelles are by their nature dynamic in solution, and they can be shearing sensitive. Therefore, Unimolecular polymeric micelles are of interest for particle formation and stabilization.[7] For particle size control, polymeric micelles of defined structure are required. In this respect, branched polymers (including dendrimer and hyperbranched polymers) provide a good alternative.

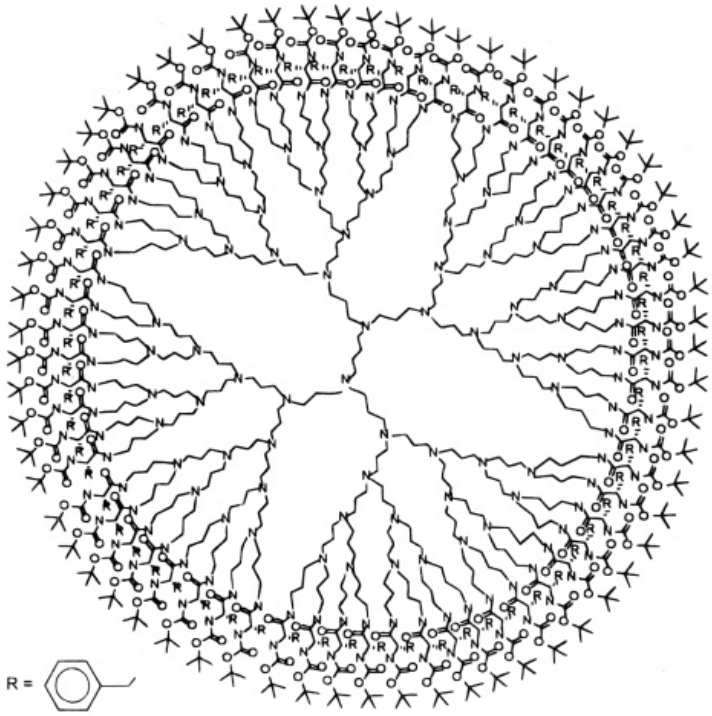

Scheme 7-1. Schematic image of dendritic box

The promising potential of dendrimers in a variety of areas, such as catalysis, materials science and biomedicine is related to their globular shape, large number of

modifiable surface functionalities and the presence of internal reservoirs.[1, 8-13] The ability to encapsulate guest molecules or catalytically active moieties represents an important structural peculiarity of dendrimers.

Encapsulation can be achieved by core-shell amphiphilicity, as pioneered by Newkome[14] et al. with the concept of the "unimolecular micelle" as well as via steric densification of the periphery, introduced by Meijer et al. as a "dendritic box".[15] (Scheme 7-1) Their use in liquid-liquid phase transfer protocols, based on the encapsulation of guest molecules as drug delivery vehicles for pharmaceutical application represents an important issue.[14, 16-19]

Unfortunately, as we mentioned in the first chapter already, dendrimer synthesis is time-consuming, which currently limits practical use to laboratory scale. For this reason, hyperbranched polymers prepared from AB_m-type monomers in one-step processes have gained increasing interest.[20-22] The development of the slow monomer addition technique has resulted in well-defined hyperbranched polymers ($1.3<M_w/M_n<1.5$) of narrow polydispersity with peculiar functional group distribution throughout the polymer scaffold, as demonstrated in detailed studies for hyperbranched polyglycerols.[23-25] (Please also refer to the first chapter)

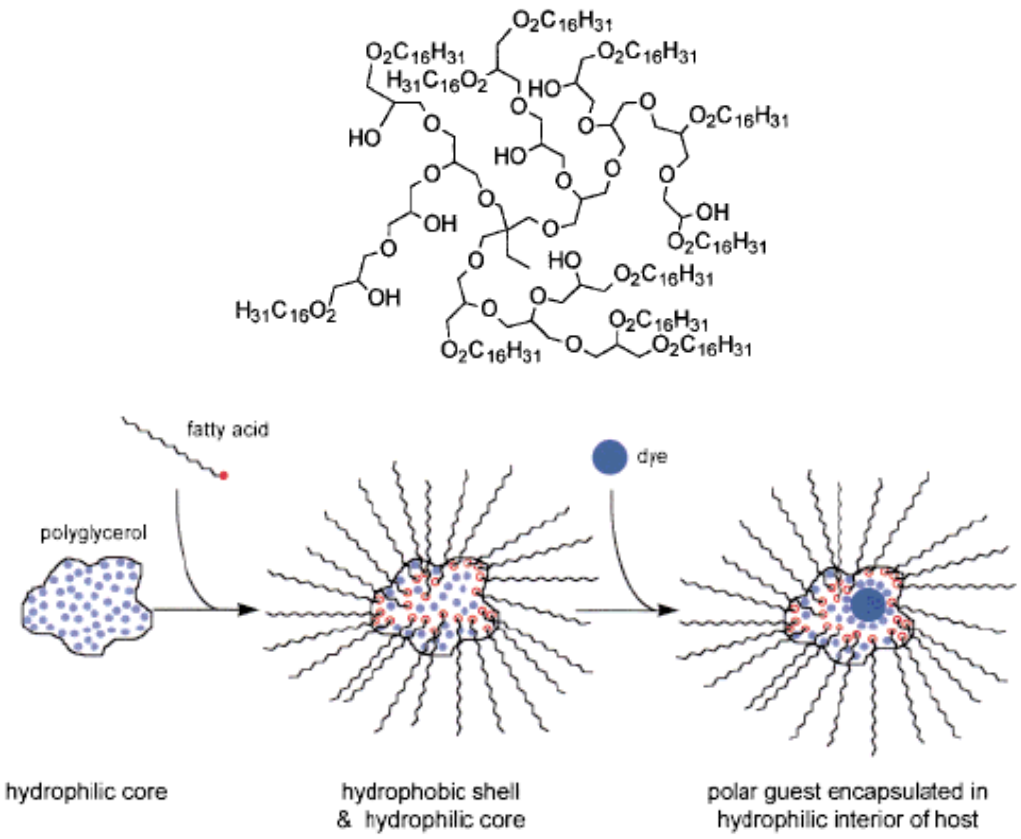

Scheme 7-2. Formation of unimolecular micelles from modification of PG

Partial modification of these hyperbranched polyethers with fatty acids or ketones leads to amphiphilic hyperbranched materials with compact core-shell structures. These structures exhibit dendrimer-like properties, such as the formation of unimolecular micelles.[26, 27] (structure can be seen from Scheme 7-2) In another paper a selective core-functionalization route for hyperbranched polyglycerol cores based on acetal formation has been presented, however, no detailed study of encapsulation properties was carried out. [26, 27]

Hyperbranched polyethylenimines (HPEI) have been used for a long time for various industrial purposes, e.g., as flocculating agents, thickeners and dispersion stabilizers and have recently been studied as a prototype for "weak" polyelectrolytes, as a component in hydrogenation processes and for quantum dot nanocomposites.[28, 29] Recently, partial functionalization of HPEI via amidation with long alkyl chains afforded amphiphilic hyperbranched polymers with core-shell-type architectures, capable of stabilizing silver nanoparticles and transferring polar dyes into organic solvents.[30, 31]

In this chapter we will describe a comparison of the amidated HPEI with the linear analogue with respect to solution properties and phase transfer. Furthermore, the influence of the polarity difference of "core" and "shell" components in the specific function of a "molecular nanocapsule" prepared from hyperbranched polymers has not yet been detailed. Herein we give a comparative analysis of amidated HPEI versus the linear analogue in solution and summarize the results of a study of the effect of core polarity on guest encapsulation, using quaternized and amidated HPEI. The combination of selective external and internal functionalization of hyperbranched polymers to fine-tune their properties has hardly been addressed. Apart from amidation, we could also modify HPEI with hydrophilic side chain to serve the purpose of stabilizing organic soluble guests in water.

7.2. Results and Discussion

7.2.1. Syntheses of palmitoyl chloride modified hyperbranched PEI

Two commercially available hyperbranched PEI samples, namely HPEI10K (M_n = 10^4 g/mol, M_w/M_n = 2.5, DP = 232) and HPEI25K (M_n = 2.5x10^4 g/mol, M_w/M_n = 2.5, DP = 581) have been partially amidated with palmitoyl chloride as previously reported,[30] affording organo-soluble, HPEI10K-$C16_x$ and HPEI25K-$C16_x$. ^{1}H NMR analysis confirmed a degree of amidation X. In order to enhance the polarity

difference of core-shell in palmitoyl chloride modified HPEI, the residual amine groups of HPEI10KC16$_x$ (HPEI25K-C16$_x$) were further quaternized by methyl iodide and termed as HPEI10KC16$_x$N$^+_{1-x.}$ (HPEI25K-C16$_{0.6}$N$^+_{1-x}$) (Scheme 7-3)

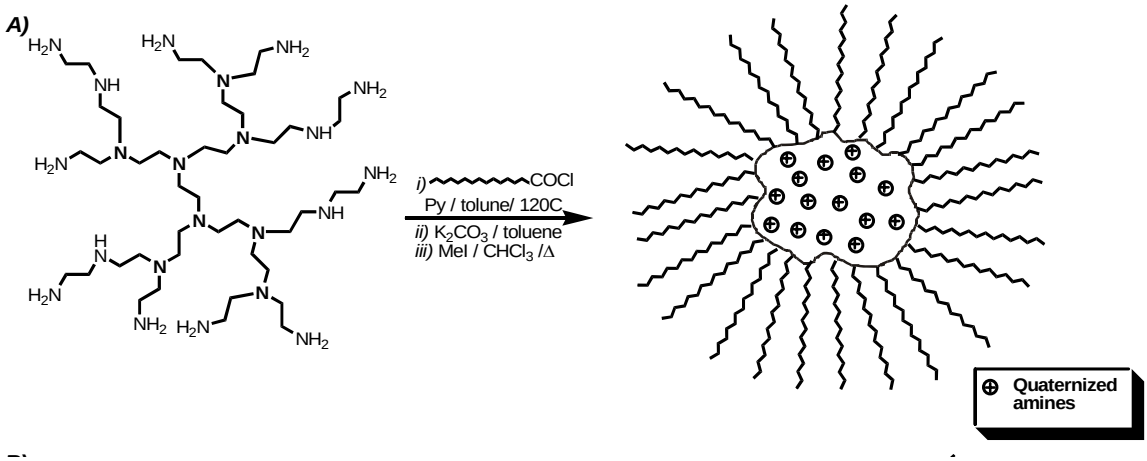

Scheme 7-3. Schematic representation of the synthesis of amidated hyperbranched polyethylenimine, displaying core-shell structure in hydrophobic organic solvent

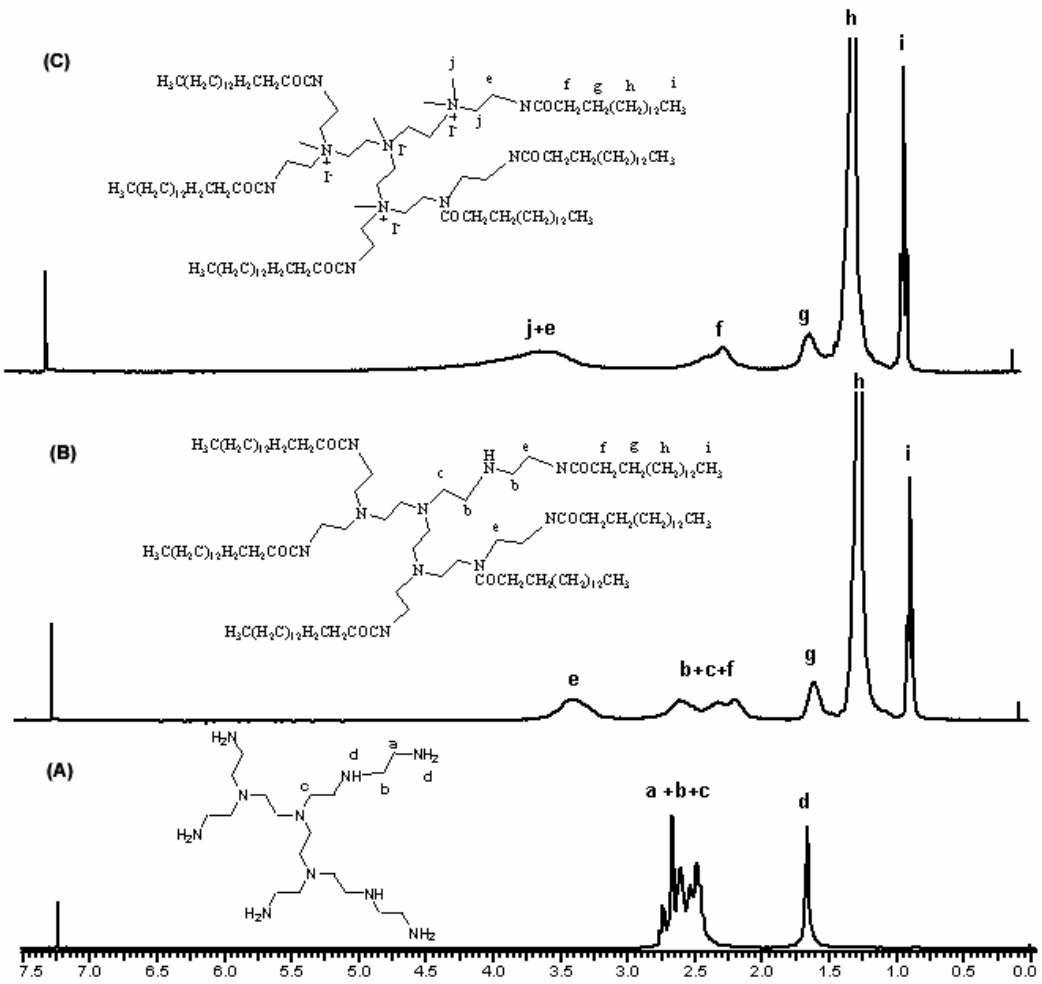

Figure 7-1. ^{1}H NMR spectra of (**A**) HPEI10K, (B) HPEI10KC16$_{0.6}$ and (C) HPEI10KC16$_{0.6}$N$^+_{0.4}$

The typical ^{1}H NMR spectrum of HPEI10K, HPEI10KC16$_{0.6}$ and HPEI10K-C16$_{0.6}$N$^{+}_{0.4}$ are shown in Figure 7-1. Compared with the ^{1}H NMR spectrum of HPEI, the new signals in Figure 7-1B, e (CH_2 connected to the amide groups) and f-i (CH_2 and CH_3 of palmitamide) evidence the successful synthesis of HPEI10KC16$_{0.6}$. In addition, the successful synthesis of HPEI10KC16$_{0.6}$ is also be supported by the FTIR spectra shown in Figure 7-2. The signal at 1635 cm^{-1} is the typical peak of amide groups. The peak broadening at around 3.5 ppm in Figure 7-1C was due to the partial overlap of the new signal from CH_2 and CH_3 attached to the quaternized amine with the original CH_2 connected to amide groups. The disappearance of the resonance at around 2.55 ppm (CH_2 connected to amine groups) was the evidence that the residual amine groups in HPEI10KC16$_{0.6}$ were quaternized. Comparing the integration of signal f-i in Figure 1C, it is obvious that the signal located at 2.5-2.0 ppm belongs to the CH_2–groups of palmitamide, not the CH_2 connected with the residual amine groups. The FTIR spectra of HPEI10KC16$_{0.6}$ and HPEI10KC16$_{0.6}$N$^{+}_{0.4}$ were similar, (Figure 7-2) without evident difference.

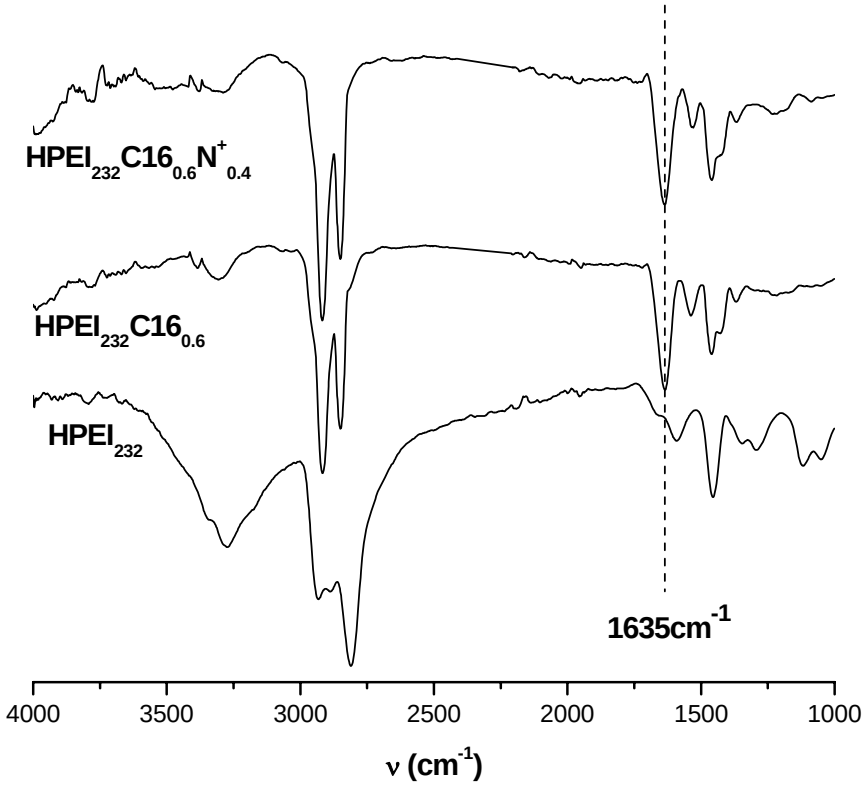

Figure 7-2. Comparison of the FT-IR spectra of HPEI10K, HPEI10KC16$_{0.6}$ and HPEI10KC16$_{0.6}$N$^{+}_{0.4}$

7.2.2. Syntheses of palmitoyl chloride modified linear PEI

High molecular weight linear PEI (LPEI) could not be obtained directly by the cationic polymerization of aziridine. The common method to synthesize LPEI is by the hydrolysis reaction of polyoxazolines,[32] as shown in Scheme 7-4. Therefore the linear analogue of HPEI with high molecular weight, LPEI15K ($\overline{M}_n$ = 1.5x10^4 g/mol), was obtained after hydrolysis of poly(2-ethyl-2-oxazoline) and subsequent partial amidation of the secondary amine groups, yielding LPEI15K-C16$_y$ (Scheme 7-4, here y is the degree of amidation).

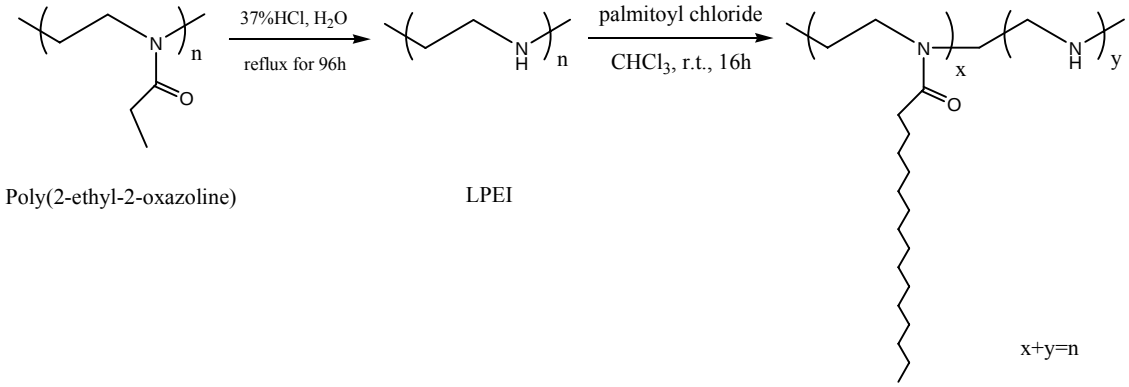

Scheme 7-4. Schematic representation of the synthesis of amidated LPEI

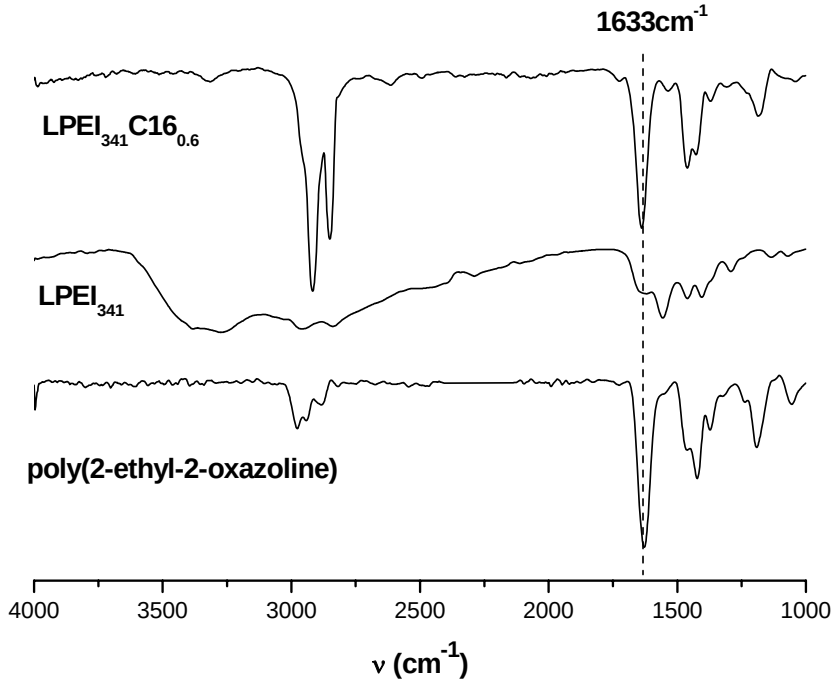

Figure 7-3. Comparison of the FTIR spectra of poly(2-ethyl 2-oxazoline), LPEI (LPEI15K) and palmitoyl chloride-modified LPEI (LPEI15KC16$_{0.6}$)

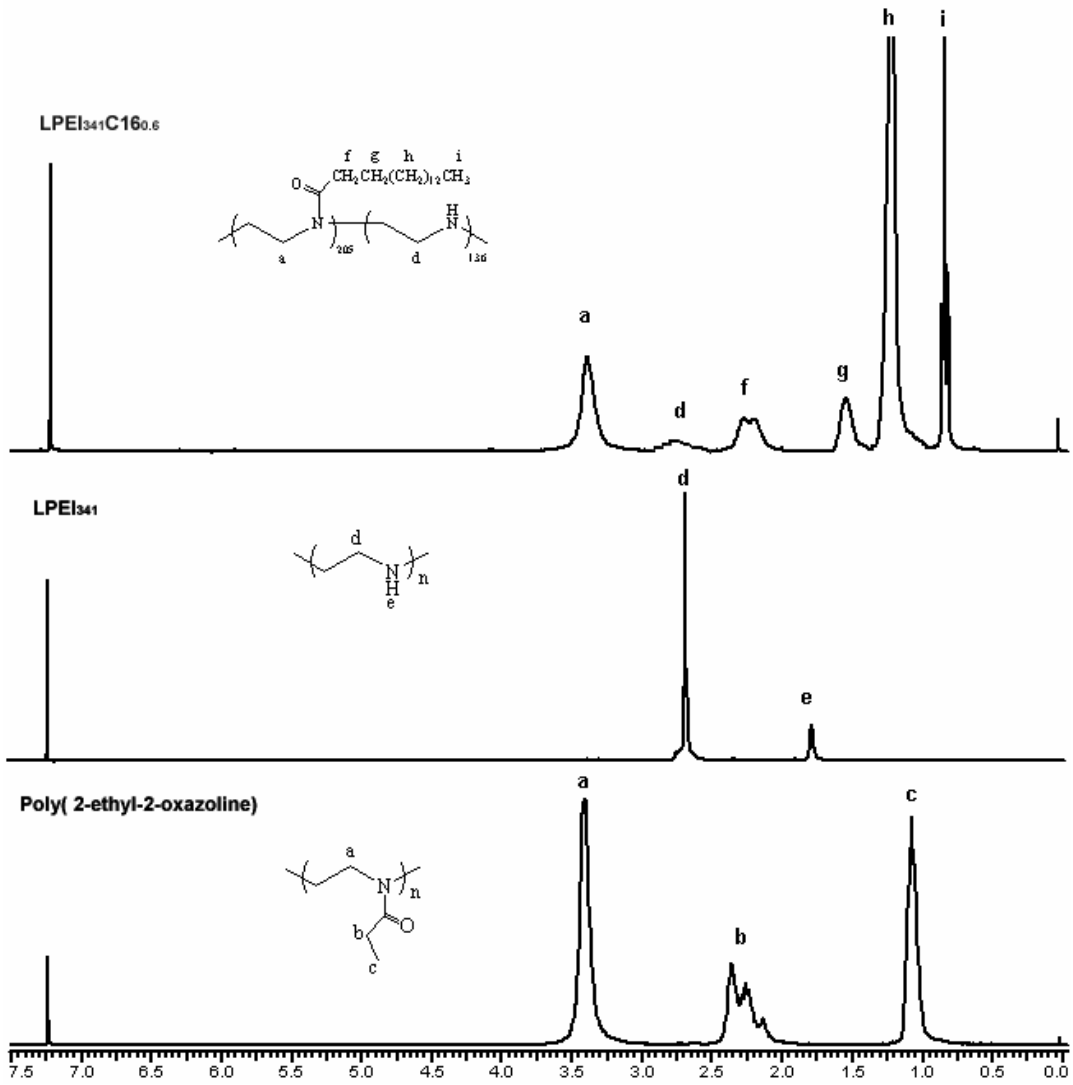

Figure 7-4. Comparison of the ^{1}H NMR spectra of poly(2-ethyl 2-oxazoline), linear PEI (LPEI15K) and palmitoyl chloride modified LPEI ($LPEI15KC16_{0.6}$)

FTIR was used to following the reaction. As shown in Figure7-3, the vibration of the carbonyl groups (1633 cm^{-1}) disappeared after hydrolysis, while the band of the secondary amine groups (3400 cm^{-1}) appears. This process can also be monitored in ^{1}H NMR spectra. (Figure 7-4) The peaks at 1.05 (CH_3) and 3.40 ppm (CH_2) disappear after hydrolysis, while the resonance of CH_2 backbone groups shifts from 2.25 to 2.75 ppm. After further amidation with palmitic acid, the peak at 1633 cm^{-1} reappears, while the amine vibration band cannot be detected. ^{1}H NMR results confirmed the formation of the desired amidated products.

The thermal characteristics and GPC data of all the obtained amidated samples are listed in the experimental part.

7.2.3. Dye encapsulation

Amidation of PEI with apolar aliphatic acid derivatives can afford polymers that are soluble in apolar organic solvents. Covalently modified hyperbranched polymers with hydrophobic shell have been shown to sequester polar dyes from the aqueous phase into organic media.[31] To confirm the micellar properties of the amidated hyperbranched PEI with both neutral and cationic cores, their capacity for polar guest encapsulation has been evaluated and compared with that of the modified linear PEI. To serve this purpose, four water-soluble dye probes, namely Eosin Y (EY), Fluorescein Sodium (FS), Methyl Orange (MO) and Congo Red (CR) have been utilized (Structures are listed in Scheme 7-5). The encapsulation effects can be seen from Figure 7-5.

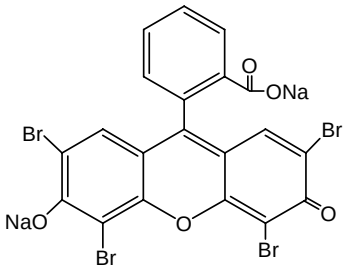

Eosin Y (EY)

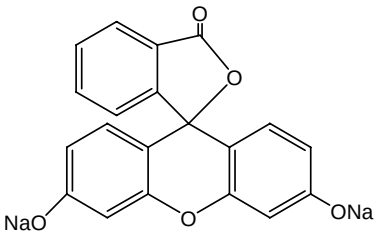

Fluorescein Sodium (FS)

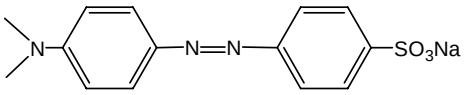

Methyl Orange (MO)

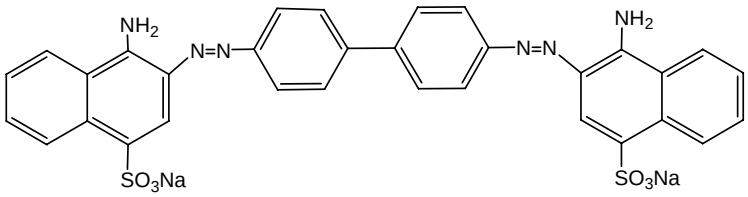

Congo Red (CR)

Scheme 7-5. Water-soluble dye structures

The encapsulated dye was quaternized calculated by the following "titration" method: Congo Red solution was mixed with nanocapsule solution (with constant concentration) first. The corresponding absorption band of the chloroform phase was measured as a function of the concentration of the CR dye in the aqueous solution. The ratio of [CR]/[Capsules] was plotted vs. absorbance. Typical UV-spectra and

titration plots from HPEI25KC16$_{0.6}$ and HPEI25KC16$_{0.6}$N$^{+}_{0.4}$ are exemplified in Figures 7-6 and 7-7. From the titration plot it is obvious that the absorbance reaches a constant value at a certain [CR]/[Capsules] ratio. The ratio at the transition point was used to calculate the maximum concentration of dye that the capsules can encapsulate. The maximum absorbance from four kinds of encapsulated dyes is exemplified in Table 7-4. (Experimental Part)

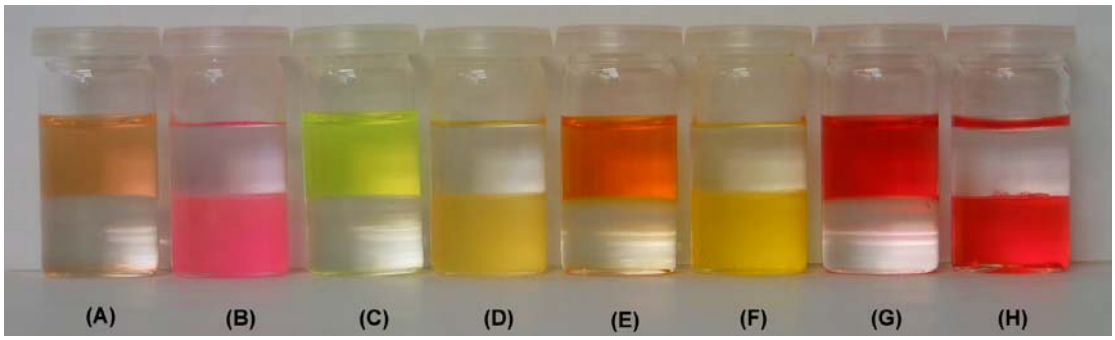

Figure 7-5. Demonstration of the solubilization effect (bottom layer: chloroform, upper layer: water). (A) Eosin Y; no polymer in organic layer; (B) Eosin Y; HPEI10K C16$_{0.6}$ in organic layer; (C) Fluorescein Sodium; no polymer in organic layer; (D) Fluorescein Sodium; HPEI10K C16$_{0.6}$ in organic layer; (E) Methyl Orange; no polymer in organic layer; (F) Methyl Orange; HPEI10K C16$_{0.6}$ in organic layer; (G) Congo Red; no polymer in organic layer; (H) Congo Red; HPEI10K C16$_{0.6}$ in organic layer

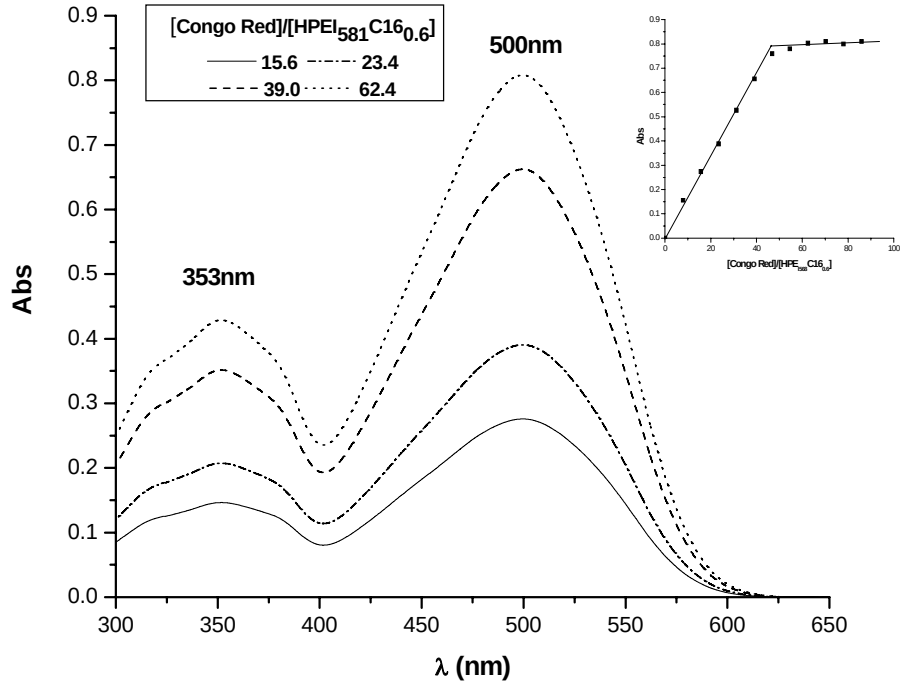

Figure 7-6. UV-Vis spectra and titration curve (inset) for HPEI25KC16$_{0.6}$ for encapsulation of Congo red (CR) in chloroform phase

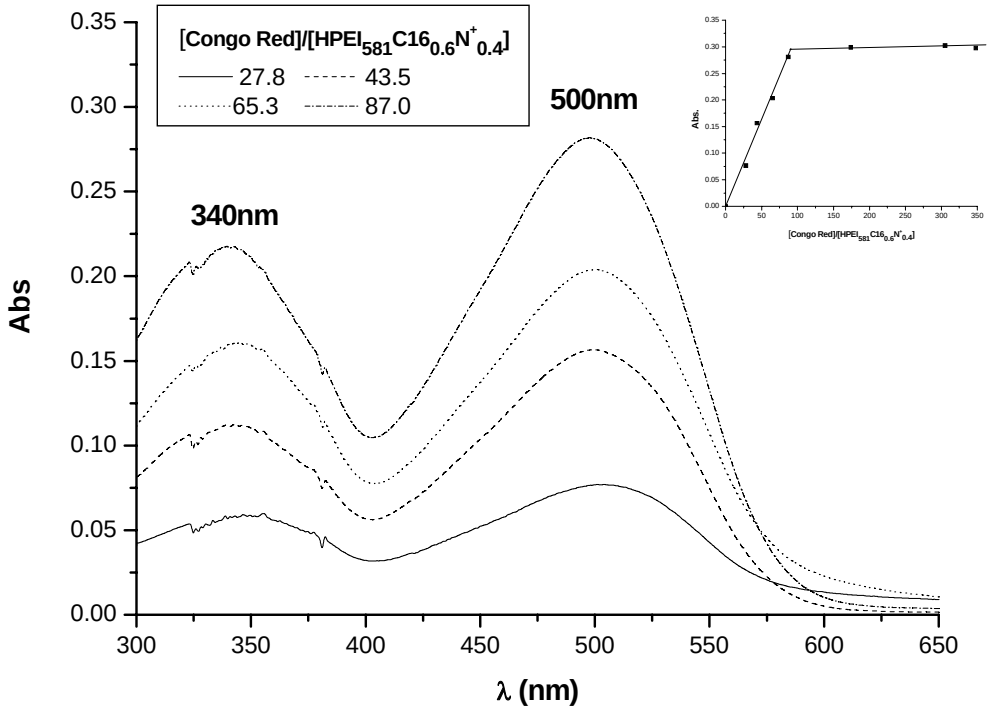

Figure 7-7. UV-Vis spectra and titration curve (inset) for HPEI25K$C16_{0.6}N^{+}_{0.4}$ encapsulating Congo red (CR) in chloroform phase

From the above titration curves and absorbances, the maximum numbers of dye molecules encapsulated by each nanocapsule were calculated. The data are listed in Table 7-1.

Table 7-1. Encapsulation capacities of amide-modified polyethylenimine samples

Polymers [a]	Dye loading capacity			
	N (EY) [b]	N(FS)	N(MO)	N(CR)
HPEI10K-$C16_{0.6}$	14.4	7.0	25.6	16.9
HPEI25K-$C16_{0.6}$	38.4	14.2	57.4	44.5
HPEI10K-$C16_{0.6}N^{+}_{0.4}$	41.2	12.2	56.6	49.3
HPEI25K-$C16_{0.6}$ $N^{+}_{0.4}$	71.4	41.7	153	90.1
LPEI15K-$C16_{0.6}$	4.2	0.9	5.3	0

[a] Nomenclature: HPEIX-$C16_y$: HPEI, hyperbranched scaffold; X: M_n of HPEI; C16, length of alkyl chain; y degree of functionalization. In the case of quaternized polymers N^{+}_{z} was used, where z indicates the degree of quaternized amines. [b] N(dye): transported dye number.

We could see the linear polymer LPEI15KC16$_{0.6}$ can only transport dyes to an insignificant extent, while the hyperbranched amidated HPEI10KC16$_{0.6}$ and HPEI25KC16$_{0.6}$ encapsulate all dyes in large amounts more efficiently than the previously reported HPEI containing an imine-bound shell.[31] The higher encapsulation capacity of the amide shell in the HPEI-based systems is ascribed to the additional contribution of the amide functional groups via hydrogen-bonding interactions. Such multiple secondary interactions originating from the presence of amide groups have been previously used to encapsulate and assemble end groups in a reversible way at the interior as well as at the periphery of dendrimers.[15, 19, 33, 34] Remarkably, the number of encapsulated dye molecules increased by a factor of about 3 after quaternization. For instance, the loading of encapsulated CR changed from 14.4 in HPEI10KC16$_{0.6}$ to 41.2 dye molecules in the sample HPEI10KC16$_{0.6}$N$^{+}_{0.4}$.

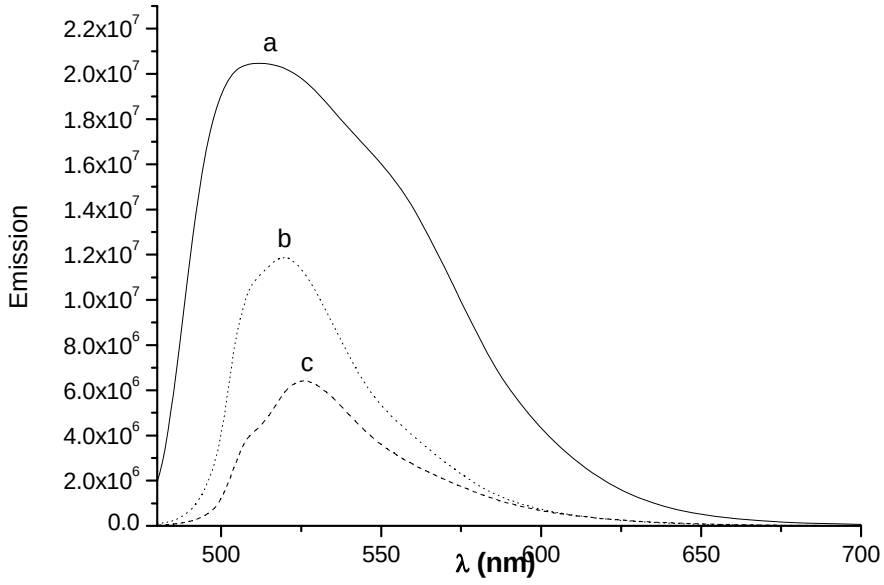

Figure 7-8**.** The fluorescence spectra of (a) Fluorescein sodium in water (Abs = 0.047, λ_{ex} = 488 nm), (b) Fluorescein sodium encapsulated by PG$_{269}$C16$_{0.6}$ in chloroform (Abs = 0.048, λ_{ex} = 506 nm) and (c) Fluorescein sodium encapsulated by HPEI25K C16$_{0.6}$ in chloroform (Abs = 0.048, λ_{ex} = 506 nm)

The low loading of dyes by the linear amidated polymer was not unexpected, since a previous study on hyperbranched and linear polyglycerols had confirmed the peculiarity of the hyperbranched structure in the context of phase transfer.[27] In the case of LPEI, we attribute the low, but not negligible fraction of dye transported to the

weak interaction of dyes with the remaining secondary amine groups. In contrast, the compact core-shell structure in the amidated HPEI is relevant for encapsulating a higher amount of dye in the polar interior. The results show that an additional increase of the polarity of the core strongly enhances the guest encapsulation capacity of the "molecular nanocapsules". This is most probably due to the thermodynamically favored environment for the anionic dyes. Further evidence for efficient dye encapsulation arises from fluorescence quenching of the encapsulated FS dyes, indicating their location within the Förster distance of the internal amine quenchers. (Figure 7-8)

Experiments to assess the selectivity of dye encapsulation of the amidated HPEIs have also been performed, using two different mixtures of FS: MO and EY: FS dyes, respectively, in 1:1 ratio. Both dyes were extracted, as observed from UV-vis spectra. However, a reasonable quantification of the ratio of the amount of transported dye was difficult due to the featureless and overlapping maximum absorption bands in the corresponding UV-vis spectra of the encapsulated dyes.

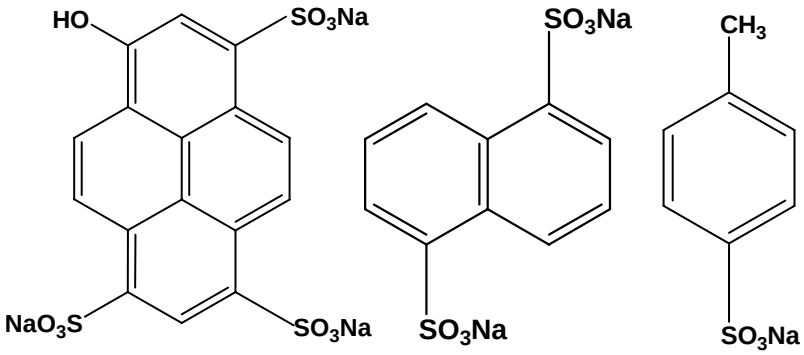

Scheme 7-6. Structures of molecules used for competitive encapsulation

Detailed competitive experiments have further been tried using the above three compounds since they possess different chromophores and their absorbances do not completely overlap. However, an exact number of "guests" cannot be quantitively calculated due to the broadened absorbance band.

Since HCl is generated during the capsule preparation by amidation of HPEI with palmitic acid chloride, traces of HCl might couple with the unreacted tertiary amines inside the capsule to form core-quaternized capsules. Thus, for comparison, samples obtained from amidation with palmitic acid under CDI conditions were used to test

the effect. The encapsulation results are summarized in Table 7-3.

Table 7-3. Encapsulation capacities of amide-modified polyethylenimine samples obtained from reaction with palmitic acid under CDI conditions

Polymers [a]	MO		FS		EY	
	n_d/n_p [b]	w_d/w_p [c]	n_d/n_p	w_d/w_p	n_d/n_p	w_d/w_p
HPEI10K-C16$_{0.3}$	67.6	0.83	15.9	0.22	38.3	1
HPEI10K-C16$_{0.6}$	62.3	0.47	14.2	0.12	25.8	0.41
HPEI10K-C16$_{0.73}$	51.9	0.34	14.1	0.11	25.2	0.35
HPEI25K-C16$_{0.73}$	132	0.34	23.3	0.07	63.5	0.35
LPEI15K-C16$_{0.73}$	17.3	0.075	1.1	0.005	13.4	0.12
HPEI10K-C16$_{0.6}$ N$^+_{0.4}$	97.2	0.56	38	0.25	55	0.67
HPEI10K-C16$_{0.6}$ HCl$_{0.4}$	74.2	0.52	23	0.19	27.3	0.40
HPEI10K-C16$_{0.73}$ N$^+_{0.27}$	87.4	0.48	24.6	0.16	45.6	0.53
HPEI25K-C16$_{0.73}$ N$^+_{0.27}$	211	0.46	66.7	0.17	107	0.50
LPEI15K-C16$_{0.73}$N$^+_{0.27}$	88.1	0.32	27.3	0.11	51.8	0.40

[a] Nomenclature: HPEIX-C16$_y$: HPEI, hyperbranched scaffold; X: M_n of HPEI; C16, length of alkyl chain; y: degree of functionalization. In the case of quaternized polymers N^+_z was used, where z indicates the fraction of quaternized amines. [b] n_d/n_p: the average number of dye transported into one polymer capsule; [c] w_d/w_p: the average weight ratio of dyes transported into the polymer capsule with the polymer capsules.

From the above results it is obvious that that the difference of encapsulation for the nanocapsules prepared by the two different methods is not large. Surprisingly we can also notice that HPEI10K with 30% alkyl modification shows very high encapsulation capacity. This could be due to the following reasons: 1) with lower degree of modification, more polar amine groups are preserved and the inner part is thus more polar to attract a higher fraction of dye; 2) the formation of larger micelles. Viscosity results support the first explanation, since the amphiphilic structures show very low and comparable viscosity with other capsules. Interestingly, when we

convert the number ratio to the weight ratio it is impressive that for the capsule HPEI10K-$C16_{0.6}$ $N^{+}_{0.4}$, 1 gram of this material can encapsulate 0.56 g MO, which represents a very high transport capacity.

7.2.4. Viscosity measurements

To obtain insight into the structure of the modified HPEI in solution, viscosimetry studies have been performed. Figure 7-9 shows the relationship between specific viscosity and concentration for modified HPEI systems from chloride reaction.

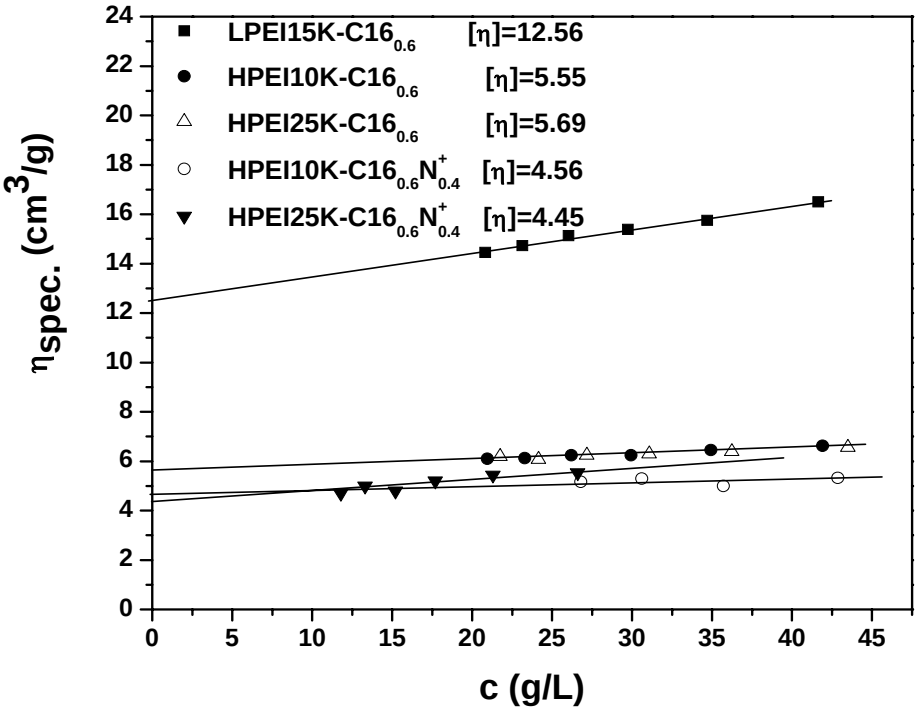

Figure 7-9. Representation of specific viscosity vs. concentration for modified HPEI systems.

As shown in Figure 7-9, the hyperbranched polymers showed remarkably low viscosity values and the viscosities changed mildly upon dilution and resulted in a relative flat line with very small slope compared with the case for linear PEI. Moreover, the viscosity values increased insignificantly with the increase of the molecular weight. These phenomena were characteristic of compact spheroid structure,[35, 36] usually exhibited by dendritic polymers[27] and star polymers.[37]

The low intrinsic viscosity values [η] were around 5.6 mL/g for both HPEI10K-$C16_{0.6}$ and HPEI25K-$C16_{0.6}$, twice lower than for the linear analogue LPEI15K-$C16_{0.6}$ ([η] = 12.5 mL/g). The quaternized polymers HPEI10K-$C16_{0.6}N^{+}_{0.4}$ and HPEI25K-

$C16_{0.6}N^{+}_{0.4}$ show even lower intrinsic viscosity ([η] = 4.6 mL/g). The specific viscosity values measured for the linear material LPEI15K-$C16_{0.6}$ are considerably higher than those observed for the hyperbranched polymers.

The viscosity of all the new samples from amidation with palmitic acid under CDI conditions has also been measured for comparison and are shown in Figures 7-10, 7-11 and 7-12.

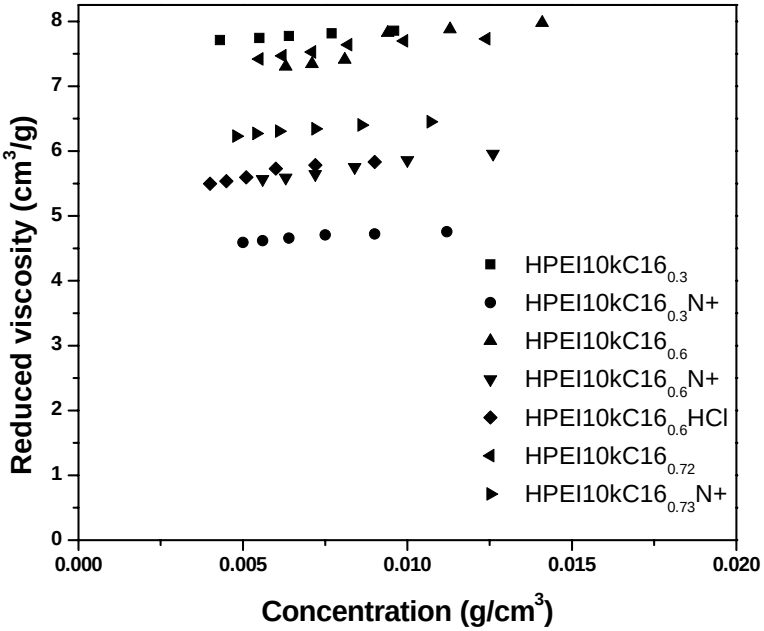

Figure 7-10. Specific viscosity vs. concentration for HPEI10K samples modified with palmitic acid under CDI conditions.

Similar as shown in Figure 7-9, all the hyperbranched polymers showed low viscosity values and the viscosities values changed mildly upon dilution, which are characteristic of hyperbranched structure. Those viscosity values increased insignificantly with the increase of the molecular weight.

From all the Figures above, it can be seen that the amidated HPEI species with cationic interior showed a little lower viscosity values compared with those without cationic interior, which is attributed to the very compact structure adopted for the quaternized HPEIs in apolar media, caused by unfavorable interaction of the charged, polar interior with the apolar solvent. This obviously results in a "collapsed" topology. These properties associated with the modified HPEIs are displayed at similar but a little higher concentration in comparison to the phase transfer experiments.[12] The amidated LPEI shows higher viscosity value than its

hyperbranched analogue. It can be concluded that the amidated LPEI in chloroform will not take the compact core-shell conformation exhibited by its hyperbranched analogues, but a relative extended conformation.

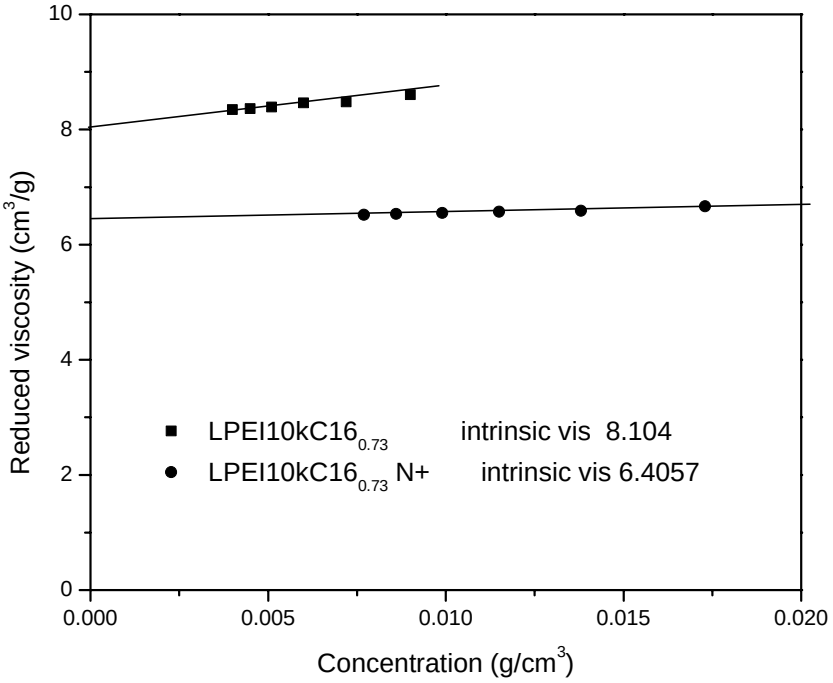

Figure 7-11. Specific viscosity vs. concentration for modified LPEI samples with palmitic acid under CDI conditions.

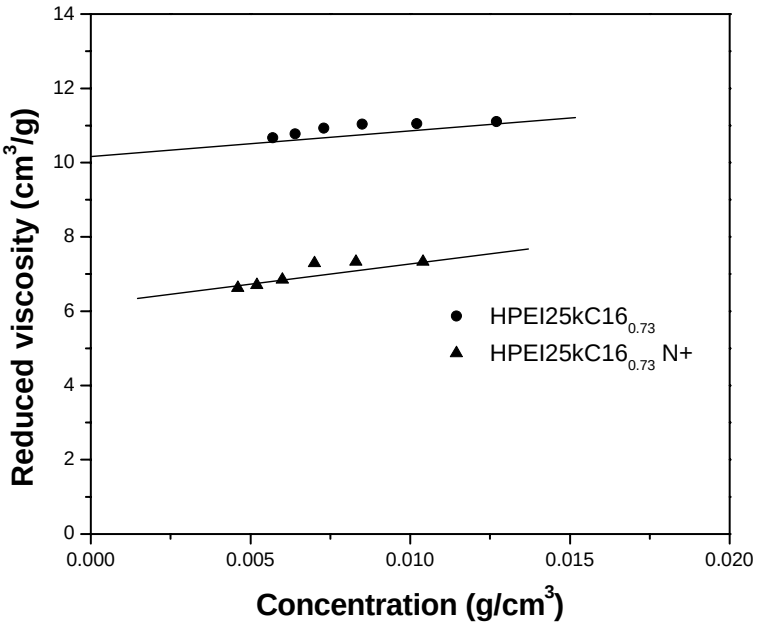

Figure 7-12. Specific viscosity vs. concentration for modified HPEI25K samples with palmitic acid under CDI conditions.

Since dilute solutions have been used for the phase transfer protocols, determination of the polymer structure in this concentration range was necessary. Dynamic Light Scattering (DLS) experiments have been performed, confirming the absence of clustering between modified HPEI and indicating single particle behavior of HPEI10K-$C16_{0.6}$ and HPEI25K-$C16_{0.6}$ with a hydrodynamic size of approximately 6±0.05 and 9±0.05 nm, respectively, while the quaternized species HPEI10K-$C16_{0.6}N^{+}_{0.4}$ and HPEI25K-$C16_{0.6}N^{+}_{0.4}$ display a size of 5±0.05 and 7±0.05 nm, respectively, pointing to an inverted unimicellar behavior of the amidated-HPEI species with both neutral and cationic interior.

When the concentrations of $LPEI_{341}C16_{0.6}$, HPEI10K$C16_{0.6}N^{+}_{0.35}$, HPEI10K $C16_{0.6}$ and HPEI25K$C16_{0.6}$ are $2x10^{-5}$ M (1.28 g/l), $9.1x10^{-5}$ M (5g /l), $5x10^{-5}$ M (2.13 g/l) and $2x10^{-5}$ M (2.13 g/l), respectively, no aggregates were found by DLS. The concentrations of $LPEI_{341}C16_{0.6}$, HPEI10K $C16_{0.6}N^{+}_{0.35}$, HPEI10K $C16_{0.6}$ and HPEI25K $C16_{0.6}$ used for the dye encapsulation are $3.13x10^{-6}$ M, $9.65x10^{-7}$ M, $2.36x10^{-6}$ M and $9.45x10^{-7}$ M, respectively. This means that the dyes are encapsulated by unimolecular nanocapsules instead of aggregated ones.

7.2.5. Water-soluble Au nanoparticle encapsulation

These amidated HPEI nanocapsules have been used as “nanoreactor” for the synthesis of a silver particles. Stabilized silver nanoparticles (NPs) possess antimicrobial properties. [9] However, due to the size distribution of the HPEI core, the obtained silver particles possess relative broad size distribution.

Besides for transferring dyes, as described above, we also used the amidated HPEI nanocapsules to encapsulate metal NPs. The respective NPs were synthesized by conventional methods. Subsequently they were encapsulated by HPEI capsules. By this method, we can transfer water-soluble NPs into the organic phase without ligand exchange, and these hybrid materials contain evenly distributed particles with narrow size distribution, which are protected by polymers.

Gold NPs, which can be easily synthesized in water, have been used for encapsulation studies.

Au NPs of 5 nm and 12 nm size have been synthesized. Their UV absorbance spectra are shown in Figure 7-14. They exhibit a distinct surface plasmon absorption

band, centered at 517 nm and 523 nm, respectively. Figure 7-13 shows a photograph of the gold NPs with a size of 12 nm.

Figure7-13. Photos of gold nanoparticle solutions with 12nm particles (left) and transported by the HPEI10K-$C16_{0.6}N^{+}_{0.4}$ capsules (right) into the chloroform phase

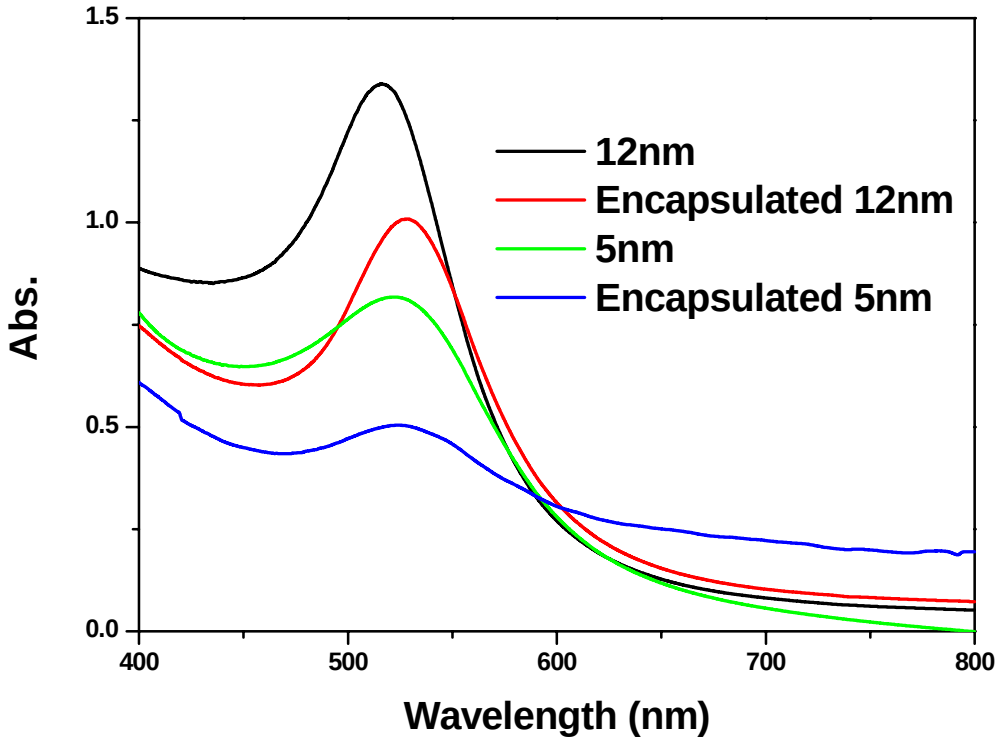

Figure 7-14. UV-spectra of water-soluble Gold nanoparticles before and after encapsulation by the nanocapsules HPEI10K-$C16_{0.6}N^{+}_{0.4}$

The same method to extract dyes as described in section 7.2.3 was used to encapsulate NPs from the water phase: mixing the water solution of Au NPs with the chloroform solution of the nanocapsules. The encapsulation effect can be seen from Figure 7-13. It is clear that water soluble Au NPs can be successfully transferred into the organic phase. The solution is turbid due to the formation of an emulsion. From Figure 14, UV-vis absorbance of the NPs moved to longer wavelength for NPs of 12 nm, while for the NPs with size of 5 nm, the plasmon absorption band did not show an obvious shift. The reason for the size change is still not clear. Tentatively, we ascribe this to the stronger coordination of Au with N, the citric acid was released during the transfer process, and the size of the NPs might be altered.

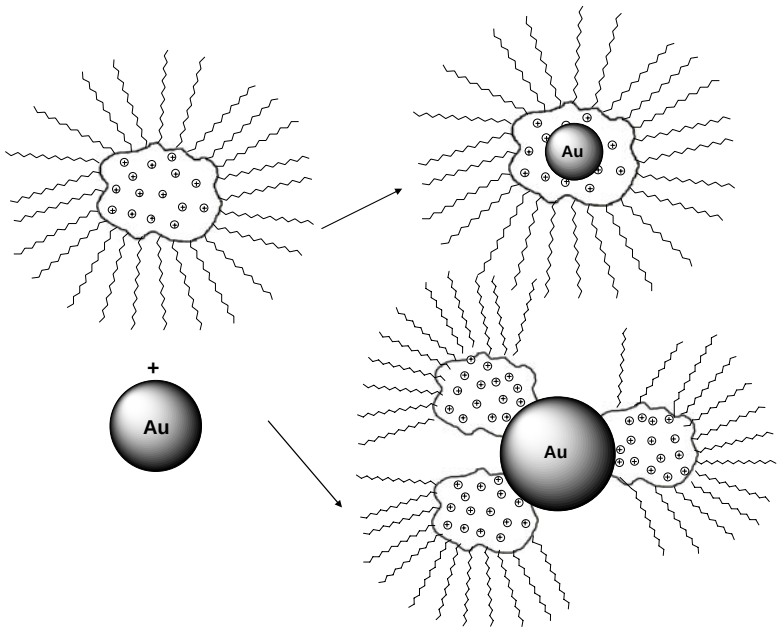

Scheme 7-7. Possible encapsulation mechanisms for the gold nanoparticles

The encapsulation mechanism is still not clear; it can be unimolecular transfer or several amphiphilic polymer molecules stabilizing the rather large nanoparticles (as shown in Scheme 7-7). However, this represents a "proof of principle" experiment supporting the possibility of transport into the organic phase.

7.2.6. Encapsulation of apolar probe molecules in the water phase

The above works are focused on extracting water-soluble guests into an organic phase, since aliphatic chain-modified capsules are soluble in organic solvents.

Accordingly, we can also modify HPEI with water-soluble chains to obtain double hydrophilic core-shell structures for stabilizing guests in the water phase. Here an example is given for encapsulating pyrene into water.

The respective nanocapsular structure is synthesized by a one step Michael-Addition: HPEI10K is reacted with PEO acrylate. The reaction is shown in Scheme 7-8. The degree of modification is 54% and the sample is termed as $HPEI10KPEO_{0.54}$.

This water soluble capsule ($HPEI10K\text{-}PEO_{0.54}$) was used for stabilizing pyrene in water. The process is shown in Scheme 7-9 and the effect is shown in Figure 7-15.

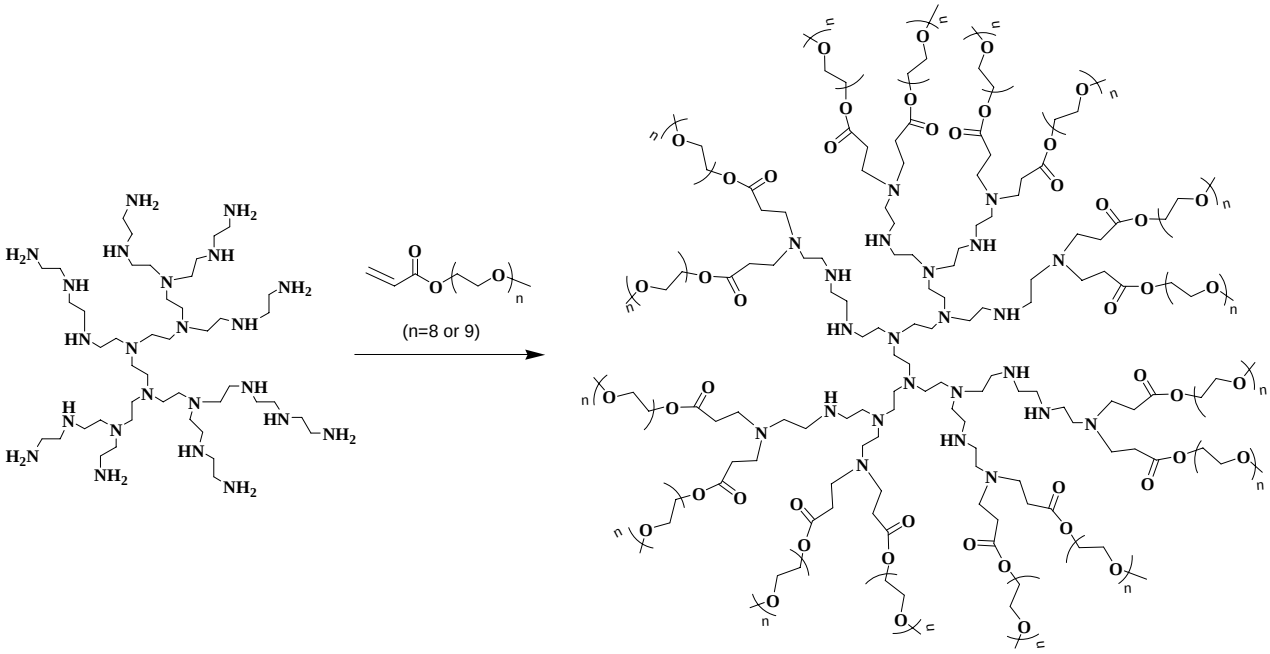

Scheme 7-8. Synthesis of double hydrophilic core-shell structure from HPEI

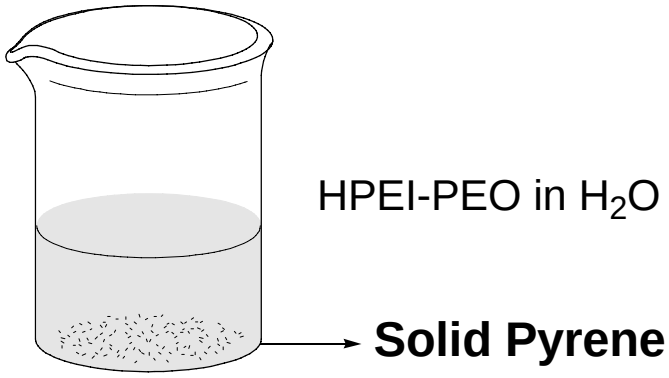

Scheme 7-9. Method to stabilize pyrene in H_2O using $HPEI10KPEO_{0.54}$ capsules

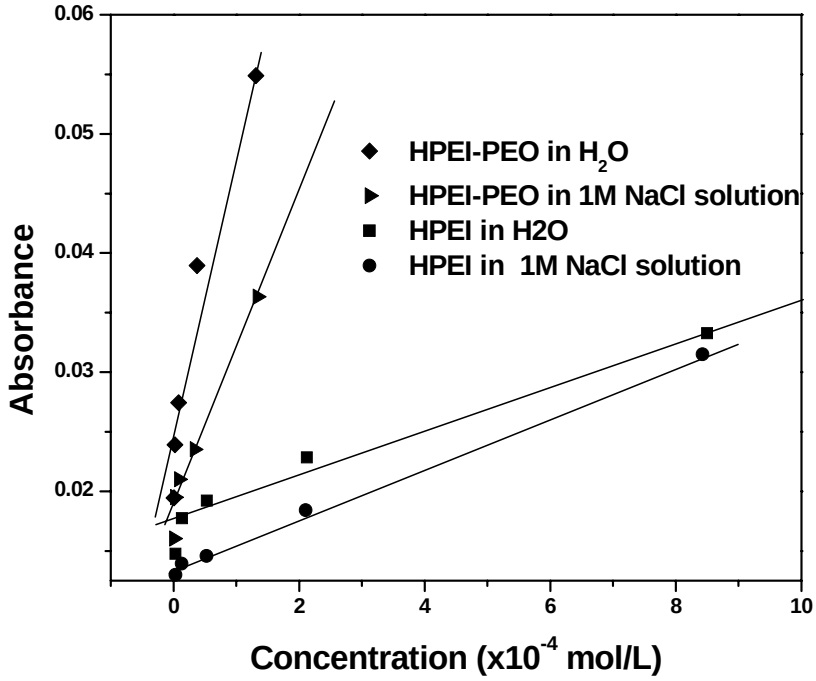

Figure 7-15. Solubility enhancement of pyrene in water with the presence of the modified HPEI10K$PEO_{0.54}$ capsules

As it can be seen from Figure 7-15, the solubility of pyrene in water was strongly enhanced by the presence of the modified HPEI10K$PEO_{0.54}$ capsules either under neutral conditions or with the presence of NaCl. If only unmodified HPEI10K was used, an enhancement of pyrene encapsulation is not obvious or detectable. By this example, it is clear that proper modification of HPEI can enlarge its application range for guest molecule transfer into environments of different polarity.

7.3. Conclusion

In conclusion, we have demonstrated that HPEI can be functionalized for the transport of different guest molecules.

Partially amidated HPEIs with cationic interior are attractive compounds to obtain unimolecular, hyperbranched nanocapsules for phase-transfer applications. It can be used to transfer water soluble dye into organic phase, the irreversible dye loading capacity is enhanced considerably by the increase of the interior polarity by quaternization. In comparison to the branched compounds, the linear analogue showed lower capacity for guest molecule transfer, which strongly supports the conclusion that the hyperbranched structure is crucial for encapsulation. Preliminary

tests also show that this capsule can be used to transfer water-soluble gold nanoparticles into the organic phase.

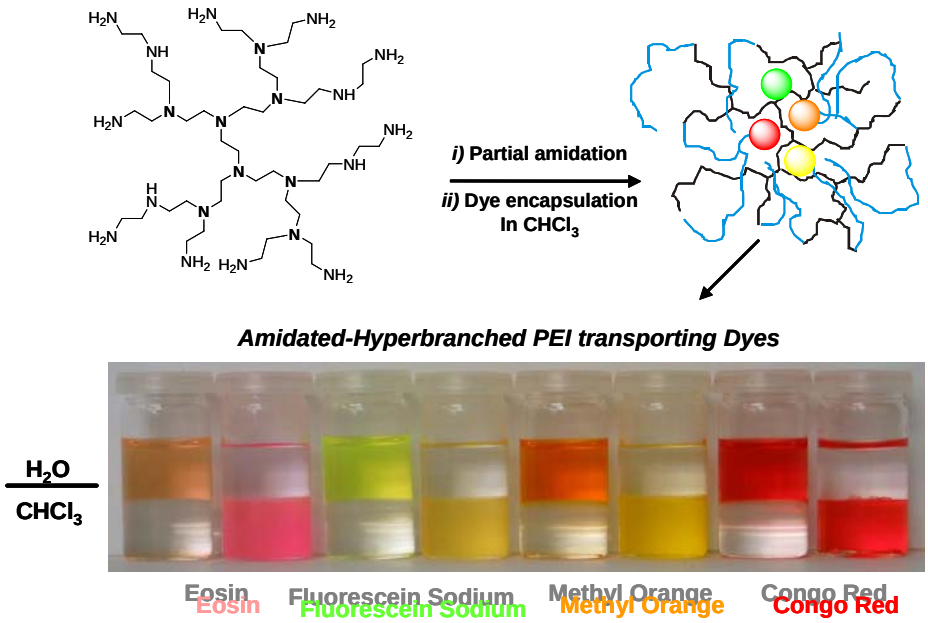

Modified HPEI-PEO possesses double hydrophilic core shell structure. It can be used to enhance the solubility of pyrene in water.

7.4. Experimental Part

7.4.1. Materials

Hyperbranched polyethylenimine HPEI10K (M_n = 1x10^4 g/mol, M_w/M_n = 2.5) was purchased from Aldrich. HPEI25K (M_n = 2.5x10^4 g/mol, M_w/M_n = 2.5) was provided from Hyperpolymers GmbH (Freiburg, Germany). Poly(2-ethyl-2-oxazoline) (M_w = 5x10^4 g/mol) was ordered from Aldrich. The polydispersity was found to be 1.44 by SEC using THF as eluent, indicating that M_n of this polymer is 3.5 x10^4 g/mol. Methyl iodide was purchased from Acros. Palmitoyl chloride (99%) was used as received from Fluka. Benzoylated cellulose tubing (MWCO 1,000) was purchased from SIGMA.

7.4.2. Amidation of hyperbranched polyethylenimine using palmitoyl chloride

The preparative procedure for partial amidation of HPEI10k (T = 33.3%, D = 26.7%, L = 40%), and HPEI25k (T = 33.3%, D = 26.9%, L = 39.8%) affording HPEI10kC16$_{0.6}$, HPEI25kC16$_{0.6}$, respectively, was carried out as described in the following.

The synthesis of 60% amidated polyethylenimine (HPEI) is exemplified for the polymer HPEI10K-C16$_{0.60}$: To1g (0.1 mmol) of HPEI10K (M_n = 10^4 g/mol, M_w/ M_n = 2.5) in 10 ml of pyridine, drop in 4.24 ml (14.0 mmol) palmitoyl chloride. The mixture was stirred overnight at room temperature, after removing all the pyridine at the presence of toluene, dissolve the sample in chloroform and washed with water, the final organic phase was dialyzed against chloroform to obtain pure polymers. HPEI10KC16$_{0.6}$**:** ^{1}H NMR ($CDCl_3$, as can be seen from Figure 7-1): = 3.36 (br, -$CH_2C\underline{H}_2NHCO$-, -$CH_2C\underline{H}_2NCO$-); 2.55 (m, -$CH_2C\underline{H}_2NH$-, -$CH_2C\underline{H}_2N$-); 2.40-2.00 (br, -$NCOC\underline{H}_2$-); 1.56 (br, -$NCOCH_2C\underline{H}_2$-); 1.22 (br, -$NCOCH_2CH_2(C\underline{H}_2)_{12}CH_3$); 0.85 (t, -$NCOCH_2CH_2\,(CH_2)_{12}C\underline{H}_3$). IR: =1635 cm^{-1} (amide group)

7.4.3. Amidation of hyperbranched polyethylenimine using palmitic acid

The syntheses of 30-60% amidated polyethylenimine (HPEI) are exemplified for the polymer HPEI10K-C16$_{0.6}$: 4.52 g (27.88 mmol) of 1,1'-carbonyldiimidazole (CDI) was slowly added to the solution of 7.16g (27.88 mmol) of palmitic acid in 40 ml of chloroform. The solution was stirred at room temperature for 1h, and then 2 g (0.2 mmol) of HPEI10K (M_n = 10^4 g/mol, M_w/ M_n = 2.5) in 10 ml of chloroform was added. The mixture was stirred at room temperature for 4 h, and then at 50 ^{o}C overnight. After cooling down, the mixture was washed three times by NaCl aq. The organic phase was dried by anhydrous $NaSO_4$. After filtration and removal of the volatiles, the residue was kept at 40 ºC in vacuum oven overnight. A higher amount of pure material can be obtained by dialysis against chloroform.

The syntheses of 73% amidated HPEI are exemplified for the polymer **HPEI10K-C16$_{0.73}$**: 3.39 g (20.91 mmol) of 1,1'-carbonyldiimidazole (CDI) was slowly added to the solution of 5.37 g (20.91 mmol) of palmitic acid in 30 ml of chloroform. The solution was stirred at room temperature for 1h, and then 1g (0.1 mmol) of HPEI10K (M_n = 10^4 g/mol, M_w/ M_n = 2.5) in 5 ml of chloroform was added. The mixture was refluxed overnight. After cooling down, the mixture was dialyzed against chloroform to obtain pure polymers.

7.4.4. The quaternization of HPEI10KC16$_{0.6}$ by methyl iodide

HPEI10KC16$_{0.6}$ (1.97 g) was dissolved in 25 ml of chloroform, and then 0.72 g of K_2CO_3 and 2.93 ml of methyl iodide (10 eq. relative to the remaining amine groups of HPEI10KC16$_{0.6}$) was added. The mixture was refluxed for 36 h. After filtration and

removal of the volatile, partially quaternized polymer HPEI10KC16$_{0.6}$N$^{+}_{0.4}$ was obtained. ^{1}H NMR ($CDCl_3$): = 4.39-3.03 (br, -$CH_2C\underline{H}_2NHCO$-, -$CH_2C\underline{H}_2NCO$-, -$CH_2C\underline{H}_2N^{+}$-, $C\underline{H}_3N^{+}$-); 2.50-2.00 (br, -$NCOC\underline{H}_2$-); 1.56 (br, -$NCOCH_2C\underline{H}_2$-); 1.22 (br, -$NCOCH_2CH_2$ $(C\underline{H}_2)_{12}CH_3$); 0.85 (t, -$NCOCH_2CH_2(CH_2)_{12}C\underline{H}_3$). IR: =1635 cm^{-1} (amide group).

7.4.5. The quaternization of HPEI10KC16$_{0.6}$ by HCl

HPEI10KC16$_{0.6}$ (1.97 g) was dissolved in 25 ml of chloroform, and then 0.72 g of K_2CO_3 and 2.93 ml of methyl iodide (10 eq. relative to the remaining amine groups of PEI10KC16$_{0.6}$) was added. The mixture was refluxed for 36 h. After filtration and removal of the volatile, partially quaternized polymer HPEI10KC16$_{0.6}$N$^{+}_{0.4}$ was obtained. ^{1}H NMR ($CDCl_3$): = 4.39-3.03 (br, -$CH_2C\underline{H}_2NHCO$-, -$CH_2C\underline{H}_2NCO$-, -$CH_2C\underline{H}_2N^{+}$-, $C\underline{H}_3N^{+}$-); 2.50-2.00 (br, -$NCOC\underline{H}_2$-); 1.56 (br, -$NCOCH_2C\underline{H}_2$-); 1.22 (br, -$NCOCH_2CH_2$ $(C\underline{H}_2)_{12}CH_3$); 0.85 (t, -$NCOCH_2CH_2(CH_2)_{12}C\underline{H}_3$). IR: =1635 cm^{-1} (amide group).

7.4.6. Preparation of the linear polyethylenimine LPEI$_{348}$

Linear PEI was prepared from poly(2-ethyl-2-oxazoline), the procedure can be found from chapter 6.

7.4.7. Amidation of the linear polyethylenimine LPEI$_{348}$

The amidation of the linear polyethylenimine was performed as reported for the hyperbranched isomers.[3] Polymer LPEI$_{348}$C16$_{0.6}$: ^{1}H NMR ($CDCl_3$): = 3.40 (br, -$CH_2C\underline{H}_2NCO$-); 2.67 (br. –$C\underline{H}_2NH$-); 2.39-2.06 (m, -$CH_2C\underline{H}_2NH$-, -$NCOC\underline{H}_2$-); 1.56 (br, -$NCOCH_2C\underline{H}_2$-); 1.22 (br, -$NCOCH_2CH_2(C\underline{H}_2)_{12}CH_3$); 0.85 (t, -$NCOCH_2CH_2$ $(CH_2)_{12}C\underline{H}_3$). IR: =1633 cm^{-1} (amide group)

7.4.8. The measurement of dye transport using HPEI nanocapsules

In a typical UV-Vis experiment, 4 mL of an aqueous Congo red solution (λ_{max} = 498 nm, ε_{max} = 2.50x10^{4} L mol^{-1} cm^{-1}) with a concentration in the range of 7.1x10^{-6}-7.8x10^{-5} M was shaken for 10 minutes with 4 mL of a chloroform solution of HPEI25KC16$_{0.6}$ (c = 9.07x10^{-7} M). After standing and phase separation, a sample of the clear red chloroform solution was transferred into a UV-Vis cuvette and its

absorption spectrum was measured.

7.4.9. Thermal and viscosity data

Table 7-3. DSC and viscosity data of amidified HPEI using Palmtic Chloride

Samples	M_n (x10^{-4})	M_w/M_n	$\eta_{spec.}$ (mL/g)[a]	$\eta_{dynamic}$ (mPa·s)[b]	T_m (°C)	T_g (°C)	H (J/g)
HPEI10KC16$_{0.6}$	4.32	2.4	6.31	5.46	76	n.d. [c]	61
HPEI10KC16$_{0.6}$N$^+_{0.4}$	5.68	2.5	5.15	4.45	70	7	12
HPEI25KC16$_{0.6}$	11.7	2.3	6.34	5.48	50 and 70	n.d. [c]	35 and 18
HPEI25KC16$_{0.6}$N$^+_{0.4}$	15.0	2.4	5.78	5.00			
LPEI15KC16$_{0.6}$	6.48	1.7	15.4	13.3	68	12	52
PG$_{269}$C16$_{0.6}$	5.87	1.3	6.68	5.78	46.6	n.d. [c]	65

[a] The specific viscosities correspond to toluene solutions of the related polymer at 30 g/L; [b] dynamic viscosities were determined at 30 g/L and determined from the following equation: $\eta_{dynamic} = \upsilon \cdot \rho$, where υ (mm^2/s) and ρ = 0.865 g/cm^3 are the absolute (kinetic) viscosity and the density of toluene at 20 °C respectively; [c] n.d. = not determined.

Table 7-4. GPC and DSC data HPEI-polyamide with palmitic acid

Samples	M_n (x10^{-4})	M_w/M_n	Delta H
HPEI10K-C16$_{0.3}$	2.66		16.656
HPEI10K-C16$_{0.6}$	4.33	1.56	33.755
HPEI10K-C16$_{0.73}$	5.05	1.97	33.796
HPEI25K-C16$_{0.73}$	12.6	1.55	49.218
LPEI15K-C16$_{0.73}$	7.57	1.87	48.572
HPEI10K-C16$_{0.6}$ N$^+_{0.4}$	5.69		33.635
HPEI10K-C16$_{0.6}$ HCl$_{0.4}$	4.67	1.28	24.589
HPEI10K-C16$_{0.73}$ N$^+_{0.27}$	5.94	2.14	33.692
HPEI25K-C16$_{0.73}$ N$^+_{0.27}$	14.9	1.71	27.839
LPEI15K-C16$_{0.73}$N$^+_{0.27}$	9.04		45.539

7.4.10. UV-vis and fluorescence measurements

Table 7-5. UV-vis data of hydrophilic dyes in water and in chloroform solution containing amidated HPEI

Solution	EY		FS		MO		CR	
	λ_{max} (nm)	ε_{max} x 10^{-4}	λ_{max} (nm)	ε_{max} x 10^{-4}	λ_{max} (nm)	ε_{max} x 10^{-4}	λ_{max} (nm)	ε_{max} x 10^{-4}
H_2O	516	8.65	488	6.06	464	2.16	498	2.50
HPEI25KC16$_{0.6}$[a]	533	4.86	506	1.58	428	2.32	500	1.72
HPEI10KC16$_{0.6}$N$^+_{0.4}$[a]	533	5.32	506	3.02	428	2.60	500	2.15
PG$_{269}$C16$_{0.6}$[a]	533	4.13	502	1.73	423	2.66	510	2.93

[a] The encapsulated dyes in HPEI nanocapsules have been measured in chloroform solution

7.4.11. Synthesis of Au Nanoparticles

12 nm Au NPs were prepared by citrate reduction of $HAuCl_4$ in the presence of citrate acid. Typically, 10 mL 1% (w/v) sodium citrate solution was added into a boiling solution of 290 mL 0.015% (w/v) $HAuCl_4$. Within 3 min the solution turned out wine-red, indicating the formation of Au NPs. After further boiling for 10 min, the heat source was removed and the dispersion was cooled down to room temperature. The Au NPs obtained were about 15 nm in size, determined by means of TEM and DLS. They exhibit a distinct surface plasmon absorption band, centered at 520 nm.

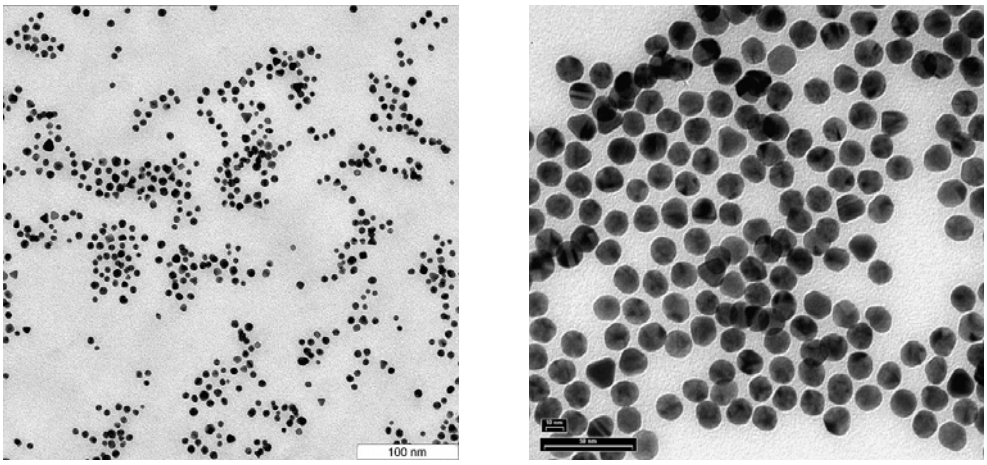

Figure 7-16. TEM of Au NPs, 5 nm (left), 12 nm (right)

The synthesis of 5 nm Au nanoparticles is quite similar to that of the 12 nm nanoparticles. In a typical experiment, a freshly prepared 100 ml solution of 0.01% $HAuCl_4$ is transferred to a 500 mL flask, stirred vigorously and is brought to the boiling in 6-7 minutes. Then, the reducing agent (2 mL of 1% sodium citrate and 0.45 mL of 1% tannic acid) is added, inducing a violet color immediately. Within 30

seconds, the solution becomes clear-red. After further boiling for 10 minutes, the heat source is removed and the dispersion is cooled down to room temperature. In this case, the size of the flask and the rate of addition of reducing solution have significant influence on the quality of the product.

7.4.12. Synthesis of the Hyperbranched HPEI10K-$PEO_{0.54}$ star polymer via Michael-Addition of Poly (ethylene glycol methylether) acrylate (PEOA) with HPEI10K

The synthetic procedure for partially PEOA modified HPEI is exemplified for HPEI10K-$PEO_{0.54}$: 1.00 g of HPEI10k (Aldrich, $M_n = 1.00 \times 10^4$, 23.3 mmol amine groups, NH_2+NH+N) was dispersed in 5 ml $CHCl_3$, then 4.30 ml (10.3 mmol, 44% to amine groups) of PEOA (Aldrich, Mn = 454, d = 1.09) was added. The mixture was stirred at room temperature for 4 days. The products are dialyzed against $CHCl_3$ to remove small molecule impurities using a benzoylated cellulose membrane (MWCO 1000 g/mol). The product is a yellow honey-like polymer.

^{1}H NMR (300 MHz, $CDCl_3$): δ = 1.22 (very weak, might from NH) 2.38-2.73 (-$NCH_2C\underline{H}_2COO$-, -$NC\underline{H}_2CH_2COO$-, -$NC\underline{H}_2C\underline{H}_2N$- of PEI), 3.36(-O-$C\underline{H}_3$), 3.50 & 3.61 (-O- $C\underline{H}_2$- $C\underline{H}_2$-O-), 4.18 (-$COOC\underline{H}_2$-CH_2-);

7.5. References

[1] Hecht, S.; Fréchet, J. M. J. *Angew. Chem. Int. Edit.* **2001,** 40, 74.
[2] Crooks, R. M.; Zhao, M.; Sun, L.; Chechik, V.; Yeung, L. K. *Acc. Chem. Res.* **2001,** 34, 181.
[3] Sauer, M.; Meier, W. *In Colloids and Colloid Assemblies, Caruso, F., Ed.; Wiley-VCH: Weinheim,* **2004**, pp 150.
[4] Ng, C.; Chan, Y.; Craig, G. S. W.; Schrock, R. R.; Cohen, R. E. *Chem. Mater.* **1992,** 4, 885.
[5] Antonietti, M.; Wenz, E.; Bronstein, L.; Seregina, M. *Adv. Mater.* **1995,** 7, 1000.
[6] Moffitt, M.; Eisenberg, A. *Chem. Mat.* **1995,** 7, 1178.
[7] Kurihara, K.; Fendler, J. H. *J. Am. Chem. Soc.* **1983,** 105, 6152.
[8] Bosman, A. W.; Janssen, H. M.; Meijer, E. W. *Chem. Rev.* **1999,** 99, 1665.
[9] Fischer, M.; Vogtle, F. *Angew. Chem. Int. Edit.* **1999,** 38, 885.
[10] Newkome, G. R.; Moorefield, C. N.; Vögtle, F. *Dendritic Molecules: Concepts, Syhthesis, Perspectives, VCH, Weinheim* **2001**.
[11] Zheng, F. W.; Zimmerman, S. C. *Chem. Rev.* **1997,** 97, 1681.
[12] Fréchet, J. M. J. *J. Polym. Sci. Polym. Chem.* **2003,** 41, 3713.
[13] Hecht, S. *J. Polym. Sci. Polym. Chem.* **2003,** 41, 1047.
[14] Newkome, G. R.; Moorefield, C. N.; Baker, G. R.; M. J. Saunders, M. J.; Grossman, S. H. *Angew. Chem. Int. Edit.* **1991,** 30, 1178.

[15] Jansen, J.; Debrabander-van den berg, E. M. M.; Meijer, E. W. *Science* **1994,** 266, 1226.
[16] Duncan, R. *Nature Reviews Drug Discovery* **2003,** 2, 347.
[17] Haag, R. *Angew. Chem -Int. Edit.* **2002,** 43, 278.
[18] Stiriba, S. E.; Frey, H.; Haag, R. *Angew. Chem. Int. Edit.* **2002,** 41, 1329.
[19] Pittelkow, M.; Christensen, J. B.; Meijer, E. W. *J. Polym. Sci. Polym. Chem.* **2004,** 42, 3792.
[20] Sunder, A.; Heinemann, J.; Frey, H. *Chem. Eur. J.* **2000,** 6, 2499.
[21] Gao, C.; Yan, D. *Prog. Polym. Sci.* **2004,** 29, 183.
[22] Voit, B. *J. Polym. Sci. Polym. Chem.* **2000,** 38, 2505.
[23] Sunder, A.; Hanselmann, R.; Frey, H.; Mülhaupt, R. *Macromolecules* **1999,** 32, 4240.
[24] Sunder, A.; Kramer, M.; Hanselmann, R.; Mülhaupt, R.; Frey, H. *Angew. Chem. Int. Ed.* **1999,** 38, 3552.
[25] Sunder, A.; Mülhaupt, R.; Haag, R.; Frey, H. *Adv. Mater.* **2000,** 12, 235.
[26] Slagt, M. Q.; Stiriba, S. E.; Gebbink, R.; Kautz, H.; Frey, H.; van Koten, G. *Macromolecules* **2002,** 35, 5734.
[27] Stiriba, S. E.; Kautz, H.; Frey, H. *J. Am. Chem. Soc.* **2002,** 124, 9698.
[28] Huang, J.; Sooklal, K.; Murphy, C. J.; Ploehn, H. *J. Chem. Mater* **1999,** 11, 3595.
[29] Dedinaite, A.; Meszaros, R.; Claesson, P. M. *J. Phys. Chem. B* **2004,** 108, 11645.
[30] Aymonier, C.; Schlotterbeck, U.; Antonietti, L.; Zacharias, P.; Thomann, R.; Tiller, J. C.; Mecking, S. *Chem. Comm.* **2002**, 3018.
[31] Kraemer, M.; Stumbe, J. F.; Turk, H.; Krause, S.; Komp, A.; Delineau, L.; Prokhorova, S.; Kautz, H.; Haag, R. *Angew. Chem. Int. Ed.* **2002,** 41, 4252.
[32] Kem, K. M. *J. Polym. Sci. Polym. Chem. Ed* **1979,** 17, 1997.
[33] Baars, M. W. P. L.; Froehling, P. E.; Meijer, E. W. *Chem. Comm.* **1997**, 1959.
[34] Baars, M. W. P. L.; Karlsson, A.; J.; Sorokin, V.; de Waal, B. F. W.; Meijer, E. W. *Angew. Chem. Int. Ed.* **2000,** 39, 4262.
[35] Lias, H.-G., *An Introduction to Polymer Science;* Wiely VCH, Weinheim:, Germany, : 1997; p Chapter 5. 8.
[36] Kulicke, W. M.; Clasen, C., *Viscosimetry of Polymers and Polyelectrolytes;* Springer: Heidelberg, Germany,: 2004.
[37] Chen, Y.; Shen, Z.; Barriau, E.; Kautz, H.; Frey, H. *Biomacromolecules* **2006,** 7, 919.

Chapter 8. Summary

Dendrimers and their less defined hyperbranched macromolecular analogues are attracting tremendous interest due to their specific shape and multifunctionality. They have been found to be powerful motifs for the design of supramolecular assemblies and nanomaterials. Since the preparation of dendrimers traditionally suffers from its time-consuming nature and expensive cost, hyperbranched polymers obtained from AB_m-type monomer in one step have been emerged as excellent alternatives. One of these materials with specific properties is hyperbranched polyglycerol that can be prepared in a controlled manner with low polydispersity.

Part I: Works based on Hyperbranched Polyglycerol

Chapter 2

Well-defined multi-arm star block copolymer polyglycerol-*b*-poly(*tert*-butyl acrylate) (PG-*b*-P*t*BA) with average 17, 27, 36, 66 and 90 arms have been prepared via a *core-first* strategy.

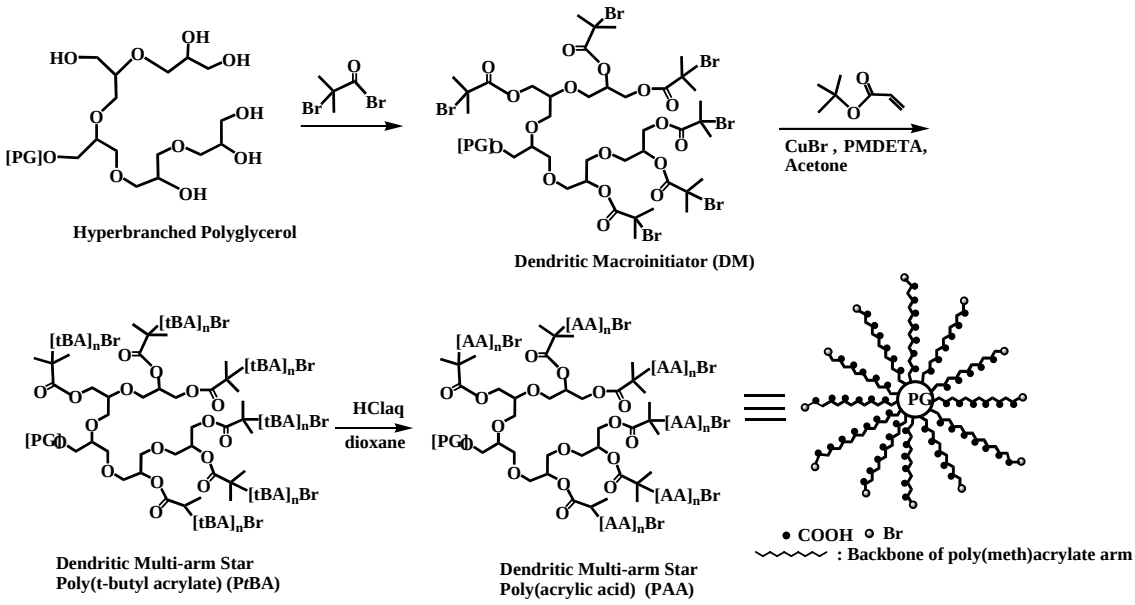

Scheme 8-1. Synthetic route of star PAA using PG as core

The hyperbranched macroinitiators employed were prepared on the basis of hyperbranched polyglycerol by esterification with 2-bromo-isobutyryl bromide. The arms were grafted by atom transfer radical polymerization (ATRP) of *t*BA in acetone. Under optimized conditions, the absolute M_n values of the obtained multi-arm-star polymers were similar to the calculated ones. Molecular weight range of the star P*t*BAs are roughly in the scope from 1×10^4 to 1×10^5. The polydispersites of the new multi-arm stars were mainly in the range of 1.22 to 1.4. Kinetic data characterized by ^{1}H NMR show a linear dependence of $\ln([M]_0/[M]_t)$ on time and molecular weights, which increase linearly with conversion, confirming that the polymerizations are controlled.

Furthermore, we have demonstrated the relationship of to which degree we can control the polymerization *vs* arm numbers of star polymers for the first time experimentally. This is due to the easy preparation of polyglycerol with different molecular weights and end group functionality.

Applying the obtained PG-*b*-P(*t*BA) with excess concentrated HCl in refluxing dioxane, full hydrolysis of the *tert*-butyl ester groups was achieved, resulting in multi-arm star polyelectrolytes, polyglycerol-*b*-poly(acrylic acid) (PG-*b*-PAA).

Chapter 3

Solution viscosity measurements in water demonstrate that the star PAAs show typical polyelectrolyte behavior characterized by an increase of the reduced viscosity at low concentration range, and no minimum apparent molar mass is needed to display a polyelectrolyte effect.

An empirical intrinsic viscosity was calculated using the Fuoss equations. The calculated intrinsic viscosity is in the range of 14.40 and 26.60 ml/g. The overlap concentration [C*] can also be obtained in the range of 37.6 mg/ml to 69.4 mg/ml.

The viscosity of the star PAAs measured in buffer solutions also shows typical polyelectrolyte behavior. Under this situation, star PAA is a charged spherical colloid. AFM measurements provided support for the formation of charged spherical colloids.

The average size of these structures is around 30 nm. The polyelectrolyte behavior was suppressed in 1 M NaCl solution.

Silver nanoparticles can be obtained using star PAA as template, reducing with either DMF or $NaBH_4$. The size of the obtained NPs depends on the size of the star PAA used.

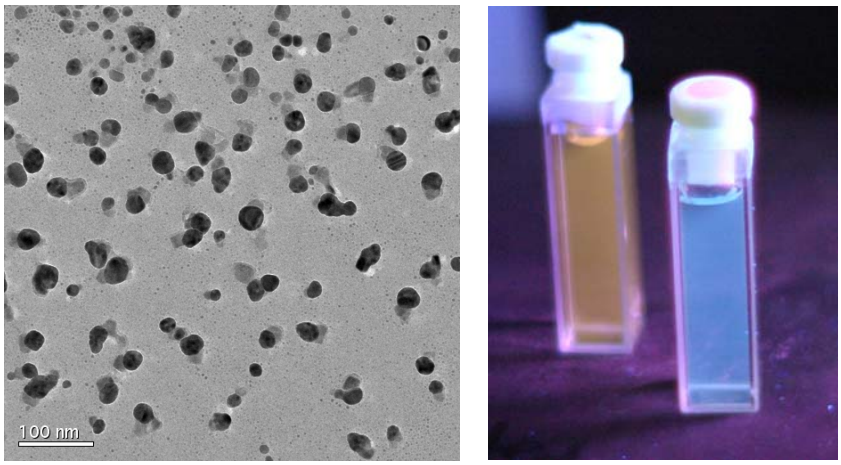

Scheme 8-2. Silver NPs (left) and fluorescent nanoclusters from star PAA template

The nanoclusters obtained from star PAA template via UV-reduction show fluorescent properties. The "cage effect" associated with densely grafted PAA and strong binding of protonated AA groups with Ag^+ are two essential factors for the formation of the fluorescent nanoclusters. The fluorescent properties show both arm-density dependence and arm length dependence. It can be expected that stable fluorescent nanoclusters will represent an interesting alternative to quantum dots as a new class of fluorescent labels, favored by the extremely small size,[37] stability and biocompatibility of these materials.

Chapter 4

Well-defined multi-arm star block copolymer polyglycerol-*b*-poly(*DMAEMA*) with an average 36 arms have been prepared via a *core-first* strategy. The arms were grafted by atom transfer radical polymerization (ATRP) of DMAEMA in either ethyl acetate or anisole. The polydispersities of the new multi-arm stars can be controlled within the range of 1.4-1.9. The kinetic data do not show a linear dependence of

$\ln([M]_0/[M]_t)$ on time, indicating that the polymerizations are only in a relative controlled mode.

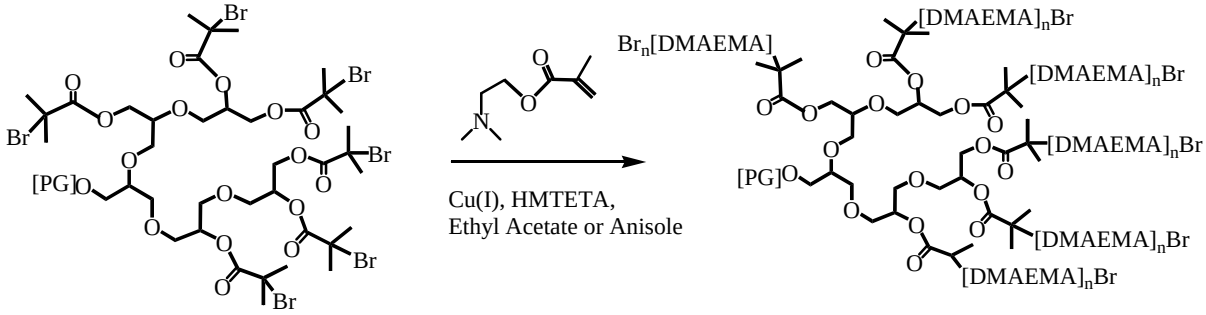

Dendritic Macroinitiator (DM)

Multi-arm Star PDMAEMA

Scheme 4-4. Synthesis of multi-arm star PG-b-PDMAEMA

The star polymers can be converted to inverted micelles by further modification with aliphatic bromides. These inverted micelles can be used to transfer water soluble dyes into the organic phase.

Part II: Works based on Hyperbranched Polyethylenimine

In continuation of our program aimed to design and construct new supramolecular systems based hyperbranched polymers, hyperbranched polyethylenimine (HPEI) was used for the preparation of both non-covalently and covalently bonded nanocapsules for liquid-liquid phase transfer protocols.

Chapter 5

Hyperbranched macroligands were successfully prepared by facile Michael addition reaction of HPEI with EA or BA. The resulting hyperbranched macroligand/Cu(I) complexes are efficient catalyst systems for the ATRP of MMA. The ATRP of MMA with hyperbranched macroligands is a controlled process, since $\ln([M]_0/[M]_t)$ is a linear function of time. Molecular weights of the resulting PMMA increase linearly with conversion and the molecular weight distributions are fairly narrow (M_w/M_n<1.4) even at very high conversion. However, the initiation efficiency of the polymerization using hyperbranched macroligands is less than 100%, usually in the range of 0.41-0.83. The compact structure not only leads to very low viscosity compared to the synthesized linear PMMA, but also imparts facile separation from the PMMA product by precipitation of the polymerization mixture in methanol. Copper is

separated together with the hyperbranched macroligands and no additional steps are required to purify the polymer from copper contamination. The hyperbranched macroligand/CuCl system can be recycled for the ATRP of MMA, keeping relatively high activity. The obtained PMMAs do not exhibit unusual tacticity.

These macroligands can also be utilized for the ATRP of BA or Styrene, however, additional optimization of the polymerization conditions is necessary.

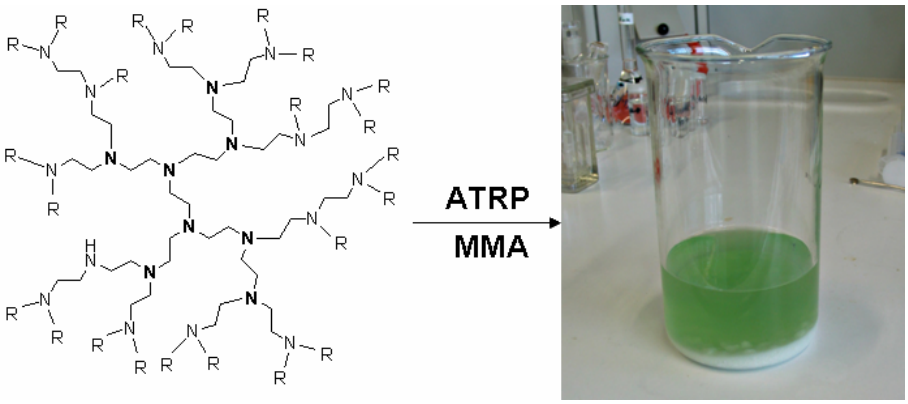

Scheme 8-4. Modified HPEI as effective ligand for ATRP

Chapter 6

Supramolecular self-assembly of a HPEI can be used to construct new molecular nanocapsules together with fatty acids for phase transfer processes.

An arrangement of fatty acids around the HPEI in a composite structure that resembles an inverted micelle, having a hydrophilic interior and hydrophobic shell that assures solubility for the entire new system was suggested. The synergy between both components affords phase transfer properties due to the polyelectrolyte-surfactant complexes. These self-assembled molecular nanocapsules were demonstrated to be of unimolecular nature, as evidenced from light scattering analysis. Viscosity measurements show compact structures. Proof of that arises from their comparison with LPEI assembled with fatty acids.

The HPEI-fatty acids synergism in the self-assembled inverted micelles leads to molecular nanocapsules able to sequester polar dyes, as demonstrated by encapsulation of water-soluble dyes like Congo Red and methyl orange. Dye loading was found to be molecular weight-dependent.

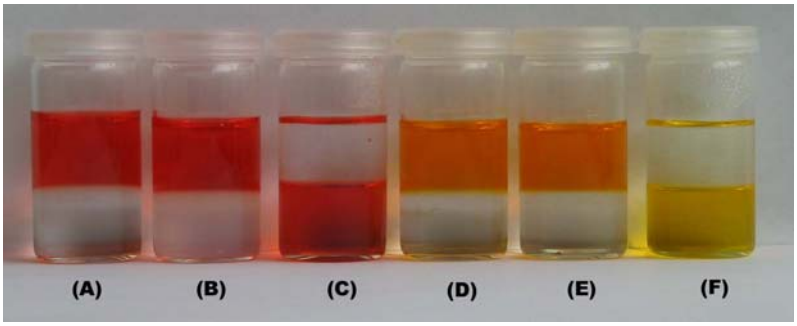

Scheme 8-5. Dye encapsulation from non-covalent HPEI based nanocapsules

Chapter 7

HPEI can be functionalized for the transport of different guest molecules.

Partially amidated HPEIs with cationic interior are attractive compounds to obtain unimolecular, hyperbranched nanocapsules for phase-transfer applications. It can be used to transfer water soluble dye into organic phase, the irreversible dye loading capacity is enhanced considerably by the increase of the interior polarity by quaternization. In comparison to the branched compounds, the linear analogue showed lower capacity for guest molecule transfer, which strongly supports the conclusion that the hyperbranched structure is crucial for encapsulation. Preliminary tests also show that this capsule can be used to transfer water-soluble gold nanoparticles into the organic phase.

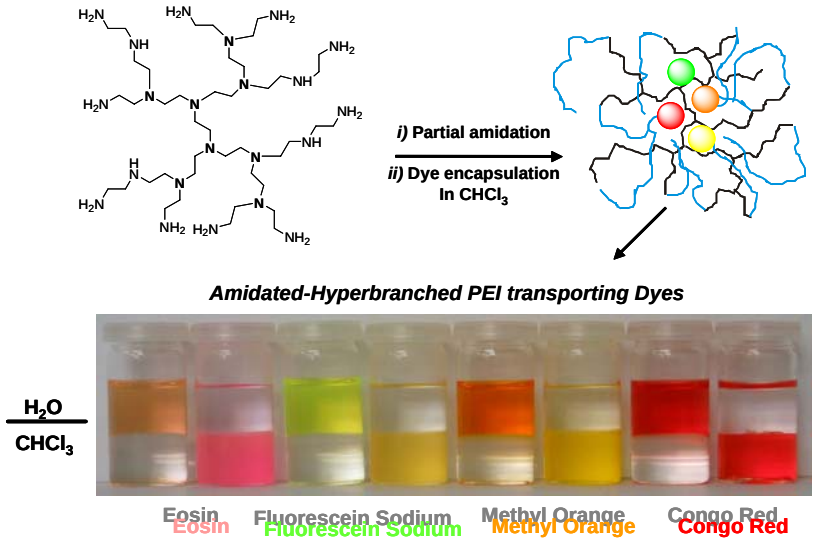

Scheme 8-6. Dye encapsulation from covalent HPEI based nanocapsules

Chapter 9. Methods and Instrumental Characterization

9. 1. NMR

^{1}H and ^{13}C NMR spectra were recorded on a Bruker ARX 300 spectrometer, operating at 300 MHz and 75.4 MHz, respectively. The chemical shifts are given in parts per million (ppm).

9. 2. SEC (Size Exclusion Chromatography)

Size Exclusion Chromatography (SEC), also known as Gel Permeation Chromatography (GPC), is an important relative method to determine the molecular weight and molecular weight distribution of macromolecules. The separation of polymer molecules is based on a size exclusion mechanism. And elution volume is dependent on the molecular size.

In contrast to light scattering or membrane osmosis, SEC is a relative method for the determination of molar masses and therefore needs calibration. Molar masses and molar mass distributions can only be determined quantitatively if the calibration standards and the unknown sample are chemically identical, i.e. consist of identical monomers and exhibit the same chain architecture. The reason for this restrictive condition is that the hydrodynamic volume is different for different polymers with the same molar mass.

$CHCl_3$ GPC: Molecular weights and molecular weight distributions were determined on a Size Exclusion Chromatography (SEC) consisting of a Waters 717 plus autosampler, a TSP Spectra Series P 100 pump and a set of three PSS-SDV 5 µ columns with 10^2, 10^3, and 10^4 Å porosity. Samples were measured with a Optilab DSP interferometric refractometer (RI detector) in Chloroform (30 °C, flow rate of 1.0mL/min) by injection of 150 µl of the polymer solution. Polystyrene standards provided by Polymer Standards Service were used for calibration.

THF GPC: Gel permeation chromatography in THF was performed on an instrument consisting of a Waters 717 plus autosampler, a TSP Spectra Series P 100 pump and a set of three PSS-SDV 5 µ colums with 100, 1.000, und 9.000 Å porosity. THF was used as an eluent at 25 °C and a flow rate of 1 ml min^{-1}. The specific refractive index increment (dn/dc) was measured at 25 °C on an Optilab DSP interferometric refractometer (also RI detector) and determined with the Wyatt ASTRA IV software

(Version 4.90.08). Calibration was carried out using poly(styrene) standards provided by Polymer Standards Service. Absolute molecular weights were measured in THF on the GPC equipped with multiangle light scattering (MALLS) detector.

DMF GPC: Measurements were performed with a Knauer microgel set C11 using DMF as an eluent at 45 °C and a Polymer Labaratories evaporative mass detector EMD 960 operating at 110 °C.

9.3. Infrared spectroscopy

FT-IR spectra were recorded on a Nicolet 5DXC FTIR spectrometer on/in KBr or using a Graseby Specac "golden gate" attenuated total reflexion (ATR) unit.

9.4. UV/VIS spectroscopy

UV-vis spectroscopy is the quantitative measurement of the absorption of near-ultraviolet and visible light by a sample. UV/VIS measurements were carried out on a Perkin-Elmer Lambda 2 UV/VIS Spectrophotometer using 10 mm quartz-glass cuvettes.

9.5. UV Reducing of silver

The experimental procedure that induces the chemical reaction of molecules by using Ultraviolet (UV) light in the suitable range is called UV Reducing. In general, UV light ranges from 10 - 400 nm. Because of its relatively short wavelength, the high energy of UV light is able to initiate photoreactions of molecules. The advantage of UV is faster, lower reaction temperature, less odor, etc. In this thesis, a Vilber Lourmat UV lamp (France, Model VL-6.LC, 6W, an average UV intensity of 0.5mW cm^{-2}, measure with a photo meter) were used to irradiate the solution filled in a cuvette at the wavelength $\lambda = 365$ nm.

9.6. Fluorescence Spectroscopy

Fluorescence is the emission which results from the return to the lower orbital of the paired electron. Fluorescence spectral data are generally presented as emission spectra: a plot of emission against wavelength for any given excitation wavelength. Fluorescence is dependent on the environment than absorption spectra and extinction coefficients. In current study, fluorescence spectra were obtained from Spex Fluorolog 2 1681 spectrometer.

9.7. Atomic Force Microscopy (AFM)

The atomic force microscope (AFM) is a member of a new class of microscopes termed the scanning probe microscopes (SPM). It was used to characterize the size and shape of the single particles and the clusters. Samples were spin coated from highly diluted MeOH solutions of the star PAA (C = 0.05g/l) onto freshly cleaved graphite. These surfaces were scanned with a nanoscope IIIa, Digital Instruments (Santa Barbara, CA), operating in tapping mode.

9.8. Transmission Electron Microscopy (TEM)

A Philips EM-420 transmission electron microscope operating at an acceleration voltage of 120 kV was used to analyze the size and size distribution of the silver nanoparticles obtained. The nanoparticles were deposited from diluted solutions onto copper grids with carbon support, and observed after they had been dried in air overnight.

9.9. Dynamic Light Scattering (DLS)

Light scattering occurs when polarizable particles in a sample are placed in the oscillating electric field of a beam of light. The varying field induces oscillating dipoles in the particles and these radiate lights in all directions. It can be utilized to determine particle size, molecular weight, shape, thermodynamic properties, diffusion coefficients etc.

Average hydrodynamic radii (Rh) of the polymers have been determined by dynamic light scattering (DLS) using an experimental setup consisting of a He-Ne laser (JDS Uniphase 1145p-3083, JDS Uniphase, 632.8 nm, 25 mW output power), goniometer SP-86 (ALV), and an ALV-3000 digital correlator/structurator. All light scattering measurements have been carried out with filtered samples (Millipore dimex-13 filter, pore size 0.2 μm). The refractive index increment necessary for the SLS experiments was measured with a home-built interferometer using a laser diode (613 nm wavelength). All the measurements were carried out at 20 ºC.

9. 9. Viscosimetry

Viscosities were measured by Lauda Processor-Viscosity-System 2.52a using $CHCl_3$ as solvent at 20 °C, 25 °C or 30 °C. Different standard Ubbelohde

viscosimeters with different capillary diameters were used. Huggins and Kraemer plots were used to obtain the intrinsic viscosity.

9.11. DSC

Measurements were carried out on a Perkin Elmer 7 Series Thermal Analysis System in the temperature range of -100 ^{o}C to 180 ^{o}C at different heating rates like 10 K/min under nitrogen. The Tg was obtained by extrapolation to heating rate 0 from these measurements. The melting point of indium (156 ^{o}C) was used for calibration.

9.12. Thermogravimetric analysis (TGA)

Thermogravimetric measurements under air and nitrogen were carried out on a Netsch thermoanalyis apparatus STA409 using corund crucibles with 10 to 20 mg sample mass.

9.13. Atomic Absorption Spectra

Atomic absorption spectroscopy (AAS) was used to determine copper residues in the final polymer products. Samples were measured in THF solution with a Perkin Elmer 5100 ZL with a Zeeman Fumace module (Oven).